THERMODYNAMICS STUDY OF SLAGS CONTAINING $FeO, Fe_2O_3, SiO_2, TiO_2$ AND CaO

by

ISMAIL IBRAHIM GHITA

B.Sc.(Met.) Eng., Cairo University

A thesis submitted to the Department of Metallurgy, University of Strathclyde in fulfilment of the requirements for the Degree of Doctor of Philosophy.

JUNE, 1981

ABSTRACT

Phase relationships on the liquidus surface in the system $FeO-TiO_2-SiO_2$ have been studied under an argon atmosphere. The crystal phases which separated from melts heated in iron crucibles were fayalite ($2FeO.SiO_2$), ulvöspinel ($2FeO.TiO_2$), ilmenite ($FeO.TiO_2$), pseudobrookite ($FeO.2TiO_2$), silica (SiO_2), rutile (TiO_2) and wüstite (FeO).

A prominent feature of the liquidus surface is a large two-liquid region which appears on the equilibrium diagram as an area extending from the $FeO-SiO_2$ to the SiO_2-TiO_2 side of the triangle $FeO-TiO_2-SiO_2$.

The system $FeO-TiO_2-SiO_2$ can be divided into five composition triangles and paths of crystallization of representative mixtures in the system, with reference to these triangles, are described.

Four ternary eutectic points have been determined in this study at the compositions, $FeO:TiO_2:SiO_2$, 70.70:6.1:23.2, 58.0:13.0:29.0, 52.5:37.5:10 and 40.0:52.5:7.5, by mole percentage, their liquidus temperatures being 1135 ± 10°C, 1140 ± 10°C, 1320 ± 10°C and 1330 ± 10°C, respectively.

The liquidus surface in the system Fe-Ti-Si-O has been studied by equilibrating mixtures of iron oxide, titania and silica in platinum crucibles at oxygen pressures ranging approximately from 10^{-6} to 10^{-2} atmospheres at 1500°C. These atmospheres cons isted of CO_2, CO and N_2 and air and N_2 mixtures.

The effect of titania content on the liquidus temperatures was determined at given oxygen pressures. Titania has not a great

effect on the liquidus temperatures at $\frac{N_{SiO_2}}{\Sigma N_{Fe}}$ ratio varying from 0.67 to the phase boundary of two-liquid region, but up to a ratio $\frac{N_{SiO_2}}{\Sigma N_{Fe}}$ of 0.33 titania increases the liquidus temperatures, at constant $\frac{N_{SiO_2}}{\Sigma N_{Fe}}$.

The results of the present work permit the construction of curves relating the $\frac{Fe^{3+}}{Fe^{2+}}$ ratio to silica and titania concentration for given temperature and oxygen pressures. Titania and silica have qualitatively similar effect but the magnitude is slightly different, e.g.

$$\frac{N_{Fe_2O_3}}{\Sigma N_{FeO}} = 0.28 \text{ and at } N_{SiO_2} = 0.35 \text{ to } \frac{N_{Fe_2O_3}}{\Sigma N_{FeO}} = 0.25$$

at constant ΣN_{FeO} and oxygen pressure about 10^{-5} atmosphere and 1500°C.

In this study the sulphide capacities of $FeO-TiO_2-SiO_2$, $FeO-TiO_2-CaO$ and $FeO-TiO_2-SiO_2-CaO$ slags were measured by allowing them to come to equilibrium with a gas mixture ($CO_2/H_2/SO_2/N_2$) of known sulphurising potential at 1500°C. The results show that, titania and silica decrease the sulphide capacity while lime and iron oxide increase C_S. By increasing the titania content in the melts from 14-17 m/o at constant silica of 24 m/o, the C_S decreases approximately by a factor of 4 at given oxygen and sulphur pressures at 1500°C in the $FeO-TiO_2-SiO_2$ slags.

On the other hand titania increases the sulphide capacity of the TiO_2-SiO_2-CaO and $TiO_2-SiO_2-CaO-Al_2O_3$ slags, which were measured under equilibrium with a gas mixture ($H_2O/H_2/H_2S/Ar$) to give

low oxygen pressures. If SiO_2 is replaced by titania, the C_S increases by a factor of 3 as composition changes from 15-55 m/o TiO_2 at 30 m/o CaO in the TiO_2-SiO_2-CaO slags. The increase in sulphur solubility by increase in iron oxide, lime and titania (in slags free from iron oxide) is tentatively explained in terms of an increase in N_O^{2-} in the slag.

There was a high degree of correlation between the sulphide capacities of titanate slags (iron oxide free) and the optical basicity scale.

The calculation of slag/metal sulphur partition show that $\frac{(\%S)}{[\%S]}$ for the FeO-TiO_2-CaO slag is higher than for FeO-TiO_2-SiO_2 slags, e.g. at 0.65 N_{FeO}, 0.20 N_{TiO_2} and 0.15 N_{CaO}, the $\frac{(\%S)}{[\%S]}$ = 1.1, while at the same concentration of FeO, TiO_2 and 0.15 N_{SiO_2}, the $\frac{(\%S)}{[\%S]}$ = 0.40 in the FeO-TiO_2-CaO and FeO-TiO_2-SiO_2 slags respectively.

CONTENTS

FIGURE CAPTIONS

INTRODUCTION

Probably no other metal can match the meteoric rise of titanium, from being a mere laboratory curiosity about thirty years ago to its present position in the forefront of modern industrial technology. The time span of the commercial titanium industry as it exists today is equally brief, covering only just over three decades since the industry was started in the U.S.A. in 1947/8 under the spur of military pressure.

Titanium, having now obtained wider acceptance of its advantages, is today regarded as a practical engineering metal and can no longer be classed as one of the "new metals".

This is not surprising, for the metal has a higher melting point than steel and low density of 4.51 g/cm^3 making its weight up to 45% less than some steel and only 60% more than aluminium. Its strength, in alloy form, is two to three times better than aluminium alloys, it has five times the strength of competitive lightweight magnesium alloys, and it is even stronger than some of the alloy steel. With its excellent toughness, fatigue strength and corrosion resistance backed by an ability to retain a large proportion of its strength at high temperatures, well above those for aluminium and magnesium alloys, it is no wonder that it was eagerly seized upon by the aerospace industry in the early days of jet aircraft development.

As an oxide, it has been used in the making of electrical components, particularly in high power capacitors and other dielectric components. Titanium oxide and its other compounds is also finding

greater use in the manufacture of paints.

In geological terms the metal is a characteristic constituent of igneous and metamorphic rocks, and of sediments derived from them such as beach sand. Those categories of ancient rock magmas, formed during the cooling of the earth's crust, which are in general rich in silica and poor in the base-forming elements, iron and magnesium, deposited their titanium content as oxide. Those containing high amounts of calcium and silicon, on the other hand, provided calcium titanate, whilst those highest in iron and lowest in acid-forming oxide (e.g. silica) provided us with iron titanates, ilmenite.

Ilmenite ($FeTiO_3$), as such is present in the ore mainly as small granules, constituting only a minor percentage of overall titanium content. Titanium further occurs as ulvöspinel (Fe_2TiO_4) and as intergrowths of ilmenite with particularly magnetite (Fe_3O_4), but also with other ore constituents.

The industrial value of titanate slags is becoming more important in view of current practices in Canada, Japan, South Africa, Malaysia, Australia, New Zealand and Brazil.

One of the world's unique smelting operations today is that of the Quebec Iron and Titanium Corporation (QIT) in Canada. Its operational practice consists of the feeding of ilmenite ore and coal into electric arc furnaces, reacting these at temperatures in excess of 1550°C, and tapping out a high-carbon iron and a slag containing about 72% TiO_2 (Sorelslag).

In South Africa, the Highveld and Vanadium Corporation produce steel and vanadium-rich slag from titaniferous magnetites ore in submerged arc electric furnaces. The process, as finally developed, is as follows: The ore, together with coal and flux

consisting of limestone delomite and silica is passed through a rotary kiln at temperature of 900°C-950°C, so effecting about a 55% reduction of the iron oxide content of the ore and also preheating the charge. This partially reduced charge is then fed to submerged arc furnaces. The products from the smelting operation are pig iron containing the vanadium and a titaniferous slag containing the gangue from the ore. The hot metal is blown with oxygen in a shaking ladle for the removal of vanadium oxide, before being transferred to the steel plant.

Another source for producing iron of titanate slags is that ore pellets containing titania are being used in electric arc furnaces in New Zealand.

In order to contribute to the understanding of the behaviour of titania in metallurgical slags, the objective of the present study was to determine the phase diagram ($FeO-TiO_2-SiO_2$) and measure the liquidus temperatures of $FeO-TiO_2-SiO_2$ and Fe-Si-Ti-O systems. Specifically, the aim was also to examine the thermodynamic properties of titanate slags in iron systems.

Thus in the literature review which follows, the approach is to review the data on the ferrous silicate systems in order that that data subsequently obtained from the ferrous titanate systems, can be compared with the relevant silicate system. This would appear to be a logical point from which to begin the study of the titanate slag systems as there is now a fairly extensive knowledge of the behaviour and properties of simple silicate systems.

For simplicity, during the writing of this thesis certain abbreviations have been used. Thus, fayalite-$2FeO-SiO_2$, ulvöspinel-$2FeO.TiO_2$, ilmenite-$FeO.TiO_2$ and pseudobrookite $FeO.2TiO_2$, wüstite,

magnetite and hematite, become, F_2S, F_2T, FT. FT_2, W, M and H respectively. All temperatures and pressures unless otherwise stated are in degrees centigrade and atmospheres respectively.

SECTION A

CHAPTER 1

LITERATURE REVIEW

A.1 LITERATURE REVIEW

A.1.1 LIMITING SYSTEMS

A.1.1.1 The $FeO-TiO_2$ Binary System

A basic building of block of the Fe-Ti-O system is the $FeO-TiO_2$ binary system. Phase diagrams for this system have been proposed by Grieve and White[1] and also by MacChesney and Muan[2]. A modification of the TiO_2-rich side of the $FeO-TiO_2$ phase diagram was proposed by Grau[3]. The diagram of MacChesney and Muan is the one generally accepted and is reproduced in Figure (A.1.1). They[2] determined phase relations in the system $FeO-TiO_2$ by heating oxide mixtures at oxygen pressures defined by the iron-wüstite equilibrium and subsequently used a quenching technique to cool the mixtures to room temperature. The oxide mixtures were heated in iron crucibles in a nitrogen atmosphere.

It may be seen in Figure (A.1.1) that the TiO_2-rich side of this diagram is characterised by the existence of two congruently melting compounds, namely ilmenite ($FeO-TiO_2$) and ferrous dititanate ($FeO-2TiO_2$), the latter having a pseudobrookite type structure. In this region, there would be two eutectic points, the first marking the co-existence of the solid phases ilmenite and pseudobrookite with a liquid of approximately 58% TiO_2 and the second corresponding to the equilibrium between pseudobrookite, rutile (TiO_2) and a molten phase containing about 80% TiO_2.

There are certain basic differences between the results of MacChesney and Muan[2] and those of Grieve and White[1]. It was suggested that Grieve and White had incorrectly named the compound

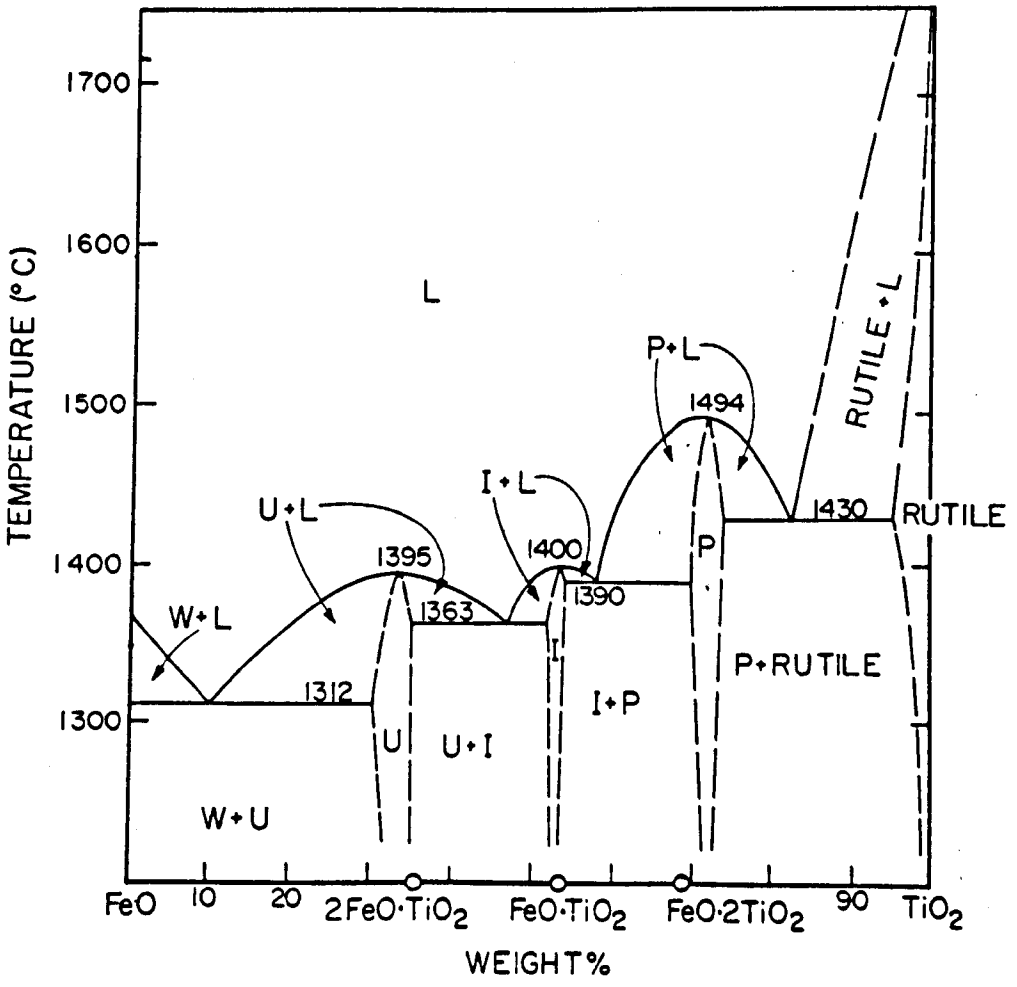

Fig. A.1.1 Phase diagram for the binary system $FeO-TiO_2$, based on data of MacChesney and Muan[2].

$2FeO-TiO_2$ as pseudobrookit and not ulvöspinel and had not incorporated $FeO.2TiO_2$ (pseudobrookit) as a phase. It was also suggested that the use of molybdenum crucibles in poorly defined atmospheres by Grieve and White, and that the compound ($FeO-2TiO_2$) was generally unknown as a natural mineral , might have been the reason for the difference of opinion.

According to the diagram of Figure (A.1.1), slags containing up to 85% TiO_2 would melt at temperatures below 1500°C. However, attempts made by Grau[3] to melt $FeO-TiO_2$ mixtures held in molybdenum crucibles by heating them to 1500°C under purified argon were unsuccessful. Similar results had been previously reported by Smith and Bell[4] who found that a temperature of 1475°C was insufficient to melt $FeO-TiO_2$ slags (contained in iron crucibles) in the 79-85% TiO_2 composition range. Since then Grau[3] carried out series of experiments to determine the liquidus temperature of $FeO-TiO_2$ slags in the range between 52-70% TiO_2 (ilmenite composition) and 80% TiO_2, using the cooling curve technique. In this technique the slag temperature is continuously recorded during a cooling cycle and the liquidus point was determined from the arrest in the time-temperature curve which indicates the beginning of the crystallisation. Grau[3] found that pseudobrookit melted incongruently at about 1475°C producing a rutile phase and a liquid containing approximately 67 or 68% TiO_2. The eutectic point which MacChesney and Muan located at about 80% TiO_2 was eliminated. The discrepancies between the results of Grau's work and those of MacChesney cannot be easily explained. These authors[2] used the quenching technique and the phases present at equilibrium were identified by x-ray and microscopic examination. The application of this technique to $FeO-TiO_2$ mixtures may encounter

difficulties in the rapid transitions which seem to take place even under quenching conditions. The rapid dentritic growth reported by MacChesney and Muan in some cases made their microscopic observation very difficult. The second problem reported by these authors[2] was the presence of metallic iron globules in the quenched samples, the formation of which was attributed to interaction between the iron crucibles and the $FeO-TiO_2$ mixtures. In spite of this, Grau[3] found that the molybdenum crucibles used in his determinations were always in very good condition and completely free of oxidation, the chemical analysis of the slag recovered after the experiments indicated in all cases the presence of molybdenum varying between 0.6% for a 52% TiO_2 slag and 2.2% for a 79.5% TiO_2 slag. Since the molybdenum detected by the chemical analysis was present as fine metallic iron, it was suggested that molybdenum is less satisfactory as a container for melts containing iron oxide and lower oxygen pressures which was confirmed by Bigger[5].

The authors[1,2] did not fix the melting point of TiO_2 with any certainty, merely stating that it was probably about 1800°C. The most reliable estimate of the melting point of TiO_2 would appear to be the 1830 ± 10°C, estimate given by Rase and Roy[6], which is in good agreement with the value of 1825°C reported by Bunting[7] and by De Vries et al[8], as well as the value of 1840°C reported by Coughonour and De Prasse[9] and by Tuset[10].

A.1.1.2 The $FeO-SiO_2$ Binary System

The first and best known determination of the $FeO-SiO_2$ binary system was by Bowen and Schairer[11]. They carried this out by using iron crucibles in a purified, nitrogen atmosphere. Hence metallic iron was always present as a phase, and the compositions of

the oxide phases present in equilibrium were those of the boundary curve between iron and the oxide phases, wüstite, fayalite and silica as shown in the $FeO-Fe_2O_3-SiO_2$ system in Figure (A.1.4). The phase relations were illustrated by projection of the composition of the condensed phases along oxygen reaction lines onto the join $FeO.SiO_2$, which is close to the iron boundary curve. This amounts to the same as recalculating all the iron as FeO. The resulting diagram, shown in Figure(A.1.2), has the appearance of a binary system and can also be treated like a binary system as far as dicussion of equilibrium crystallisation is concerned.

It can be seen that in Figure (A.1.2) there is one compound $2FeO.SiO_2$ (fayalite) at composition 70% FeO, 30% SiO_2 and melting point 1205°C in addition to the end-members FeO (wüstite) and SiO_2 (tridymite or cristobalite). A concentration range at the SiO_2 end of the binary system is characterised by the equilibrium existence of two liquid phases from approximately 62% to 97% SiO_2 at temperatures above 1698°C. The silica liquidus curve rises steeply up to this temperature.

The first attempt to obtain information on phase relationships of iron oxide and silica mixtures at different oxygen pressures, and to determine the melting points of iron oxides under various atmospheric conditions was made by Greig[12] and Darken[13]. Darken did not determine experimentally the composition of the metls and liquidus temperatures but discussed the principles involved in applying the phase rule to the system. Muan[14,15] investigated the phase relations in the system iron oxide-silica in air (P_{O_2} = 0.21 atmospheres).

A structural study of the molten $FeO-SiO_2$ system has been

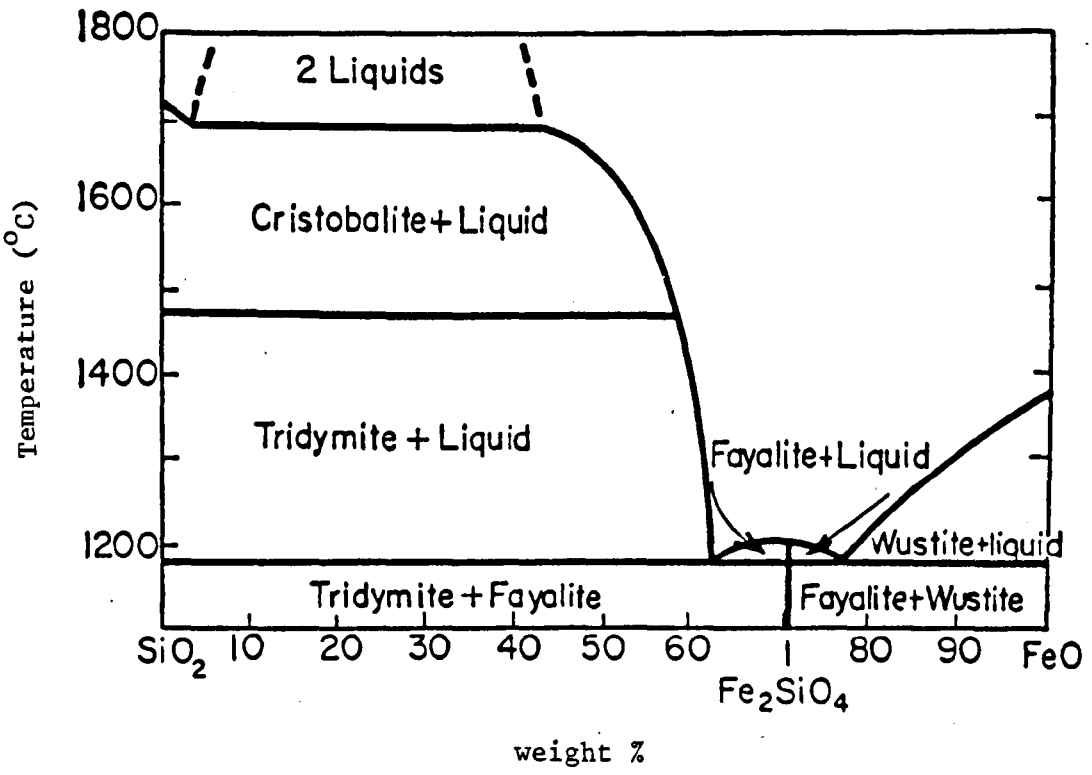

Fig. A.1.2 Phase diagram for the binary system SiO_2-FeO, based on data of Bowen and Schairer[11].

carried out by means of a high temperature x-ray technique by Waseda and Toguri[16], the composition range studied was from N_{SiO_2} = 0.0 to 0.44. From the calculated interference function, the radial distribution function was evaluated from which average interionic distances and co-ordination numbers were obtained. They found that SiO_4 tetrahedra exist from N_{SiO_2} = 0.17 towards the SiO_2 rich region, as confirmed by the nearly constant value of 4 for the co-ordination numbers of Si-O pairs in this composition range. The Si-Si distance, which corresponds to the inter SiO_4 distance, gradually decreases as the silica content increases from N_{SiO_2} = 0.2 and then shows a nearly constant value at compositions beyond N_{SiO_2} = 0.39. This constant value is comparable with the value of the Si-O-Si distance with an angle of less than 180 deg. This indicates that some of SiO_4^{4-} tetrahedra polymerize to form silicate anions. The interionic distance Fe-Si and Fe-O varies in a similar manner with Si-Si correlation.

The structure of pure molten FeO can be approximated to a molten salt-like structure such as NaCl[17]. Waseda[16] also found that the distance and co-ordination numbers corresponding to SiO_4 tetrahedra do not critically depend on temperature.

A.1.1.3 <u>The TiO_2-SiO_2 Binary System</u>

The equilibrium diagram for the system TiO_2-SiO_2 has been revised from that of Bunting[7] who was unable to completely fuse mixtures containing more than 20% TiO_2 and thus no data were reported beyond that composition towards TiO_2 except for the melting point of rutile.

The TiO_2-SiO_2 phase diagram has been studied also by De Vries et al[8] who confirmed Bunting's eutectic point composition (10.5% TiO_2). Their results showed the addition of TiO_2 to SiO_2

caused a drop from 1713°C to 1550°C in the liquidus temperature as the TiO_2 concentration increased to 10.5% TiO_2 as shown in Figure (A.1.3).

A region of two liquids extends over the major part of the binary system (from 19 to 93% TiO_2) at temperatures above 1780°C. This two-liquid region is noteworthy for its extent, and for the fact that it exists on the TiO_2 rather than on the SiO_2 side of the eutectic, and also for its effect in maintaining the very high liquidus temperature to high silica concentration (1780°C in melts containing down to 21% SiO_2). At 1780°C the two liquids form and separate almost immediately, this may be owing to the difference in physical properties as will be discussed later. It seems extremely likely that Si^{4+} cations insist on the tetrahedral co-ordination of O^{2-} anions to form SiO_4^{4-} or more complex polymerised anions, while Ti^{4+} prefers the O^{2-} anions to be in octahedral co-ordination, as do the cations of the basic oxides.

In view of the viscosity and electrical conductivity data of slags containing TiO_2 and SiO_2, it is of interest to know some theories about their structure. The most important and relevant results are those of Handfield and Charette[18] who studied Sorel-slags originating in electric arc furnaces. They found very low viscosity values of ≃30Cp, typical of melts with cations in octahedral co-ordination and very much lower than for silicates, which is indicative of the absence of large directionally bonded polymeric anions in these titanate melts. Turning to the electrical conductivity, there is qualitative agreement among the result of Mori[19], Reznichenko[20] and Denisov et al[21] that the values of specific electrical conductivity are also high, from ≃10 to ≃300 $ohm^{-1}cm^{-1}$

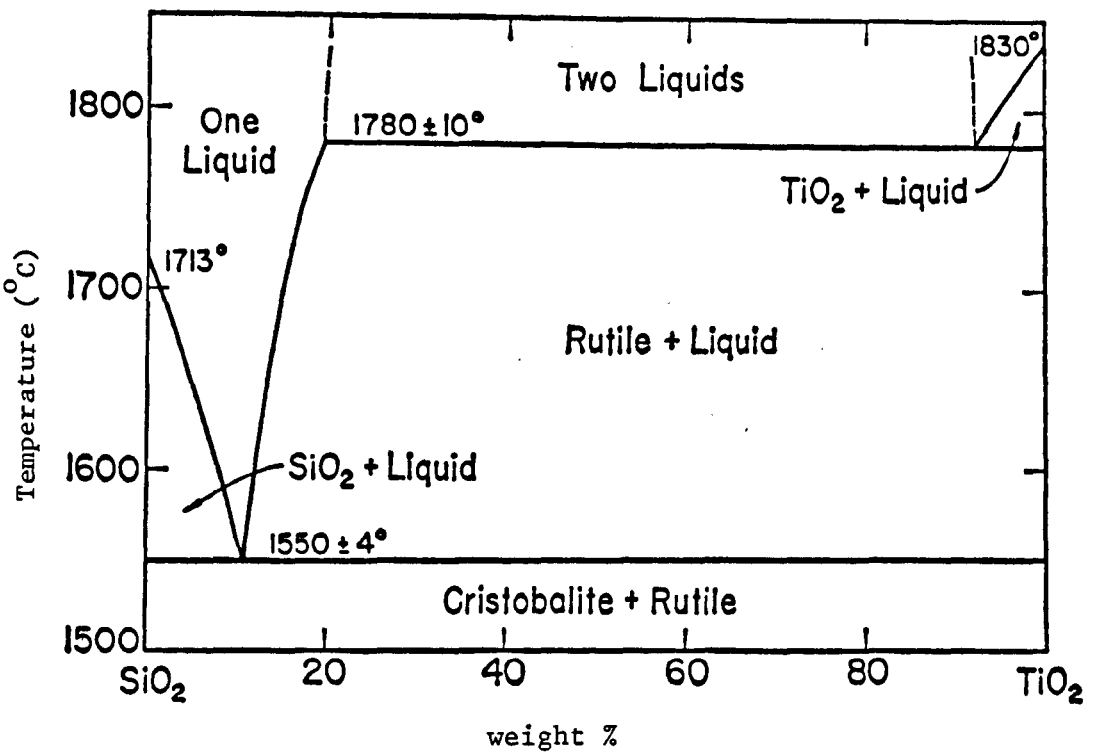

Fig. A.1.3 Phase diagram for the binary system SiO_2-TiO_2, based on the data of De Vries, Roy and Osborn[8].

for slags containing TiO_2 but no silica. These values can be compared with those for molten silicates which are usually in the range 0.1-1.0 $ohm^{-1}cm^{-1}$. On the other hand the activity behaviour is a thermodyanmic effect and it is not necessarily related to viscosity or conductivity. Hence the behaviour of the activities of titania and silica in their respective binary systems with FeO, are similar in nature both showing negative deviations from their respective ideality curves, as reported by Schuhmann and Ensio[22] and Smith[23]. Thus the physical properties of these melts suggest that liquid titanates and liquid silicates might differ structurally, but complete understanding of the structure of these slags may well wait a more general theory to account for their semiconducting properties.

A.1.1.4 The $FeO-Fe_2O_3-SiO_2$ Ternary System

An equilateral triangle is the most suitable figure for representing compositions in a ternary system. The composition triangle for the system $FeO-Fe_2O_3-SiO_2$ is part of the ternary system Fe-Si-O. A complete picture of phase relationships and composition may only be obtained by varying the gas composition over a wide range. White[24] equilibrated $FeO-Fe_2O_3$ and $FeO-Fe_2O_3-SiO_2$ melts under various oxygen pressures ranging from 1.0 to 5.9×10^{-2} atmospheres at temperatures from 1558°C to 1619°C. White's results showed that the $\frac{Fe^{3+}}{Fe^{2+}}$ ion ratio decreases with an increasing mole fraction of silica at a given oxygen pressure. It was noted that for a given partial pressure of oxygen, e.g. P_{O_2} = 0.2 atmospheres, the value of $\frac{Fe^{3+}}{Fe^{2+}}$ decreases with a rise in temperature. It was also found that by increasing the oxygen potential of the gas at constant temperature and concentration of silica, the ferric oxide content of the melt increased.

Darken and Gurry[25,26] studied the phase relationships of the $FeO-Fe_2O_3$ system. The variation of the composition of liquid and solid phases was measured as a function of the temperature and oxygen pressure. In a recent study Schuhmann et al[22,27] determined experimentally the composition of iron silicate melts in equilibrium with various CO_2/CO gas mixtures between temperature 1250°C and 1450°C. They investigated melts saturated with iron[22] and silica[27] and determined the liquidus surface of a portion of the ternary system[28] $FeO-Fe_2O_3-SiO_2$.

Schuhmann et al[28] used mixtures with various contents of SiO_2, FeO and Fe_2O_3 made by melting together stock mixtures in various proportions. Samples of the mixtures were heated in platinum crucibles in an inert atmosphere until equilibrium among the condensed phases was achieved. The samples were quenched to room temperature and the phases present determined by microscopic examination. Assuming that no change in composition takes place during the equilibration run in inert atmosphere, the liquidus surface can be determined, but no information was obtained regarding the partial pressure of oxygen of the gas phase in equilibrium with the condensed phases.

Muan[14] investigated the $FeO-Fe_2O_3-SiO_2$ ternary system in that the composition of the condensed phases and the liquidus surface were dependent on the partial oxygen pressures of the gas phase. Liquidus data were obtained at P_{O_2} ranging from $10^{-10.9}$ to 1.0 atmosphere. In this part of the system, there are two ternary invariant points as shown in Figure (A.1.4). At one invariant point, the phases co-existing in equilibrium at 1150°C were fayalite ($2FeO.SiO_2$), magnetite ($FeO.Fe_2O_3$), wüstite and a liquid with composition 22% SiO_2, 14% Fe_2O_3 and 64% FeO and a gas phase with partial P_{O_2} of $10^{-9.9}$

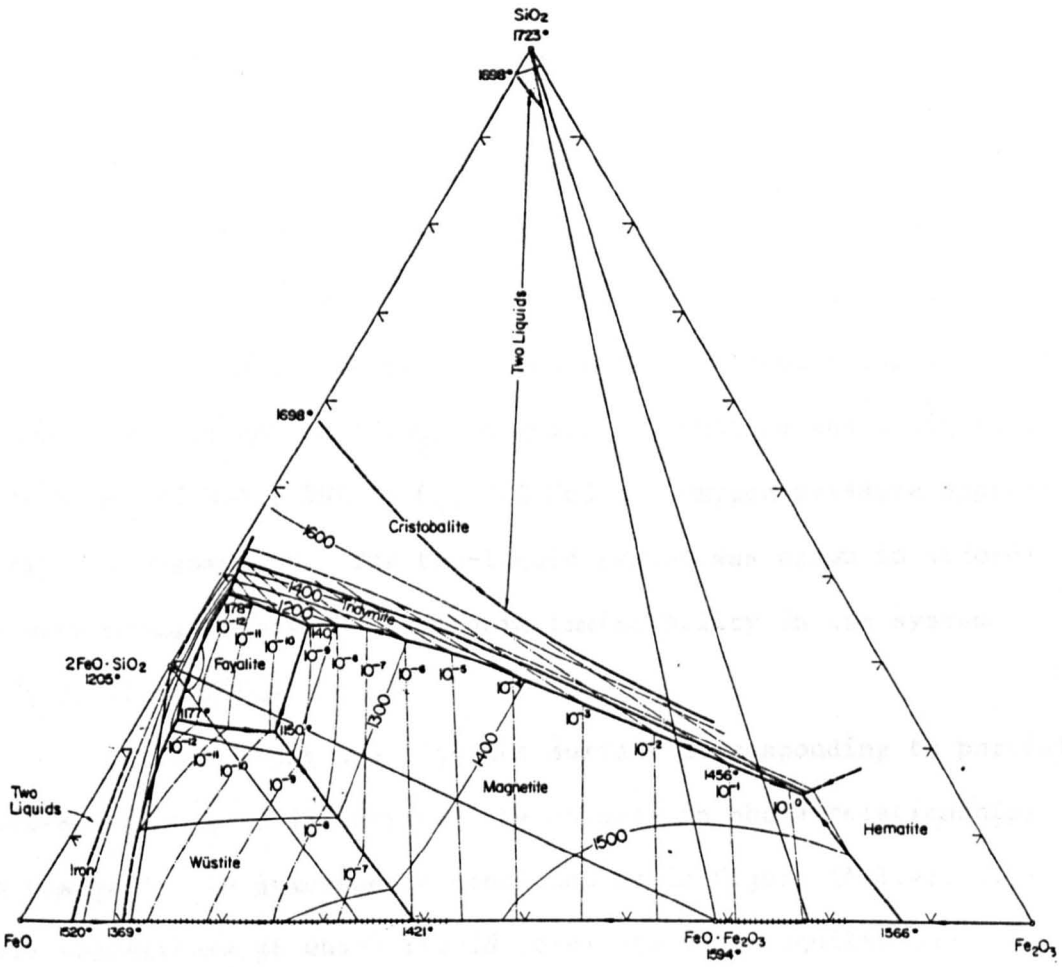

Fig. A.1.4 Phase diagram for the ternary system $FeO-Fe_2O_3-SiO_2$, based on the data of Muan[14].

atmosphere. The second invariant point, was at 1140°C, the phases co-existing in equilibrium were tridymite (SiO_2), fayalite ($2FeO\text{-}SiO_2$), magnetite ($FeO.Fe_2O_3$), a liquid with composition 35% SiO_2, 11% Fe_2O_3 and 54% FeO and a gas phase with partial pressure of 10^{-9} atmosphere. The ternary invariant point where tridymite (SiO_2), magnetite, hematie, liquid and gas are in equilibrium was not determined experimently but it was inferred to be located at a temperature of approximately 1455°C with a liquid composition approximately 15% SiO_2, 69% Fe_2O_3, 16% FeO, and P_{O_2} slightly higher than 1.0 atmosphere. Along the boundary curve tridymite, magnetite, a maximum point exists at a temperature of 1456°C with the following phases co-existing in equilibrium, i.e., tridymite (SiO_2), magnetite, hematite and a liquid of composition 19% SiO_2, 59% Fe_2O_3, 22% FeO and oxygen pressure approximately 0.1 atmosphere. The two-liquid region was drawn in accordance with Greig's data[12] on liquid immiscibility in the system $FeO\text{-}Fe_2O_3\text{-}Al_2O_3\text{-}SiO_2$.

Isobars along the liquidus surface corresponding to partial pressures of oxygen, illustrated the changes in phase relationships with change in the atmospheric condition as in Figure (A.1.4). The lowest temperature at which liquid co-exists under equilibrium conditions in an iron oxide-silica mixture is approximately 1455°C at an oxygen pressure of 1.0 atmosphere. With oxygen pressure decreasing to 10^{-1} atmosphere, the lowest temperature of liquid existence is essentially the same. With further decrease in oxygen pressure, liquid is present at rapidly decreasing temperatures, reaching a minimum of 1140°C at a P_{O_2} of 10^{-9} atmospheres for mixtures above the $2FeO.SiO_2$-silica join and a minimum of 1150°C at an oxygen pressure $10^{-9.9}$ for mixtures below the $2FeO.SiO_2$-silica join. With further

decrease in oxygen pressure, the lowest temperature of liquid existence increases somewhat until metallic iron appears as a phase at oxygen pressures between 10^{-12} and 10^{-13} atmosphere.

Turkdogan and Bills[29] investigated the variation of $\frac{Fe^{3+}}{Fe^{2+}}$ ratio with silica concentration in iron silicate melts under various $\frac{CO_2}{CO}$ atmosphere at 1550°C. They found that the $\frac{Fe^{3+}}{Fe^{2+}}$ ratio decreases as the silica content of the melts increases for a given oxygen partial pressure in $FeO-Fe_2O_3-SiO_2$ system and for a given silica content that $\frac{Fe^{3+}}{Fe^{2+}}$ ratio decreases with decrease in oxygen partial pressure as in Figure (A.1.5). The data of Turkdogan and Bills confirm White's results[24].

A.1.1.5 The $FeO-Fe_2O_3-TiO_2$ Ternary System

Several studies on the system $FeO-Fe_2O_3-TiO_2$ have been reported in the literature.

MacChesney and Muan[2] investigated the $FeO-TiO_2$ binary system as described previously in Figure (A.1.1).

Markhanavala[30] studied the same system in air at 1200°C and the phases were reported to be hematite, pseudobrookite and rutile.

The details of the ternary system $FeO-Fe_2O_3-TiO_2$ are quite complex but the most noteworthy features of the diagram are the existence of three continuous solid solution series. The first, magnetic-ulvöspinel ($FeO-Fe_2O_3-2FeO.TiO_2$, i.e. $Fe_nTi_{3-n}O_4$, where $3<n>2$) were reported to form a continuous solid-solution series at sufficiently high temperatures. This solid solution series has the cubic spinel structure and the consolute temperature is probably 600°C[31]. The second consists of hematite-ilmenite ($Fe_2O_3-FeO-TiO_2$, i.e. $Fe_mTi_{2-m}O_3$, where $2<m>1$). They have limited solid solubility in each other at

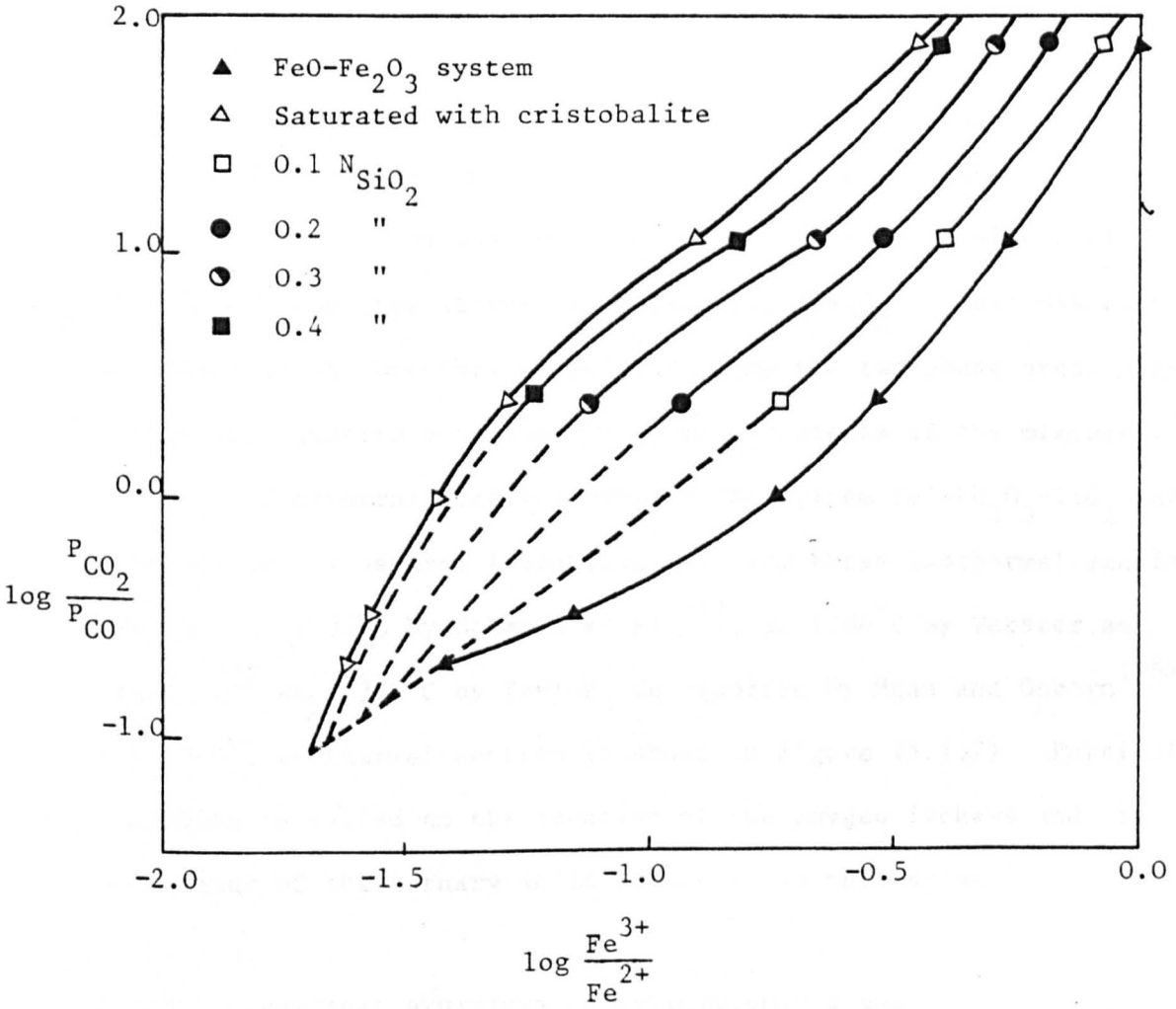

Fig. A.1.5 Variation of $\frac{Fe^{3+}}{Fe^{2+}}$ with silicate and gas composition in $FeO-Fe_2O_3-SiO_2$ system at 1550°C[29].

low temperature, but form a complete solid solution series at higher temperatures. The consolute temperature was reported to be in the region 950°C to 1050°C[32]. This solid solution series has a rhombohedral structure. The third solid solution was pseudobrookite and ferrous dititanate ($FeO.2TiO_2$-Fe_2O_3,TiO_2, i.e. $Fe_pTi_{2-p}O_5$, where $2<p>1$). They form continuous solid solution series at 1050°C[33]. Members of this series have an orthorhombic structure.

MacChesney and Muan[34] studied the FeO-TiO_2 equilibrium in the air as in Figure (A.1.6). The most remarkable feature of the phase relations shown was the very strong stabilizing effect of TiO_2 on the corundum type structure of hematite (Fe_2O_3). This was seen by the shape of the boundary curves outlining the two-phase area, magnetite and hematite with increasing TiO_2 contents of the mixtures.

Isothermal sections through the system FeO-Fe_2O_3-TiO_2 have been studied by several investigators. The three isothermal sections are that at 1000°C by Schmahl et al[35], at 1200°C by Webster and Bright[32] and 1300°C by Taylor, as reported by Muan and Osborn[36]. The 1300°C isothermal section is shown in Figure (A.1.7). Particular attention is called to the location of the oxygen isobars and the occurrence of the ternary solid solutions in this sytem.

A.1.2 PHYSICAL BEHAVIOUR OF TITANIFEROUS SLAGS

A.1.2.1 Viscosity

The viscosity of many liquids, including synthetic and industrial slags, is related to temprature according to the well known Arrhenius-Guzman equation

$$\eta = Ae^{-E_\eta/RT}$$

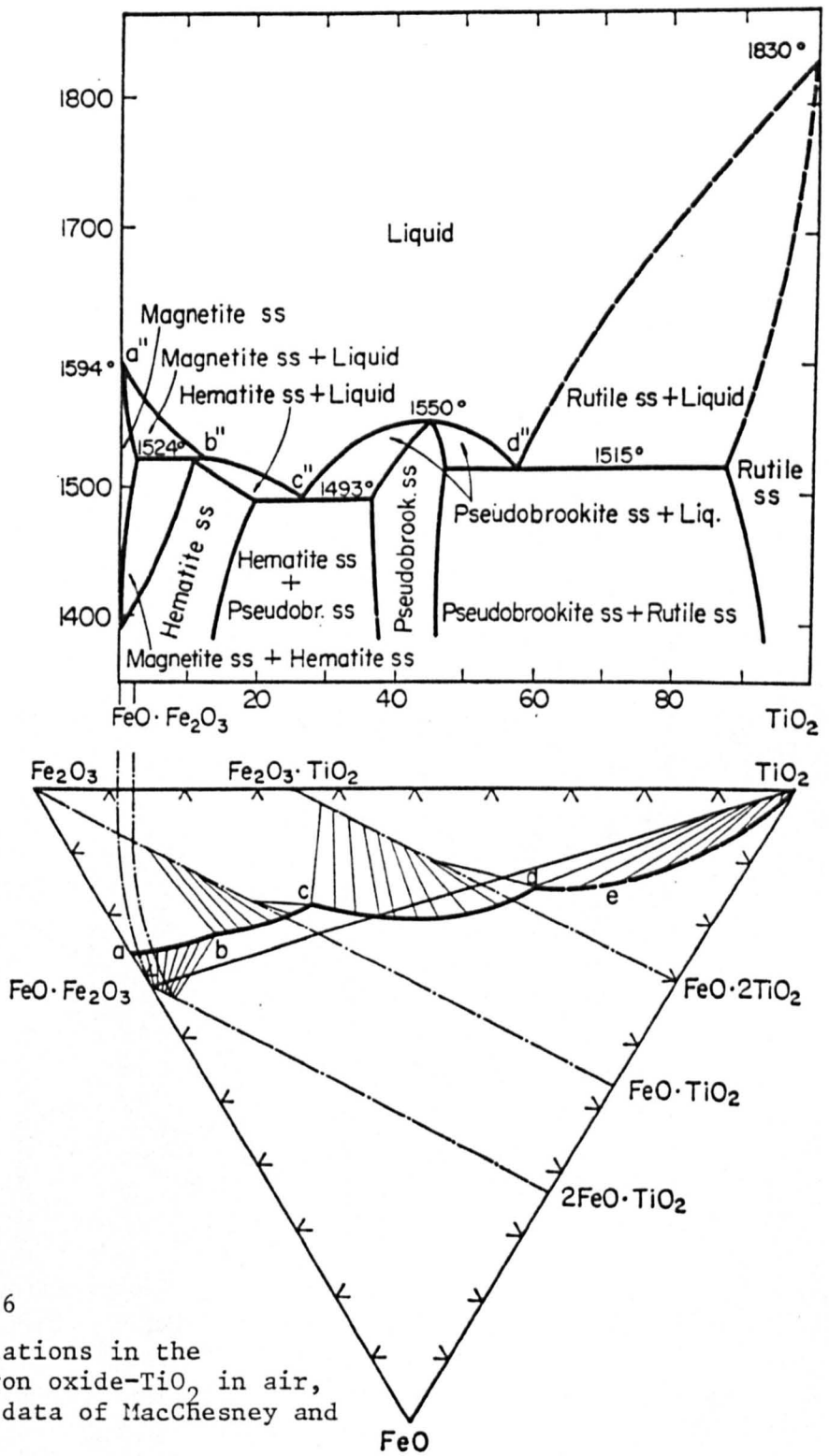

Fig. A.1.6

Phase relations in the system iron oxide-TiO_2 in air, based on data of MacChesney and Muan[34].

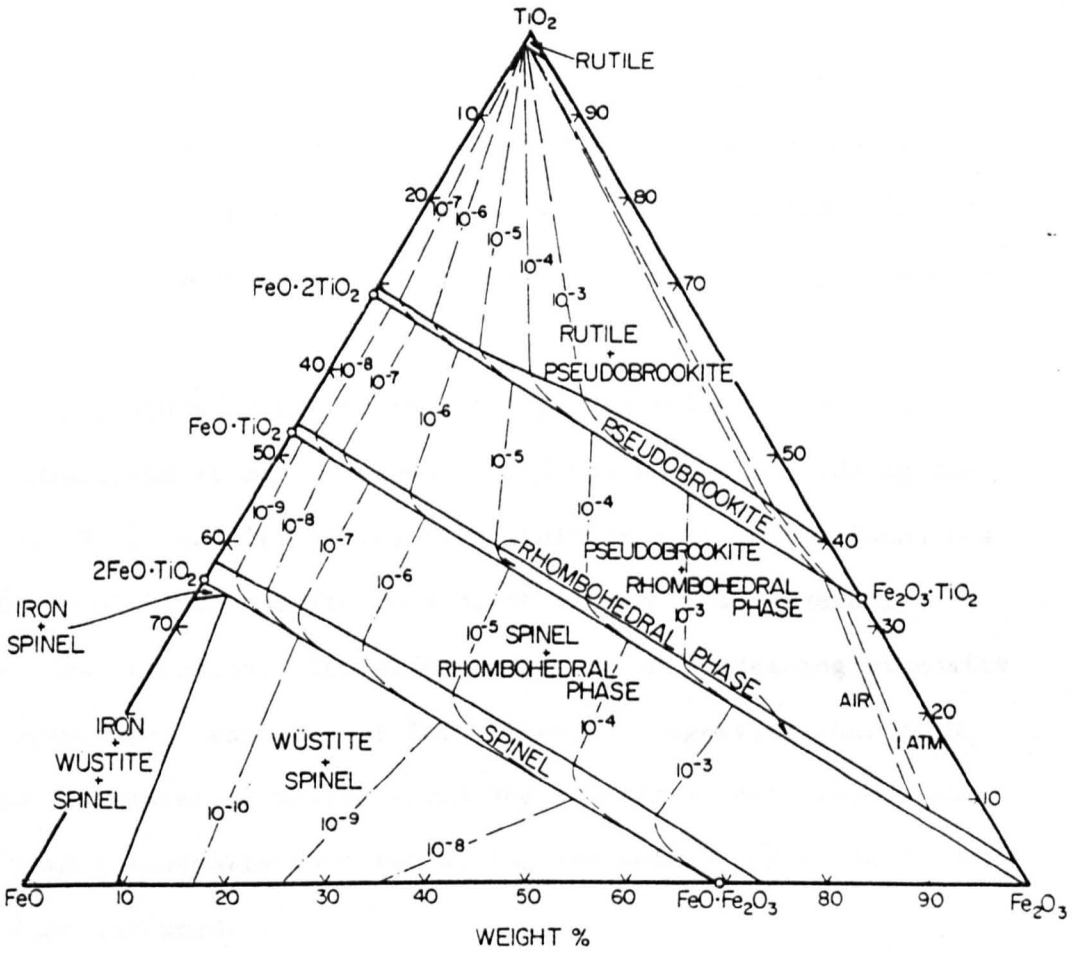

Fig. A.1.7 The 1300°C isothermal section through the system $FeO-Fe_2O_3-TiO_2$, after Muan and Osborn[36].

where η is absolute viscosity

A and R are constant

T is the absolute temperature

E_η is an activation energy for viscous flow and obtained from the slope of the straight line relating to log η and $\frac{1}{T}$. Since the viscosity of a slag depends on the difference between the actual and the liquidus temperature (i.e. superheat) and on the precipitation of solid insoluble particles as well as on the slag structure, the effect of oxygen pressures on the viscosity of slags containing TiO_2 is complex. Eventually the result is a marked increase in viscosity but the intermediate changes seem to depend on slag composition.

In a study of the effect of slag viscosity in the blast furnace, Handfield et al[37] investigated the effects of adding the sub-oxides, Ti_2O_3 and TiO to the blast furnace slag. They found that the addition of Ti_2O_3 and TiO to a blast furnace slag generally decreased its viscosity. The effect of Ti_2O_3 in decreasing viscosity is more pronounced than that of TiO. They[38] suggested that Ti_2O_3 is a network breaker in molten slags and as much is not responsible for the higher viscosity reported during the melting of titaniferous ore in blast furnaces.

The fusibility temperature of the blast furnace slag was decreased by adding up to 10% Ti_2O_3 or TiO to it. With addition of Ti sub-oxides greater than 10% the fusibility temperature of the slag increased rapidly.

The early Russian investigations in this field have been reviewed by Frohberg et al[38,39] and Handfield and Charette[18]. Frohberg et al reported the results of their studies on the viscosity

of meltshaving a high titania content in the systems $CaO-Al_2O_3-TiO_2$, $SiO_2-Al_2O_3-TiO_2$ and $SiO_2-Al_2O_3-CaO-TiO_2$. The results show that the isokoms are nearly parallel to the lines of equal alumina content over a large concentration range in $CaO-Al_2O_3-TiO_2$ slags. Moreover the viscosity reducing effect of lime under these conditions is much more marked than that of titania. Titania has a significant effect on the viscosity in $SiO_2-TiO_2-Al_2O_3$ slags, i.e. the titania increases the fluidity in this system.

Frohberg et al[38,39] also studied the system $CaO-SiO_2-TiO_2$ by adding various amounts of Al_2O_3 at 1600°C. The effect of Al_2O_3 additions is generally to raise the viscosity, the effect being more pronounced at low levels of alumina, i.e. up to 5% Al_2O_3.

Van Bemst and De Launios as reported by Handfield and Charette[18] studied the effect of TiO_2 in the $K_2O-SiO_2-TiO_2$ system. They concluded that in this system TiO_2 behaves like an amphoteric oxide, that it acts as an acidic or basic oxide, depending on the acidity of the slag. Tuset[18] as reported studied the viscosity of melts rich in TiO_2 in $TiO_2-Ti_2O_3-MgTiO_3$ system. The composition fell within the range 58-85% TiO_2, 8-33% Ti_2O_3 and 3-21% MgO. Tuset concluded that all these melts are remarkably fluid and the viscosity measurements on completely molten slags was of the order of 50 to 100 Cp, with little dependence upon slag composition, or temperature.

Unfortunately Tuset did not tabulate or report graphically his viscosity measurements but only stated that the calculated accuracy for the viscosity data was ±15 Cp in $TiO_2-Ti_2O_3-MgTiO_2$ slags.

Ohno and Ross[40] studied the viscosity of $CaO-Al_2O_3-SiO_2-TiO_2$ slags having a liquidus temperature below 1450°C. They found that

both lime and titania lowered the viscosity while alumina increased it. Pliner et al[41] studied a slag containing 60.6% Al_2O_3, 12.8% CaO, and 10.1% TiO_2, with minor percentages of MgO, FeO and SiO_2, and had a melting point of approximately 1750°C. The activation energy for viscous flow was very small. At 1760°C the viscosity was 18 Cp and 15 Cp at 1830°C.

Handfield and Charette[18] worked on some industrial high titania slags known as Sorelslags for a range of composition extending from 3 to 15% FeO and from 80-67% TiO_2. When fully molten, such melts had viscosities of only 30 Cp, lower even than the viscosities of molten CaO, MgO, MnO and FeO near their melting points, while a melt of 30% CaO, 70% TiO_2 yielded an even lower value of 20 Cp. Handfield and Charette found that industrial high TiO_2 slags were very fluid melts once completely molten and regardless of their FeO content. The viscosity of these molten slags remain fairly constant, even with a further increase in temperature, this was confirmed by Tuset. Handfield and Charette[18] found that with such a low viscosity, molten titania slag cannot be responsible for the stability of froth or foam during the smelting of ilmenite in the electric arc furnaces. The main factor seriously affecting the fluidity of industrial high titania slags was the presence of solid particles in the melt.

McRea et al[42] found that the viscosities of the titaniferous slags were low for slags containing CaO-MgO-SiO_2-Al_2O_3 with 37.19% TiO_2, and that the viscosity at constant temperature, decreased slightly with increase in the $\frac{\%MgO}{\%CaO}$ ratio in slags with a constant (%CaO + %MgO). This may be attributed to the fact that Mg^{2+} has a cation field strength considerably greater than Ca^{2+} and hence

has greater tendency to co-ordinate itself with oxygen. At constant temperature, the viscosity decreases with increasing basicity of the slag which was confirmed by Ohno and Ross[40].

Gruzdev et al[43] investigated the viscosity of slags of the $CaO-MgO-Al_2O_3-SiO_2-TiO_2$ system. At TiO_2 content less than 9% the viscosity at 1550°C decreases with increase in titanium oxide in the melts and with increase in basicity. With further additions of TiO_2 above 9% the viscosity increased rapidly. The influence of mass % addition (20%) of TiO_2 and Ti_2O_3 upon the viscosity of both acid and basic oxide slags was also investigated. Both oxides caused a reduction of viscosity, the effect of TiO_2 being considerably more pronounced. The location of the region of minimum slag viscosity does not change with decrease in temperature.

Mikhailov and Belyakova[44] studied the effect on viscosity of the addition of up to approximately 25% TiO_2 in $CaO-Al_2O_3-TiO_2-SiO_2$ slags. They found that increase in the concentration of TiO_2 in the melts lowered the viscosity of acid slags, while the viscosity of basic slags was increased.

Van der Colf[45] investigated the viscosity of slags in the $CaO-MgO-Al_2O_3-SiO_2-TiO_2$ system comparable in composition to those produced during submerged arc melting by the Highveld Steel and Vanadium Corporation. Using the inner rotating cylinder technique with molybdenum components, he measured viscosities in a number of slags in this system. The variation of TiO_2 content was insufficient to show a clear effect on viscosity, although an increase in (TiO_2 + Al_2O_3) caused an increase in the activation energy for viscous flow (E_η). All his values lie in the range 50-500 Cp at 1550°C and at 50°C above the liquidus temperature. The inverse relationship

between viscosity and basicity of the melts was the most important parameter influencing viscosity. The effect of $\frac{CaO}{MgO}$ ratio was only significant at low basicity.

A.1.2.2 Electrical Conductivity

Slag resistivity is considered to be an important parameter in submerged arc furnace smelting, but it has no practical importance in blast furnace operations.

Most investigations of electrical conductivity of slags containing titania have yielded such high values that electronic conductivity involving valency exchange is clearly predominating over ionic conductivity.

Reznichenko[46] reported that molten slags with a TiO_2 content ranging from 40 to 70% had a specific electrical conductivity of the order of 10 to 30 $ohm^{-1}cm^{-1}$, while at 90% TiO_2, these slags had a specific electrical conductivity of more than 200 $ohm^{-1}cm^{-1}$. Mori[19] found that the specific electrical conductivity was 30 $ohm^{-1}cm^{-1}$ at 40% TiO_2, while Inouye et al[47] found that the specific electrical conductivity for pure iron oxide was 300 $ohm^{-1}cm^{-1}$. Mori's finding that a minimum conductivity exists in the system is in qualitative agreement with the effect of adding FeO to TiO_2-rich slags[21] and with the effect of adding TiO_2 to FeO, as shown by Nikitin et al[48].

The $FeO-SiO_2-CaO-Al_2O_3-TiO_2$ system has been studied by Nikitin et al[48]. The predominant process in conductivity is electron exchange between Fe^{2+} and Fe^{3+} ions, since replacement of ferrous oxide by titania, which is an electronic conductor with an oxygen-defective crystal lattice in the solid state, lowers the conductivity of the system.

Mori[49] investigated the electrical conductivity of melts in the $CaO-SiO_2-TiO_2$ system. The values of specific electrical conductivity were 0.1-1.0 $ohm^{-1}cm^{-1}$ at temperature of 1200°C to 1470°C, clearly in the ionic conductivity range, the mobile ion being considered to be Ca^{2+}. Conductivity increased with TiO_2 content at constant $\frac{CaO}{SiO_2}$ ratio and with increasing $\frac{CaO}{SiO_2}$ ratio at constant TiO_2 content. Mori indicated that TiO_2 is acting as a network breaker. In agreement with this, Kato and Minowa[50] found that TiO_2 addition of up to 8% to a blast furnace slag increased its conductivity by an amount comparable to that caused by similar additions of FeO,MnO and MgO and decreased the activation energy for conduction (E_k).

In fact, Degtyarev et al[51] considered that FeO content can be used as a control parameter in the industrial situation. Indeed Denisove and Degtyarev[21] observed during the smelting of titania concentrates that the electrical conductivity of the slags strongly depend upon the reducing conditions. They reported that the specific electrical conductivity increased from 25-35 $ohm^{-1}cm^{-1}$ for high FeO slags, to 150-170 $ohm^{-1}cm^{-1}$ for low FeO slags. These are such high values for electrical conductivity that the slags cannot correspond to purely ionic melts, where the specific electrical conductivity never exceeds 5 $ohm^{-1}cm^{-1}$ and this value cannot be expected to shed much light on the ionic constitution of such slags. This hypothesis is further supported by the work of Musithin et al[52] who studied the electrical properties of quaternary oxide mixtures involving CaO, MgO, Al_2O_3 and SiO_2 and sub-oxides of Ti. Some electronic conductivity was detected with minor concentrations of titanium oxide. They also observed that the binary melts containing 80% TiO_2 and 20% CaO or Al_2O_3 were n-type semiconductors. Van der Colf[45] and Musithin

et al[52] found that the electrical conductivity was increased by slight reduction.

In the unreduced $CaO-MgO-Al_2O_3-SiO_2-TiO_2$ slags Van der Colf obtained specific electrical conductivity values in the range 0.5-2.0 $ohm^{-1} cm^{-1}$ for compositions around 30% TiO_2. Conductivity was directly related to the ratio $\frac{CaO + MgO}{SiO_2}$ and to the $(TiO_2 + Al_2O_3)$ content, but was inversely related to the $\frac{CaO}{MgO}$ ratio.

A.1.2.3 Structure related to the Viscosity and Electrical Conductivity

The majority of modern theories of viscous flow are based on the assumption of a direct relationship between the viscosity and the structure of a liquid. Many investigators have compared the viscosity with the size of the structure units in a liquid and have shown that both are directly related to each other.

Pure melts of SiO_2, B_2O_3 etc. have high viscosity values of the order of 10^5-10^7 cp[18], Viscosities of this order of magnitude are generally found in oxides having low co-ordination numbers (3 and 4) and strongly polymerized liquids , and their viscosities decrease with increase in temprature.

Within a given temperature range if the degree of polymerization is constant, then the activation energy of viscous flow is also constant. The activation energy is obtained from the gradient of a plot of logarithm of viscosity as a function of the inverse absolute temperature i.e.

$$\eta = Ae^{\frac{-E_\eta}{RT}}$$

or

$$\ln \eta = \ln A - \frac{E_\eta}{RT}$$

If structural regrouping of the melt occurs as a result of increased or decreased polymerization, the activation energy of viscous flow changes. A continuous change in the liquid structure with changing temperature will be characterized by a curved log η vs $\frac{1}{T}$ relationship, while a sudden change of the liquid structure will give a break in the straight line log η vs $\frac{1}{T}$ relationship.

On the other hand, a very low viscosity seems to be the characteristic property of oxides with high co-ordination numbers (6 or more) of the metal atoms. Molten CaO, Mno, MgO and Feo all have viscosities of the order of 50 Cp near their melting points.

The ionic or molecular theories of titania slags can only be applied to establish the themodynamic behaviour. These theories were developed to explain the physicochemical properties and structure of silicate type melts. As shown previously, the viscosity values and their variation with temprature are drastically different for TiO_2 slags as compared to the polymerized melts. Some their were developed pertaining to liquid semiconductors.

It is believed that Sorelslag like other melts rich in TiO_2, are semiconductors and have 80 times higher conductivity than the normal slags.

Wyatt's work[53] showed that the resistivity of high titania slags was much lower than that of normal silicous slags. The electrical properties of the slags similar to Sorelslags have been found by Reznichenko[46] to change very little in passing from the solid to the liquid state. This means that the structure of these semiconducting slags is hardly affected by the melting process. Hence, the structure of molten high TiO_2 slags should be similar to that of the corresponding solid slag. This probably leads to the structure of these complex solids.

Reznichenko et al as quoted by Handfield and Charette[18] proposed a general formula for the anosovite minerals representing a solid solution based on the Ti_3O_5 type of structure (orthorhombic), which takes into account the extensive mutual dissolution of the various slag constituents. This formula was as follows:

$$m[(Ti, Mg, Mn, \text{or } Fe)O \cdot 2\ TiO_2]$$

$$n[(Ti, Fe, Al, Cr, \text{or } V)_2O_3 \cdot TiO_2]$$

The variable valence of Ti in the compound

$$TiO \cdot 2\ TiO_2 \leftarrow Ti_3O_5 \rightarrow Ti_2O_3 \cdot TiO_2$$

assumes the possibility of mutual dissolution of compounds of the type $MeO.2\ TiO_2$ (where Me may be Ti, Mg, Mn or Fe) as well as those of the $Me_2O_3 \cdot TiO_2$ (where Me may be Ti, Fe, Al, Cr or V).

Reznichenko et al also proposed a general formula for tagirovite minerals representing as solid solution having the Ti_2O_3 type of structure (rhombohedral).

$$a[(Ti, Mg, Mn \text{ or } Fe)O, TiO_2]$$

$$b[(Ti, Al, Cr, V \text{ or } Fe)_2O_3]$$

where Ti has a mixed valency

$$TiO \cdot TiO_2 \leftarrow \quad \rightarrow Ti_2O_3$$

The silicate phase found in industrial high-titania slags also represents a very complex composition of solid solution consisting of feldopathic materials (anorthite, albite and orthoclase) and amporphus or glassy substance.

For the titaniferrous portion of these slags, the mutual dissolution of the elements to form a wide region of solid solutions is explained by the close ionic radii of the constituent elements and small difference, which in most cases does not exceed 4 to 5%, existing in the lattice constant of the meta-titanates ($MeO \cdot TiO_2$),

(Me_2O_3. TiO_2) and the dititanates (MeO. 2 TiO_2) making up the main portion of these slags.

Forman et al as reported by Handfield and Charette worked on the separation and identification of the titaniferrous and siliceous constituents of a series of Sorelslags. They concluded that the main constituents of QIT's slags have one of the two following basic chemical formulae, RO. 2 TiO_2 (where R may be Mg^{2+}, Fe^{2+} or Ti^{2+}) or R_2O_3. TiO_2 (where R may be Fe^{3+}, Al^{3+} or Ti^{3+}), which is in good agreement with Reznichenko et al.

Quite recently both Thakur, as quoted by Marboe and Weyl[54] and Reznichenko[46] have suggested that molten high TiO_2 slags are constructed mainly from simple anions of the type TiO_6^{8-} based on the fact that the TiO_6 octahedron in the basic structure unit in solid ansovite[55], while Esin and Lepinskikh[56] favoured TiO_4^{4-} and TiO_3^{2-}. Mori[19] considered the ions in FeO-TiO_2 melts to be the simplest possible, namely Ti^{4+}, Fe^{2+} and O^{2-}, but while the electronic conductivity implies a fair amount of valency exchange between divalent and trivalent iron and between trivalent and quadrivalent titanium, it does not necessarily imply the presence of simple Fe^{2+}, Ti^{3+}, Fe^{3+} and Ti^{4+} ions. In view of the clear preference of Ti^{4+} for octahedral co-ordination, the ions suggested by Esin and Lepinskikh do not seem very likely and thus despite its rejection by Handfield and Charette[18], TiO_6^{8-} seems to be the likeliest of the suggestions to date since it is consistent with the observed viscosities, crystallisation characteristics and the structure of solid anosvite. However, it is clearly not the building unit of a network analogous to that obtained in silicate melts.

On the other hand the only two clues seem to be the electronic structure and high polarization of the Ti^{4+} ion. Being the

ion of a transition element, Ti^{4+} is not a noble gas ion[57], as opposed to Si^{4+} and Al^{3+} which are both of noble type. This means that its charge field is not necessarily symmetrical, which could have two repercussions. At high $\frac{SiO_2}{TiO_2}$ ratios, when titanium may be forced to assume tetrahedral co-ordination within the silicate network[58,59], such assymetry will tend to produce inherently distortable sites in the network, so that its break-up will be facilitated. However, probably more important is the fact that because the force field is not spherically symmetrical and is easily distorted, the effective ionic radius could be appreciably larger and therefore its effective ion-oxygen attraction is appreciably smaller than the values normally ascribed (0.68$\AA^{O}$ and 1.85 respectively). Thus effectively the ion will be more basic in both its structural and thermodynamic behaviour. Such an effect will be strongly reinforced by any reduction to the trivalent state which occurs so readily, since for Ti^{3+} the ion-oxygen attraction is considerably smaller than for Ti^{4+}. Thus there appears to be a decrease in the mean field strength of Ti^{4+} such as cannot occur for either Si^{4+} or Al^{3+}, which effectively reverses the positions of Ti^{4+} and Al^{3+} in terms of ion-oxygen attraction and renders Ti^{4+} more basic than Al^{3+}, so that it becomes a network-breaker rather than a network-former, which is in good agreement with Schenck and Frohberg[39].

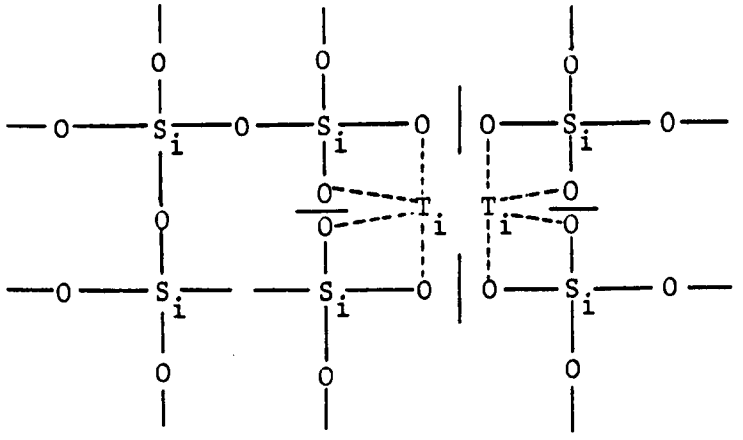

A.1.3 REDUCTION BEHAVIOUR IN TITANIFEROUS SLAGS

The problems associated with the smelting of titaniferrous ores appear only after a period of time. This suggests that reduction kinetics play an important part and that one solution is to slow down the reduction of titania sufficiently that the slag can be discharged from the furnace before it can cause any harm.

Mikhailov and Belyakova[44] found that the rate of reduction as TiO_2 ultimately to TiC was faster in basic than in acid slags, an observation subsequently confirmed by Ohno and Ross[60]. Chukukere and Ross[61] also determined overall reduction rates of $CaO-SiO_2-TiO_2-Al_2O_3-FeO$ slags by carbon-saturated iron at 1500°C. The reduction proceeds faster and further with increasing the basicity $(\frac{CaO}{SiO_2})$ for any given titania content in slags. In this work the acid slags retained more iron oxide in solution than did the basic slags. The results showed that as the titania in slags increases, the amount of iron oxide retained in the slag decreases for any given $\frac{CaO}{SiO_2}$ ratio. These observations indicate that the effect of titania on the activity of iron oxide in the slag, particularly in acid slags, is qualitatively similar to that of lime. Van der Colf[45] found in his reduction experiments that for the more basic slags there was a clear break in the order of reaction which occurred at an $\frac{O}{Ti}$ ratio of around 1.8, the order being one during the first stage and 3/4 in the second, whereas for more acid slags this was not obtained. He deduced that the reduction was probably chemical reaction controlled over the first part, and diffusion controlled in the thickening slags during the second part. McRea et al[42] found that the titania can exist as non-stoichiometric phase with $\frac{O}{Ti}$ less than 2:1 in $MgO-TiO_2-Al_2O_3-CaO$ slags. Somerville et al[62] have indicated that a small

concentration of TiO_2 in a slag of a composition typical of the blast furnace may be reduced almost as far as Ti_3O_5 reasonably rapidly and independently of SiO_2. This is also consistent with the thermodynamics of the situation since simple calculations indicate that reduction of TiO_2 by carbon to Ti_3O_5 or Ti_2O_3 is possible at oxygen potentials comparable to those for reducing small concentrations of FeO, but above those necessary for reducing SiO_2 to silicon dissolved in liquid iron. The amount of reduction free of interference by SiO_2 will decrease in more acid slags in which the activity of SiO_2 is higher, and eventually this first stage will disappear altogether, as observed by Van der Colf in acid slags.

A.1.4 IDENTIFICATION OF PHASES AND DETERMINATION OF LIQUIDUS TEMPERATURE

Phase changes in a material will be accompanied by change in a number of its properties. Accurate measurements of any one of these properties at known temperatures and compositions will build up a complete picture of the material's phase diagram.

De Vries et al[63] have studied the SiO_2-CaO-TiO_2 system. The phases were determined by examination of the quenched sample under a photographic microscope using transmitted light. The identity of the phases was further confirmed by x-ray techniques using copper radiation filtered through nickel.

Rouf[64] and Van der Colf[45] have used the hot stage microscope and micro-differential thermal analyser for determination of liquid temperatures for slags containing CaO, MgO, TiO_2, Al_2O_3 and SiO_2. Rouf also used the hot stage microscope for the determination of the solidus temperatures. However, Roxburgh[65] and Mansor[66] used hot stage microscope for determination of liquidus

temperatures and micro D.T.A. for solidus temperatures. This technique has been used[64-66] and was applied for the identification of primary phases by using the x-ray powder differaction technique with a copper target and a nickel filter to give CuK_{α} radiation for diffraction patterns.

The technique used in the present study was not the same as that used by the previous authors. Due to the presence of iron oxide in slags and its optical properties, it was impossible in the hot stage microscope to identify crystals from liquid in the slags or to measure their liquidus temperature. The x-ray technique used by Mansor[66], was used in this work, but a chromium target and vanadium filter have been used instead of a copper target and nickel filter. The copper target was not suitable and gave poor lines for slags containing iron oxide. The technique used for phase identification and liquidus surface determination will be described later.

SECTION A

CHAPTER 2

EXPERIMENTAL TECHNIQUE

A.2 EXPERIMENTAL TECHNIQUE

There were two different experimental techniques used to study the $FeO-TiO_2-SiO_2$ system. The first technique used to study this system was at iron saturation and the system contained as components only the relative stable oxides made up from cations appearing in only one predominant state of oxidation. In such systems the gas phase can usually be ignored and the total composition of condensed phases remain constant.

The second technique involved varying oxygen pressures at constant temperatures. The compositions of the condensed phases might vary with variation in compositions of the gas phase, and hence the latter must be considered in the representation of phase relations in such system.

A.2.1 STARTING MATERIAL

A.2.1.1 Titania

The purest form of commercial titania (TiO_2) was used, i.e. a Griffen certified reagent, having a purity not less than 99%.

A.2.1.2 Silica

SiO_2 was prepared by washing silica sand and repeatedly washing with concentrated hydrochloric acid, until no trace of iron remained. It was then washed with hydrogen peroxide and deionized water after which it was dried and heated at 1000°C for 5 hours.

A.2.1.3 Ferrous Oxide

FeO was prepared by the controlled decomposition of ferrous oxalate at 1000°C. The decomposition was carried out in a sealed iron reaction tube with a valve to release the carbon monoxide and carbon dioxide given off, according to the reaction,

$$(COO)_2Fe + H_2O \rightarrow (CO + CO_2)\uparrow + FeO + H_2O$$

After the decomposition reached completion, the reaction tube was completely sealed, withdrawn from the furnace and rapidly quenched in water. The ferrous oxide produced was ground to -150 mesh, demagnetized and analysed for its iron content.

For each sample the correct quantity of reagent was weighed out, mixed and put into a crucible.

A.2.2 GAS MIXING APPARATUS

The method used for controlling oxygen pressures was similar to that used by Johnston and Walker[67] and later improved by Darken and Gurry[25].

The oxygen pressure was controlled at 0.021 atmosphere using a mixture of air and nitrogen, but runs were made at lower oxygen pressures, obtained by mixing carbon monoxide, carbon dioxide and nitrogen in various proportions at 1500°C.

Four flowmeters were used to establish the equilibrating gas mixtures, which function on the basis of a constant pressure drop through each of the capillaries (to proportion the gas composition), and this pressure drop was measured by manometers. The calibrated gases were intimately mixed in a vertical column packed with glass beads. After monitoring the flowrate, all gases were passed through purification columns, consisting of layers of magnesium perchlorate and silica gel to remove any moisture present in the gas. Vacuum oil was used as a liquid in the flowmeters (either the manometers or the constant pressure columns) because it has a low vapour pressure and does not react with the gas used. The flowmeters were calibrated by using a soap-bubble meter.

A Schematic diagram of the flowmeters arrangement is shown in Figure (A.2.1).

A.2.3 FURNACES AND TEMPERATURE CONTROL

As mentioned previously there were two methods used in this section. The furnace which was used for the equilibration of melts of $FeO-TiO_2-SiO_2$ systems at a constant total pressure of 1 atmosphere was a vertical furnace because of the size of iron crucibles (to minimise the creeping of liquid slags) which could not be accommodated in the horizontal furnace.

The furnace had a resistance winding of platinum, supported on alumina tube. The furnace tube was wound over a 30.5cm length with platinum wire. A "purox" grade recrystallized alumina reaction tube of 1.9cm internal diameter and 61cm long, was held centrally inside the furnace tube, as shown in Figure (A.2.2).

The temperature of the melts was measured during the experiments by a 20/Rh/Pt-5/Rh/Pt thermocouple contained within an alumina-thermocouple sheath. The controlling thermocouple was positioned between these tubes so that it was just touching the coating over the winding at the hot zone. This thermocouple was connected to a Eurotherm temperature controller. The hot zone of the reaction tube was calibrated with another Pt-13/Rh/Pt thermocouple connected to a potentiometer. The temperature variation was about $\pm 2^{\circ}C$ during the melting time given a 4cm length of hot zone.

The second furnace used was a horizontal furnace with a mullite reaction tube (95cm long and 3.9cm internal diameter), as in Figure (A.2.3). This furnace was heated by six silicon carbide elements and the temperature was monitored by a Pt-13/Rh/Pt thermocouple,

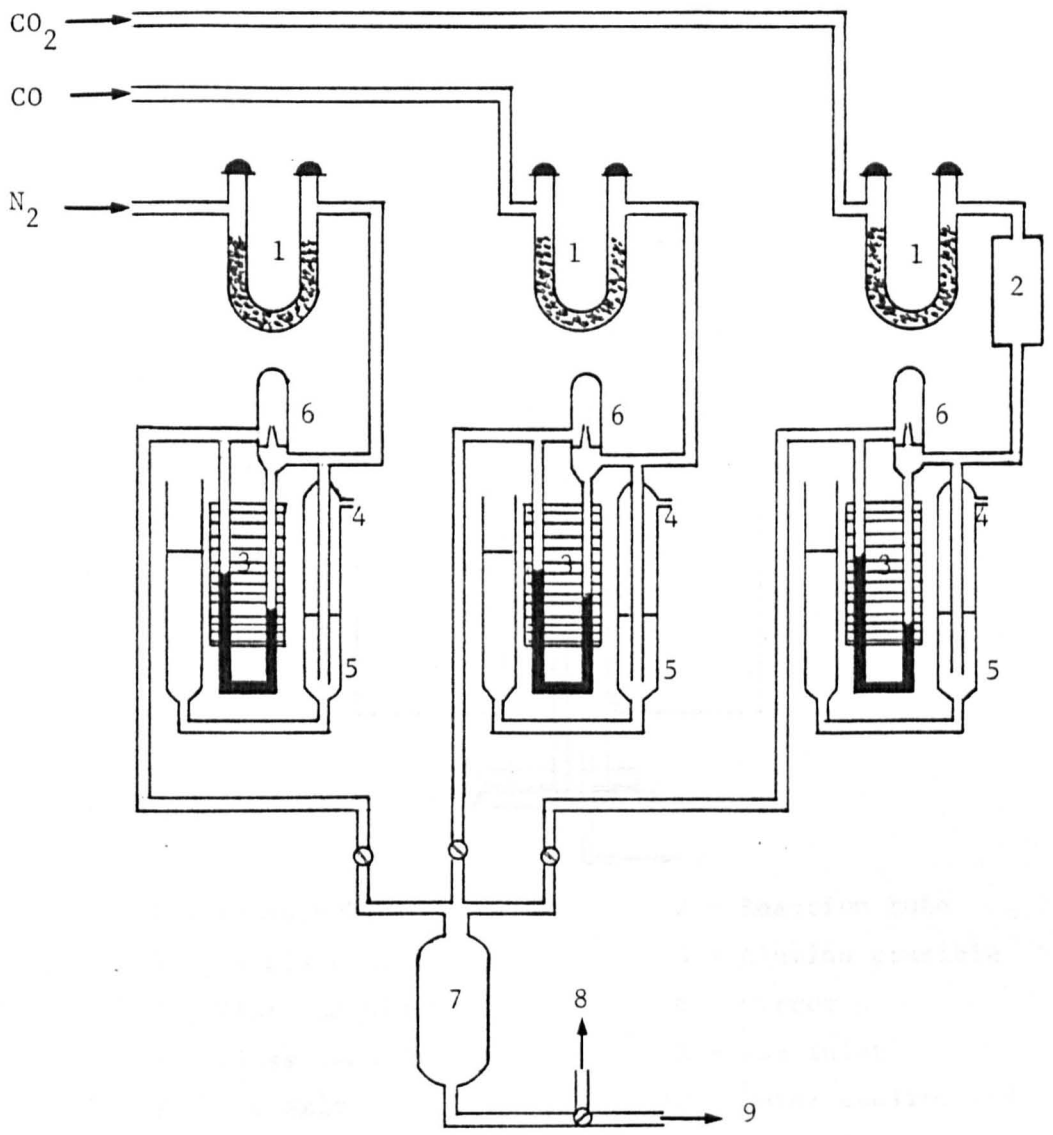

1 - Magnesium perchlorate
2 - SiliCagel
3 - Manometer
4 - Excess gas outlet
5 - Constant pressure column
6 - Capillary
7 - Gas-mixer
8 - Exhaust
9 - To the furnace

Fig. A.2.1 Gas Mixing Apparatus.

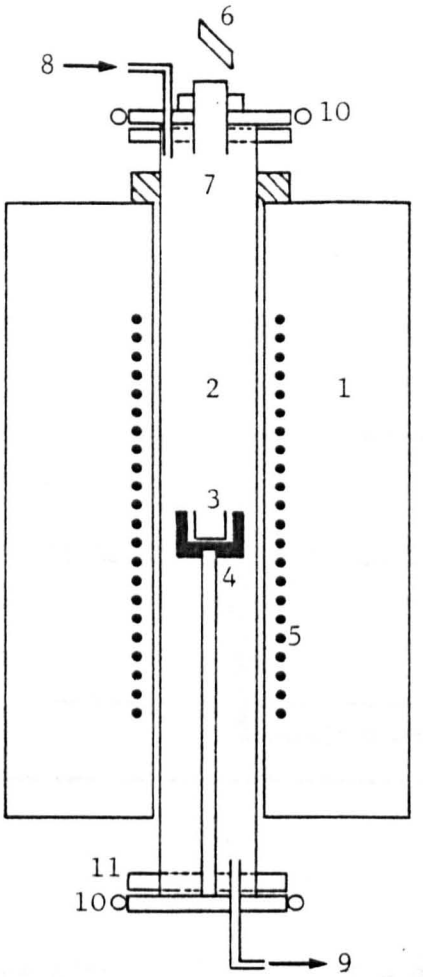

1 - Furnace body
2 - Reaction tube
3 - Sample crucible
4 - Alumina crucible
5 - Platinum winding
6 - Mirror
7 - Glass lens
8 - gas inlet
9 - Gas exit
10 - Water cooling coil
11 - Brass furnace ends

Fig. A.2.2 Vertical furnace assembly.

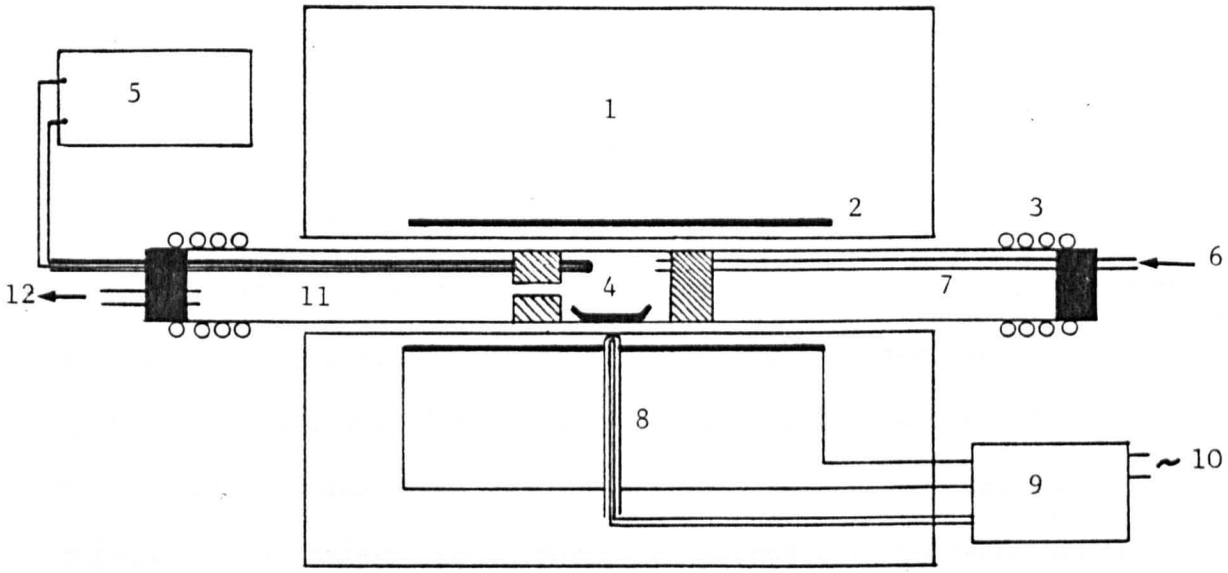

1 - Furnace body
2 - Heating elements
3 - Cooling coils
4 - Sample tray
5 - Potentiometer
6 - Gas inlet
7 - Reaction tube
8 - Controller thermocouple
9 - Temperature controller
10 - Power input
11 - Mullite sheath and thermocouple.

Fig. A.2.3 Schematic diagram of horizontal furnace.

connected to a West-Carbolite temperature controller. The temperature at the reaction zone was determined by employing another Pt-13/Rh/Pt thermocouple connected to a potentiometer. The same thermocouple was used to determine the temperature profiles of the furnace and it was found that there was a hot zone approximately 5cm ($\pm 3^{o}C$) at the centre of the furnace.

A.2.4 EXPERIMENTAL PROCEDURE

A "purox" recrystallized alumina rod carrying an Armco iron crucible 15mm length, 15mm diameter and 1.5mm thickness and containing 4.0g of different slag mixture, was placed in the hot zone of the vertical furnace. The furnace was then switched on and the temperature was raised over a period of around five to seven hours to the working temperature. During this time argon was passed continuously through the reaction tube.

Once the correct temperature had been reached, one hour was allowed to ensure complete melting and homogenity of the slag mixture, then the furnace was switched off and cooled to room temperature while the argon continued to pass through the reaction tube. Most of the slags after reaching equilibrium were withdrawn from the furnace and quenched.

After each run the crucible was compressed to break away the slag, which was crushed to -150 mesh. The crushing of the slag took usually only a few minutes to avoid any possibility of oxidation of the ferrous oxide by the atmosphere.

In the other technique the horizontal furnace was used. For each run two 1g samples of slag were taken and placed in two platinum crucibles of 9.50mm diameter and 9.5-12.5mm high, which

were pressed from 0.025mm thick platinum foil. The two crucibles were placed on an alumina tray and pushed slowly into the furnace hot zone. A small flow of nitrogen was passed into the reaction tube to flush out the furnace tube. An hour after the temperature controller had begun to operate, the nitrogen was switched off and the gas mixture of CO_2-CO and N_2 passed over the samples to give a flow rate of 400ml/minute. At the end of four hours, the samples reached equilibrium and the alumina tray was withdrawn from the furnace and quenched. After the slags had cooled, they were removed from their platinum crucibles and crushed to -150 mesh.

A.2.5 CHEMICAL ANALYSIS OF SLAG

After every run the samples were analysed to check the accuracy of the slag composition.

A.2.5.1 Titania Analysis

Four standard solutions of known titanium concentration were made to construct the calibration curve for the A.A. stock. These standards were prepared by heating 0.30g of sodium tetraborate ($Na_2B_4O_7 \cdot 10H_2O$) in a platinum cup over a meker burner until the water was removed. The platinum cup was then cooled and 0.10g of titania and 0.70g of sodium carbonate were added, then it was heated again until complete fusion had taken place. The fused mixture was then dissolved in 20ml (1 :1) hydrochloric acid. The solution was transferred to a 100ml graduated flask and diluted up to volume with deionized water.

This was a "stock standard" solution and contained only titania. The "stock samples" solution were prepared the same way as the standard solution, by fusing 0.10g of slag with 0.30g of sodium

tetraborate and 0.70g sodium carbonate. The melt was then dissolved in 20 (1:1) hydrochloric acid and diluted to 100ml.

To prepare the actual solution for titania analysis 50ml of the stock solutions was measured and then transferred into another 100ml graduated flask. This operation allowed the concentration of all the titania solutions to be brought into the linear range of atomic absorption titania analysis (333 ppm) for the titania content, used in the slags.

Iron in the samples increased the titania sensitivity, therefore, the manual of the atomic absorption spectrophotometer recommends that all solutions contain 2000μg/ml KCl to remove this interference.

The standard solutions were then aspirated into a nitrous oxide-acetylene flame on a Perkin-Elmer atomic absorption spectrophotometer, Model No. 103. Values of the percentage absorption were obtained for the various standards allowing a calibration curve to be drawn. The melts to be determined were then aspirated into the flame and the percentage absorption measured. The concentration of titania in the melt was determined by consulting the calibration curve.

A.2.5.2 Silica Analysis

The solution of the sample for silica analysis was achieved in the same way as for titania samples by fusing the slag with sodium tetraborate and sodium carbonate. Therefore, the "stock sample" solution prepared for titania can be used for silica determination, but without any additions to overcome interference.

Silica standard solutions were prepared from a solution containing 1000 ppm of silica. The standard solution was prepared by fusing 0.10g of silica with 0.30g of sodium tetraborate and 0.70g

of sodium carbonate dissolving in hydrochloric acid and diluting to 100ml in a graduated flask. 5, 15, 30 and 50ml aliquots were transferred by pipette into 100ml graduated flasks and diluted to mark with standard iron and titania solutions. This operation gives standards of 5, 15, 30 amd 50 wt% silica.

Samples and standards were then aspirated into the atomic absorption spectrophotometer flame as described above and calibration curves drawn allowing determination of the silica concentration within the slag samples.

A.2.5.3 Total Iron Analysis

The total iron was determined by dissolving 0.1g samples in boiling 25 (1:1) hydrochloric acid in a graduated flask. When steam was evolved, some dropwise addition of hydrofluoric acid was made to dissolve the silica[68] and the solution was allowed to boil slowly for approximately 5 minutes, until all HF was given off. Stannous chloride solution was then added dropwise to reduce the ferric iron and 2-3 drops excess after the yellow iron colour was discharged. The solution was then cooled rapidly to room temperature, and the excess of stannous chloride was removed by an addition of 10ml mercuric chloride solution. A fine silky preciate was obtained at this stage. The flask was then shaken thoroughly and allowed to stand for 2-3 minutes before adding 15ml of orthophospharic-sulphuric acid mixture and 8-10 drops of diphenylamine sodium sulphonate as internal indicator. The solution was then titrated with $N/_{10}$ potassium dicromate until one drop of the dicromate solution produced a colour change from green to purple. This determination gives an estimation of the total iron content of the sample.

A.2.5.4 Ferrous Iron Analysis

The FeO content of slag was determined in the same way as for total iron analysis, but a stream of argon was used continuously during dissolution of the sample to avoid the oxidation of ferrous oxide. Obviously to titrate the ferrous iron, stannous chloride reduction was not performed.

A.2.5.5 Ferric Iron Analysis

Fe_2O_3 was determined by difference from the ferrous oxide and the total iron content of the melt.

A.2.6 X-RAY TECHNIQUE

The primary phases after equilibrium were determined from the x-ray powder patterns, using a Debye Scherrer camera and a Guiner camera.

For Debye Scherrer, the powder sample was mixed with gum tragacanth, rolled on glass strips into a needle approximately 0.40mm thick and 8mm long and allowed to dry for 2 hours. A dried cylindrical sample was mounted on the specimen holder and focussed by rotation. While exposing the film with x-rays, the specimen was rotated using a PM1033 synchronous motor.

The powder sample which was used for the Guiner camera was put on a thin strip of transparent cellotape and mounted on the camera.

A chromium target with a vanadium filter was used in the present study.

Before any research was begun a series of x-ray powder photographs were taken of the compounds likely to be expected in the work - TiO_2, FeO, SiO_2, F_2T, FT, FT_2 and F_2S and these were checked

with the ASTMS x-ray indexes. They were then used as standards for phase identification.

To establish the primary phase fields within the system, the samples has to be quenched before they could be x-rayed. Exposure time varied from an hour to 8 hours for samples mounted on the Guinier camera and between 45 minutes to 5 hours using the Debije Scherrer camera.

The measures (θ) angle was used to calculate "d" spacing from Bragg's law, i.e.

$$\lambda = 2 d \sin \theta$$

A.2.7 LIQUIDUS TEMPERATURE DETERMINATION

As mentioned previously in Chapter 1, a hot stage microscope used for measurements of liquidus temperature[64-66] was not good for $FeO-TiO_2-SiO_2$ systems due to the presence of iron oxide.

Some modifications were made to the Burgess[69] apparatus for determination of the melting points of the iron group by knowing the emissivity of some substance such as molybdenum and platinum.

The schematic diagram for the apparatus arrangement is shown in Figure (A.2.4).

Approximately 0.001g of slag was placed on a molybdenum strip in a brass cylinder container, which connected with the water cooling pipe. The molybdenum strip was heated by a finely adjustable current supplied from 240 volt mains through a variac and step-down transformer.

Molybdenum easily oxidises to give a volatile oxide which tends to cloud over the cylinder window with a fine deposit. Therefore it was necessary to carry out the melting in an inert atmosphere,

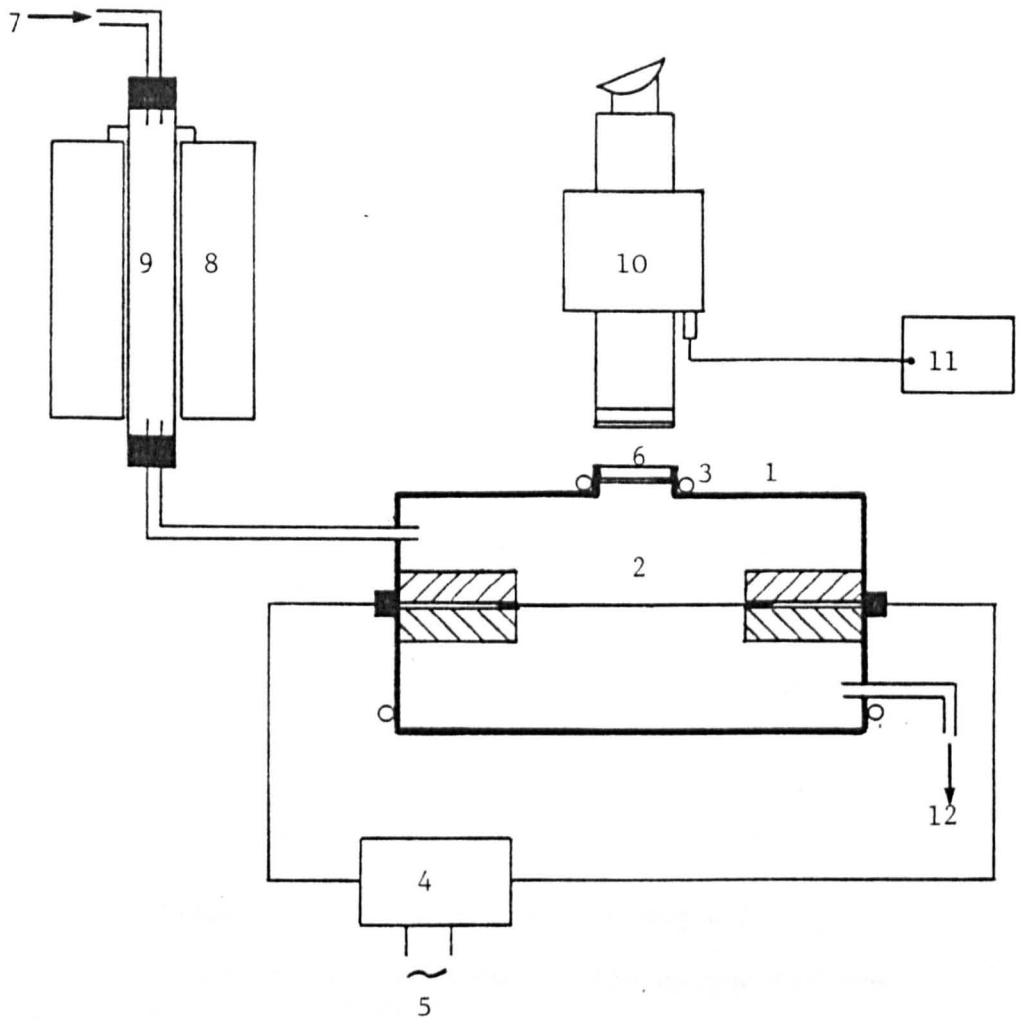

1 - Brass cylinder
2 - Molybdenum strip
3 - Cooling water
4 - Variac and transformer
5 - Power
6 - Cylinder window
7 - Argon inlet
8 - Furnace
9 - Granulated calcium
10 - Optical pyrometer
11 - Potentiometer
12 - Argon outlet

Fig. A.2.4 Liquidus temperatures measurement apparatus

so argon was used. Before passing argon into the brass container it was allowed to pass through a small furnace containing pure granulated calcium at 600°C. The calcium reacts with any oxygen traces in the argon forming calcium oxide which ensured that there was no oxygen to affect the molybdenum strip. To measure the sample melting point, the molybdenum strip was slowly heated until the melting point was approached, at the same time the disappearing filament pyrometer was adjusted to measure the temperature of the strip. The melting point was then measured directly from the potentiometer.

Calibration of the optical pyrometer was made in accordance with Wien's law[70] concerning the spectral distribution of energy in the emission spectrum

$$J_A = C_1 E_\lambda \lambda^{-5} e^{-C_2/\lambda T}$$

where J_A = intensity of radiation of wavelength λ.

λ = wavelength of radiation = 0.653 micron for the optical pyrometer

e = base of natural logarithms

T = absolute temperature

C_1 and C_2 = constant of known value, hence C_2 = 1.438cm.deg.

E = emissivity of body at wavelength λ, i.e. 0.353 for molybdenum and 0.295 for platinum.

if Ta is the temperature of standard source, and its brightness at this temperature is the same as that of the unknown, then

$$C_1 E_\lambda \lambda^{-5} e^{-C_2/\lambda T} = C_1 \lambda^{-5} e^{-C_2/\lambda Ta},$$

with

$$\ln E_\lambda = \frac{C_2}{\lambda}\left(\frac{1}{T} - \frac{1}{Ta}\right)$$

Initially a check of the calibration was carried out by measuring the liquidus temperature of standard materials (Gehlenite, $2CaO.Al_2O_3.SiO_3$, has melting point at 1593°C and Alite, $Al_2O_3.6\ SiO_2.Na_2O$, a melting point at 1118°C).

The accuracy of the measurements within the high and low (up to 1300°C) temperature was estimated to be ±10°C and ±13°C respectively. The measurements of liquidus temperatures for the $FeO-Fe_2O_3-TiO_2-SiO_2$ system were carried out under the same experimental flow rate of gas mixtures of CO_2, CO and nitrogen, or air and nitrogen, used in their preparation to minimise any change of slag composition. Platinum strip was used instead of molybdenum strip, and the same calibration was made, according to the emissivity of the platinum.

A.2.8 EXPERIMENTAL DIFFICULTIES

A.2.8.1 Thermal Diffusion

In a mixture of gases of unlike molecular weight, any temperature gradient tends to produce a corresponding composition gradient, the less dense gas diffusing towards the hotter region, while the heavier gas molecules tend to concentrate in the cooler zone. This is a well known effect which has given rise to troublesome errors in many studies of gas/metal reactions. When the metal is heated by induction, a sharp temprature gradient may be set up near its surface.

Gillespie[71] simplified the treatment of the phenomenon which showed that the thermal separation is diminished by mixing with a gas of high molecular weight. According to this theory the thermal diffusion was inversely proportional to the square root of the mean molecular weight of the gas mixture and could, therefore, be decreased by the addition of a third gas of high molecular weight.

Emmet and Schultz[72] reported that thermal diffusion was responsible for an error of as much as 40% in the water vapour-

hydrogen ratios used during a study of the equilibrium H_2O-H_2-FeO-Fe by a static method. Darken and Gurry[25] studying the iron-oxygen system found that the upward flow of the gas mixture in this type of system was preferable to downward flow if the degree of thermal separation within the gas mixture was to be a minimum.

Fontana and Chipman[73] and Dastur and Chipman[74] concluded that the error could be minimised by preheating the gases entering the system, so as to eliminate, as far as possible, the thermal gradient near the surface of the melt.

Floridis and Chipman[75] found that diluting the gas mixture with argon in a ratio of six parts argon to one part hydrogen was sufficient to eliminate errors due to thermal diffusion and that preheat was not necessary. On the other hand, McLean and Bell[76] studied the reaction

$$Al_2O_3 + 3H_2 = 3H_2O + 2Al$$

with and without preheat. They found that the substantial errors were possible when the gas was not preheated.

The technique whereby the gas mixture was bubbled through the melt has been used by many investigators[75-80]. This technique is one of the most reliable methods of minimising errors due to thermal diffusion, but it has the disadvantage of being rather difficult to perform successfully.

The general conclusions to be drawn from the work mentioned above to eliminate the thermal diffusion may be summarised as follows.

1. Preheating the incoming gases to a temperature close to that of the melt, to reduce as much as possible the sharp temperature gradient.

2. Dilution of the gas mixture by the addition of an inert gas of high molecular weight.

3. By bubbling the gas mixture through the melt.

In the present study a silicon-carbide element furnace was used in which the gas mixture received a considerable degree of preheat and in conjunction with the addition of an inert gas such as argon and nitrogen. It was considered that this was sufficient to avoid errors due to thermal diffusion.

A.2.8.2 Creep in the Slags

This creeping phenomena obviously caused experimental difficulties in that frequently there was not sufficient slag left in the crucible after an equilibration run to carry out an effective chemical analysis. Normally in such an instance where part of the slag sample had crept, the sample remaining in the crucible was found to be a somewhat different composition from what would have been expected if the slag had been successfully equilibrated. Fincham and Richardson[81] attempted to study some compositions on the FeO-SiO_2 binary system varying from 62% FeO and 38% SiO_2 to 72. FeO and 28% SiO_2 (by weight). These slags were held in iron crucibles (roughly hemispherical in shape, and had a radius of about 6mm). In all the experiments, however, the melt crept out of the iron crucibles, and no way of overcoming this difficulty, without a radical alteration in technique, could be found. However, Fincham and Richardson suggested that platinum spirals be put in the centre of the platinum crucible (similar to the iron crucibles) which would minimise creeping in silicate slags. The spirals allowed the slags to creep and fall back in the crucible.

MacChesney and Muan[2] studied the binary system FeO-TiO_2

at low oxygen pressure, and found creeping in these slags. They attempted to study the slags in a nitrogen atmosphere but loss of liquid slag by creeping on the crucible walls caused the same difficulties. They[2] minimised the creeping by sealing an iron wustite buffer together with the sample of slag into a vitreous silica tube, in order to maintain a fixed oxygen partial pressure at any chosen temperature.

In the present study for systems $FeO-SiO_2-TiO_2$, $FeO-CaO-TiO_2$ and $FeO-TiO_2-SiO_2-CaO$, the slag creeping caused experimental difficulties. As shown in Figure (A.2.5) the critical composition zone for creep extends from $FeO-TiO_2$ towards $FeO-SiO_2$ binary system. However, creeping usually increased gradually with decreasing oxygen pressures, which is in good agreement with previous investigators.

The problem to be faced therefore was one of trying to eliminate, or at least minimise, this creeping phenomena without having to radically alter the entire experimental procedure adopted for the investigation. There were different types of crucibles used, e.g, platinum crucibles with spirals in the centre, crucibles with turned-over top edges, and crucibles with lids having holes of different diameters.

Having tried these various designs of crucibles, it was concluded that they were not a great improvement in reducing creeping, whereas those having the spiral shape in the centre, gave only a small improvement. This being the case, it would be simpler to increase the height of the crucible, keeping the initial amount of the sample in the crucible the same, but in this case the horizontal furnace could not be used.

The last attempt in the present study to eliminate

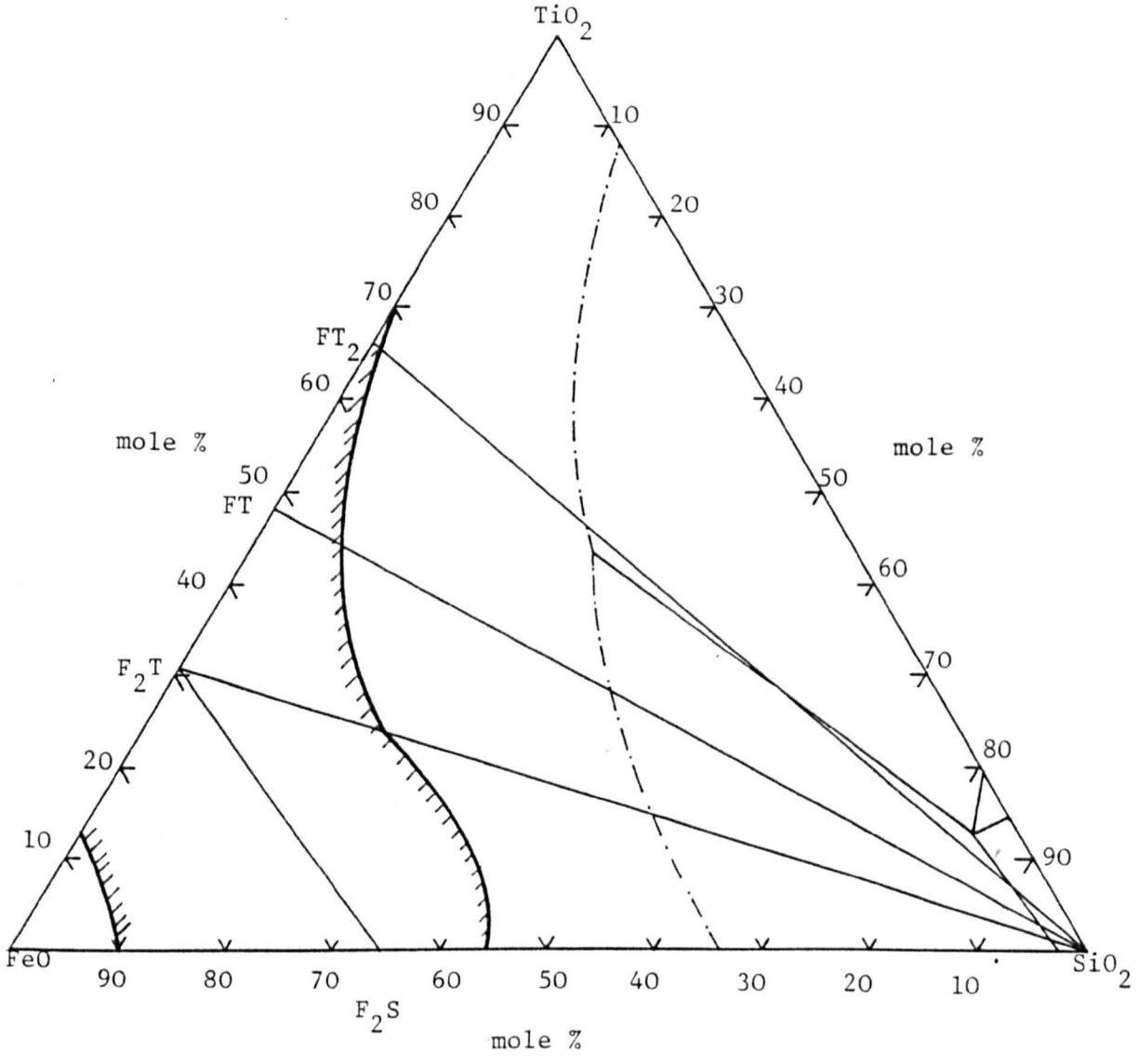

Fig. A.2.5 Creeping area in $FeO-TiO_2-SiO_2$ slag at $1500^{o}C$.

creeping was by using platinum crucibles (with 9.5mm diameter and 9.5-12.5mm high) placed in another larger crucible, hence the slag could creep from the first crucible and fall into the second crucible, or by making another wall inside the crucible of the platinum scrap, the slag would creep onto these walls and fall back into the crucible.

The main disadvantage of introducing this procedure was due to the expense of platinum. The remarkable feature of the specimens equilibrated in these crucibles was that there was little or no loss as slag was observed.

SECTION A

CHAPTER 3

RESULTS AND DISCUSSION

A.3 RESULTS AND DISCUSSION

The study of the $FeO-TiO_2-SiO_2$ system in the present work contains as components only the relatively stable oxides, i.e. the composition of condensed phases as a function of temperature, at a constant total pressure of 1 atmosphere.

This ternary system is noteworthy because of the large area of liquid immiscibility. This two-liquid region extends over the greater portion of the composition triangle of the system.

The present results showed that the $FeO-TiO_2-SiO_2$ system was divided into five composition triangles, i.e. $Fe_2SiO_4-Fe_2TiO_4-FeO$, $Fe_2TiO_4-Fe_2SiO_4-SiO_2$, $Fe_2TiO_4-FeTiO_3-SiO_2$, $FeTiO_3-FeTi_2O_5-SiO_2$ and $FeTiO_5-TiO_2-SiO_2$. All these five composition triangles are ternary systems. The three compounds at the apices of a triangle coexist in equilibrium with liquid at the temperature of the appropriate invariant point, and the composition of the liquid is that of this point. The triangles thus show the three crystalline phases of which a mixture within the triangle will be composed at subsolidus temperatures and under equilibrium conditions.

A.3.1 THE $Fe_2SiO_4-Fe_2TiO_4-FeO$ SYSTEM

Before studying any of the compositions inside the ternary, the first step in this investigation was to study the limiting binary systems of the ternary system. For the F_2S-F_2T-FeO system (Table A.1 and Figure A.3.1) the binary section $FeO-F_2S$ had been studied previously by Bowen and Schairer[11]. They gave two primary phases involving liquid + wüstite and liquid + fayalite, and a single eutectic temperature of 1175°C at a composition FeO of 16.4 mole% and F_2S of 83.6 mole% as shown in Figure (A.3.2).

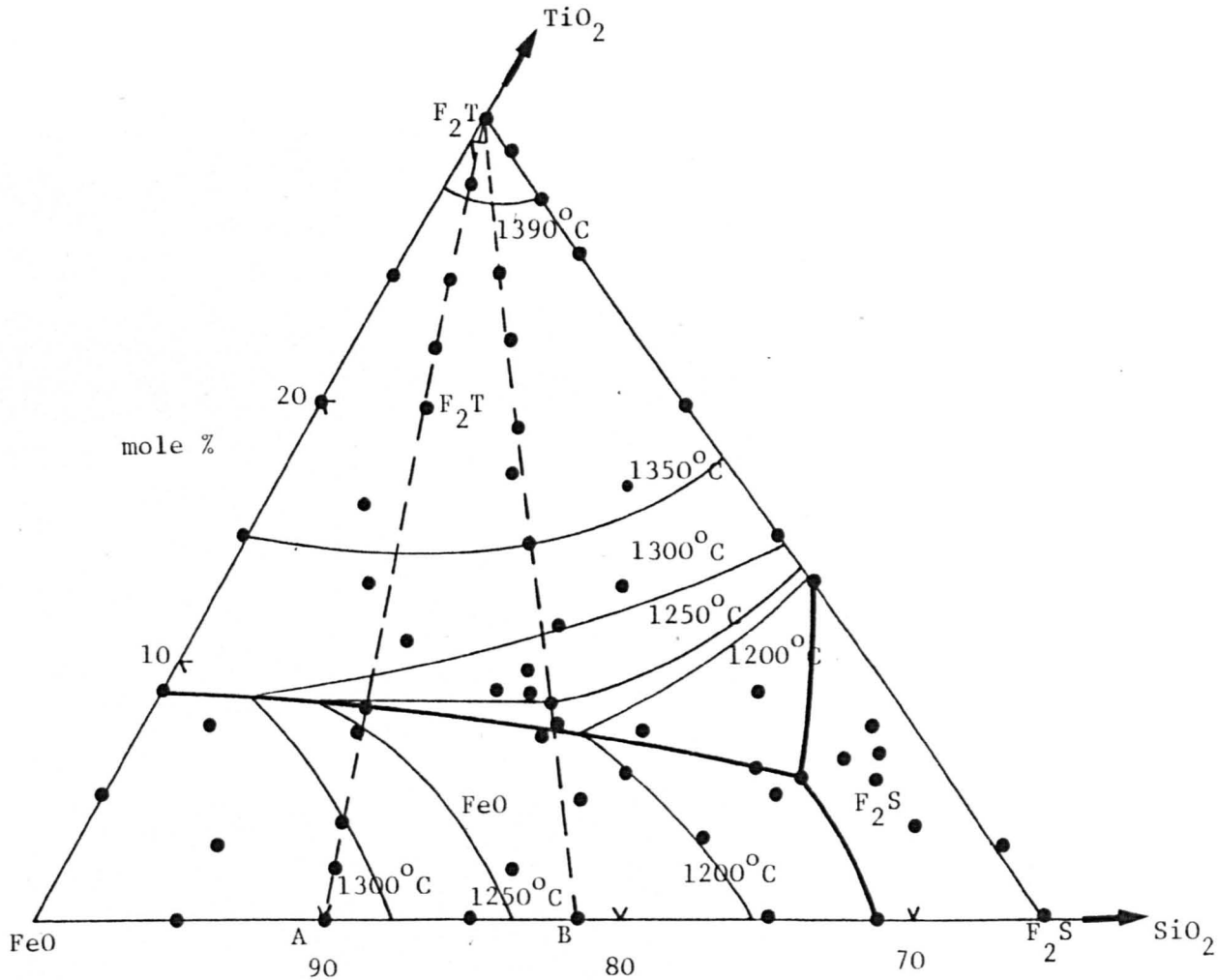

Fig. A.3.1 Phase relationships and liquidus temperatures in the system FeO-F_2T-F_2S (Table A.1)

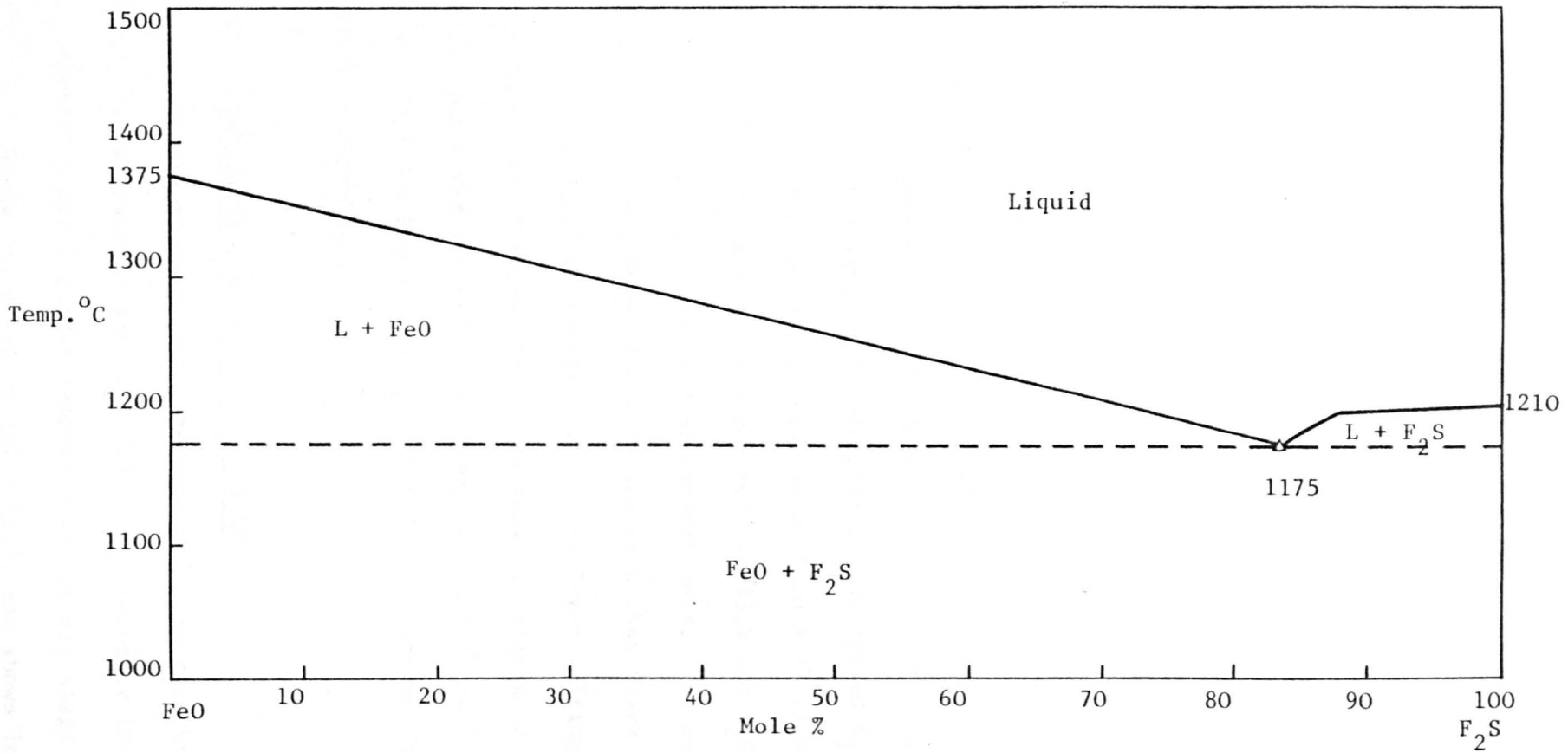

Fig. A.3.2 Liquidus profile on the slags on the join $FeO-F_2S$[11] in the $FeO-F_2T-F_2S$ system.

Initially samples were prepared for the quasi-binary join F_2S-F_2T and were studied for primary phase identification and liquidus temperature. Two primary phase fields were identified, liquid + F_2S and liquid + F_2T, and the minimum point in the liquidus curve was found. This point is eutectic involving liquid + F_2S + F_2T at temperature of 1185±10°C and composition F_2S of 58 mole% and F_2T of 42 mole% as shown in Figure (A.3.3).

The join FeO-F_2T was studied as mentioned in Chapter 1 by MacChesney and Muan[2]. They studied the liquidus temperatures for this join as a part of FeO-TiO_2 binary system, and found that the eutectic temperature at 1312°C at composition of 72 m/o FeO and 28 m/o F_2T, which was confirmed by Grau[3] as in Figure (A.3.4).

The phase equilibrium diagram of the system F_2S-F_2T-FeO with two sections through the liquidus surface A (71.5 m/o FeO and 28.5 m/o F_2S) - F_2T and B (46.5 m/o FeO and 53.5 m/o F_2S) - F_2T are shown in Figures (A.3.5 and A.3.6) respectively. The results of this investigation of the F_2S-F_2T-FeO system show that there is a small portion of the field of fayalite with much lower melting points than the greater part of spinel field, as shown in Figure (A.3.6). The eutectic point was located with a composition 6.1 m/o TiO_2, 23.2 m/o SiO_2 and 70.7 m/o FeO (since F_2T-F_2S-FeO is a portion of the ternary system FeO-SiO_2-TiO_2).

A.3.2 THE Fe_2TiO_4-Fe_2SiO_4-SiO_2 SYSTEM

Before studying any composition inside this triangle (Figure A.3.7), the quasi binary F_2T-SiO_2 was thoroughly investigated. The composition and liquidus temperatures for all slags were studied for F_2T-SiO_2 slags and given in Table (A.2) and shown in Figure (A.3.8).

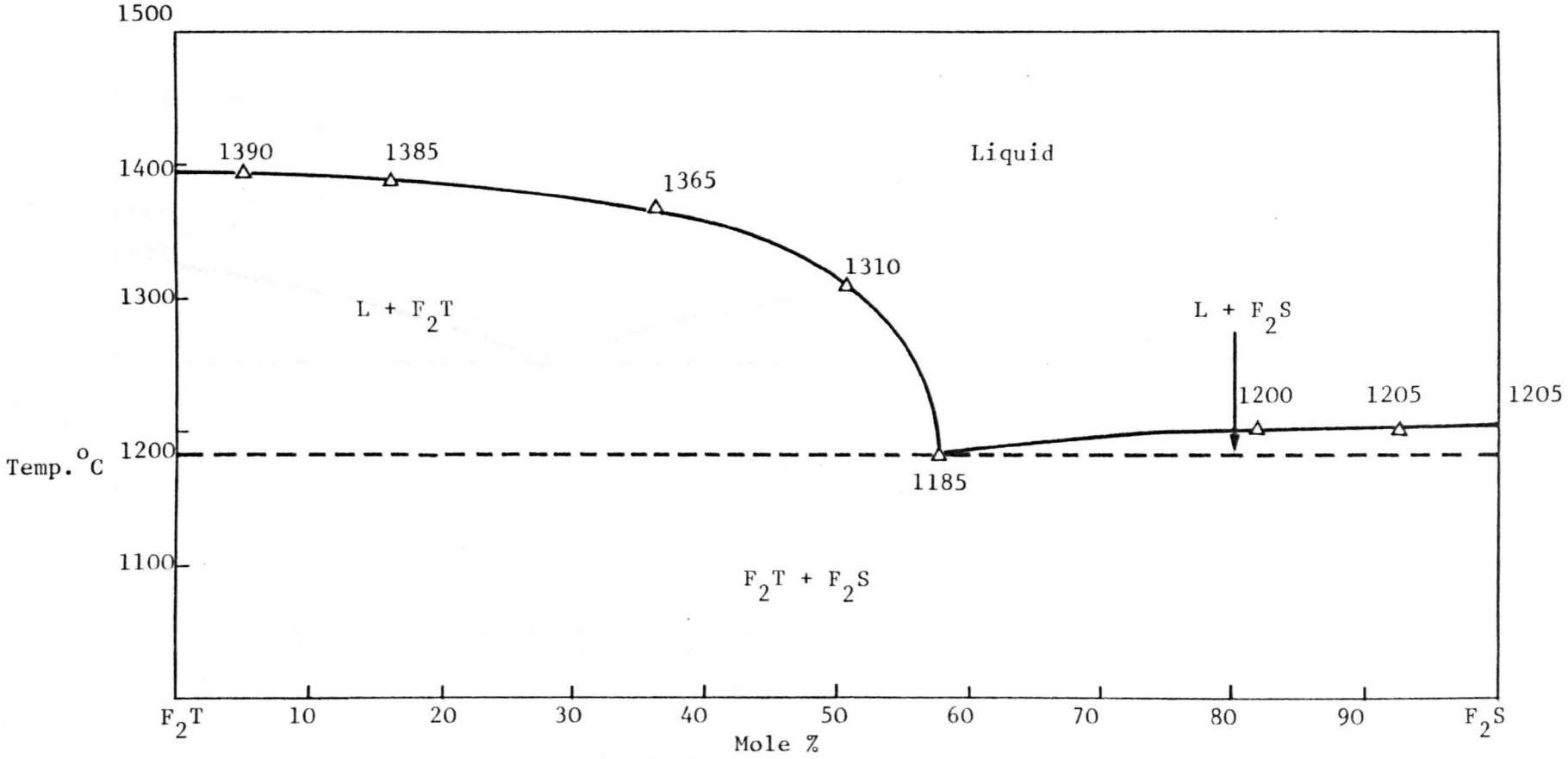

Fig. A.3.3 Liquidus profile on slags on the Quasi-Binary F_2T-F_2S

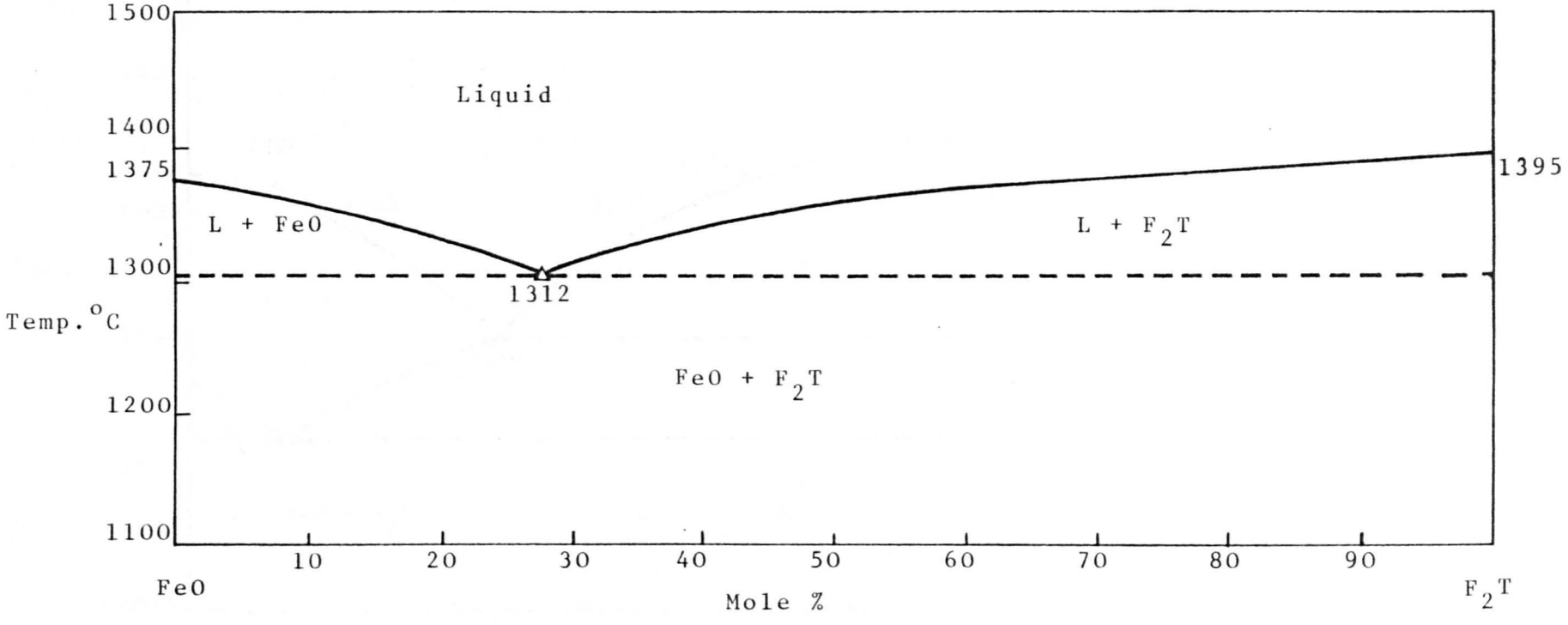

Fig. A.3.4 Liquidus profile on the slags on the join FeO-F_2T[2].

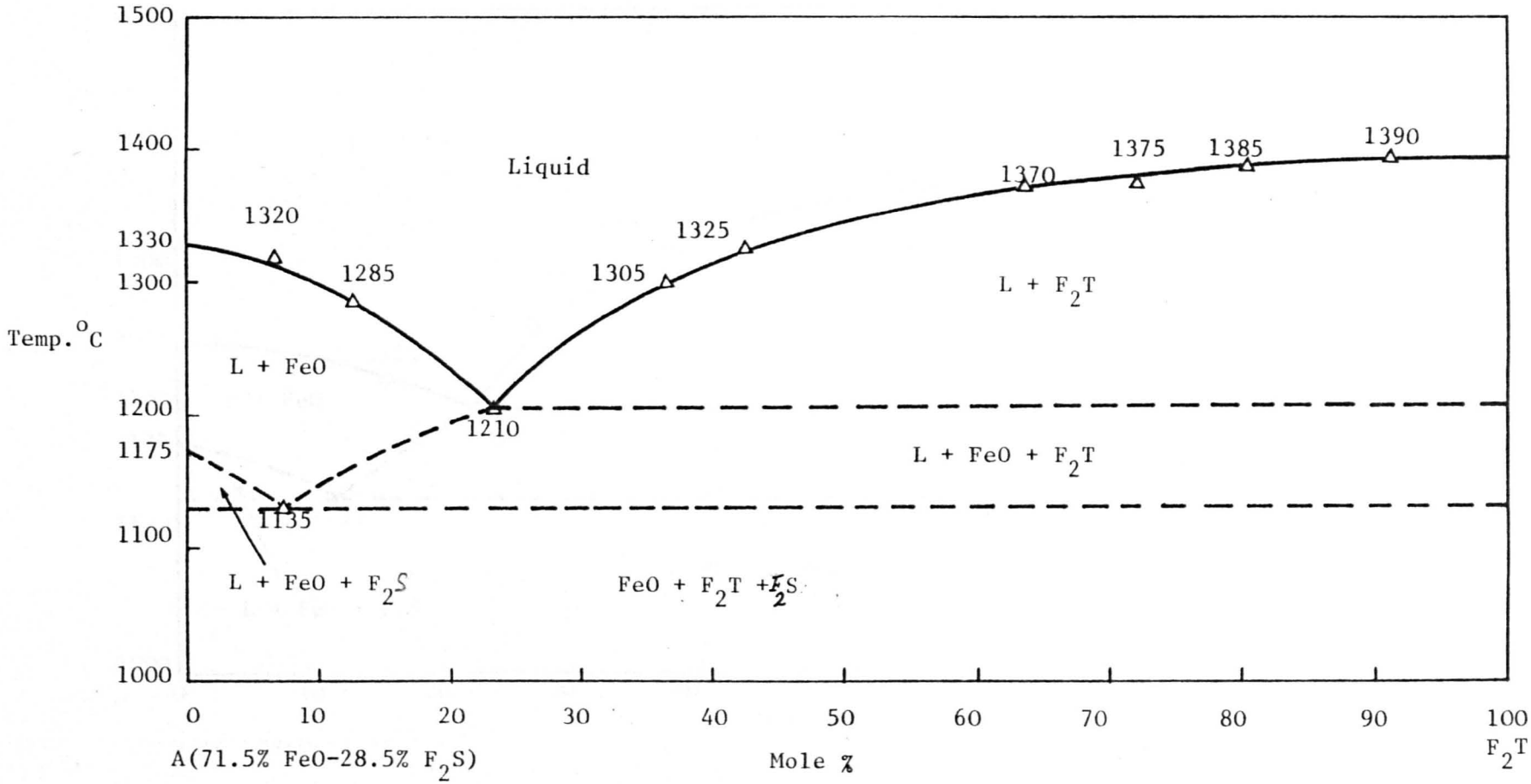

Fig. A.3.5 Liquidus profile of section on A-F_2T in the FeO-F_2T-F_2S system.

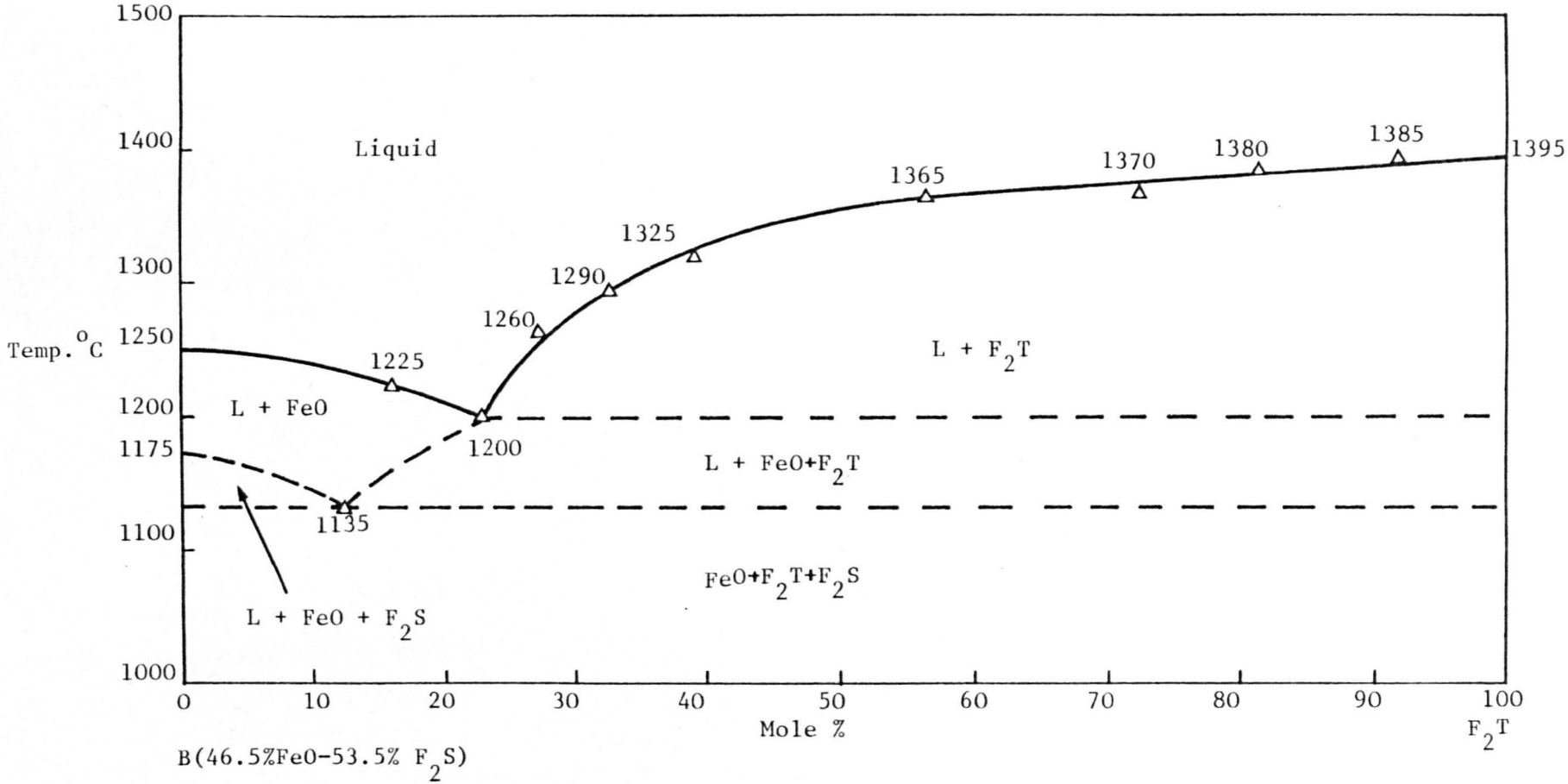

Fig. A.3.6 Liquidus profile of section on B-F_2T in the FeO-F_2T-F_2S system.

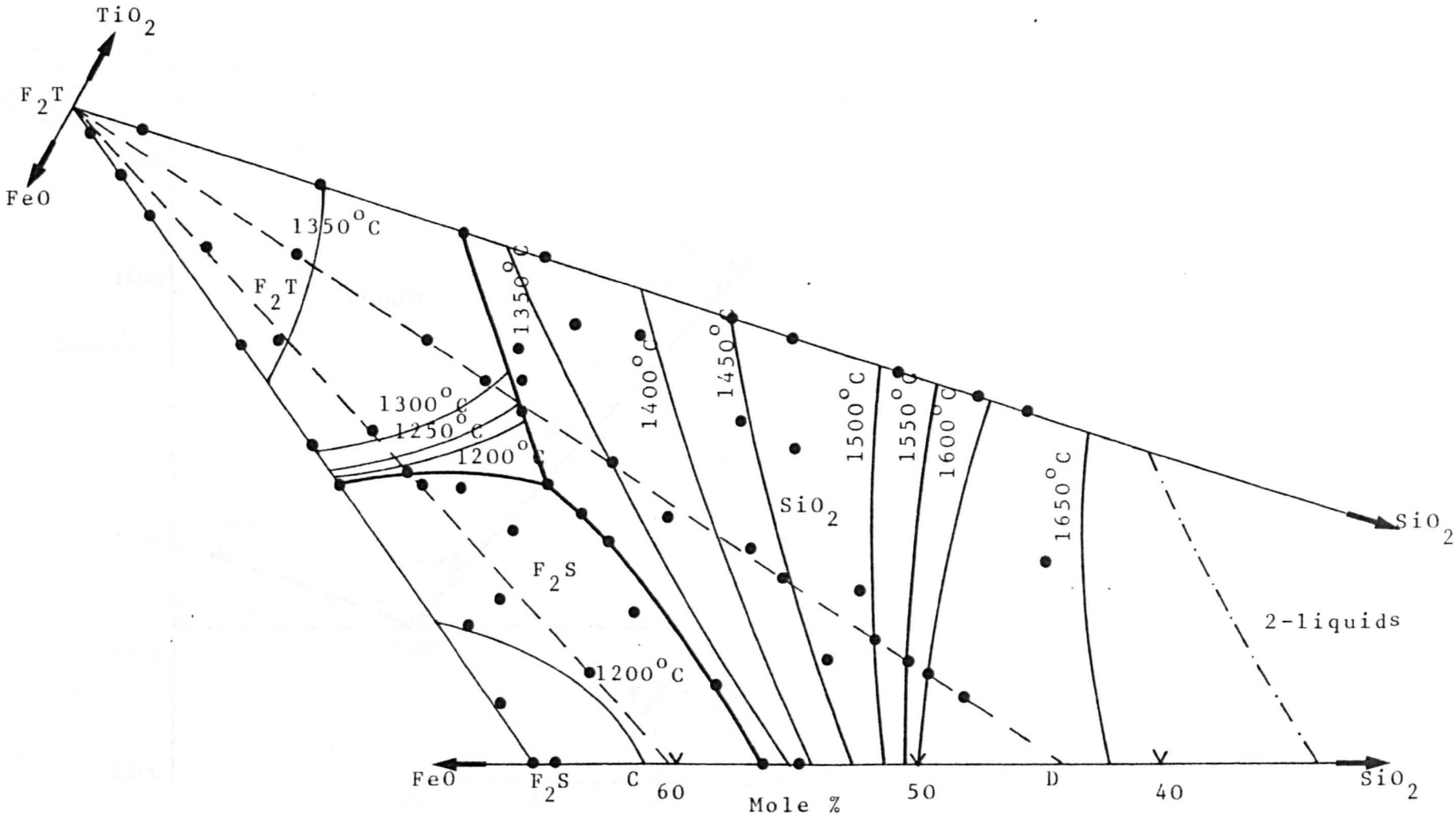

Fig. A.3.7 Phase relationships and liquidus temperatures in the F_2S-F_2T-SiO_2 system (Table A.2)

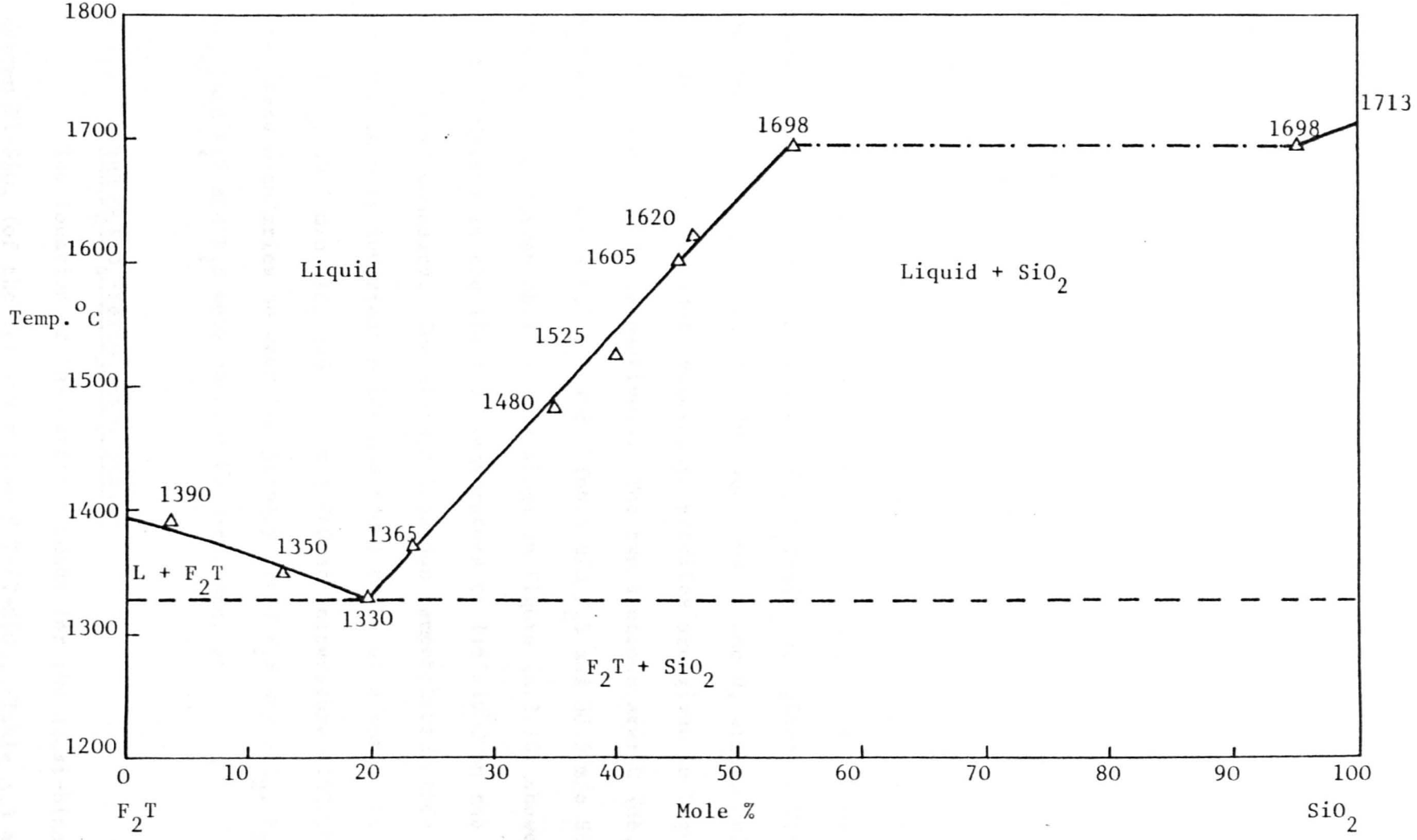

Fig. A.3.8 Liquidus profile on the slags on the Quasi-Binary F_2T-SiO_2

-·-·- two-liquid region.

The minimum liquidus temperature on the quasi-binary F_2T-SiO_2 was found to be at a composition of 19 m/o SiO_2 at 1330±10°C. The curve (Figure A.3.8) also shows that the phase boundary separating two liquids and silica appears to cross this quasi-binary at approximately 54 m/o SiO_2 and 96 m/o SiO_2. The immiscibility gap is shown by dotted line, as shown in this curve.

Bowen and Schairer[11] have studied the join F_2S-SiO_2 as part of the binary system FeO-SiO_2 (Figure A.1.2). The region of two-liquid extends over almost half the join F_2S-SiO_2 (from 51 m/o F_2S and 49 m/o SiO_2) at a temperature above 1698°C as in Figure (A.3.9).

The compositions and liquidus temperatures of the various slags on the composition triangle F_2T-F_2S-SiO_2 are given in Table (A.2) and shown in Figure (A.3.7). Two sections, C and D, within this system showing the liquidus temperature profiles are given in Figure (A.3.10 and A.3.11) respectively. The two sections are: C (86.25 m/o F_2S and 13.75 m/o SiO_2)-F_2T and D (66.5 m/o F_2S and 33.5 m/o SiO_2)-F_2T. The liquidus curves obtained for slags in Figure (A.3.10) showed a sharp decrease in the liquidus temperature to 1165±10°C on the fayalite-spinel boundary. The minimum liquidus temperature in this system was the ternary invariant point and found to be at a composition 13.0 m/o TiO_2, 29.0 m/o SiO_2 and 58.0 m/o FeO at temperature 1140±10°C. The phase boundaries between the primary field F_2S and SiO_2, F_2T and SiO_2 and F_2T and F_2S were checked by x-ray analysis.

A.3.3 THE Fe_2TiO_4-$FeTiO_3$-SiO_2 SYSTEM

The location of the eutectic point for the quasi-binary system FT-SiO_2 (of the ternary system F_2T-FT-SiO_2, (Table A.3 and Figure A.3.12)) has been found by examination of the liquidus

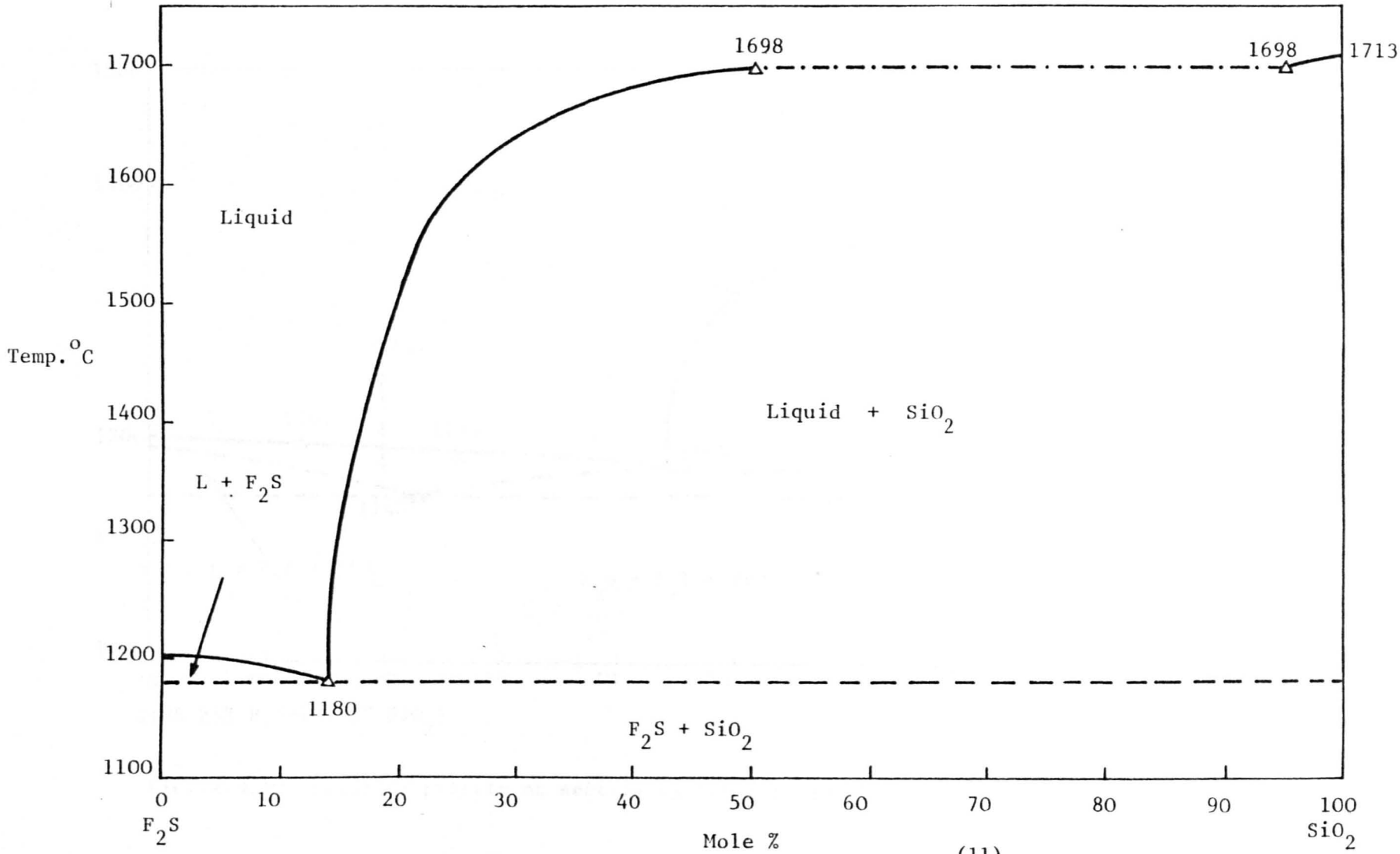

Fig. A.3.9 Liquidus profile on the slags on the join F_2S-SiO_2 (11)

-·-·- two-liquid region.

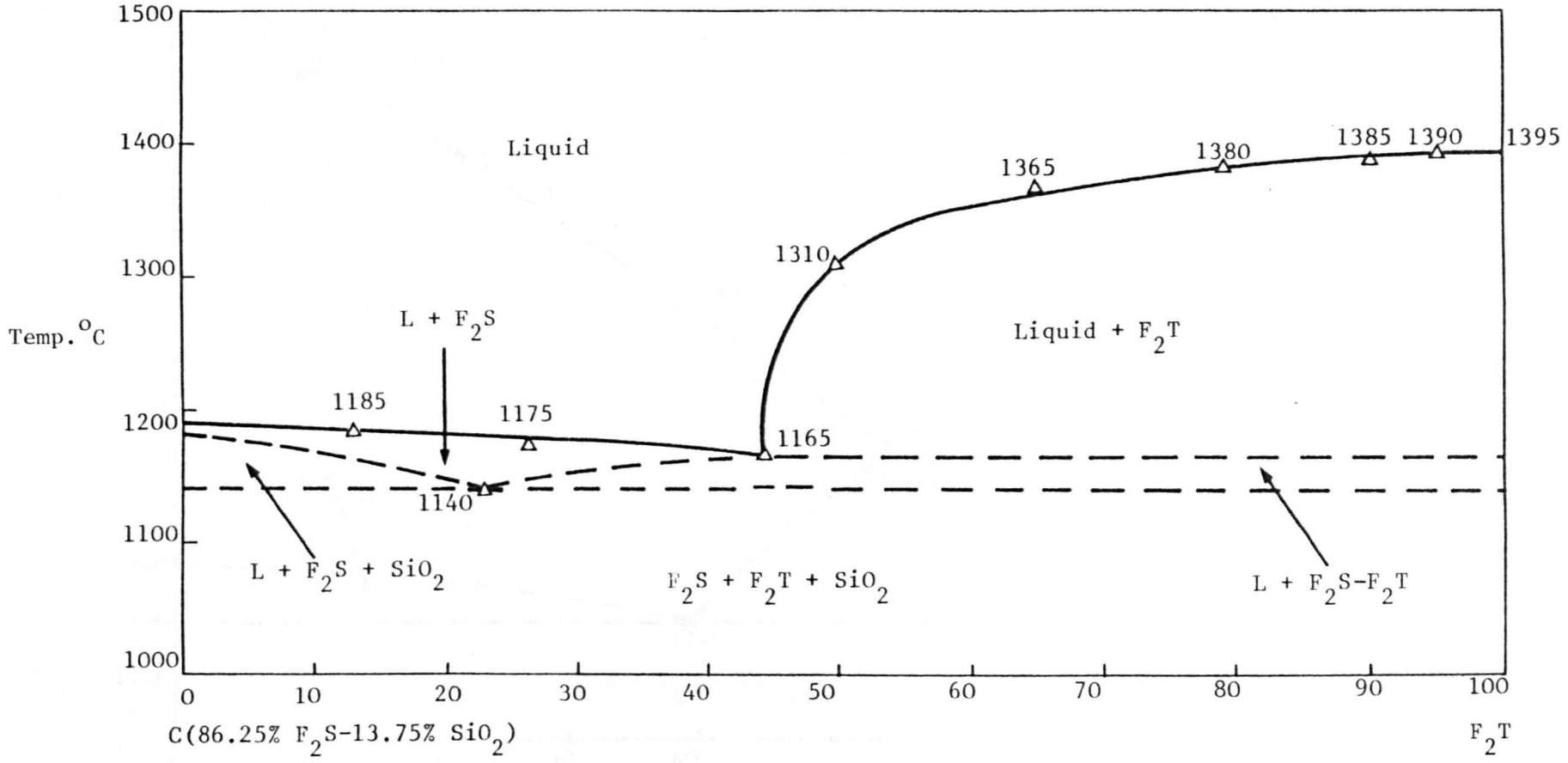

Fig. A.3.10 Liquidus profile of section on C-F_2T in the F_2S-F_2T-SiO_2 system.

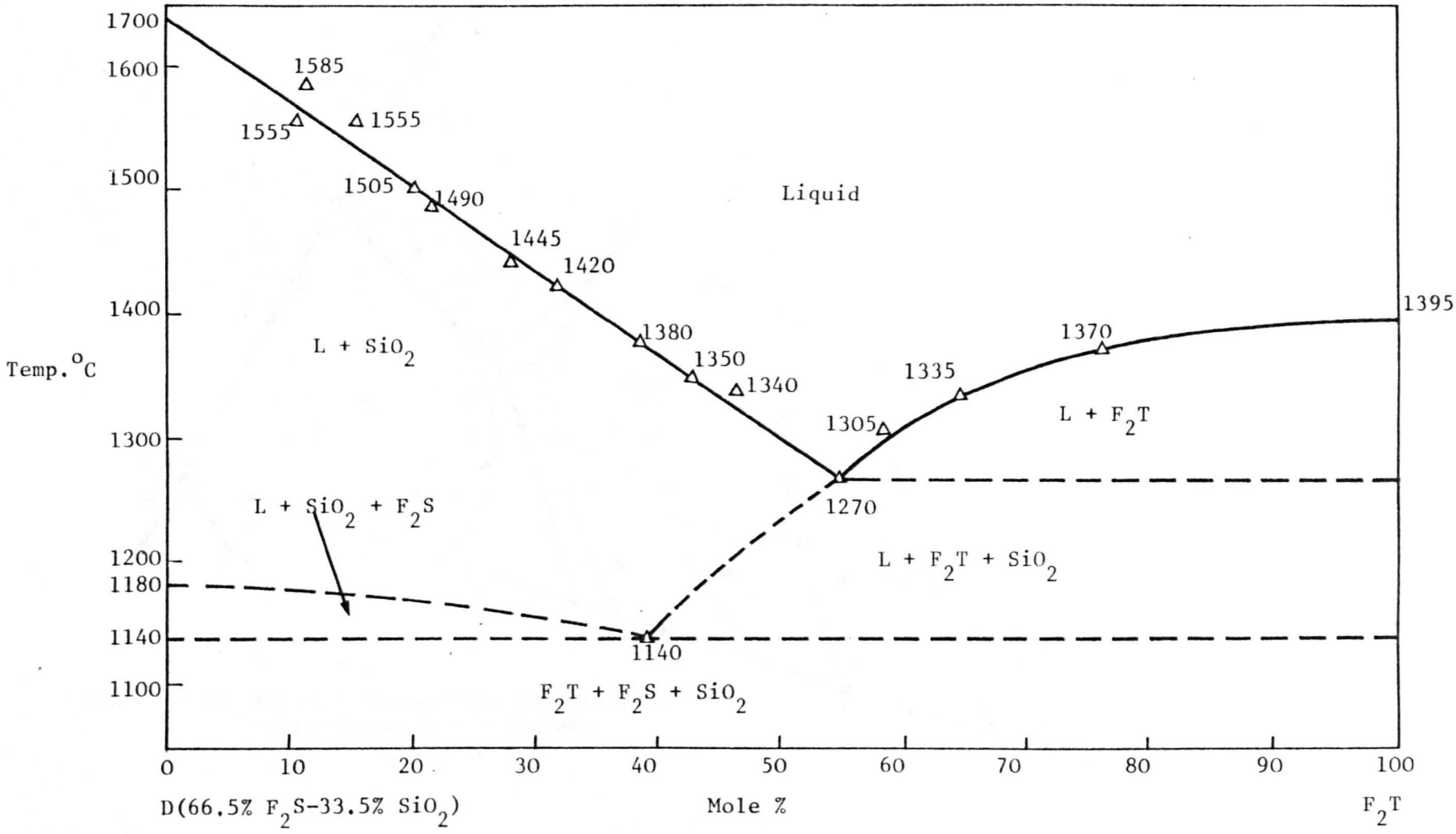

Fig. A.3.11 Liquidus profile of section on D-F_2T in the F_2S-F_2T-SiO_2 system.

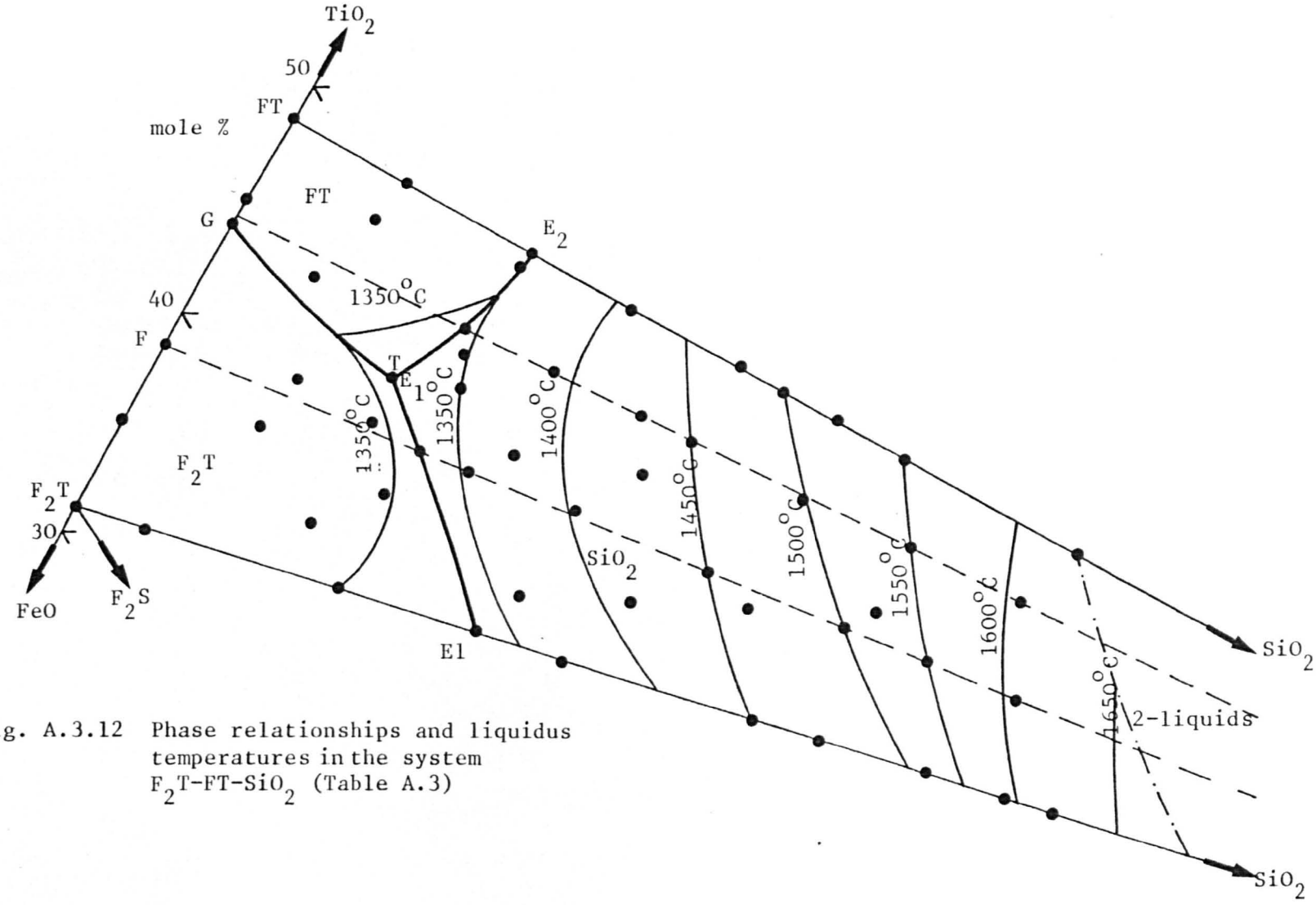

Fig. A.3.12 Phase relationships and liquidus temperatures in the system F_2T-FT-SiO_2 (Table A.3)

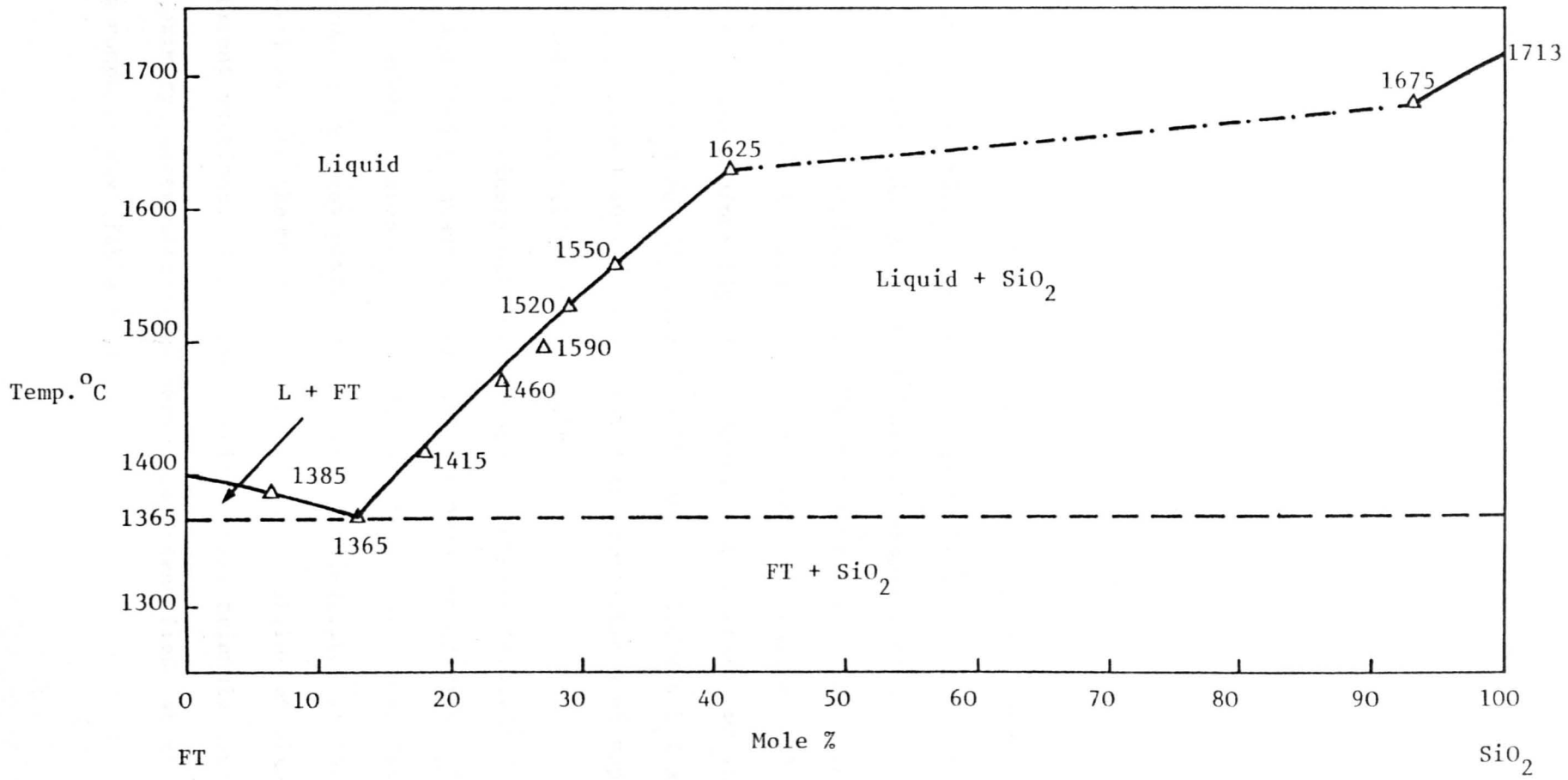

Fig. A.3.13 Liquidus profile on the slags on the Quasi-Binary FT-SiO_2.
-·-·- two-liquid region.

temperature as shown in Figure (A.3.13). The quasi-binary was found to have a eutectic at a temperature of 1365±10°C and composition of 87 m/o FT and 13 m/o SiO_2. During the present work a slag on this quasi-binary was made up of 58 m/o FT and 42 m/o SiO_2 and found to have a liquidus temperature of 1625±10°C when it was approximately on silica-two liquid boundary.

The F_2T-FT join has a eutectic point located at a composition (29 m/o F_2T and 71 m/o FT) at a temperature of 1363°C, as shown in Figure (A.3.14).

The immiscibility gap extends also over a large area of the triangle F_2T-FT-SiO_2 as shown in Figure (A.3.12). The ternary eutectic point was found at 1320±10°C and at composition 37.5 m/o TiO_2, 10 m/o SiO_2 and 52.5 m/o FeO. Two sections F and G through the liquidus surface in this section are shown in Figures (A.3.15 and A.3.16). Two minimum liquidus temperatures in these two sections F (59.0 m/o F_2T and 41.0 m/o FT)-SiO_2 and G (25.0 m/o F_2T and 75 m/o FT)-SiO_2, were 1340±10°C and located at compositions of approximately 12.5 and 12 m/o silica respectively.

The binary eutectic troughs in Figure (A.3.12) for F_2T-SiO_2 and FT-SiO_2 quasi systems and the phase boundaries $E_1T_{E_1}$ and $E_2T_{E_1}$ between phases F_2T and SiO_2, and FT and SiO_2 respectively, were determined by x-ray powder diffraction, as described in Chapter 2, as well as from the through of the liquidus profiles of slags on the different sections. The phase fields on this triangle correspond to the primary phases actually observed and identified at different slag compositions (Table A.3).

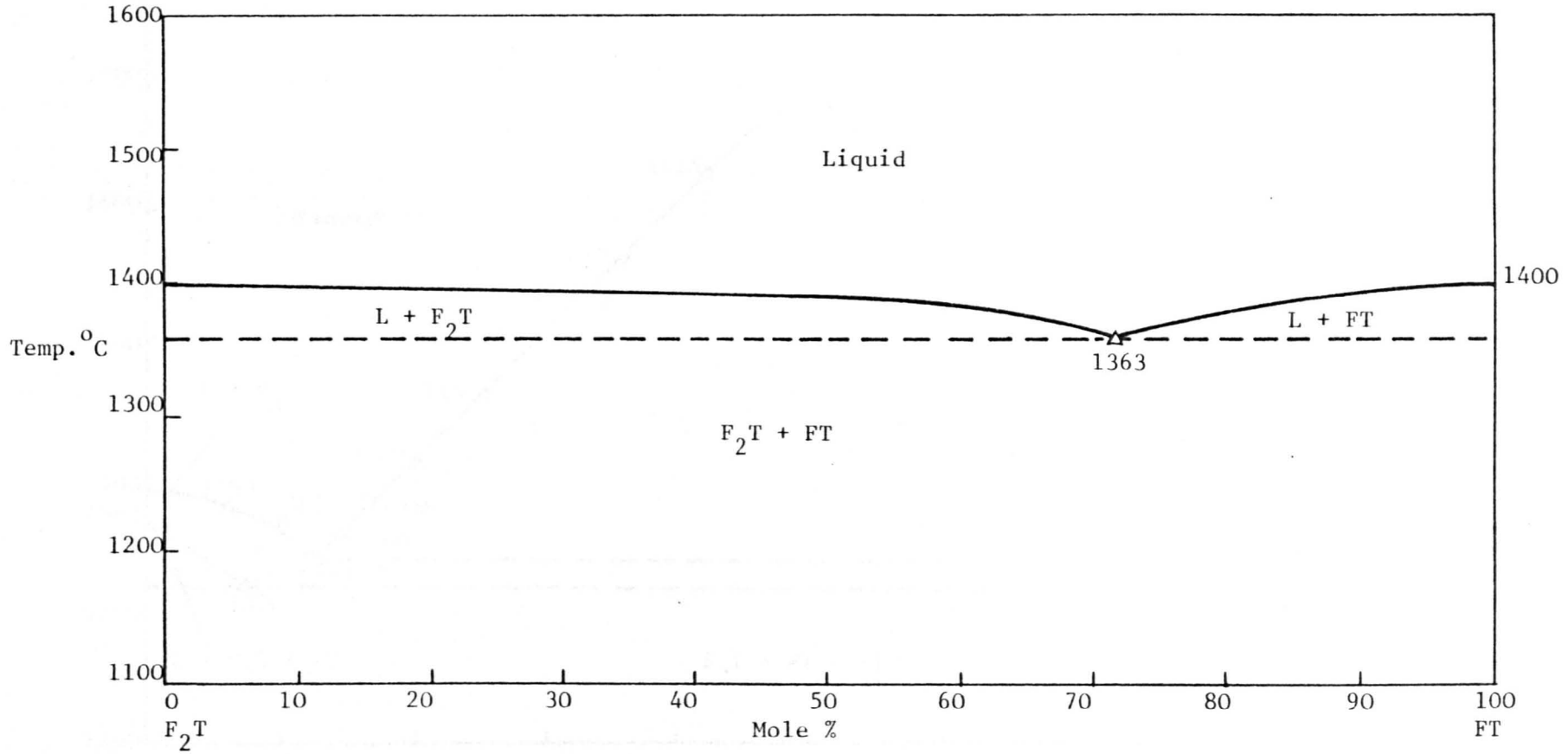

Fig. A.3.14 Liquidus profile on the slags on the join F_2T-FT[2].

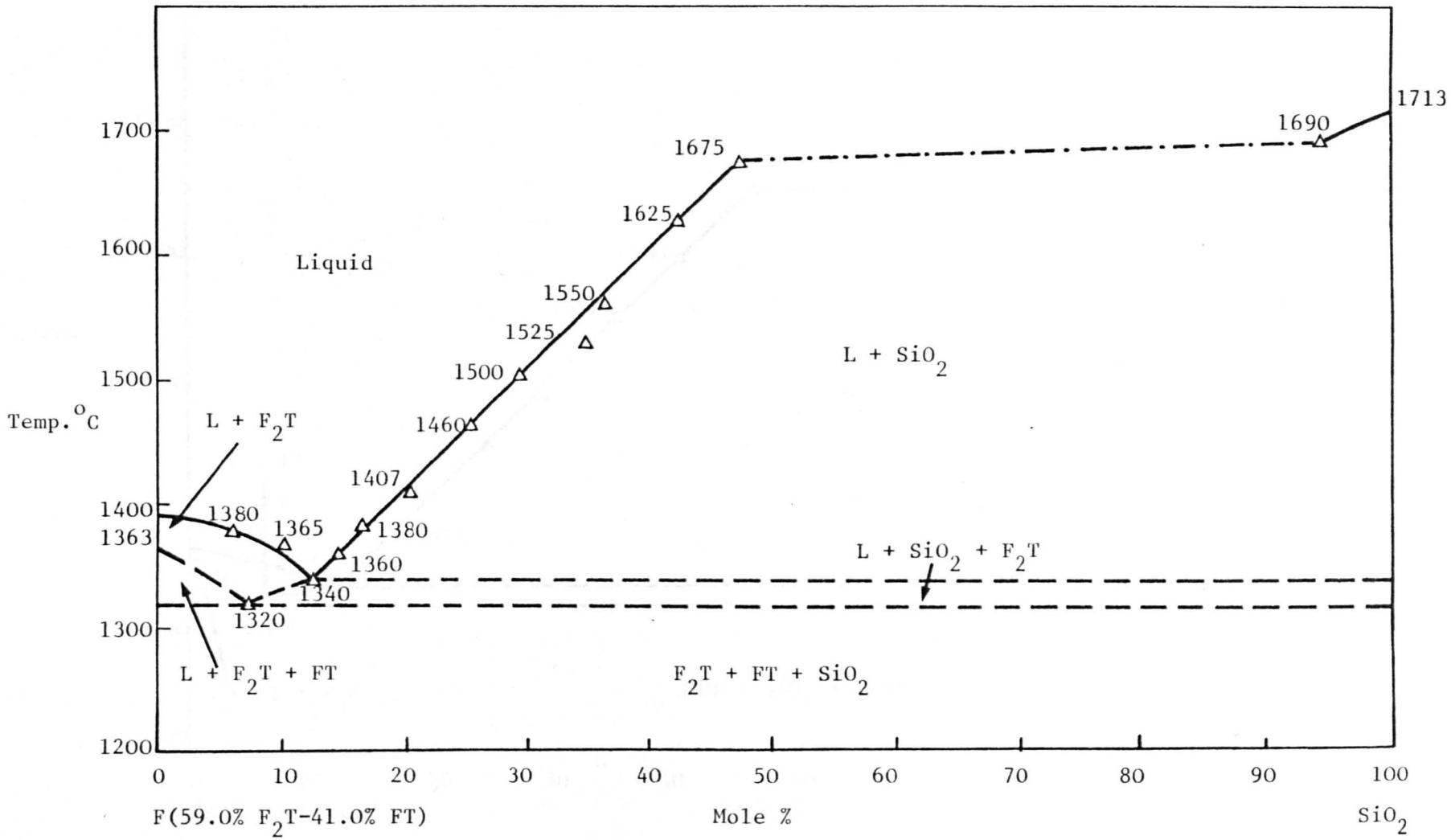

Fig. A.3.15 Liquidus profile of section on F-SiO_2 in the F_2T-FT-SiO_2 system

-·-·- two-liquid region.

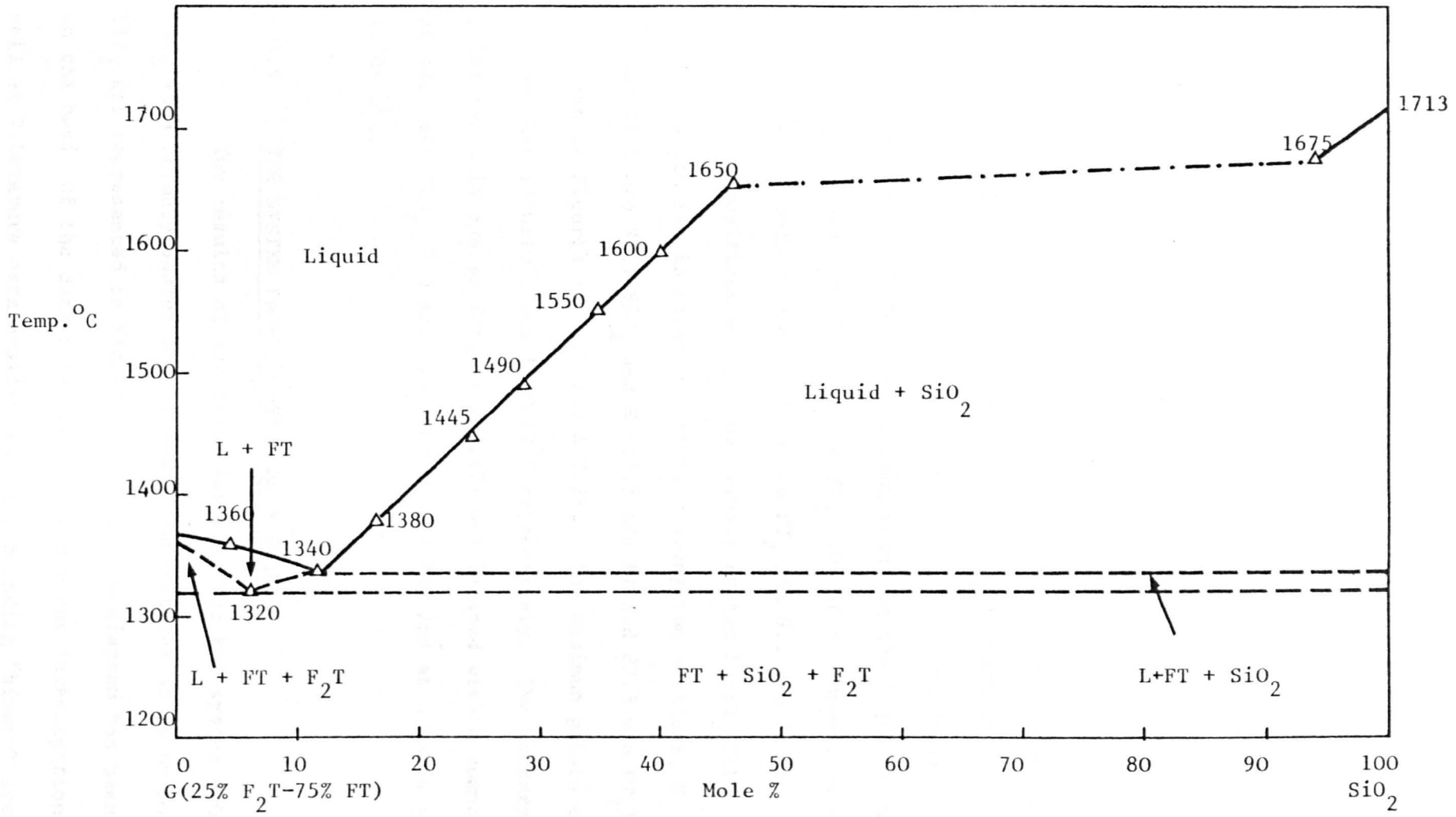

Fig. A.3.16 Liquidus profile of section on G-SiO_2 in F_2T-FT-SiO_2 system

-·-·- two-liquid region.

A.3.4 THE $FeTiO_3$-$FeTi_2O_5$-SiO_2 SYSTEM

For the system FT-FT_2-SiO_2 (Figure A.3.17), the join FT-FT_2 had been studied previously, and the results given by MacChesney and Muan[2] were used as shown in Figure (A.3.18). They gave two phase fields involving liquid+FT and liquid+FT_2, and a single eutectic temperature of 1390°C at composition 57 m/o FT and 43 m/o FT_2.

The quasi-binary FT_2-SiO_2 was studied for liquidus temperatures as well as primary phase identification before proceeding to study the composition within the FT-FT_2-SiO_2 ternary system. Two primary fields were identified, liquid+FT_2 and liquid+silica. As shown in Figure (A.3.19), one minimum point on the liquidus curve was found. This point involved liquid+FT_2+SiO_2 at a temperature of 1450±10°C and composition of 90.5 m/o FT_2 and 9.5 m/o SiO_2.

Compositions within the ternary system FT-FT_2-SiO_2 were prepared and studied in order of priority along two sections, H (78.5 m/o FT and 21.5 m/o FT_2)-SiO_2 and K (17.5 m/o FT and 82.5 m/o FT_2)-SiO_2 as shown in Figures (A.3.20 and A.3.21). The minimum points on these curves were 1350±10°C and 1440±10°C respectively. The ternary eutectic point for this system (Figure A.3.17) was located with a composition of 52.5 m/o TiO_2, 7.5 m/o SiO_2 and 40 m/o FeO and at a temperature of 1330±10°C.

A.3.5 THE SYSTEM FeO-TiO_2-SiO_2 AS A WHOLE

The results of equilibration runs for the system FeO-TiO_2-SiO_2 with primary phases and liquidus temperatures up to 66 mole% TiO_2 are represented in Figure (A.3.22). The diagram has been drawn on the basis of the data obtained in the present investigation, as well as literature data available on the bounding "binary" systems

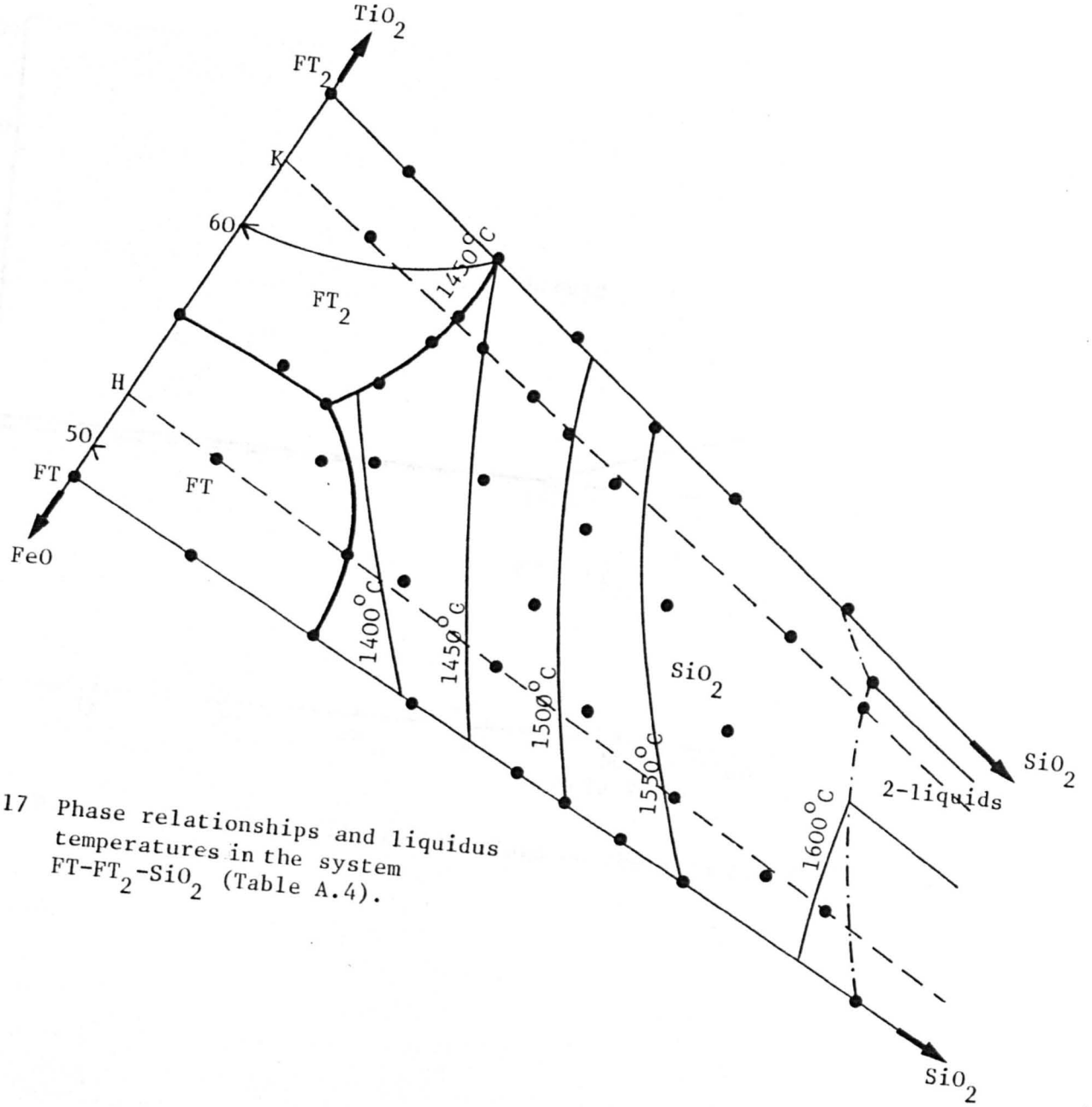

Fig. A.3.17 Phase relationships and liquidus temperatures in the system $FT-FT_2-SiO_2$ (Table A.4).

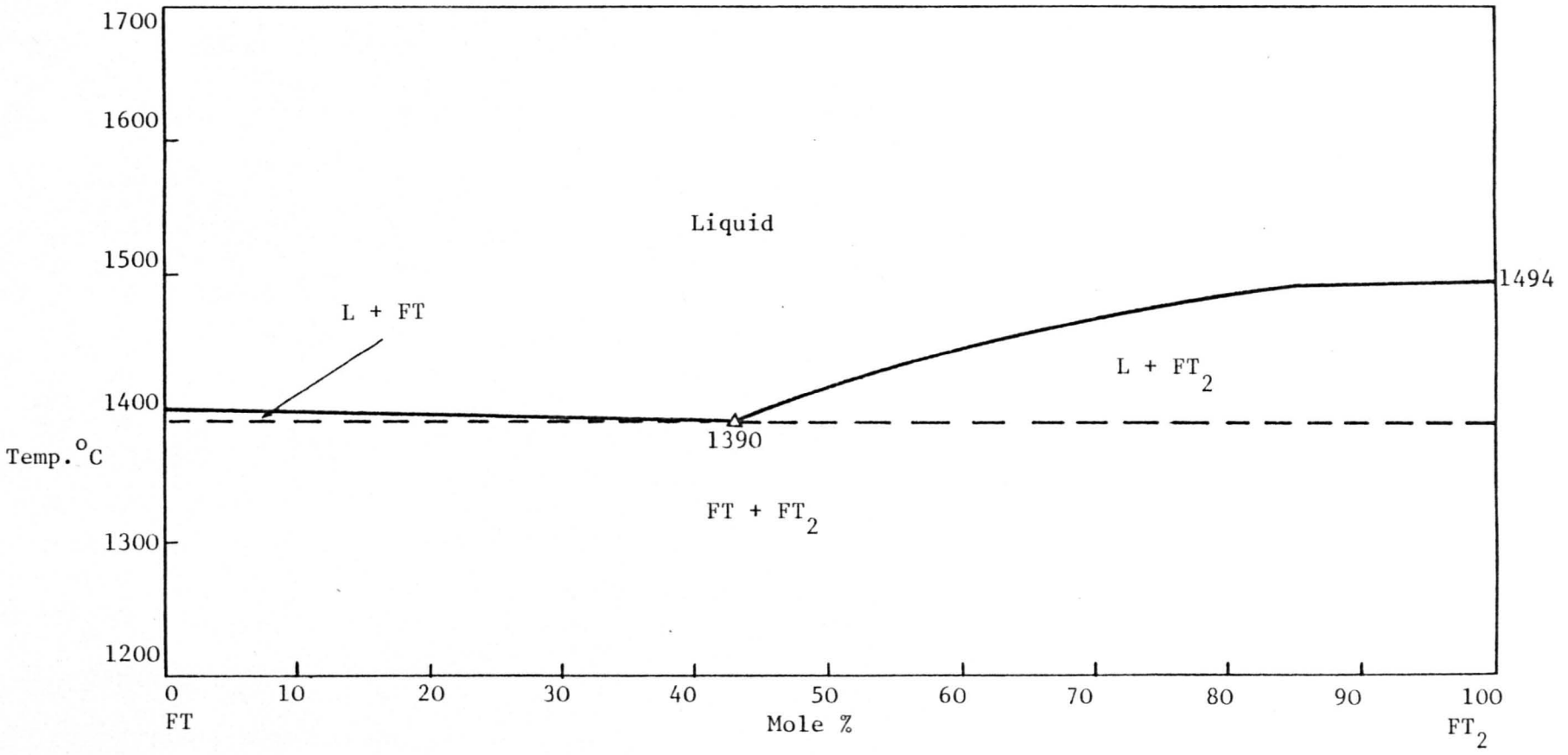

Fig. A.3.18 Liquidus profile on the slags on the join $FT-FT_2$.[2]

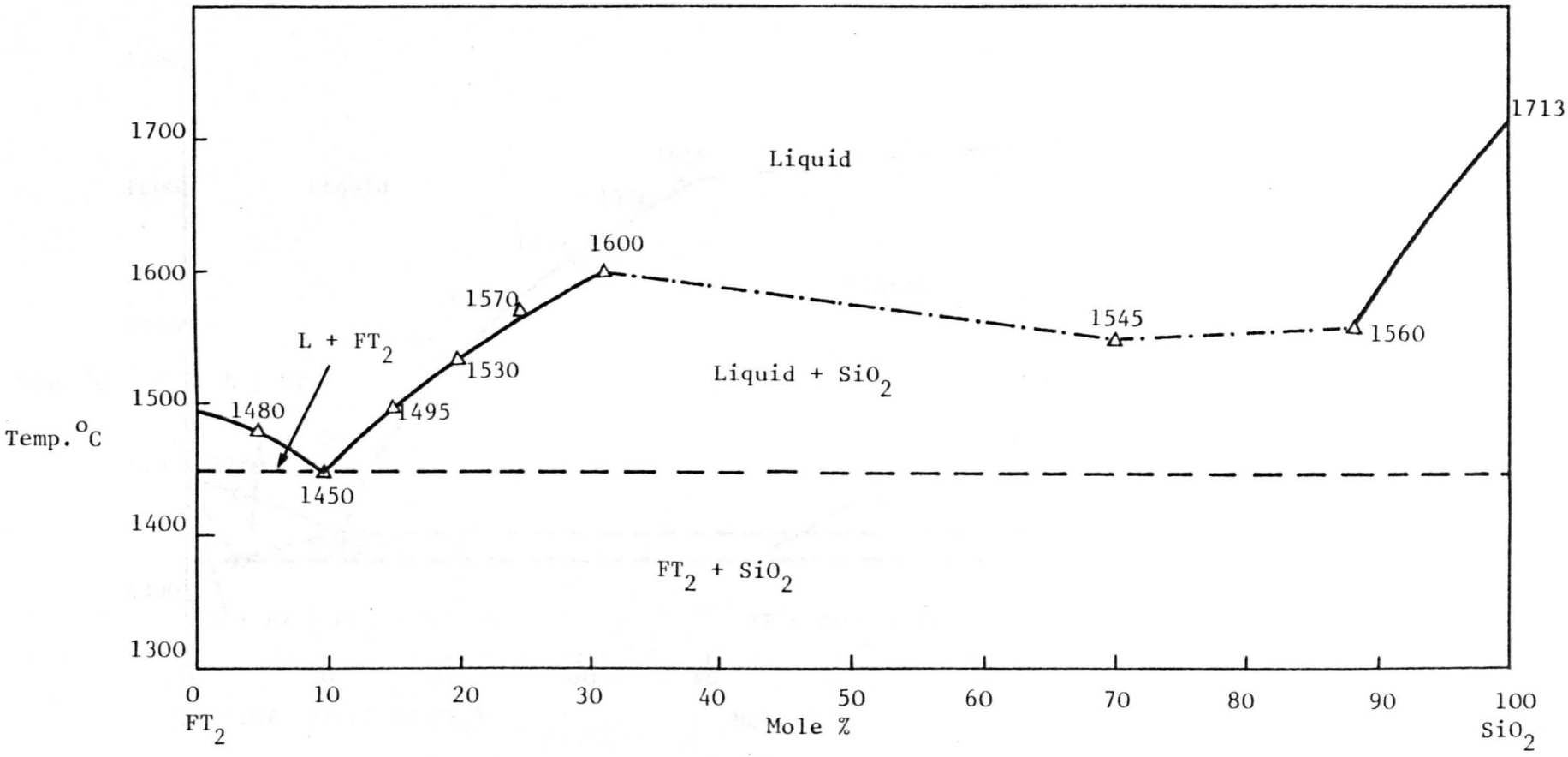

Fig. A.3.19 Liquidus profile on the slags on the Quasi-Binary FT_2-SiO_2

-·-·- two-liquid region.

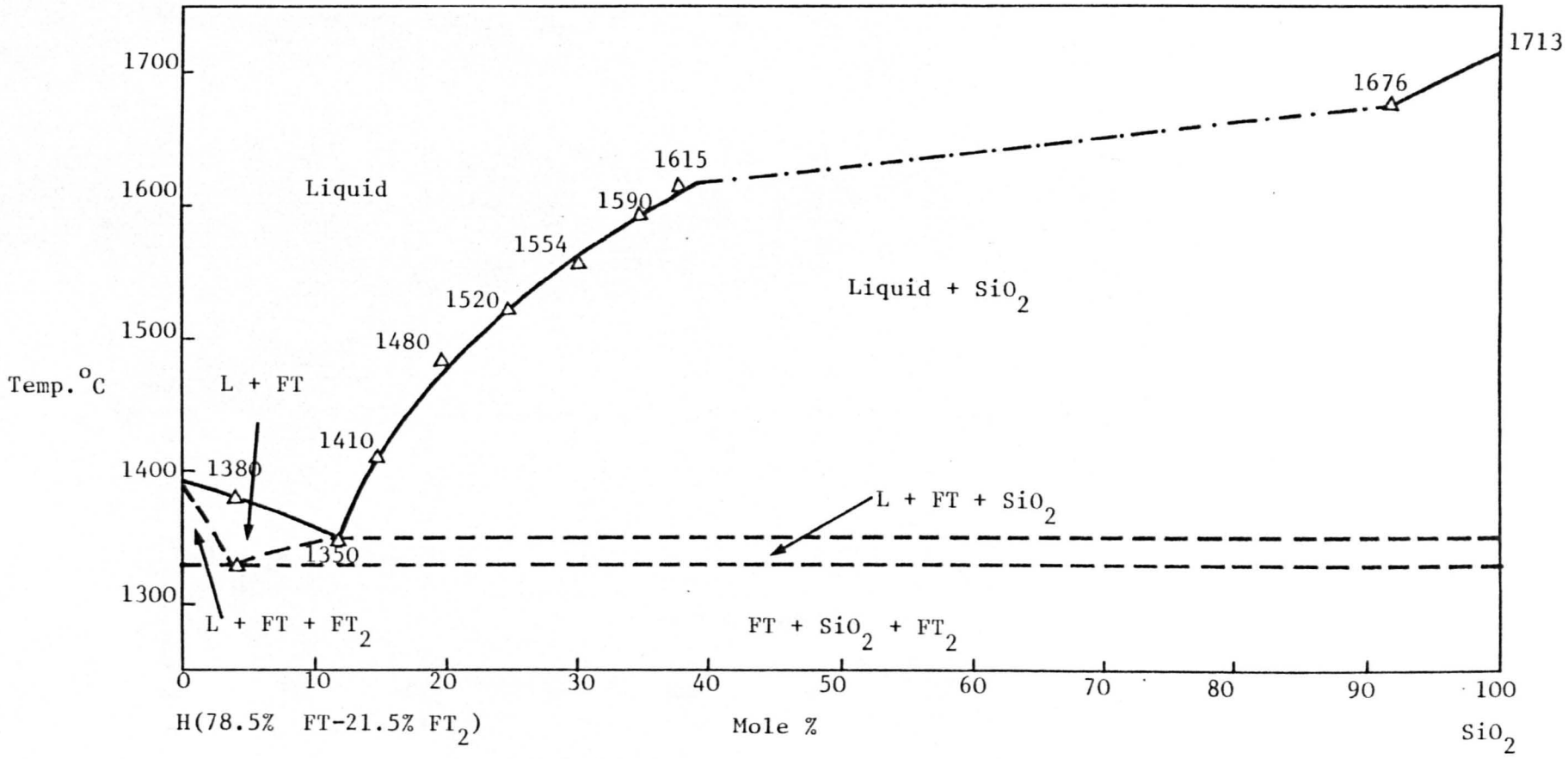

Fig. A.3.20 Liquidus profile of section on H-SiO_2 in the FT-FT_2-SiO_2 system.
-·-·- two-liquid region.

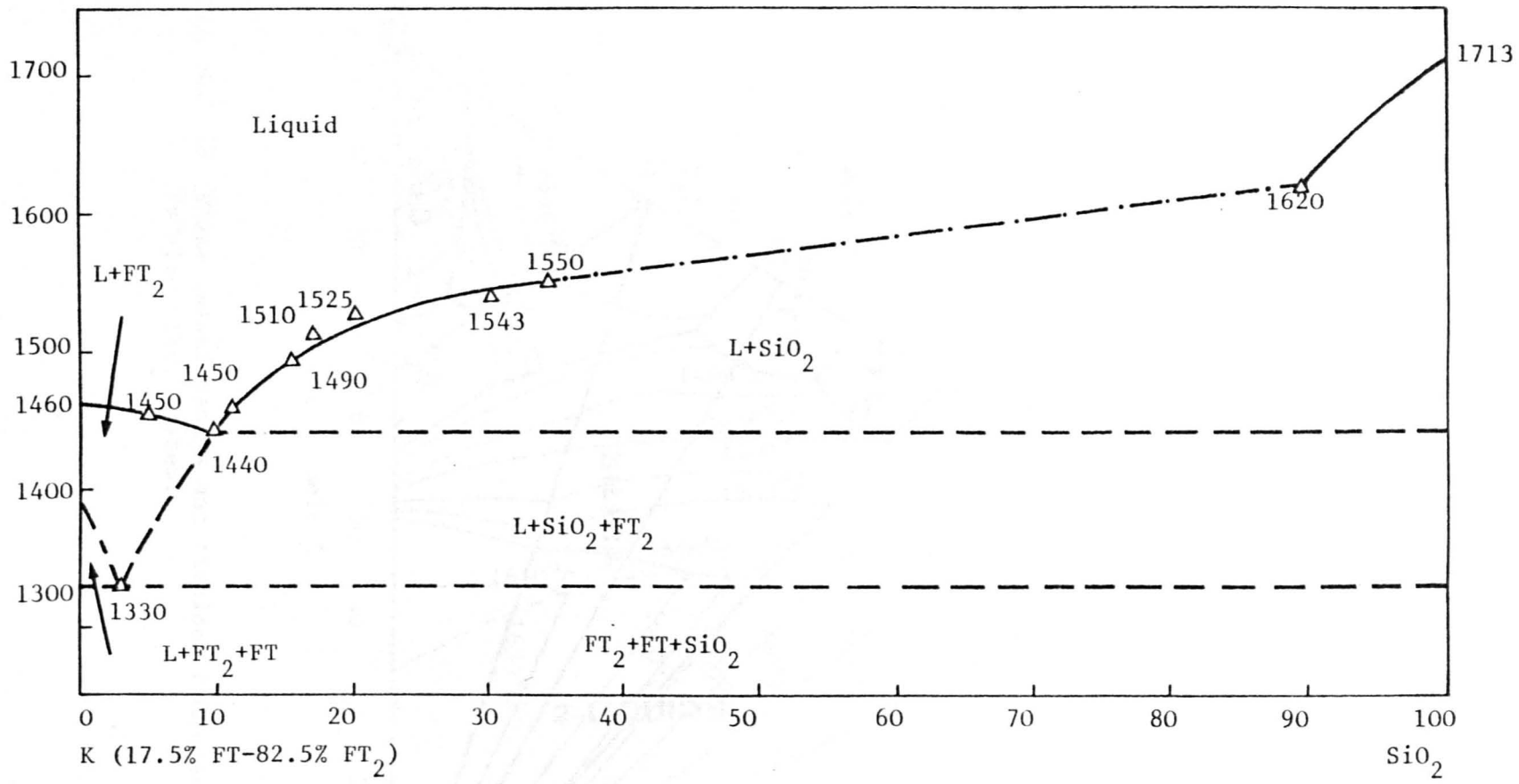

Fig. A.3.21 Liquidus profile of section on K-SiO_2 in the system FT-FT_2-SiO_2.
-·-·- two liquid region.

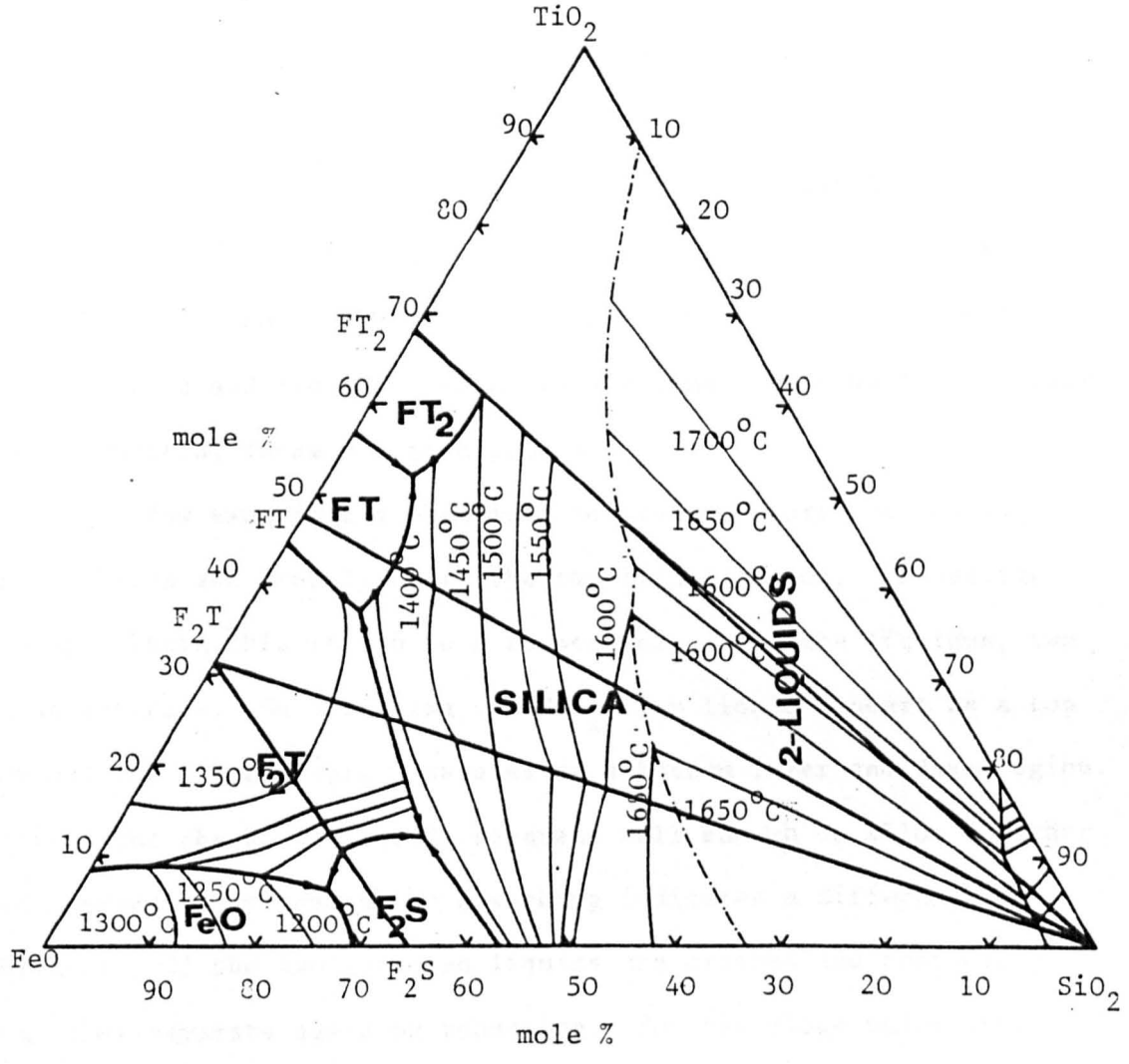

Fig. A.3.22 Phase relationships and liquidus temperatures in the $FeO-TiO_2-SiO_2$ system.

(Figures A.1.1, A.1.2 and A.1.3). - Six crystalline phases have stable existence in equilibrium with liquids, in the part of the diagram studied in the present works, i.e., wüstite, fayalite, ulvöspinel, ilmenite, pseudobrookite and silica (tridymite or cristabolite). The triangle FT_2-TiO_2-SiO_2 has not been studied in this work.

Four invariant points have been determined. Wüstite, fayalitem ulvöspinel and liquid at approximately 1135±10°C, and at 1140±10°C fayalite, ulvöspinel, silica and liquid. At approximately 1320±10°C ulvöspinel, ilmenite, silica and liquid. The fourth eutectic point was characterised by the co-existence at 1330±10°C of ilmenite, pseudobrookit, silica and liquid. Temperature maxima exists on the boundary curves connecting these eutectic points.

A few experiments were made to study mixtures containing rutile, silica and iron lying in the two-liquid region. On heating a mixture within this region to a temperature above the liquidus, two liquids separate. On quenching, the SiO_2-rich liquid appears as a top layer and the other liquid separates as a bottom layer and dark region. The fact that these two-liquids separate well enough to allow a rather clean spearation by hand after quenching indicates a difference in properties. If the two quenched liquids are crushed and thoroughly mixed, they separate again on reheating. For the slags which were examined, the two quenched liquids were separated by hand and individually analysed for TiO_2 and SiO_2 as a check on the tie-line directions. The results are depicted graphically in Figure (A.3.23). The fanning of the tie-lines across the two-liquid region confirms in general with liquidus temperare data. The ends of the tie-lines, however, do not fall on the limits of the two-liquid area as determined at liquidus temperatures, but rather fall within the boundaries. This is partly

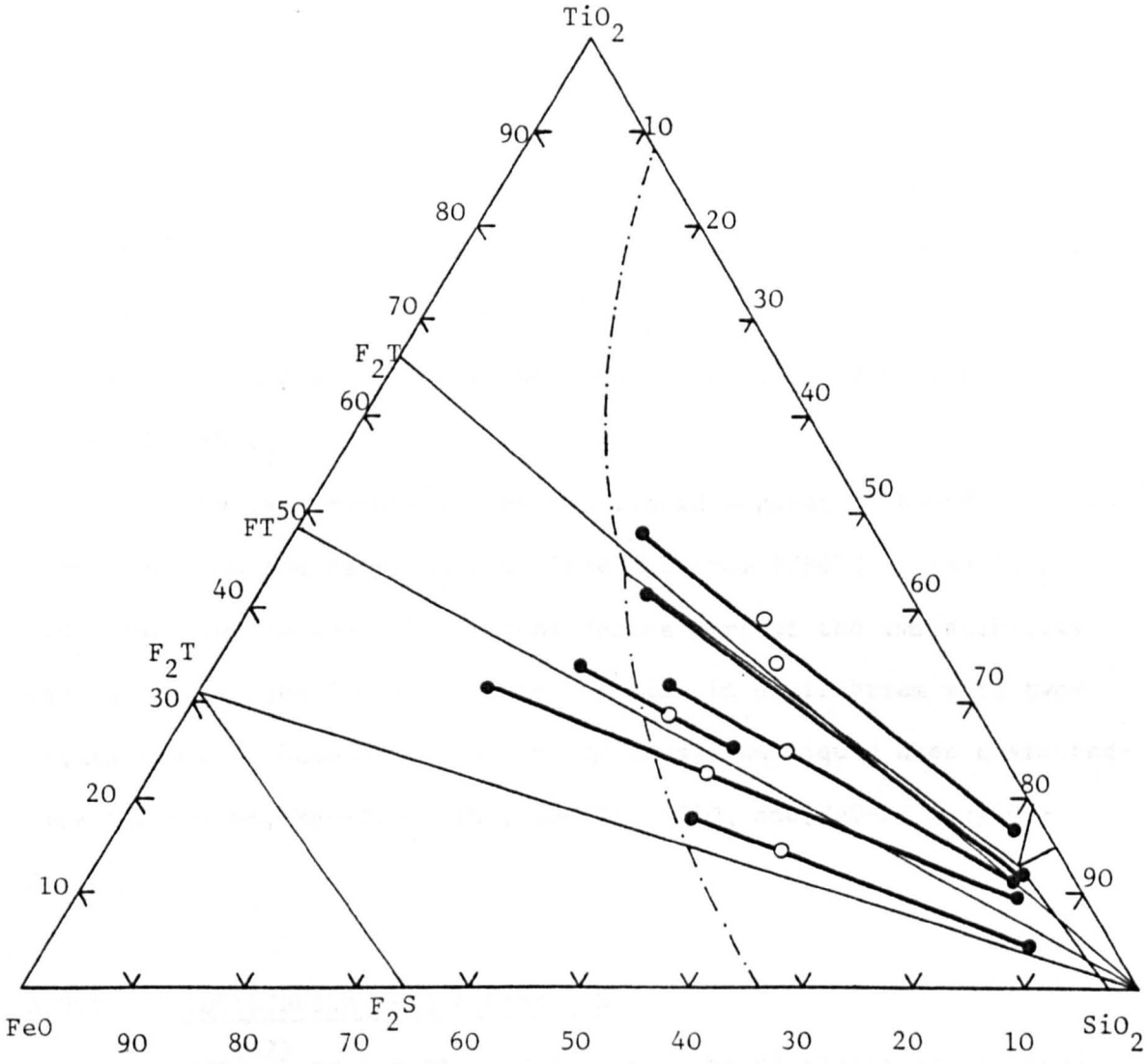

Fig. A.3.23 Tie lines in the two-liquid region as determined from chemical analysis in $FeO-TiO_2-SiO_2$ system.

○ composition of original mixture
● composition of the two liquids

due to incomplete separation which gives analytical difficulties. In as much as the mixtures for analysis were quenched from 1700°C, i.e. above the liquidus temperature, a contributing factor could be the "closing-in" of the limits of the two-liquid region with increasing temperatures above the liquidus. It was not clear why two of the tie-lines did not pass exactly through the composition of the original mixture, but this may be related to the experimental errors. The ternary evidence of two-liquid separation is consistent with the binary systems TiO_2-SiO_2 [8], FeO-SiO_2 [11] where the same type of separation takes place. In this sense the evidence from ternary relations confirms the existence of the two-liquid region reported for the system TiO_2-SiO_2.

The temperature at the two-liquid separation boundary falls from 1695°C on the FeO-SiO_2 side line and from 1780°C on the TiO_2-SiO_2 side line to 1540±10°C in the centre part of the immiscibility gap where cristabolite and rutile co-exist in equilibrium with two-liquid phases. Undoubtedly a similar large two-liquid area characterises the system, MgO-TiO_2-SiO_2, CaO-TiO_2-SiO_2 and FeO-Fe_2O_3-TiO_2-SiO_2.

A.3.6 EQUILIBRIUM CRYSTALLISATION

Geer[82] as reported, states that the crystallisation curve denotes the locus of points which present the compositions of the solutions formed on cooling any given solution from any given temperature to the temperature (quintuple point in the case of ternary systems) at which it becomes solid, under the assumption that no phase is removed during the cooling.

The relations of solid phases to liquid phases of any

system which does not have solid solution are known when the liquidus of the system is determined for all compositions. The liquidus is the temperature at which the first solid (primary phase) appears on cooling under equilibrium conditions. A knowledge of the crystallisation curve or the melting curve for any particular melt is very valuable in the study of the firing of ceramic bodies.

A summary of the equilibrium crystallisation of a representative mixture in the system $FeO-TiO_2-SiO_2$ is given in Table (A.4a) in conjunction with Figure (A.3.24). The composition triangles in Figure (A.3.22) can be divided into areas within which all mixtures have a similar sequence of phase changes. A few of these areas are listed in Table (A.4a), the phase assemblages of the mixtures which will be composed in the order in which they appear as the mixture was cooled under equilibrium conditions. For example in the area F_2T, L, m, a of the triangle $FeO-F_2T-F_2S$, and point (m) is the ternary eutectic and all crystallisation of compositions within this triangle are complete at this point. If a liquid of composition (x) is chosen and allowed to cool, the system remains liquid until the liquidus temperature is reached, at which the solid F_2T begins to crystallise. The course of the crystallisation curve from this point to boundary (m-a) follows a straight line drawn through F_2T and x. As the liquid changes in composition from x to y, solid F_2T crystallises. At point y, a second phase appears and the crystallisation curve follows boundary a-m with phases F_2T and FeO crystallising together. At lower temperature of the invariant point (m), the three phases F_2T, FeO and F_2S are in equilibrium with liquid, and below the temperature of the point (m), liquid is absent.

The composition of the solid crystallising at any instant

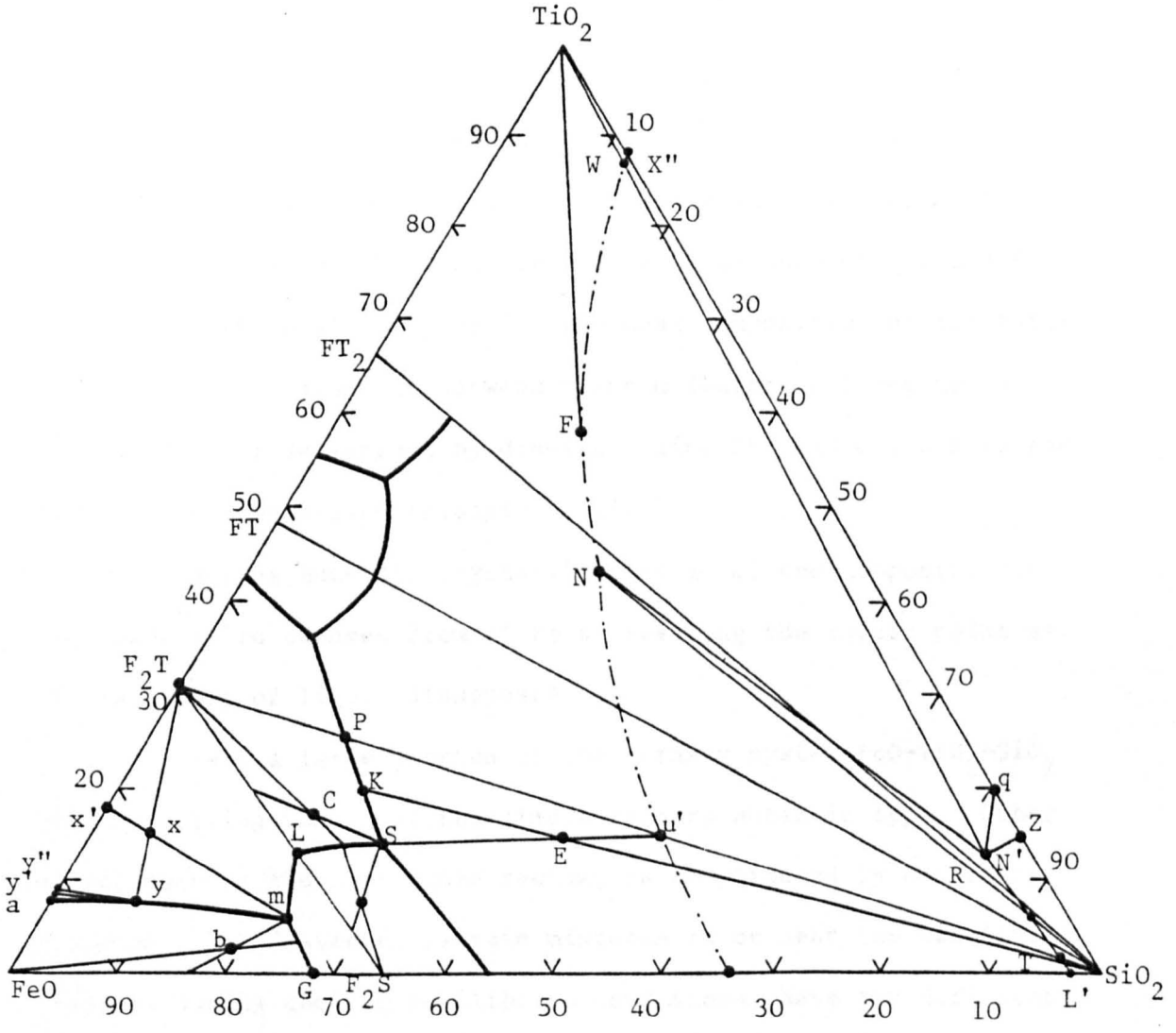

Fig. A.3.24 Designation of areas for description of equilibrium in the $FeO-TiO_2-SiO_2$ system.

along y-m is given at the point where the tangent to the crystallisation curve intersects that side of the composition triangle representing the two solid phases co-existing, i.e. at point y, it is indicated by the intersection of the tangent to the curve m-y-a at the point y with line F_2T-FeO at point y". The ratio of F_2T to FeO is given by the lever y"-FeO/y"-F_2T. The mean composition of the two solid phases that have crystallised between points y and m is represented by the intersection of a line drawn through m and y and the side of composition triangle at y'. In this case it is a mixture of F_2T and FeO in the proportion y'-FeO/y'-F_2T. The mean composition of the total solid which separated out between x and m (before F_2S begins to crystallise) is determined by drawing a line through m and x to the side of the composition triangle at x'.

During eutectic crystallisation at m, the composition of the total solid changes from x' to x, reaching the latter point as the last drop of liquid disappears.

Over a large portion of the ternary system FeO-TiO_2-SiO_2 the crystallisation is of the simple ternary eutectic type. Other parts, such as the two-liquid region, is complicated by peritectic relation. For instance, certain mixtures in or near the two-liquid area can during cooling equilibrium conditions, have two different temperature intervals during which two liquids appear in equilibrium with crystals.

Table A.4a

Triangle Fe_2TiO_4-Fe_2SiO_4-FeO

area L-m-G-F_2S	area m-G-FeO-a
L	L
L + F_2S	L + FeO
F_2S + F_2T + L	F_2S + FeO + L
F_2S + F_2T + FeO +L	FeO + F_2T + F_2S + L
F_2S + F_2T + FeO	FeO + F_2S + F_2T

Triangle Fe_2TiO_4-Fe_2SiO_4-SiO_2

area L-S-P-F_2T	area L-S-V-F_2S
L	L
L + F_2T	L + F_2S
F_2T + F_2S + L	F_2S + F_2T + L
F_2T + F_2S + SiO_2 + L	F_2S + F_2T + SiO_2 + L
F_2T + F_2S + SiO_2	F_2S + F_2T + SiO_2

area SiO_2-P-S-V

L_1 + L_2 (composition expressed along T-Rand T $^{u'}$

SiO_2 + L_1 + L_2

SiO_2 + L (composition of L along u'-P-F_2T

SiO_2 + F_2T + L (k)

SiO_2 + F_2T + F_2S

Triangle TiO_2-SiO_2-F_2T

area TiO_2-W-X"	area N-F-W-N'
L	L_1 + L_2
TiO_2 + L	TiO_2 + L_1 + L_2
TiO_2 + L_1 + L_2	TiO_2 + SiO_2(c) + L_1 + L_2(N_1+N_2)
TiO_2 + SiO_2(c)* + L	
TiO_2 + SiO_2(c)+ L_1 + L_2(N-N')	(area R-N'-N is similar)
TiO_2 + SiO_2(c)+ SiO_2(t)* + L	

Table A.4a (contd.)

area W-X"-N'-q	area SiO_2-R-T
$L_1 + L_2$	L
$TiO_2 + L_1 + L_2$	SiO_2(c) + L
TiO_2 + L	SiO_2(c) + $L_1 + L_2$
$TiO_2 + SiO_2$(c) + L	SiO_2(c) + FT_2 or (TiO_2) + L
$TiO_2 + SiO_2$(c) + L_1+L_2(N-N')	SiO_2(t) + $FT_2 + TiO_2$ + L
$TiO_2 + SiO_2$(c) + SiO_2(t) + L	SiO_2(t) + $FT_2 + TiO_2$
$TiO_2 + SiO_2$(t) + FT_2 + L	
$TiO_2 + SiO_2$(t) + FT_2	(area SiO_2-T-L' is similar)

* SiO_2(c) = cristobalite SiO_2(t) = tridymite

A.3.7 LIQUIDUS TEMPERATURE OF $FeO-Fe_2O_3-TiO_2-SiO_2$ SYSTEM

The quaternary system Fe-Ti-Si-O contains a large number of oxide phases which play important roles in ceramics as well as in the related fields of metallurgy and geochemistry.

The liquidus measurements are important in the selection of the slag compositions. The present study deals with the liquidus surface of this system at different oxygen pressures.

A clear picture of the phase volume relationships in the quaternary system $FeO-Fe_2O_3-TiO_2-SiO_2$ was obtained using a tetrahedral model. This was constructed of transparent paper with vertical planes of the same paper fixed at different oxygen pressure intervals. On the faces of the tetrahedron and on each plane are sketched the phase equilibrium relations. This allows liquidus temperatures throughout the tetrahedron, the approximate location of invariant points, and primary phases volume relationships to be readily seen.

The system $FeO-Fe_2O_3-TiO_2-SiO_2$ is shown as a regular tetrahedron in Figure (A.3.25) with one component at each apex. Phase equilibrium data were fairly complete for one of the boundary ternaries ($FeO-Fe_2O_3-SiO_2$), partially complete for two ($FeO-TiO_2-SiO_2$ and $FeO-Fe_2O_3-TiO_2$) and essentially lacking for the $Fe_2O_3-SiO_2-TiO_2$ system.

The system $Fe_2O_3-SiO_2-FeO$, the right face of the tetrahedron, and $Fe_2O_3-FeO-TiO_2$, the basel plane, have been discussed previously in Chapter 1.

MacChesney and Muan[83] studied the phase relations at liquidus temperatures in the system iron oxide-TiO_2-SiO_2 in air (0.21 atmosphere). The stable existence of the crystalline phases, magnetite (ss), hematite (ss), pseudobrookite(ss), rutile (ss) and silica (tridymite or crystobalite) in equilibrium with liquids in the system, has been established. Three isobaric eutectic situations were shown in the Fe-Ti-Si-O at an oxygen pressure of 0.21 atmosphere. At 1445°C magnetite (ss), hematite (ss) and silica are present together in equilibrium with liquid whose composition is 9% FeO, 73% Fe_2O_3, 3% TiO_2 and 15% SiO_2 (by weight percentage). Another isobaric invariant situation at 1440°C is characterised by the co-existence of hematite (ss), pseudobrookit (ss), silica and liquid of composition 10% FeO, 59% Fe_2O_3, 18% TiO_2 and 13% SiO_2 (by weight percentage). The phase assemblies at the third isobaric invariant situation at 1475°C was pseudobrookit (ss), rutile, silica and a liquid of composition 9% FeO, 29% Fe_2O_3, 52% TiO_2 and 10% SiO_2 (by weight percentage) as shown in Figure (A.3.26).

In the present study experimental work was carried out over a range of oxygen pressures from about 10^{-6} to 10^{-2} atmospheres at 1500°C.

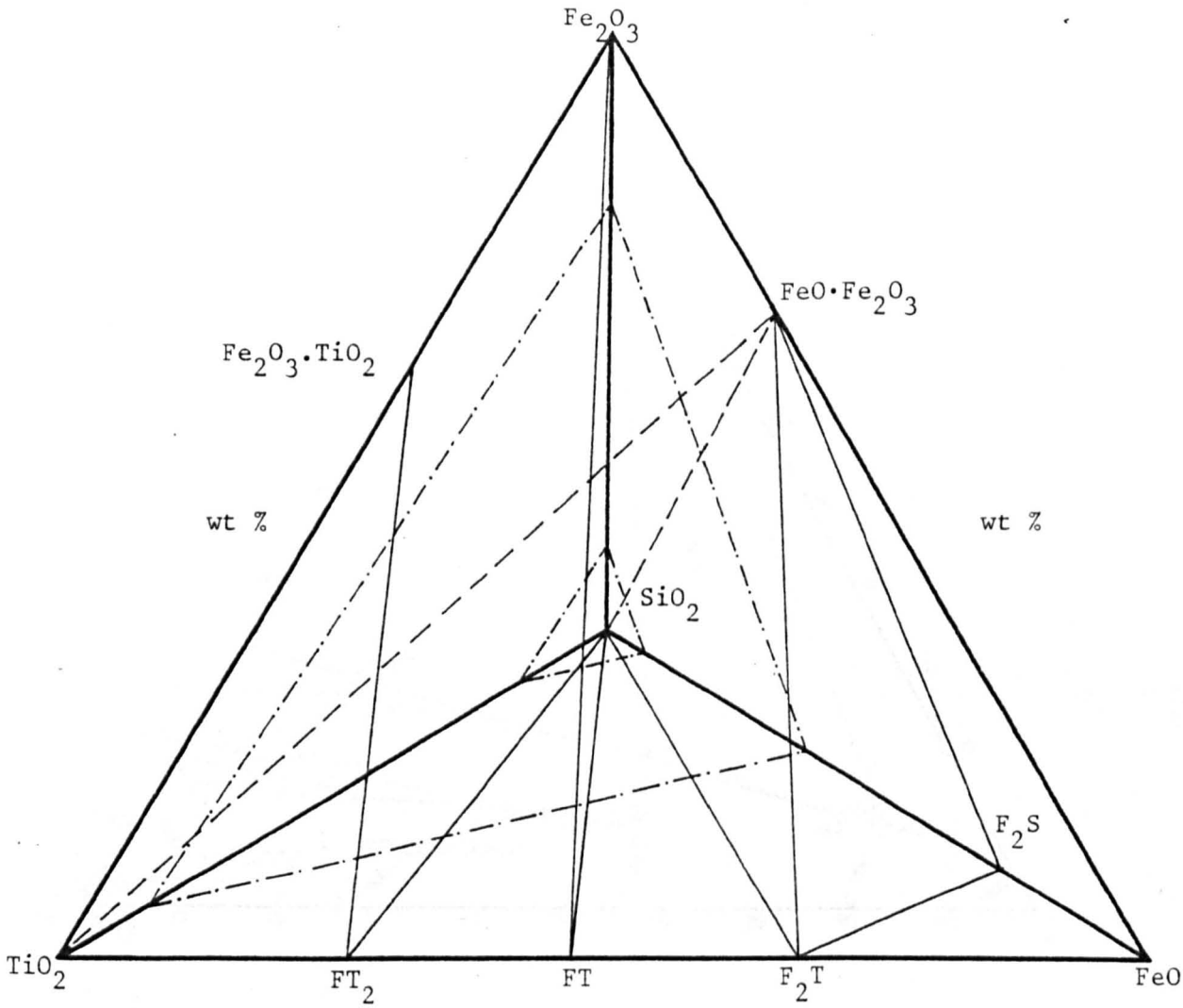

Fig. A.3.25 Diagram representing the system $FeO-Fe_2O_3-TiO_2-SiO_2$ as a regular tetrahedron with one component at each apex.

-·-·- two-liquid region

- - - The plane $FeO.Fe_2O_3-TiO_2-SiO_2$

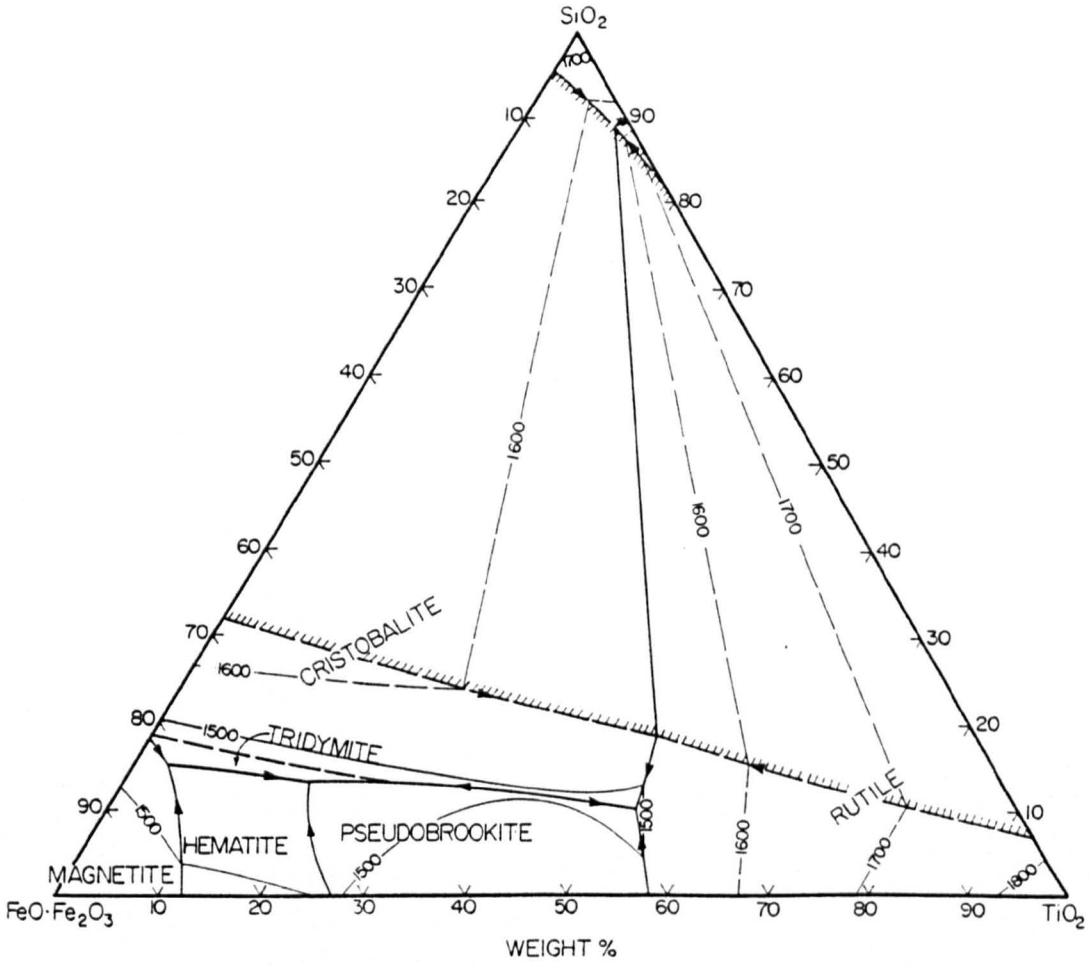

Fig. A.3.26 Phase diagram for ternary system $FeO-SiO_2-TiO_2$ in air, based on data of MacChesney and Muan(83).

The results of the quenching experiments are given in Tables (A.5-A.9) and illustrated in the diagrams of Figures (A.3.27 - A.3.41). Compositions of liquids under the experimental conditions used in this investigation are represented by points located along an irregularly curved surface extending through the tetrahedron representing the system $FeO-Fe_2O_3-TiO_2-SiO_2$, which is part of the system Fe-Ti-Si-O. For the purpose of simple illustration the phase relationships can be represented by projection of these surfaces onto triangular diagrams drawn in the plane of paper. These diagrams are then necessarily distorted pictures, but they are valuable and useful as long as one keeps the true relationship in mind and always refers back to the tetrahedron representing the quaternary system. The data obtained for mixtures along this surface are projected onto the plane $FeO.Fe_2O_3-TiO_2-SiO_2$ and the diagrams obtained have the appearance of a ternary diagram.

The corresponding diagram shown in Figure (A.3.27) is a projection into the plane $FeO.Fe_2O_3-TiO_2-SiO_2$ of phase equilibria in the approximately 10^{-2} atmosphere oxygen isobaric surface.

The crystalline phases co-existing in equilibrium with liquids at oxygen pressures of 10^{-2} atmospheres are suggested to be silica (tridymite or crystobalite), magnetite (ss), hematite (ss), pseudobrookit (ss) and rutile. Accurate compositions of the solid crystals were not determined in this present study, but in general relationships are similar to the situation in air[83]. The curves in these diagrams have not been located accurately, and the diagrams show only in a qualitative way the probable phase relationships.

Holmes et al[84] have studied the effect of titanium oxide on the liquidus temperature for $CaO-MgO-Al_2O_3-TiO_2-SiO_2$ slags. Their

results showed that titanium oxide lowers the liquidus temperature at low concentrations, which is in agreement with Ohno and Ross[40] for slags in the system $CaO-MgO-TiO_2-SiO_2$.

In the present study increase in titanium oxide has not a great effect on the liquidus temperature at $\frac{N_{SiO_2}}{\Sigma N_{Fe}}$ ratio varying from 0.67 to the phase boundary of two-liquid region at given oxygen pressures and over the range studied of the $FeO\cdot Fe_2O_3-TiO_2-SiO_2$ slags. Up to a ratio $\frac{N_{SiO_2}}{\Sigma N_{Fe}}$ of 0.33, titania increases the liquidus temperatures as shown in Figures (A.3.27 - A.3.41). All previous studies[40,84] were made in air or in dry nitrogen and argon (for slags free of iron oxides). Fine and Arac[85] have studied the effects of minor amounts of FeO, MgO, Na_2O and TiO_2 on the liquidus temperature of synthetic blast furnace slags at oxygen pressures of 10^{-15} atmospheres. They found that at low concentration of titanium oxide, the liquidus temperature increases at given oxygen pressure.

It was expected from previous work[40,84] and the present study that titanium oxide will be present as TiO_2, i.e. titanium as Ti^{4+}, but at the low oxygen potential of approximately 10^{-15} atmosphere considerable amounts of the titanium could be as Ti^{3+} and Ti^{2+}. This can be confirmed by using the data on the activity of liquid TiO_2, liquid Ti_2O_3 and liquid TiO at 1800°K[85] i.e.

$$\frac{a_{TiO_2}}{a_{Ti_2O_3}^{\frac{1}{2}}} \simeq 10^3 \, Po_2^{\frac{1}{4}} \qquad \text{(A.3.1)}$$

$$\frac{a_{Ti_2O_3}^{\frac{1}{2}}}{a_{TiO}} \simeq 10^{14} \, Po_2^{\frac{1}{4}} \qquad \text{(A.3.2)}$$

$$\frac{a_{TiO_2}}{a_{TiO}} \simeq 10^7 \, Po_2^{\frac{1}{2}} \qquad \text{(A.3.3)}$$

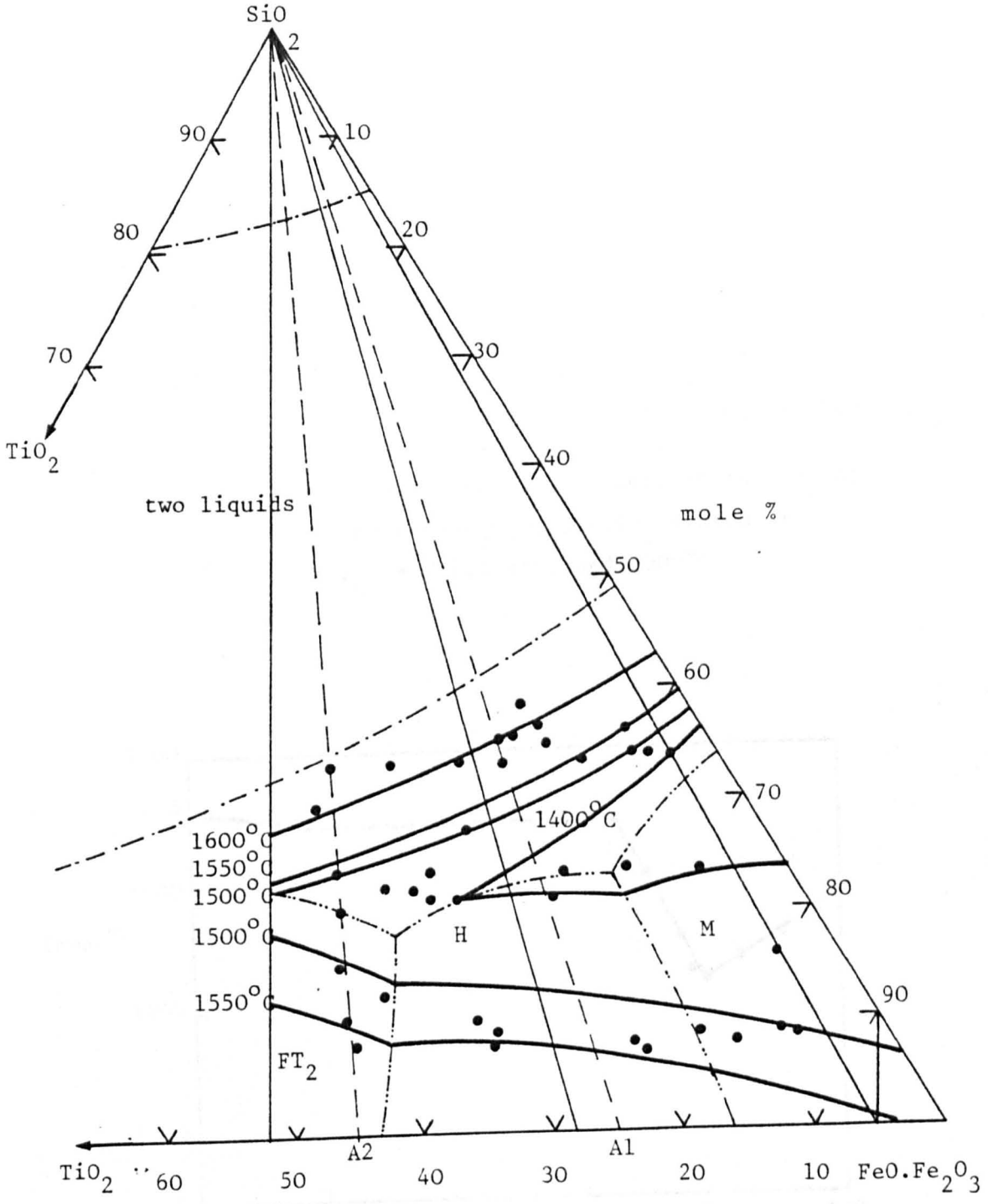

Fig. A.3.27 Liquidus temperatures in the $FeO.Fe_2O_3$-SiO_2-TiO_2 system at P_{O_2} = 0.021 atm. and 1500°C (Table A.5)

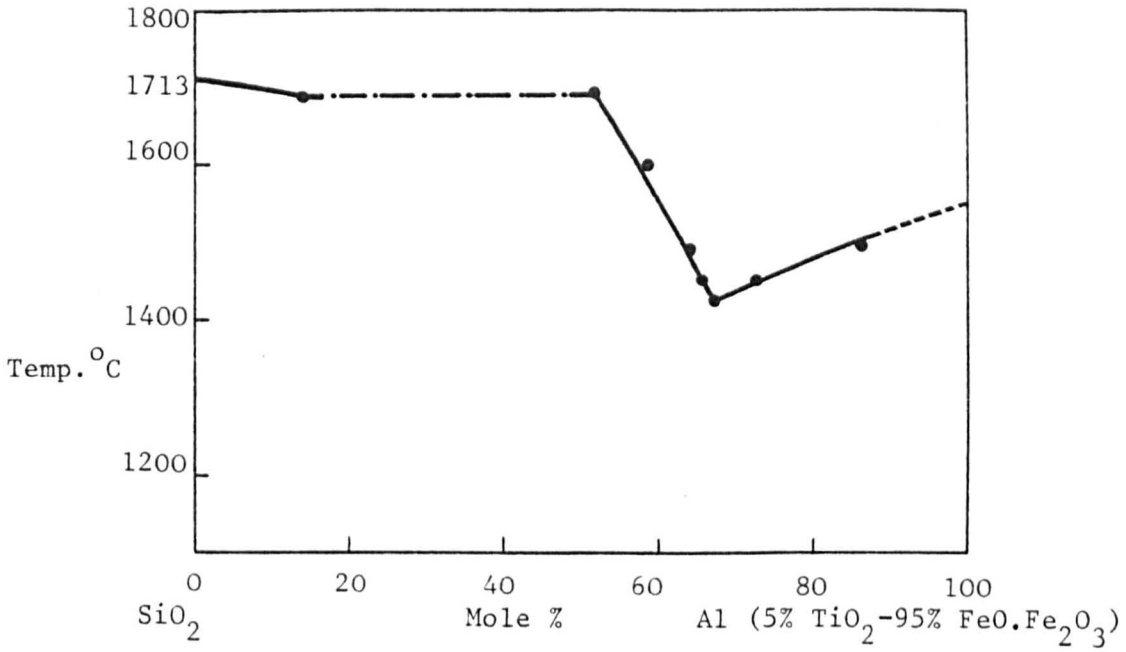

Fig. A.3.28 Liquidus profile of section on SiO_2-Al in the $FeO-Fe_2O_3-SiO_2-TiO_2$ system at P_{O_2} = 0.021 atm. and 1500°C.

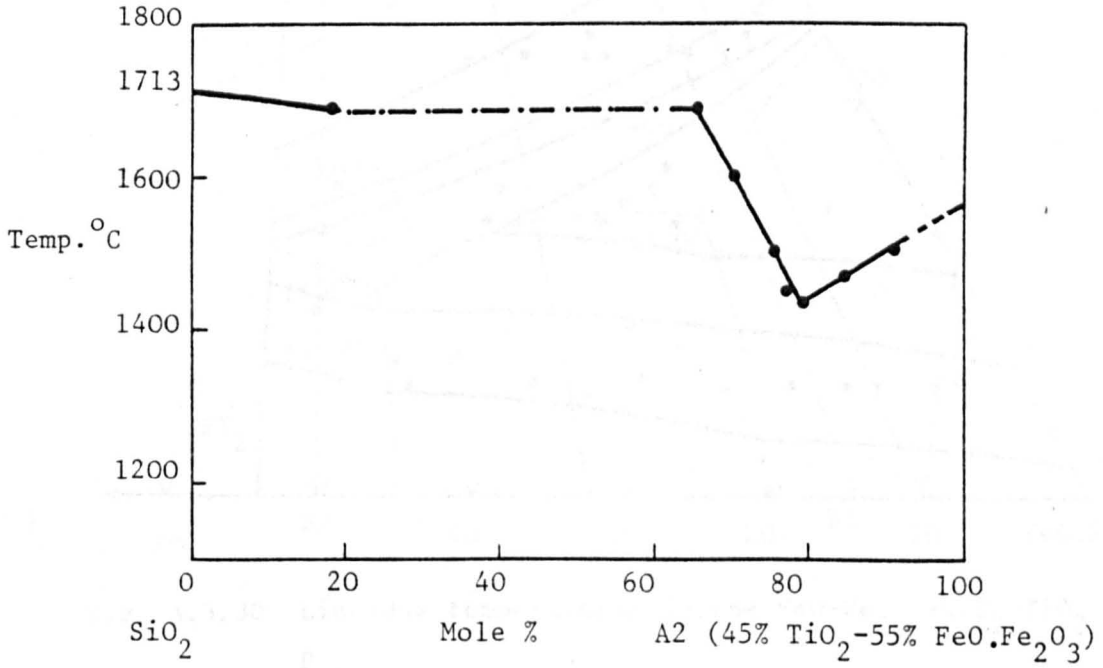

Fig. A.3.29 Liquidus profile of section on SiO_2-A2 in the $FeO-Fe_2O_3-SiO_2-TiO_2$ system at P_{O_2} = 0.021 atm. and 1500°C.

-·-·- two liquid region.

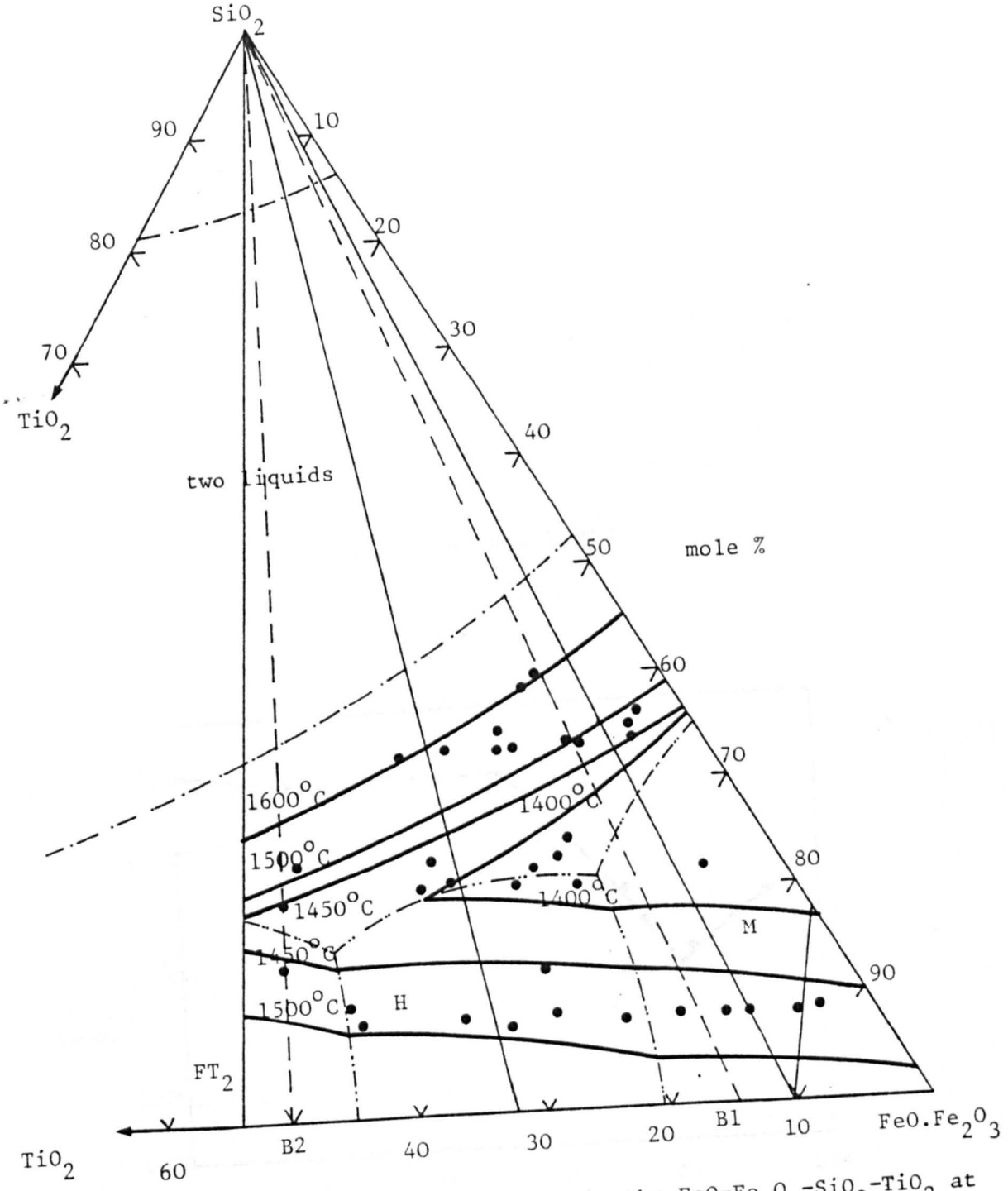

Fig. A.3.30 Liquidus temperatures in the $FeO-Fe_2O_3-SiO_2-TiO_2$ at $\frac{P_{CO_2}}{P_{CO}} = 249$ and 1500°C (Table A.6).

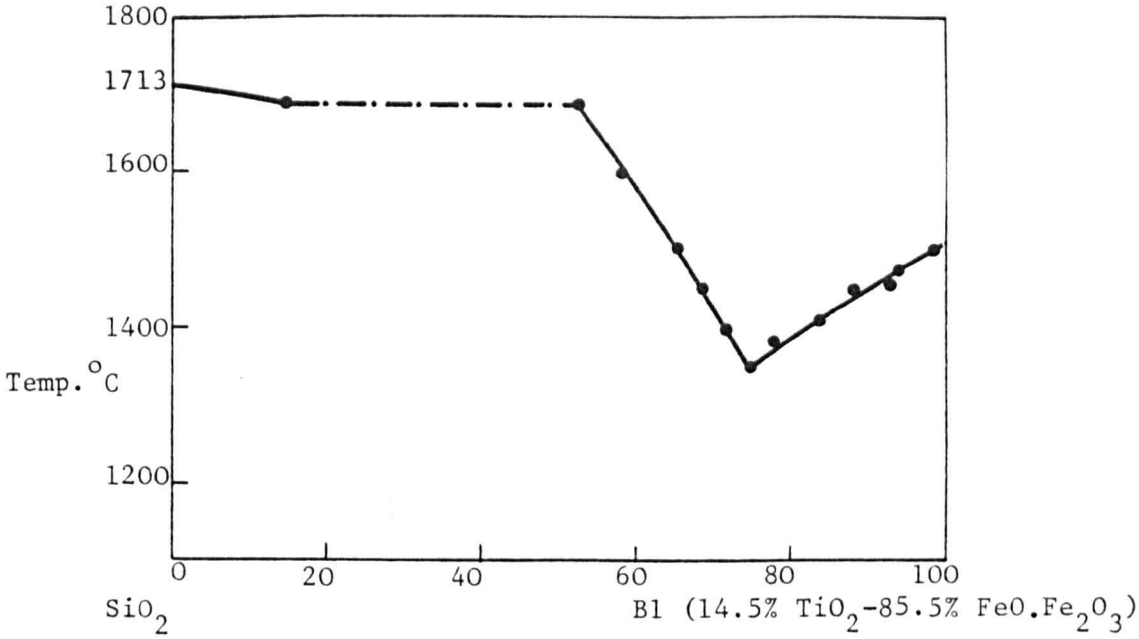

Fig. A.3.31 Liquidus profile of section on SiO_2-B1 in the system $FeO-Fe_2O_3-SiO_2-TiO_2$ at $\frac{P_{CO_2}}{P_{CO}}$ = 249 and 1500°C.

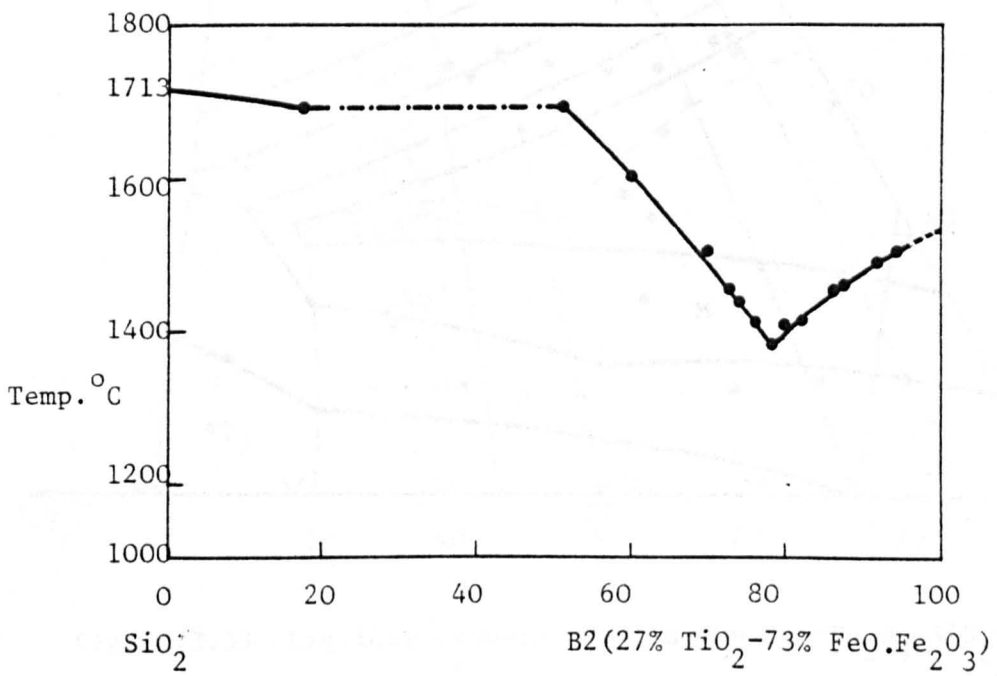

Fig. A.3.32 Liquidus profile of section on SiO_2-B2 in the $FeO-Fe_2O_3-SiO_2-TiO_2$ at $\frac{P_{CO_2}}{P_{CO}}$ = 249 and 1500°C.

-·-·- two liquid region.

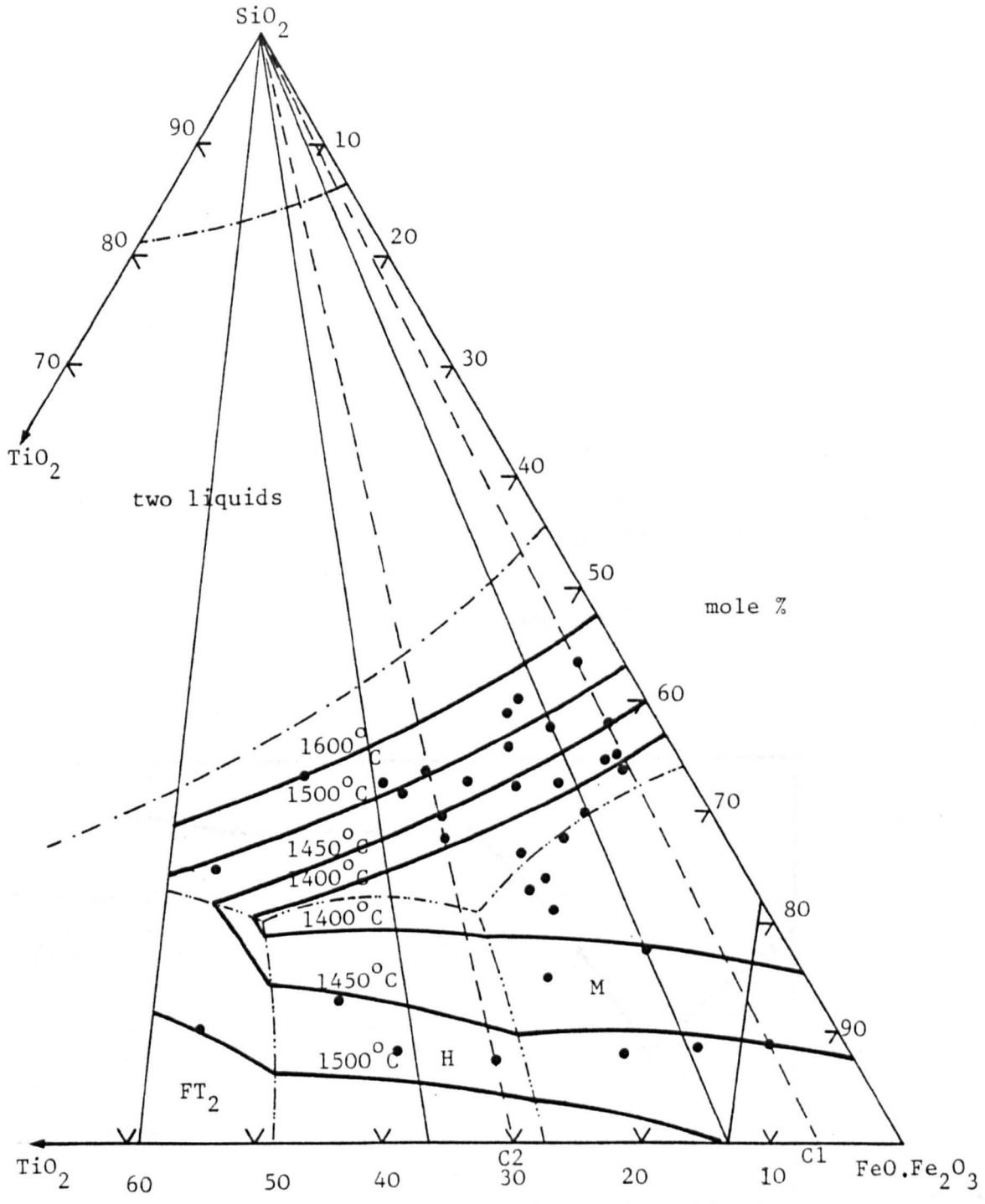

Fig. A.3.33 Liquidus temperatures in the $FeO-Fe_2O_3-SiO_2-TiO_2$ system at $\frac{P_{CO_2}}{P_{CO}} = 135.36$ and 1500°C (Table A.7).

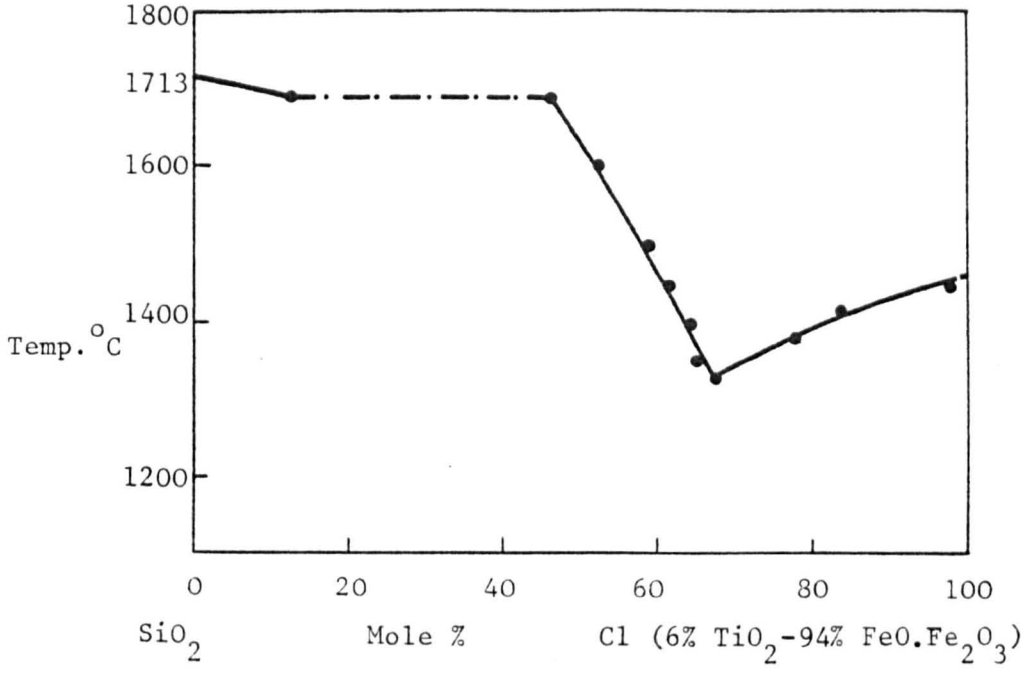

Fig. A.3.34 Liquidus temperature of section on SiO_2-Cl in the $FeO-Fe_2O_3-SiO_2-TiO_2$ system at $\frac{P_{CO_2}}{P_{CO}}$ = 135.36 and 1500°C.

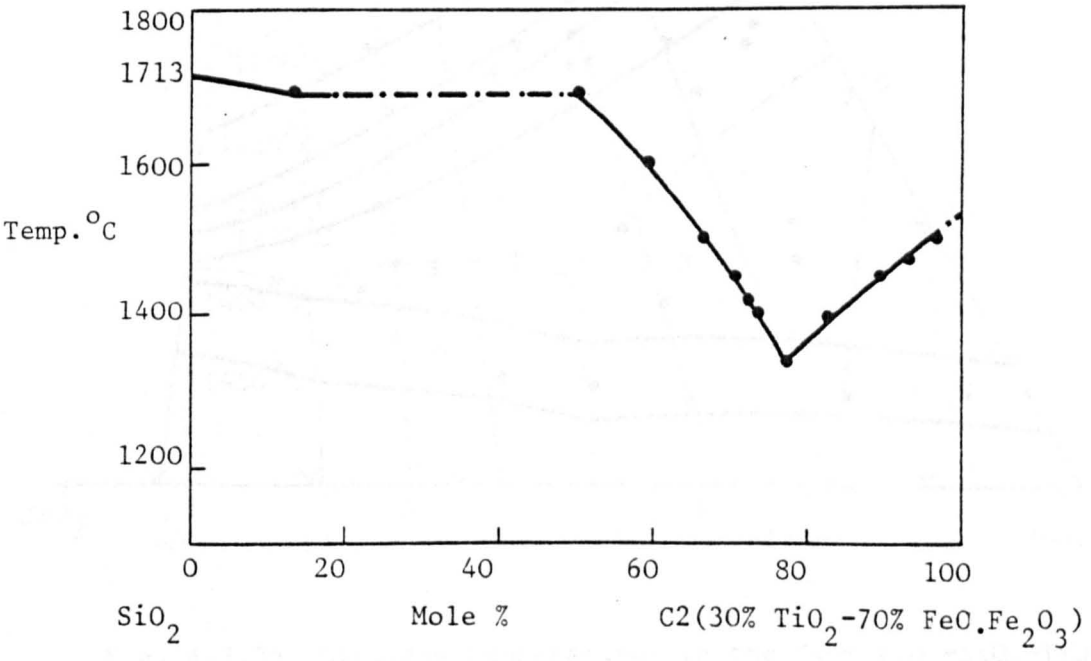

Fig. A.3.35 Liquidus profile of section on SiO_2-C2 in the $FeO-Fe_2O_3-SiO_2-TiO_2$ system at $\frac{P_{CO_2}}{P_{CO}}$ = 135.36 and 1500°C.

-·-·- two liquid region.

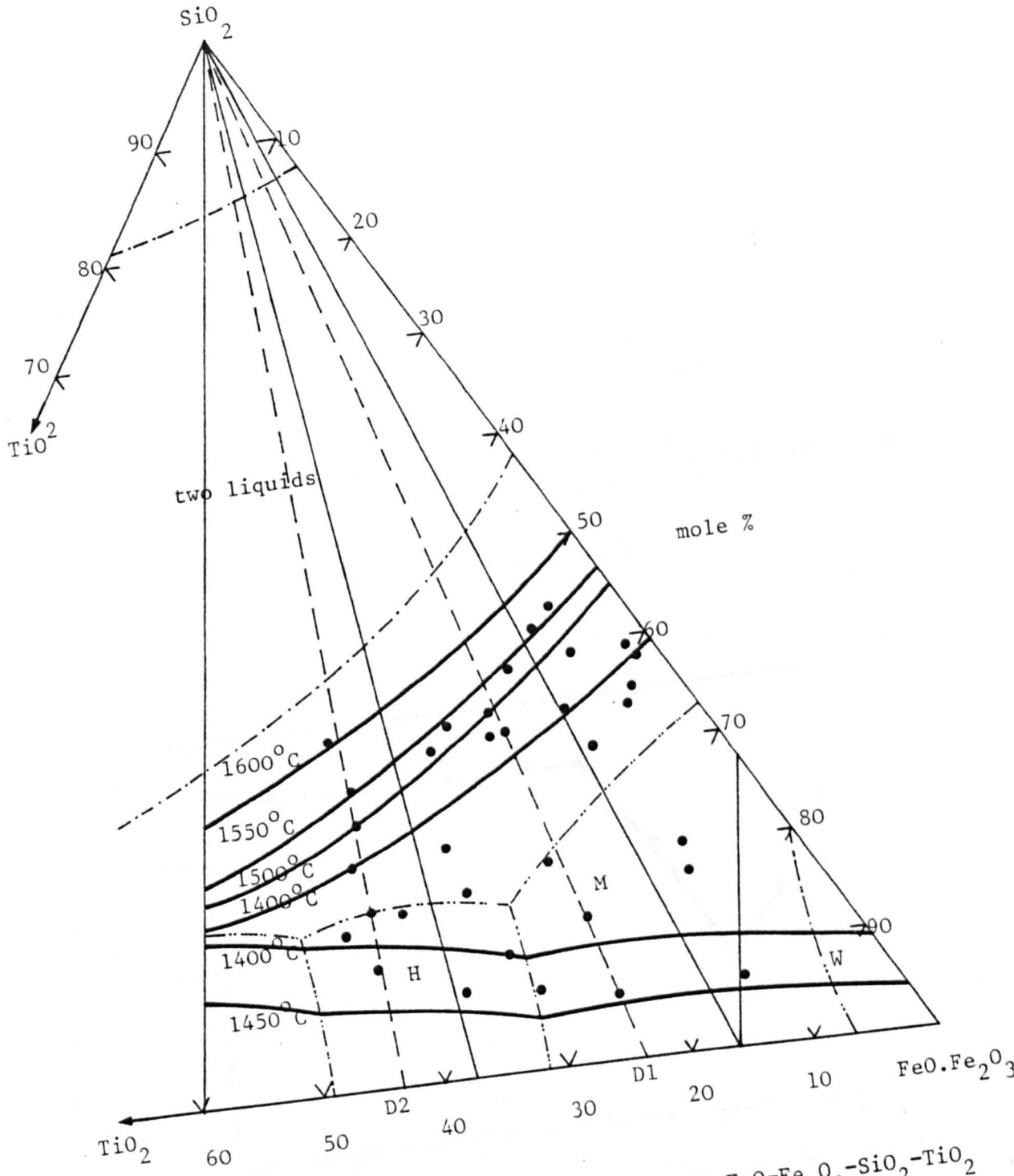

Fig. A.3.36 Liquidus temperatures in the $FeO-Fe_2O_3-SiO_2-TiO_2$ system at $\frac{P_{CO_2}}{CO} = 20.99$ and 1500°C. (Table A.8)

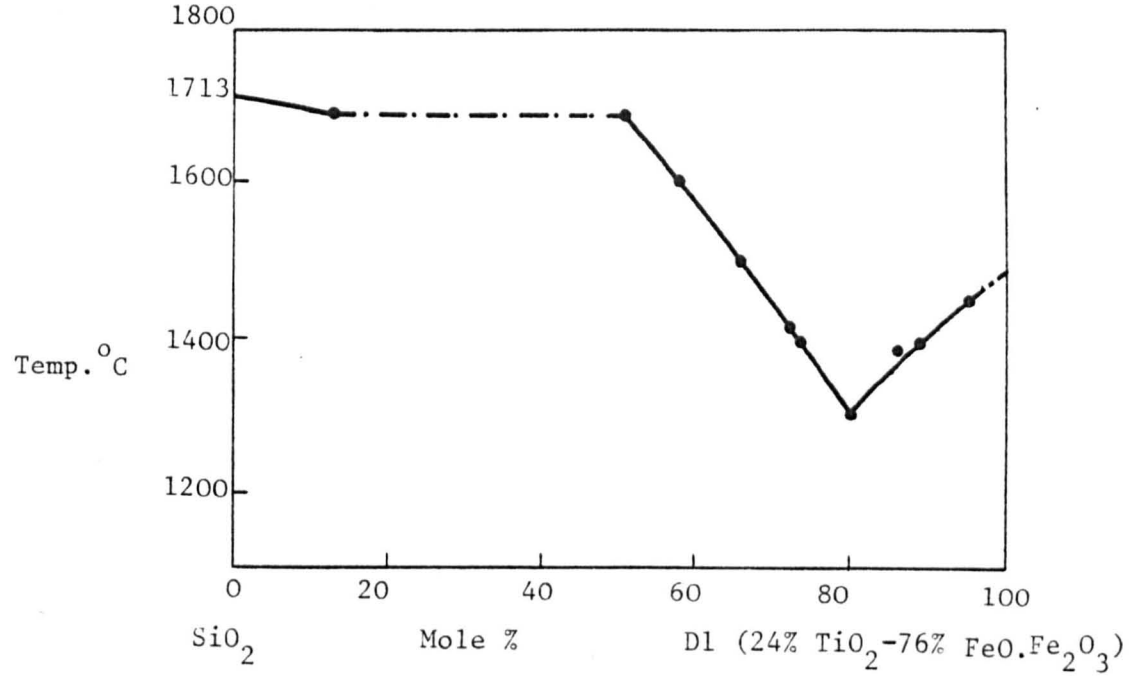

Fig. A.3.37 Liquidus profile of section on SiO_2-D1 in the $FeO-Fe_2O_3-SiO_2-TiO_2$ system at $\frac{P_{CO_2}}{P_{CO}} = 20.99$ and $1500^{\circ}C$

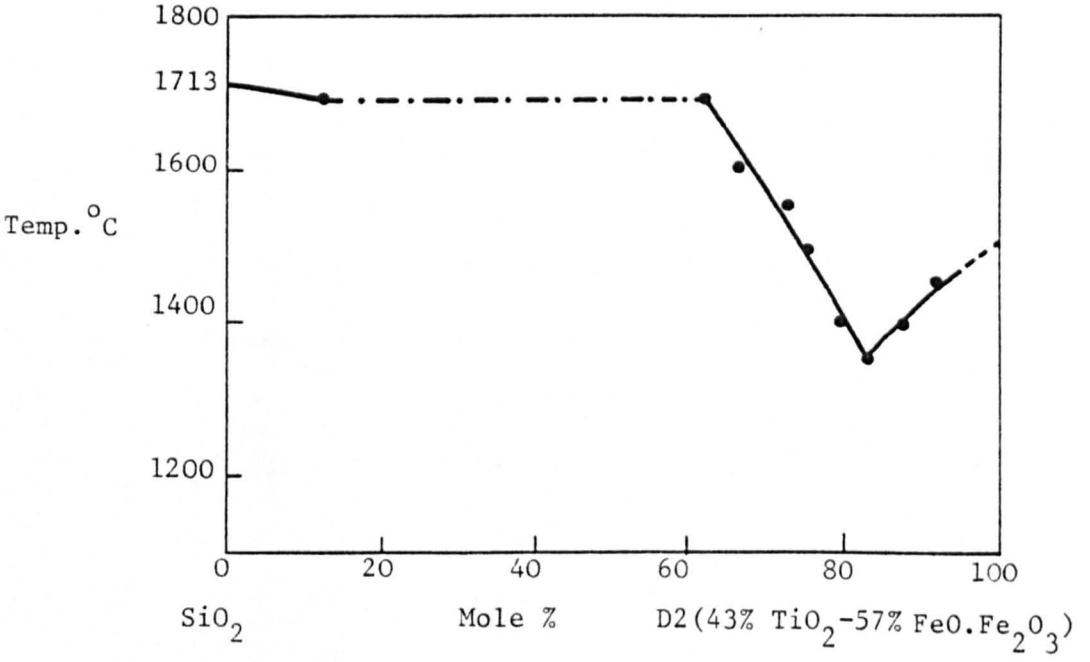

Fig. A.3.38 Liquidus profile of section on SiO_2-D2 in the $FeO-Fe_2O_3-SiO_2-TiO_2$ system at $\frac{P_{CO_2}}{P_{CO}} = 20.99$ and $1500^{\circ}C$.

-·-·- two-liquid region.

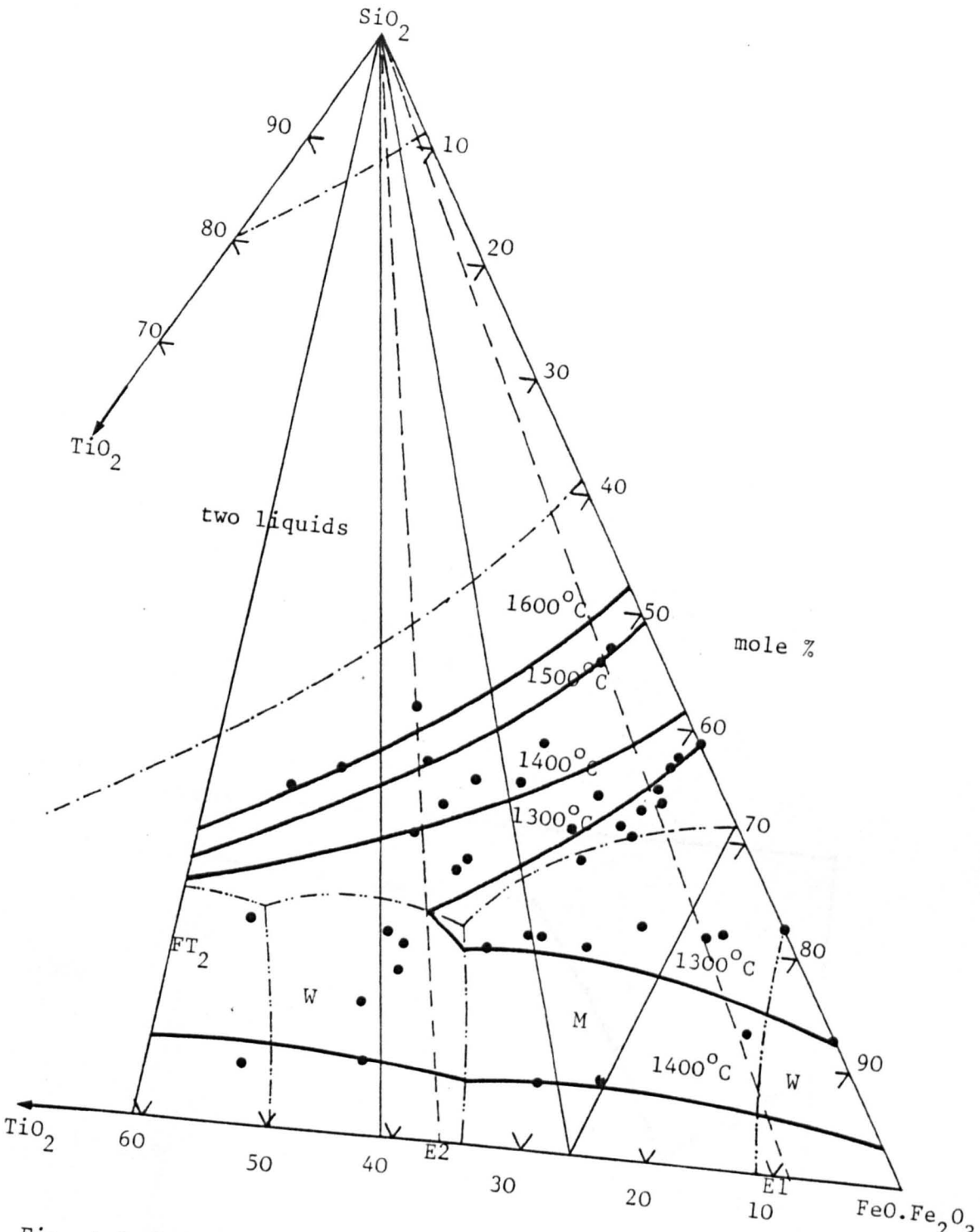

Fig. A.3.39 Liquidus temperatures in the $FeO-Fe_2O_3-SiO_2-TiO_2$ system at $\frac{P_{CO_2}}{P_{CO}} = 6.71$ and 1500^oC (Table A.9).

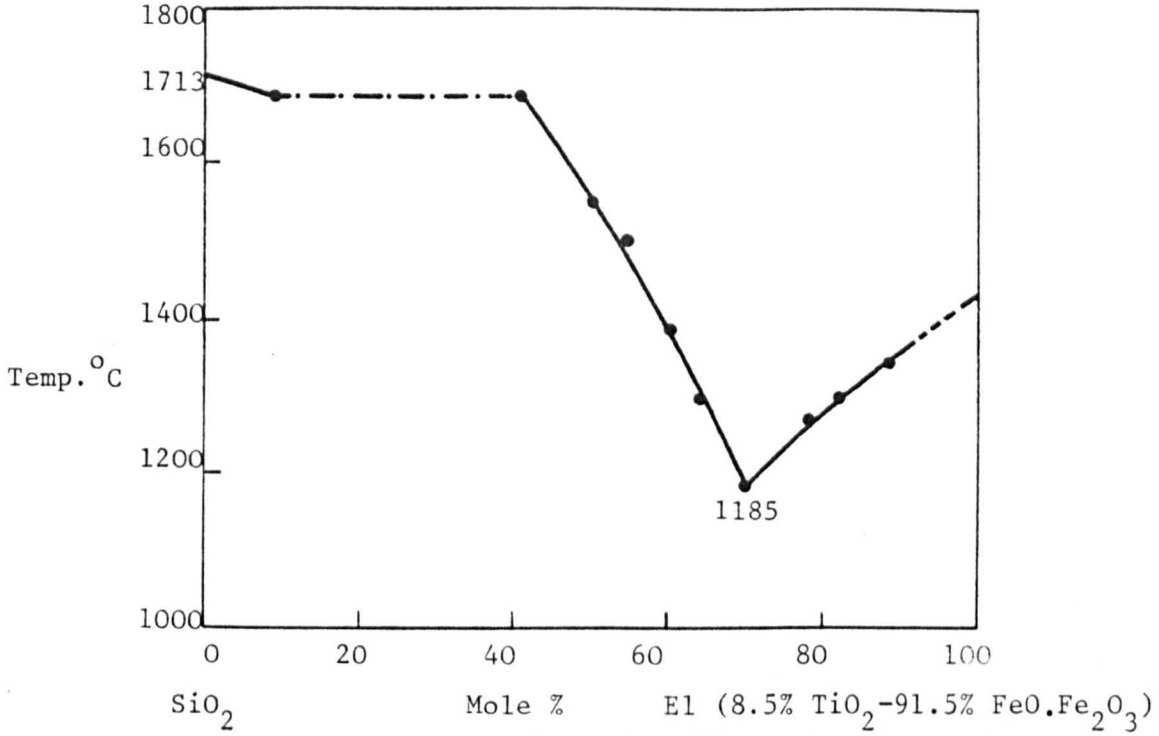

Fig. A.3.40 Liquidus profile of section on the SiO_2-E1 in the $FeO-Fe_2O_3-SiO_2-TiO_2$ system at $\frac{P_{CO_2}}{P_{CO}}$ = 6.71 and 1500°C

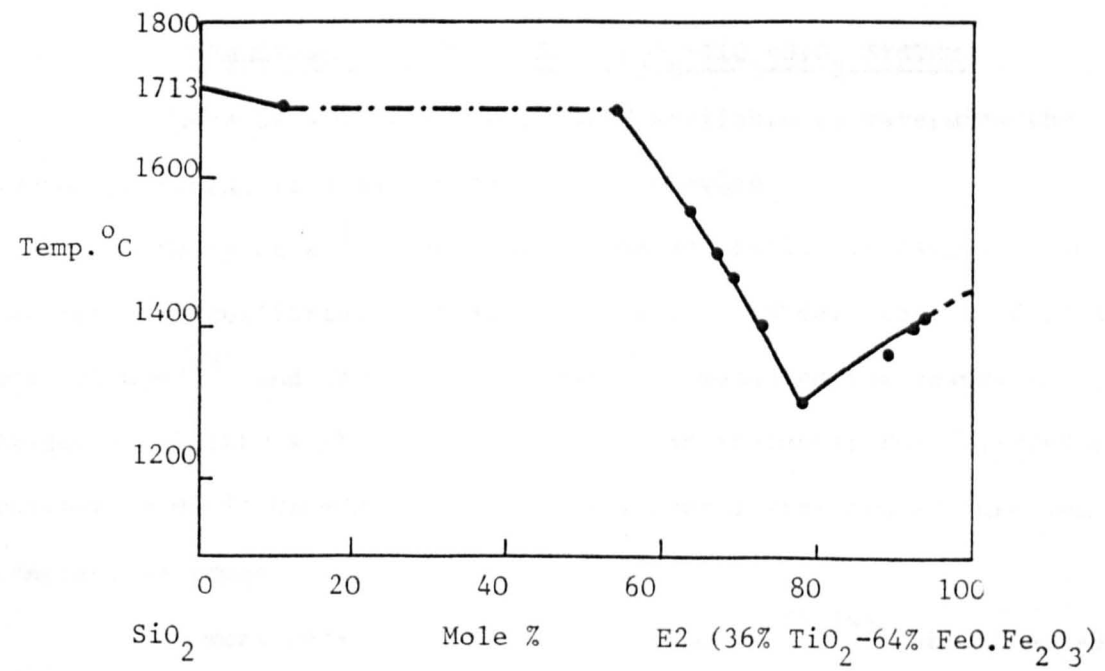

Fig. A.3.41 Liquidus profile of section on SiO_2-E2 in the $FeO-Fe_2O_3-SiO_2-TiO_2$ system at $\frac{P_{CO_2}}{P_{CO}}$ = 6.71 and 1500°C.

-·-·- two liquid region.

As mentioned previously in Chapter 1 several investigators have studied the effect of titania on the viscosities of blast furnace slags. It is interesting to note that the sub-oxides Ti_2O_3 and TiO reduce the viscosity more than TiO_2.

Baldwin[86] studied the relationship between temperature and viscosity on blast furnace slags containing iron-oxide, manganese oxide and sulphur. Baldwin showed that the viscosity of blast furnace slags decreases with the increase in temperature. Thus, the viscosity of slags containing titanium oxide was found to be strongly dependent on the oxygen potential. At higher oxygen pressures, titanium oxide has no effect on the liquidus temperature for slags containing iron oxide while at the same oxygen potential TiO_2 decreases the liquidus temperature at low concentration for slags free of iron oxide. At low oxygen potentials, titanium oxide increases the liquidus temperature of blast furnace slags.

A.3.8 THERMODYNAMIC STUDY OF $FeO-Fe_2O_3-TiO_2-SiO_2$ SYSTEM

There is a wide range of data available to determine the oxygen potential of slags containing iron oxide.

Harty et al[87] determined the solubility of oxygen in molten iron in equilibrium with almost pure iron oxide. Later, Fellers and Chipman[88] and Taylor and Chipman[89] measured the change in oxygen solubility with slag composition and evaluated the activity of ferrous oxide in $CaO-MgO-FeO-SiO_2$ slags over a wide temperature and composition range.

In more recent years Darken and Gurry[25,26] made an extensive study of the iron-oxygen system within the range 1100-1600°C by equilibrating the oxides of iron with various gases of known oxygen

potential. Gurry and Darken[90] subsequently determined the dissociation pressure of ferric oxide in $CaO-FeO-Fe_2O_3$ and $MnO-FeO-Fe_2O_3$ ternary melts at several oxygen pressures and at about 1600°C.

Schuhmann and Ensio[22] and Michal and Schuhmann[27] studied the state of equilibrium in the $FeO-Fe_2O_3-SiO_2$ system saturated with γ-iron or silica or both under low oxygen potentials and within the temperature range 1250-1350°C. Larson and Chipman[91] studied the $CaO-FeO-Fe_2O_3$ and $CaO-FeO-Fe_2O_3-SiO_2$ slags at 1550°C.

The general conclusion to be drawn from the work mentioned above may be summarised that the activities of ferrous and ferric oxides in simple and complex slags deviate from Raoult's law in varying degreees. The ratio $\frac{Fe^{3+}}{Fe^{2+}}$ increases with oxygen potential for a given temperature and slag composition, and decreases with increasing temperature for a given oxygen pressure and slag composition.

All the experiments in the present study were carried out on the system $FeO-Fe_2O_3-TiO_2-SiO_2$ as mentioned previously at 1500°C with gas ratio $\frac{P_{Co_2}}{P_{Co}}$ = 6.71,20.99,135.36,249 and oxygen pressure of 0.021 atmosphere. These experimental results are given in Tables (A.5 - A.9) for these gas ratios. For convenience, the slag composition is given in terms of weight percentages of oxides, mole fractions of oxides and atom fractions of the constituent elements, together with calculated ratios of $\frac{Fe^{3+}}{Fe^{2+}}$.

The proportions of divalent and trivalent iron are affected appreciably by the slag composition, i.e. $\frac{Fe^{3+}}{Fe^{2+}}$ decreases with the increase in both TiO_2 and SiO_2 content in the melts at $\frac{P_{CO_2}}{P_{CO}}$ = 6.71 as shown in Figs. A.2.42 and A.3.43. The reaction studied in this work may be represented by the expression

$$2Fe^{2+} + CO_2 = 2Fe^{3+} + O^{2-} + CO \qquad (A.3.4)$$

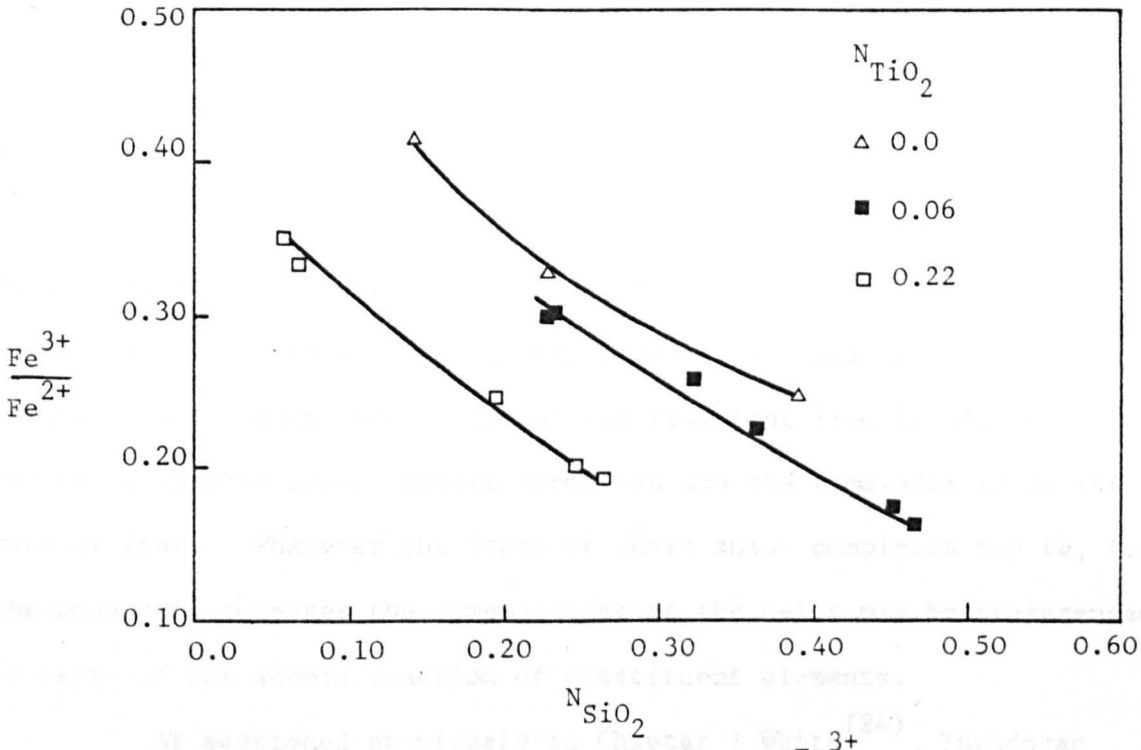

Fig. A.3.42 Effect of silica on the $\frac{Fe^{3+}}{Fe^{2+}}$ ratio in the $FeO-Fe_2O_3-SiO_2-TiO_2$ system at $\frac{P_{CO_2}}{P_{CO}} = 6.71$ and 1500°C.

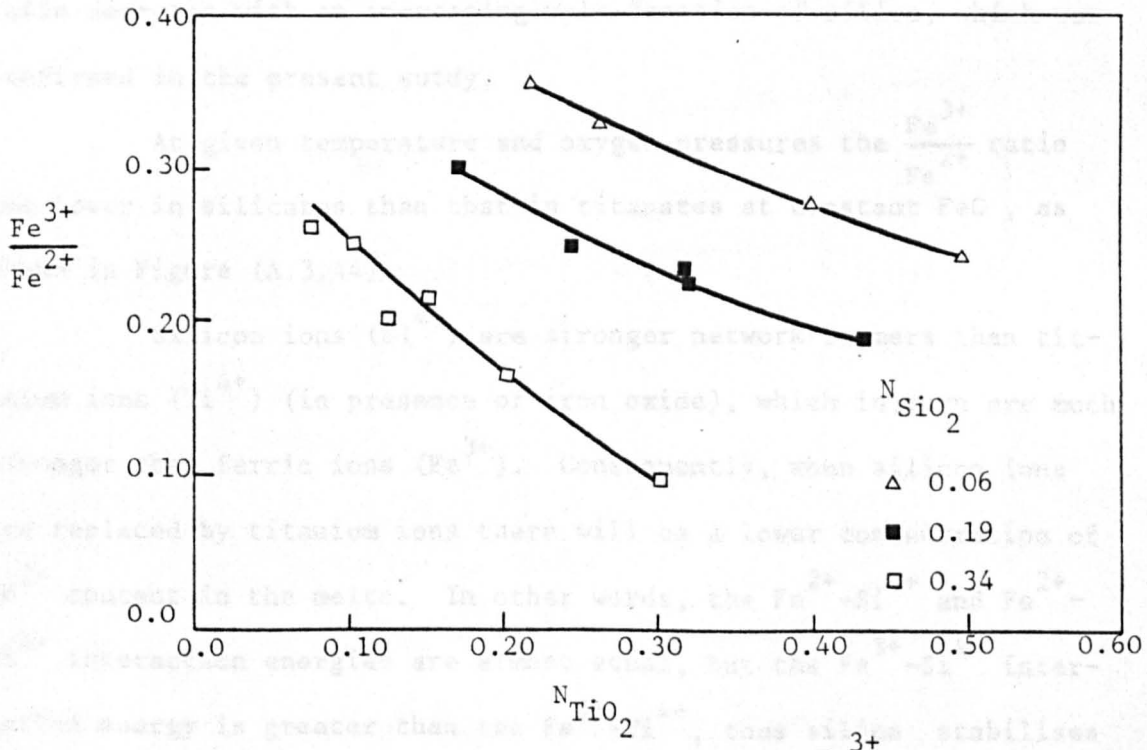

Fig. A.3.43 Effect of titania on the $\frac{Fe^{3+}}{Fe^{2+}}$ ratio in the $FeO-Fe_2O_3-SiO_2-TiO_2$ system at $\frac{P_{CO_2}}{P_{CO}} = 6.71$ and 1500°C.

or $$2Fe^{2+} + \tfrac{1}{2} O_2 = 2Fe^{3+} + O^{2-} \qquad (A.3.5)$$

For a given temperature and gas ratio any change in the composition of the melt can be related to the behaviour of the system. It is probable that in molten ferrites, silicates, titanates and their mixtures, silicon and titanium are bonded with oxygen ions forming networks or ring-link anion complexes. Part of the trivalent iron is also co-ordinated in this anion complex formation and the remainder is in the catonic state. Whatever the state of these anion complexes may be, for thermodynamic purposes,the compositions of the melts may be represented in terms of the atomic fraction of constituent elements.

As mentioned previously in Chapter 1 White[24], Turkdogan and Bills[92] and Timucin and Morris[93] have measured the oxygen dissociation pressure of various ternary and quaternary systems containing iron oxide. Their results showed that the values of the $\frac{Fe^{3+}}{Fe^{2+}}$ ratio decrease with an increasing mole fraction of silica, which was confirmed in the present sutdy.

At given temperature and oxygen pressures the $\frac{Fe^{3+}}{Fe^{2+}}$ ratio was lower in silicates than that in titanates at constant FeO , as shown in Figure (A.3.44).

Silicon ions (Si^{4+}) are stronger network-formers than titanium ions (Ti^{4+}) (in presence of iron oxide), which in turn are much stronger than ferric ions (Fe^{3+}). Consequently, when silicon ions are replaced by titanium ions there will be a lower concentration of Fe^{2+} content in the melts. In other words, the Fe^{2+}-Si^{4+} and Fe^{2+}-Ti^{4+} interaction energies are almost equal, but the Fe^{3+}-Si^{4+} interaction energy is greater than the Fe^{3+}-Ti^{4+}, thus silica stabilises Fe^{2+} more than titania.

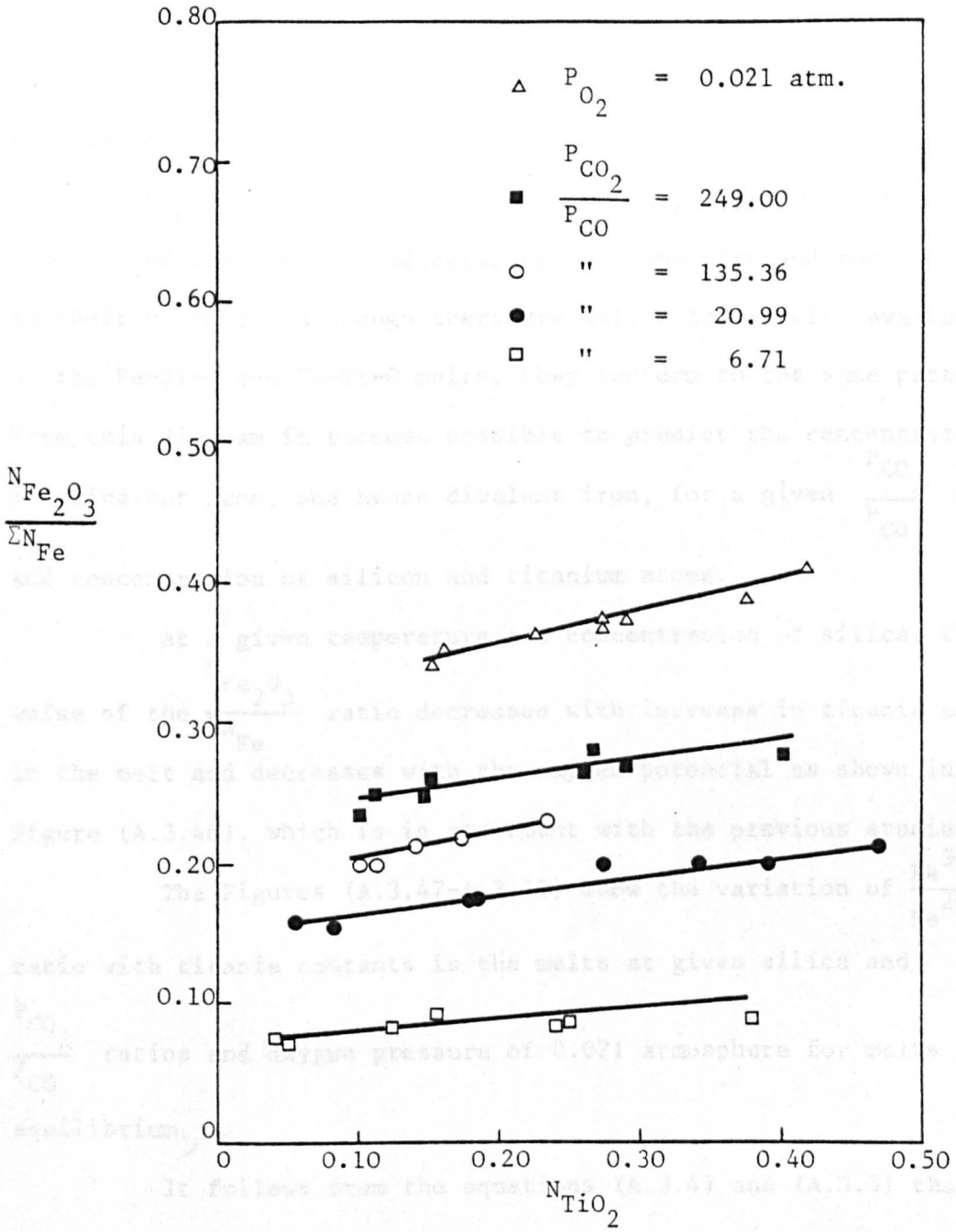

Fig. A.3.44 Variation of ferric iron with $N_{SiO_2}+N_{TiO_2} = 0.50$ and constant N_{FeO} in $FeO-Fe_2O_3-SiO_2-TiO_2$ system at varying $\frac{P_{CO_2}}{P_{CO}}$ ratios and 1500°C.

As already indicated, silicates reduce the $\frac{Fe^{3+}}{Fe^{2+}}$ ratio concentration more than the titanates. It was therefore necessary to find a relationship whereby the combined effect of these two components can be represented in a simple manner. As shown in Figure (A.3.45), $N_{Fe^{3+}}$ is plotted against $4N_{Si} + 4N_{Ti}$ where N is the atom fraction of the element indicated by the subscript and the factor 4 is their valency. Although there are only a few results available on the Fe-Si-O and Fe-Ti-O melts, they conform to the same pattern. From this diagram it becomes possible to predict the concentration of trivalent iron, and hence divalent iron, for a given $\frac{P_{CO_2}}{P_{CO}}$ ratio and concentration of silicon and titanium atoms.

At a given temperature and concentration of silica, the value of the $\frac{N_{Fe_2O_3}}{\Sigma N_{Fe}}$ ratio decreases with increase in titania content in the melt and decreases with the oxygen potential as shown in Figure (A.3.46), which is in agreement with the previous studies.

The Figures (A.3.47-A.3.50) show the variation of $\frac{Fe^{3+}}{Fe^{2+}}$ ratio with titania contents in the melts at given silica and $\frac{P_{CO_2}}{P_{CO}}$ ratios and oxygen pressure of 0.021 atmosphere for melts in equilibrium.

It follows from the equations (A.3.4) and (A.3.5) that for given temperature and oxygen pressure, a decrease in the oxide ion ($\bar{O}$) activity of the melt increases the activity ratio $\frac{a_{Fe^{3+}}}{a_{Fe^{2+}}}$. Since silicon ions and titanium ions form complex anions with oxygen, the oxide ion activity of the slag decreases with increases in silica and titania content and this brings about a rise in activity ratio $\frac{a_{Fe^{3+}}}{a_{Fe^{2+}}}$.

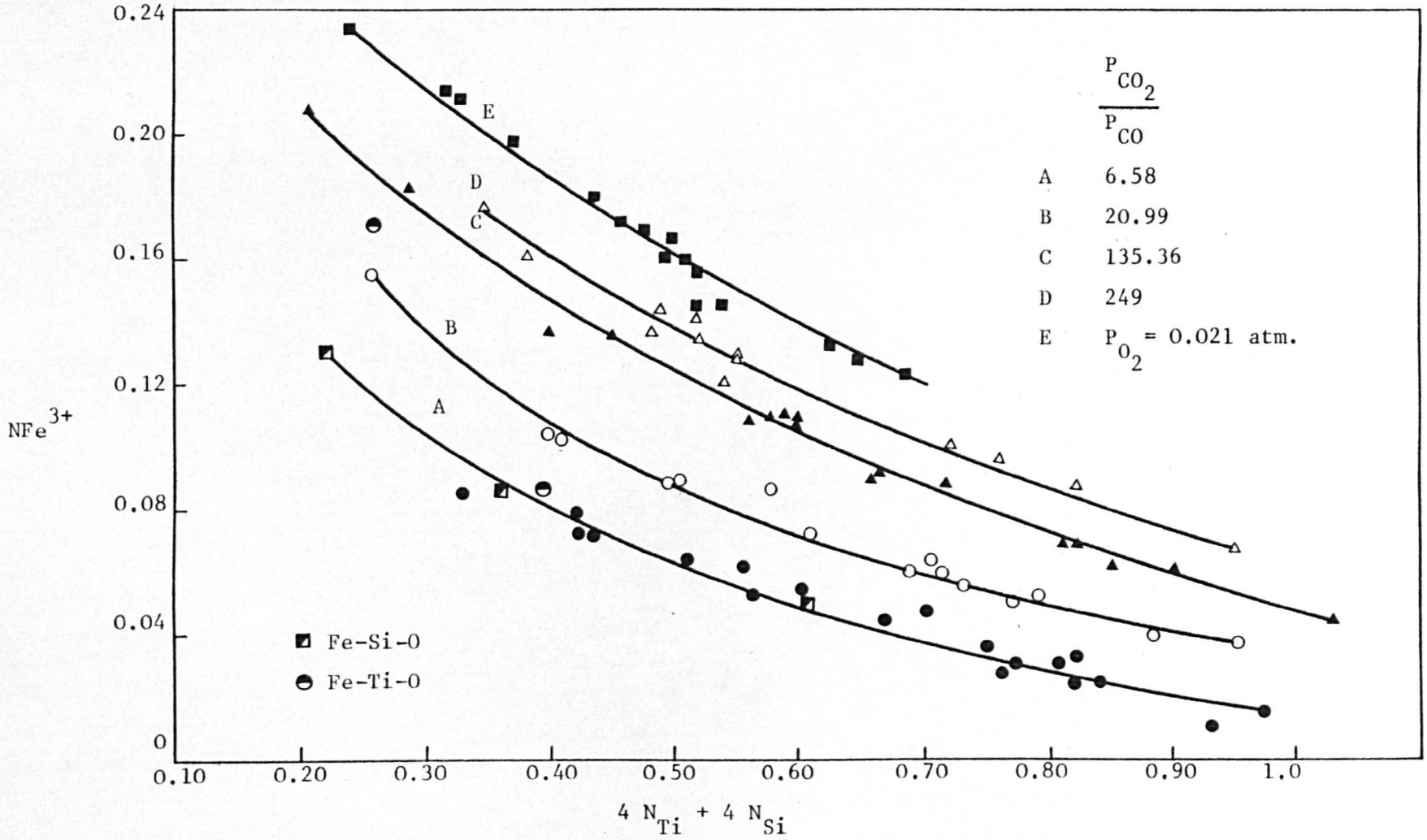

Fig. A.3.45 Variation of ferric iron with titanium and silicon concentrations in Fe-Si-Ti-O system at varying $\frac{P_{CO_2}}{P_{CO}}$ ratios and 1500°C.

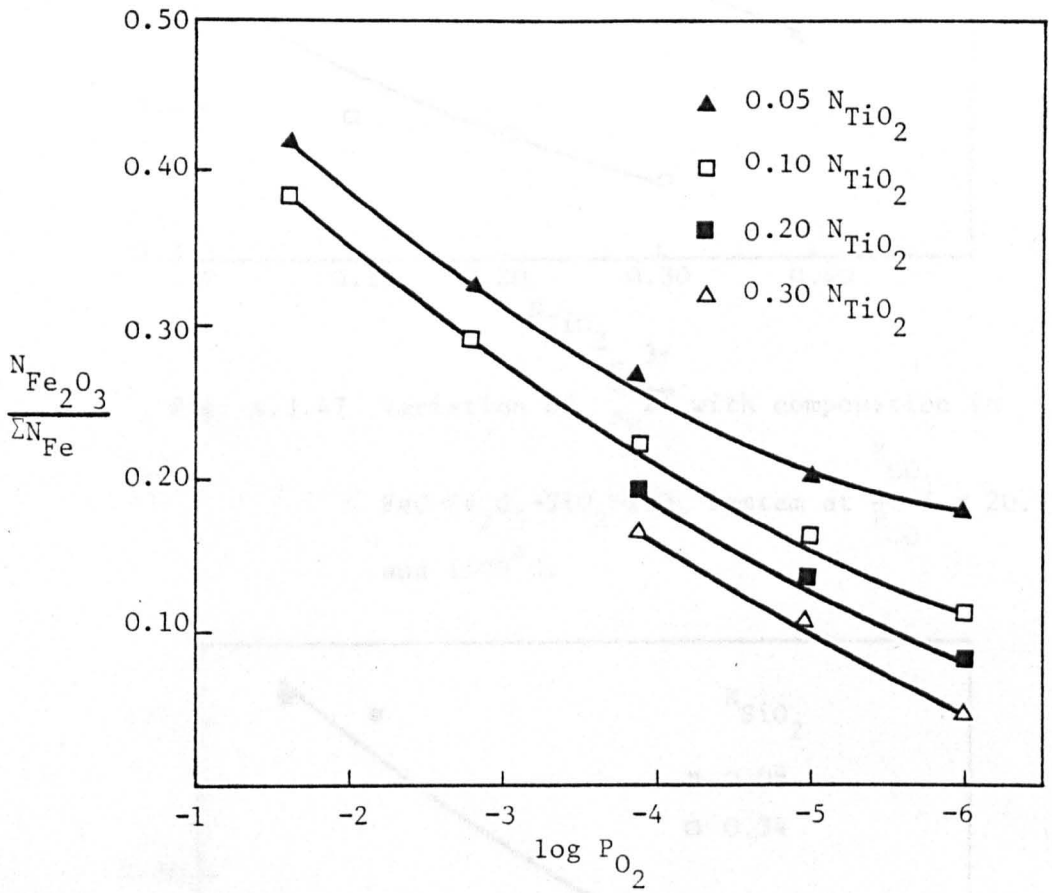

Fig. A.3.46 Variation of $\frac{N_{Fe_2O_3}}{\Sigma N_{Fe}}$ with titanate and gas composition in the $FeO-Fe_2O_3-SiO_2-TiO_2$ system at 0.34 N_{SiO_2} and 1500°C.

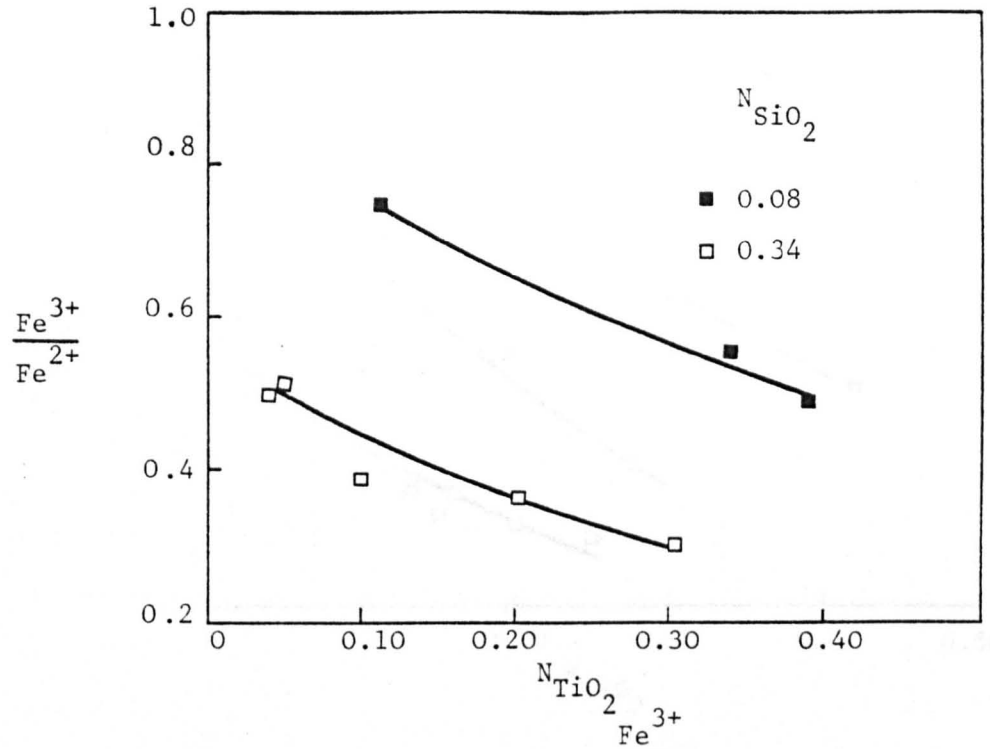

Fig. A.3.47 Variation of $\frac{Fe^{3+}}{Fe^{2+}}$ with composition in $FeO-Fe_2O_3-SiO_2-TiO_2$ system at $\frac{P_{CO_2}}{P_{CO}} = 20.99$ and $1500^{o}C$.

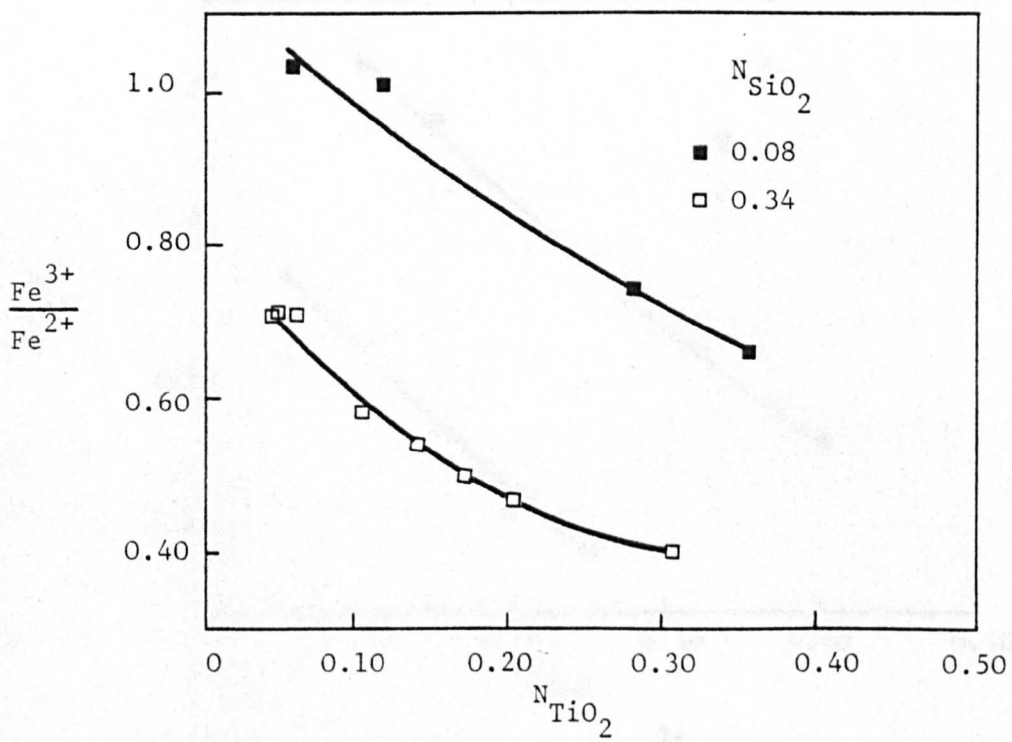

Fig. A.3.48 Variation of $\frac{Fe^{3+}}{Fe^{2+}}$ with composition in $FeO-Fe_2O_3-SiO_2-TiO_2$ system at $\frac{P_{CO_2}}{P_{CO}} = 135.36$ and $1500^{o}C$.

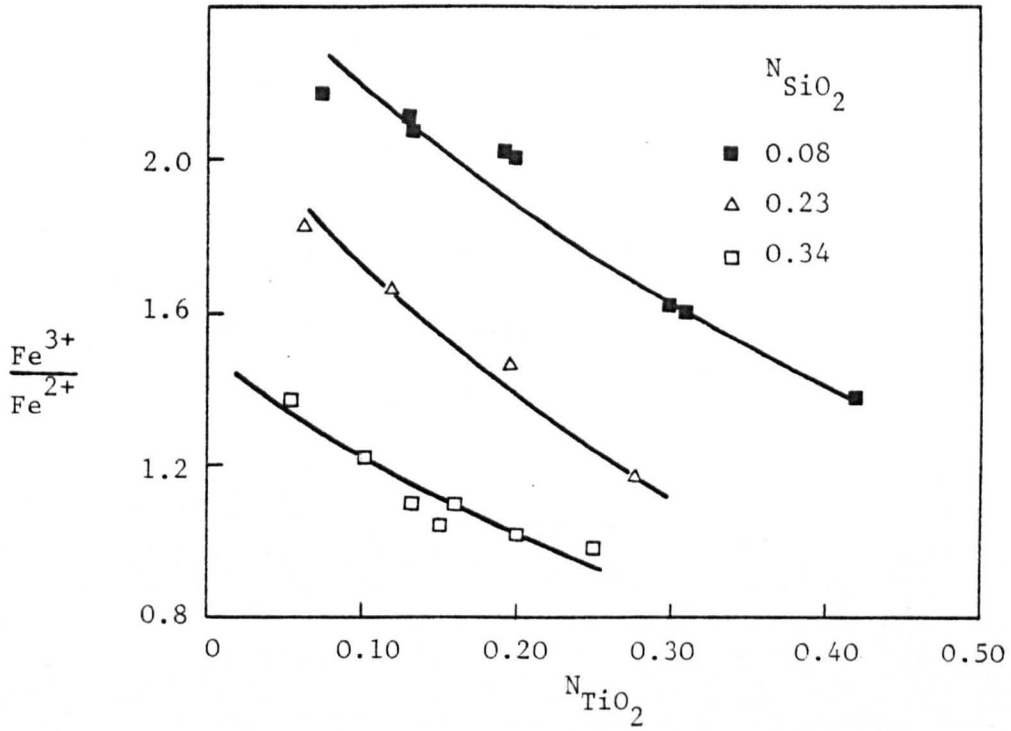

Fig. A.3.49 Variation of $\frac{Fe^{3+}}{Fe^{2+}}$ with composition in $FeO-Fe_2O_3-SiO_2-TiO_2$ system at P_{O_2} = 0.021 atm. at 1500°C.

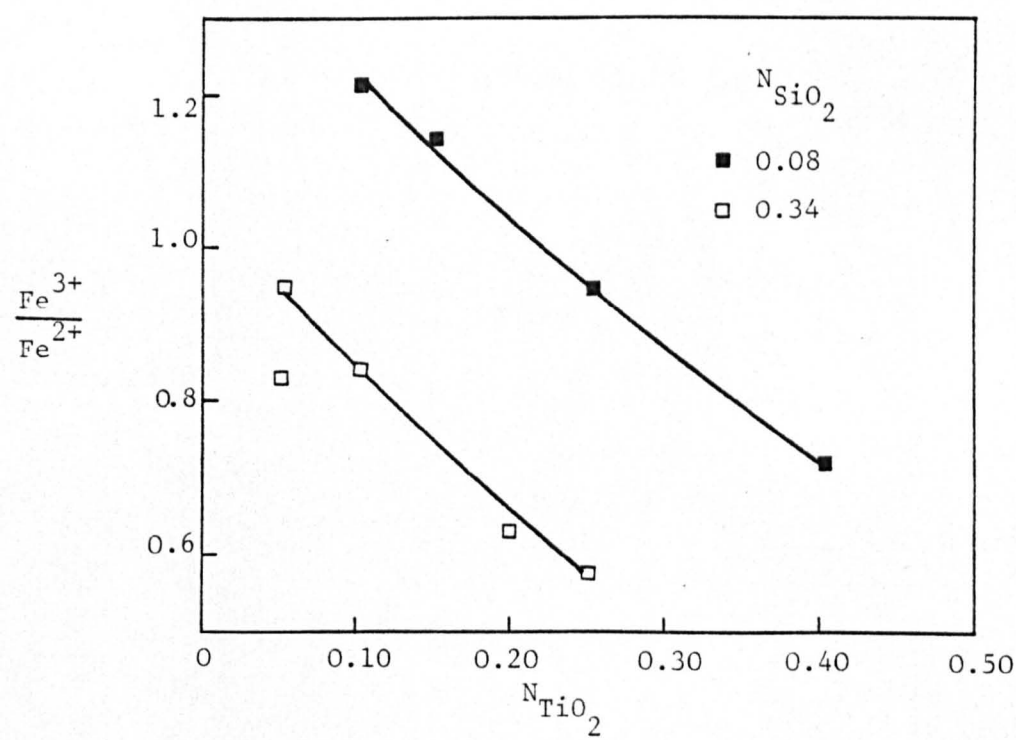

Fig. A.3.50 Variation of $\frac{Fe^{3+}}{Fe^{2+}}$ with composition in the $FeO-Fe_2O_3-SiO_2-TiO_2$ system at $\frac{P_{CO_2}}{P_{CO}}$ = 249 and 1500°C

It is interesting to note from the above discussion that titania and silica have a qualitatively similar effect on the $\frac{Fe^{3+}}{Fe^{2+}}$ ratio, which suggests that titania behaves as acidic oxide in the melts containing iron oxide.

SECTION B

CHAPTER 1

LITERATURE REVIEW

B.1 LITERATURE REVIEW

The sulphur pick up by slag from metal has been studied by[94-97], they measured the sulphur distribution between slag and metal and defined a parameter called "desulphurising power". This was defined as

$$\frac{\text{\% sulphur in the slag}}{\text{\% sulphur in the metal}}$$

and although it can act as a good comparator for slags under well defined conditions, it is not a thermodynamically based parameter.

The early experiments mentioned above had all been carried out in graphite crucibles and this may be one of the disadvantages of this technique in that it limits the range of slag compositions which can be used. Also, the activity of iron and sulphur would be affected by the presence of carbon in these phases and the prediction of actual slags desulphurising power would be in error. The slag/metal distribution technique also has the disadvantage that it is difficult experimentally in that containers are required which are inert to both slag and metal. The modern concept of the sulphide capacity and indirect methods involving a separate study of the slag and metal was first discussed by Fincham and Richardson[81,98]. They studied the partition of sulphur between sulphur containing gases and various silicate and aluminate slags.

The desulphurisation reaction can be written in a most general reaction

$$\underline{S} + O'' = S'' + \underline{O} \qquad (1.1)$$

for which the equilibrium constant is defined as

$$K_1 = \frac{a_{S''} \cdot a_{\underline{O}}}{a_{O''} \cdot a_{\underline{S}}}$$

where O" and S" represented the oxygen and sulphur anions in the slag and $\underline{O}$ and $\underline{S}$ represent those in the metal phase being desulphurised. This indirect technique has several advantages in that it allows containers to be used which are relatively inert for each study. It also gives more thermodynamic information in that gas/slag and gas/metal studies are involved and the range of composition which can be studied is much greater. An equation (1.1) can be written, using a gas phase to control the sulphur and oxygen potentials,

i.e. $$\tfrac{1}{2} S_2 + O'' = S'' + \tfrac{1}{2} O_2 \qquad (1.2)$$

where $$k_2 = \frac{a_{S''}}{a_{O''}} \cdot \frac{P_{O_2}^{\frac{1}{2}}}{P_{S_2}^{\frac{1}{2}}}$$

But it is not possible to determine experimentally a value of k. Carter and Macfarlane[99] studied an equilibrium constant for the reaction

$$CaO + \tfrac{1}{2} S_2 = CaS + \tfrac{1}{2} O_2 \qquad (1.3)$$

where $$K_3 = \frac{a_{CaS}}{a_{CaO}} \cdot \frac{P_{O_2}^{\frac{1}{2}}}{P_{S_2}^{\frac{1}{2}}}$$

$$= \frac{\gamma_{CaS}}{\gamma_{CaO}} \cdot \frac{N_{CaS}}{N_{CaO}} \cdot \frac{P_{O_2}^{\frac{1}{2}}}{P_{S_2}^{\frac{1}{2}}}$$

The equilibrium constant for the reaction (1.3) is known accurately by combining the results of Rosenqvist[100], confirmed by Filipovska and Bell[101] for the reaction

$$CaO + H_2S = CaS + H_2O \qquad \Delta G^\circ = 66{,}840 - 4.48T \text{ J.mole}^{-1}$$

with free energy of formation of H_2O and H_2S

i.e. $$CaO + \tfrac{1}{2}S_2 = CaS + \tfrac{1}{2} O_2 \qquad \Delta G^\circ = 96{,}270 - 5.61T \text{ J.mole}^{-1}$$

This is experimentally[102-5] a time consuming method, especially when considering slags more complex than binary ones, but it yields data for activities of CaO.

The definition of the sulphide capacity is

$$C_S = (\%\ S).\ \frac{P_{O_2}^{\frac{1}{2}}}{P_{S_2}^{\frac{1}{2}}} \qquad (1.4)$$

This gives for the slag sulphur concentration in weight percent in equilibrium with a given oxygen and sulphur potential. This is a very useful value and can be related to the slag/metal sulphur distribution. As shown in Figures (B.1.1a and B.1.1b) at 1500°C for oxygen pressure of less than 10^{-5} atmosphere, sulphide capacities are important, while for those greater than 10^{-4} atmosphere, sulphate capacities are important, as reported by Fincham and Richardson[81,98].

The sulphate capacity can be defined as

$$\tfrac{1}{2}\ S_2 + O'' + \tfrac{3}{2}\ O_2 = SO_4''$$

$$C_{SO_4} = (\%S)\ \frac{1}{P_{S_2}^{\frac{1}{2}} \cdot P_{O_2}^{3/2}}$$

From equation (1.2)

$$a_{O''} = \frac{a_{S''}}{k.A.}$$

where A is the ratio $\frac{P_{S_2}^{\frac{1}{2}}}{P_{O_2}^{\frac{1}{2}}}$ and called the sulphurising potential of the gas phase which is being used to equilibrate the slag. The measurement of single ion activities is impossible but ratios can be measured as mentioned previously[99] from equation (1.3)

$$k_3 = \frac{a_{CaS}}{a_{CaO} \cdot A}$$

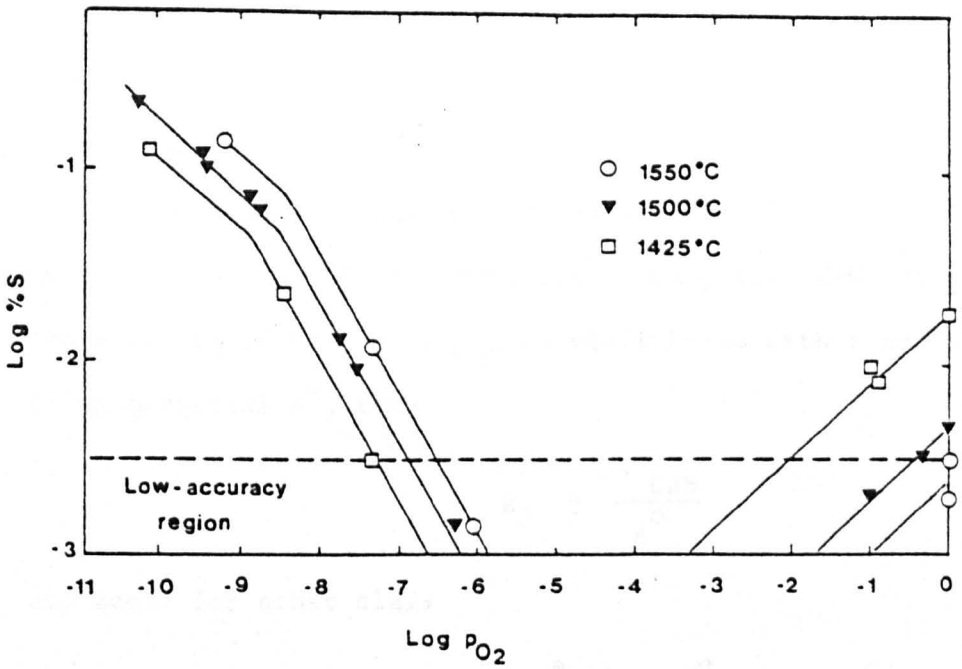

Fig. B.1.1a The effect of oxygen pressure and temperature on the sulphur content of a $CaO-Al_2O_3-SiC_2$ slags

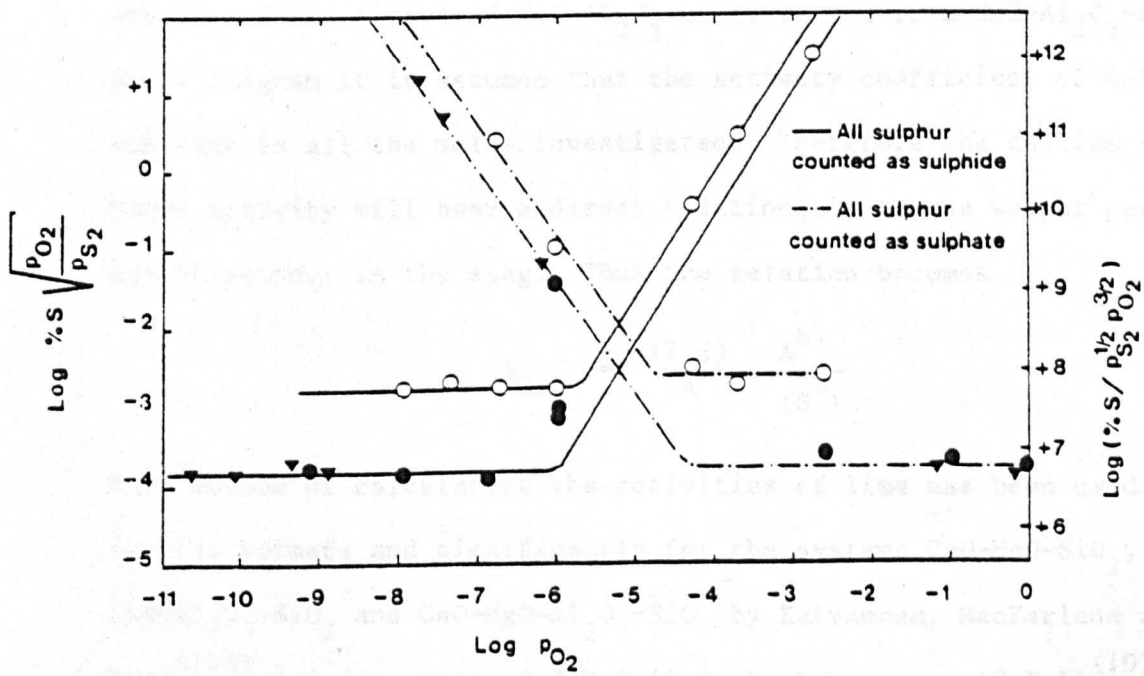

Fig. B.1.1b Variation of sulphide and sulphate capacity with oxygen potential.

$$\therefore \quad a_{CaO} = \frac{a_{CaS}}{K_3 . A}$$

Many of the slags studied are rich in calcium oxide which from thermodynamic data will be the main component reacting with sulphur (except in slags containing ferrous oxide). Carter and MacFarlane[99] considered a slag of unit activity of CaO, i.e. CaO saturated, and the activity of CaS = a^{o}_{CaS} in equilibrium with a gas of sulphurising potential A^{o}, then

$$k_3 = \frac{a^{o}_{CaS}}{A^{o}}$$

and hence for other slags

$$a_{CaO} = \frac{a_{CaS}}{A} \times \frac{A^{o}}{a^{o}_{CaS}}$$

$$= \frac{\gamma_{CaS} \cdot N_{CaS}}{A} \times \frac{A^{o}}{\gamma^{o}_{CaS} \cdot N^{o}_{CaS}}$$

At 1500°C for the slag 60.6 wt% CaO, 32.4 wt% Al_2O_3 and 7 wt% SiO_2 and then for a series of CaO-Al_2O_3 mixtures and from CaO-Al_2O_3-SiO_2 phase diagram it is assumed that the activity coefficient of CaS is the same in all the melts investigated. Therefore the calcium sulphide activity will bear a direct relationship to the weight percentage of sulphur in the slag. Thus the relation becomes

$$a_{CaO} = \frac{(\%\ S)}{A} \times \frac{A^{o}}{(S^{o})}$$

This method of calculating the activities of lime has been used by several workers and significantly for the systems CaO-MgO-SiO_2, CaO-Al_2O_3-SiO_2 and CaO-MgO-Al_2O_3-SiO_2 by Kalyanram, MacFarlane and Bell[106] and for system CaO-MgO-Al_2O_3 by Kalyanram and Bell[107].

Sharma and Richardson[104] measured the sulphide capacities and the limiting of solubilities of calcium sulphide in melts containing $CaO-Al_2O_3$ at 1500°C. They found that γ_{CaS} decreased with increasing lime in the melts, while the same authors[108] found that γ_{CaS} decreased with decreasing lime in the $CaO-SiO_2$ systems.

Abraham et al[109] calculated the activity coefficients of MnS for the $MnO-SiO_2$ system. They found that γ_{MnS} increased with decrease in concentration of MnO. Therefore the assumption of Carter and MacFarlane[99] that γ_{CaS} is independent of composition might be in error.

Sharma and Richardson[104,108] calculated the lime activity of $CaO-Al_2O_3$, and $CaO-SiO_2$ melts.

$$a_{CaO} = \frac{1}{k} \cdot \frac{P_{O_2}^{\frac{1}{2}}}{P_{S_2}^{\frac{1}{2}}}$$

When the system was saturated with CaS, i.e. $a_{CaS} = 1$ and the activity of CaO can be calculated from the equation

$$a_{CaO} = \frac{1}{K.A_{(sat.)}}$$

Cameron et al[105] also used this method of activity determination in a different form in the $CaO-Al_2O_3-SiO_2$ melts at 1550°C. Their results apparently disagree with those of Sharma and Richardson.

Wagner[110] has made an interesting analysis of the sulphur-oxygen displacement reaction in connection with $CaO-CaS-Al_2O_3$ and $CaO-CaS-SiO_2$ systems. This results in an equation connecting the activity of CaO with the concentration of CaS and Al_2O_3 in the $CaO-CaS-Al_2O_3$ system as follows:

$$\ln a_{CaO}(\xi=0) = \ln a_{CaO}(\xi_{sat}) + \xi_{sat} - \int_0^{\xi_{sat}} \xi \frac{\partial \ln C_S}{\partial \xi} d\xi - \eta \int_0^{\xi_{sat}} \frac{\partial \ln C_S}{\partial \eta} d\xi \quad (1.5)$$

where a_{CaO} ($\xi = \xi_{sat}$) is given by

$$\left[a_{CaO} = \frac{1}{k_3}\left(\frac{P_{O_2}}{P_{S_2}}\right)^{\frac{1}{2}} \right]_{a_{CaS}=1}$$

where $\xi = \frac{n_{CaS}}{n_{CaO} + n_{CaS}}$ and $\eta = \frac{n_{Al_2O_3}}{n_{CaO} + n_{CaS}}$

Referring to the work of Sharma and Richardson[104,108] equation (1.5) becomes

$$\ln a_{CaO}(\xi=0) = \ln a_{CaO}(\xi_{sat}) + \left[1 - \eta \frac{\partial \ln C_S}{\partial \eta}\right] \xi_{sat}$$

The term $(1 - \eta \frac{\partial \ln C_S}{\partial \eta})$ may be considered as a correction term for the calculation of $a_{CaO}(\xi = 0)$ from $a_{CaO}(\xi_{sat})$. The logarithm of the sulphide capacity in the system $CaO-CaS-Al_2O_3$ is in essence a linear function of η between $\eta = 0.429$ and 0.754[104]. Accordingly, $\frac{\partial \ln C_S}{\partial \eta} = -6.4$ is independent of ξ and η. Similarly for the system $CaO-CaS-SiO_2$ in order to determine the activity of lime with concentration of CaS and SiO_2, where

$$\xi = \frac{n_{SiO_2}}{n_{CaO} + n_{CaS}}$$

In this system $\frac{\partial \ln C_S}{\partial \eta}$ varies considerably with η.

B.1.1 MEASUREMENT OF SULPHIDE CAPACITY

The measurement of sulphide capacity involves the equilibration of the liquid slag by a gas mixture of known oxygen and

sulphur partial pressure, it requires a very accurate thermodynamic data and also precise calculation. Typical gas mixtures which have been used are $CO-CO_2-S\ O_2$, $H_2-H_2O-H_2S$ and $H_2-CO_2-SO_2$. In the present work a mixture of $H_2-CO_2-SO_2$ and $H_2O-H_2-H_2S$ were used. Nitrogen or argon were used as diluents to reduce thermal diffusion and avoid the formation of layers due to differencies in density of the gas constituents. At high temperatures all these gas mixtures react to form a large number of chemical species whose partial pressures will depend on their free energies of formation. The species which appear in significant amounts at 1500°C are CO_2, CO, SO_2, H_2, H_2O, H_2S, S_2, S, SO, HS, CO_3 and O_2. Thus it is necesary to have accurate thermodynamic data on the free energy of formation for each species. The thermodynamic data used in this work have been taken from "JANAF thermodynamical tables"[111] and Pierre and Chipman[112]. The method of calculation of the oxygen and sulphur potentials of gas mixture $H_2-SO_2-CO_2$ and N_2 and gas mixture $H_2-H_2O-H_2S$ and Ar at given reaction temperature are shown in Appendices (2) and (3) respectively.

The method of sulphide capacity depends on the accurate method of sulphur analysis. The method employed was that described by Fincham and Richardson[113].

A sample of the slag must be finely ground and heated in an oxidising atmosphere so that volatile oxides of sulphur are formed. These oxides must be flushed out of the furnace and titrated. From the oxidation of a sulphur bearing specimen either sulphur dioxide or sulphur trioxide can be formed. The problem arising from SO_3 is that it is readily absorbed by the ceramic materials of the furnace. Examination of the equilibrium

$$SO_2 + \tfrac{1}{2} O_2 = SO_3$$

for which, at 1400°C $\quad \Delta G^\circ = 13{,}525 \text{ cal.mole}^{-1}$

$$K = 1.71 \times 10^{-2}$$

shows that $\frac{SO_2}{SO_3}$ ratio depends on the oxygen potential of the system

$$\frac{P_{SO_2}}{P_{SO_3}} = \frac{}{P_{O_2}^{\frac{1}{2}} \cdot 1.71 \times 10^{-2}}$$

Fincham and Richardson[113] suggested the use of carbon dioxide instead of pure oxygen to avoid any formation of sulphur trioxide

$$CO_2 = CO + \tfrac{1}{2} O_2$$

for which, at 1400°C $\quad \Delta G^\circ = 32{,}976 \text{ cal.mole}^{-1}$

$$K = 4.92 \times 10^{-5}$$

Thus $$\frac{P_{CO} \cdot P_{O_2}^{\frac{1}{2}}}{P_{CO_2}} = 4.92 \times 10^{-5}$$

where $\quad CO_2 \simeq 1$ atmosphere

$$P_{CO} = 2 P_{O_2}$$

$$P_{O_2}^{\frac{1}{2}} = \sqrt[3]{\frac{4.92 \times 10^{-5}}{2}} = 0.0291$$

Combining this result with that obtained of dissociation of SO_3, we obtain a $\frac{P_{SO_2}}{P_{SO_3}}$ ratio of approximately 2011. Hence at 1400°C, when a slag containing sulphur is burnt in carbon dioxide, the ratio of sulphur dioxide to sulphur trioxide in the issuing gas will be 2011/1, which means that the loss of sulphur dioxide would be in order of 0.05%. However, as the gas is removed from the

furnace there will be a shift in the equilibrium in favour of sulphur trioxide due to the decrease in temperature until the reaction is kinetically frozen. It is estimated[113] that this, together with the fact that commercially available carbon dioxide contains some oxygen, will cause a loss of 0.7% of the sulphur as sulphur trioxide.

B.1.2 PREVIOUS WORK ON SULPHIDE CAPACITIES FOR SLAGS

B.1.2.1 Slags Free of Iron Oxide

Sharma and Richardson[104] and Cameron et al[105] studied the solubility of CaS in the slag. It has been observed that the Cameron results cannot be reconciled with those of Sharma and Richardson in lime-alumina system. In the high lime melts, the sulphur solubility values are much the same as those reported, normally about 2% but, whereas Cameron's results show first a gradual, then a rapid rise to 6.15% at the $CaO-Al_2O_3$ liquidus, Sharma and Richardson show a gradual fall to 0.6%.

Schürmann et al[114] have carried out measurements of sulphide capacities in $CaO-Al_2O_3$ melts at 1600°C by studying the partition of sulphur with iron melts, with the aid of solid (ThO_2) electrolytes to determine the oxygen potential of the system. The measurements were made in Al_2O_3 crucibles hence the slags tend to be at the low lime side of the range of composition liquid at 1600°C i.e., 44 to 68% Al_2O_3. These data are presented in the form of sulphur capacities expressed as

$$C_S = \frac{(\%S)}{[\%S]} [a_O]$$

This can be converted to the form given in equation (1.4) by using the factor 0.125 at 1600°C as reported by Bell[115].

Schürmann et al[114] compared their data with those of Cameron et al[105] at 1500°C and indicated some large discrepancies between the two sets of data, Schürmann et al indicating higher values of sulphide capacity especially in the range 42-46% CaO. Much of the discrepancy can be ascribed to the difference in temperature - the solubility of Al_2O_3 in the slag increases by 8% between 1500°C to 1600°C and sulphide capacity will increase with increase in temperature. If the higher values at 46% CaO are neglected, the data are not out of line with previous data using gas-slag studies.

Some studies have been made on the ternary slags containing $CaO-Al_2O_3-SiO_2$ because they are of considerable industrial importance. Kalyanram et al[106] studied the sulphide capacity of these slags and found that at a constant weight fraction CaO, the replacement of SiO_2 by Al_2O_3 increases the sulphide capacity of the slag.

Fincham and Richardson[81], and Abraham and Richardson[116] have given data for sulphur capacities of some slags in the same ternary system, but the actual numerical value of C_S for comparable slags are approximately twice those found in Kalynaram's work. The difference in the sulphide capacities value must be attributed to the thermodynamic data used to P_{S_2} and P_{O_2} in the different gas mixture at this time. The discrepancy has now been resolved.

Titania containing slags are of interest and there are some unpublished data on CaO, MgO and SiO_2 containing melts with TiO_2. Roxburgh[65] measured the sulphide capacities in the $CaO-MgO-TiO_2$ system. He found that as the composition varied from 50 to 75 wt% TiO_2, the sulphide capacities varied by a factor of only 1.7 while for slags in the $CaO-MgO-SiO_2$ system, which has been studied by Kalynaram et al[106], when the silica composition varies from

63 wt% to 37%, their sulphide capacities increased by a factor of ten. The sulphide capacity is reduced by a factor of 10 when the titania is replaced by silica in the system $CaO-MgO-SiO_2-TiO_2$ [65] at a CaO+MgO content of 35 wt%. There are few results from $CaO-MgO-TiO_2$ slags containing 5 wt% and 10% silica, and it is apparent that their sulphide capacities are reduced by these additions. Brown [117] measured the sulphide capacities in the $CaO-TiO_2-SiO_2$ system but there is a restricted range of compositions which can be studied at 1500°C. The results showed that the substitution of TiO_2 for SiO_2 leads to an increase in the sulphide capacity. McRea et al [42] studied the complex slag containing $CaO-MgO-TiO_2-SiO_2-Al_2O_3$ and they found that by decreasing $\frac{CaO}{MgO}$ ratio, the sulphide capacity fell from 1.7×10^{-5} to 10^{-6} when the concentration of TiO_2, SiO_2 and Al_2O_3 were kept relatively constant and the $\frac{CaO}{MgO}$ ratio has changed from 10 to 0.10. The eutectic in the binary system $CaO-TiO_2$ (containing 82 wt% TiO_2) has been studied at an oxygen pressure of 10^{-8} and 1500°C by Brown [117] and the sulphide capacity found to be 1.7×10^{-4}. The $CaO-TiO_2-Al_2O_3-SiO_2$ quaternary system has also been studied by Brown [118]. In the range of composition studied there was very little variation in the sulphide capacities as the slags became richer in TiO_2 when the slag composition moves towards the sphene composition ($CaTiSiO_5$). There is a sharp decrease in the sulphide capacity with the first addition of anorthite ($Ca.Al_2.SiO_8$) due to an increase in the alumina and silica contents of the slag, then after 10% anorthite, there is a decrease in the effect of anorthite addition on the sulphide capacities of the slag. This is possibly due to the fact that Al_2O_3 is taking over the role of TiO_2 in the depolymerisation of silicate anions, and to a lesser extent by

the mechanism suggested by Sharma and Richardson[103].

$$3(\vdots\ Si\text{-}O\text{-}Si\ \vdots) + Al_2O_3 = 6(\vdots\ Si\text{-}O^-) + 2\ Al^{3+}$$

$$2(\vdots\ Si\text{-}O^-\ \ ) + \tfrac{1}{2}\ S_2 = (\ \vdots\ Si\text{-}O\text{-}Si\ \vdots) + S^{2-} + \tfrac{1}{2}O_2$$

The overall decrease in the sulphide capacity is approximately a factor of 7 as the composition moves from 100% ($CaO.TiO_2.SiO_2$) to 20% ($CaO.TiO_2.SiO_2$) / 80% ($CaO.Al_2O_3.2\ SiO_2$).

Duffy et al[119] using an optical basicity scale (Λ) have shown a correlation with sulphide capacities of slags free of iron oxide and titania.

where $$\Lambda = \frac{X_A}{\gamma_A} + \frac{X_B}{\gamma_B} + \cdots\cdots$$

where X_A and X_B are the equivalent cation fraction of A and B. A correlation has been given between C_S values at 1500°C and basicity (Λ) as

$$\log C_S = 12.0\Lambda - 11.9$$

Figure (B.1.2)shows the sulphide capacity for these slags against optical basicity (Λ) and the technique which was involved will be discussed later in Chapter (3).

Sulphide capacities have been measured at 1500°C by Carter and MacFarlane[99] for $CaO\text{-}Al_2O_3$ and $CaO\text{-}SiO_2$ systems, Kalyanaram and Bell[107] for $CaO\text{-}Al_2O_3$ and $CaO\text{-}MgO\text{-}Al_2O_3$ systems, Kalyanaram et al[106] for $CaO\text{-}MgO\text{-}SiO_2$, $CaO\text{-}Al_2O_3\text{-}SiO_2$ and $CaO\text{-}MgO\text{-}Al_2O_3\text{-}SiO_2$ systems, Abraham et al[109] for $MnO\text{-}SiO_2$ and Fincham and Richardson[81] for $CaO\text{-}SiO_2$. Their C_S values have been plotted against mole fraction base as shown in Figure (B.1.3).

B.1.2.2 Slags Containing Iron Oxide

It is evident that the distribution of sulphur between slag

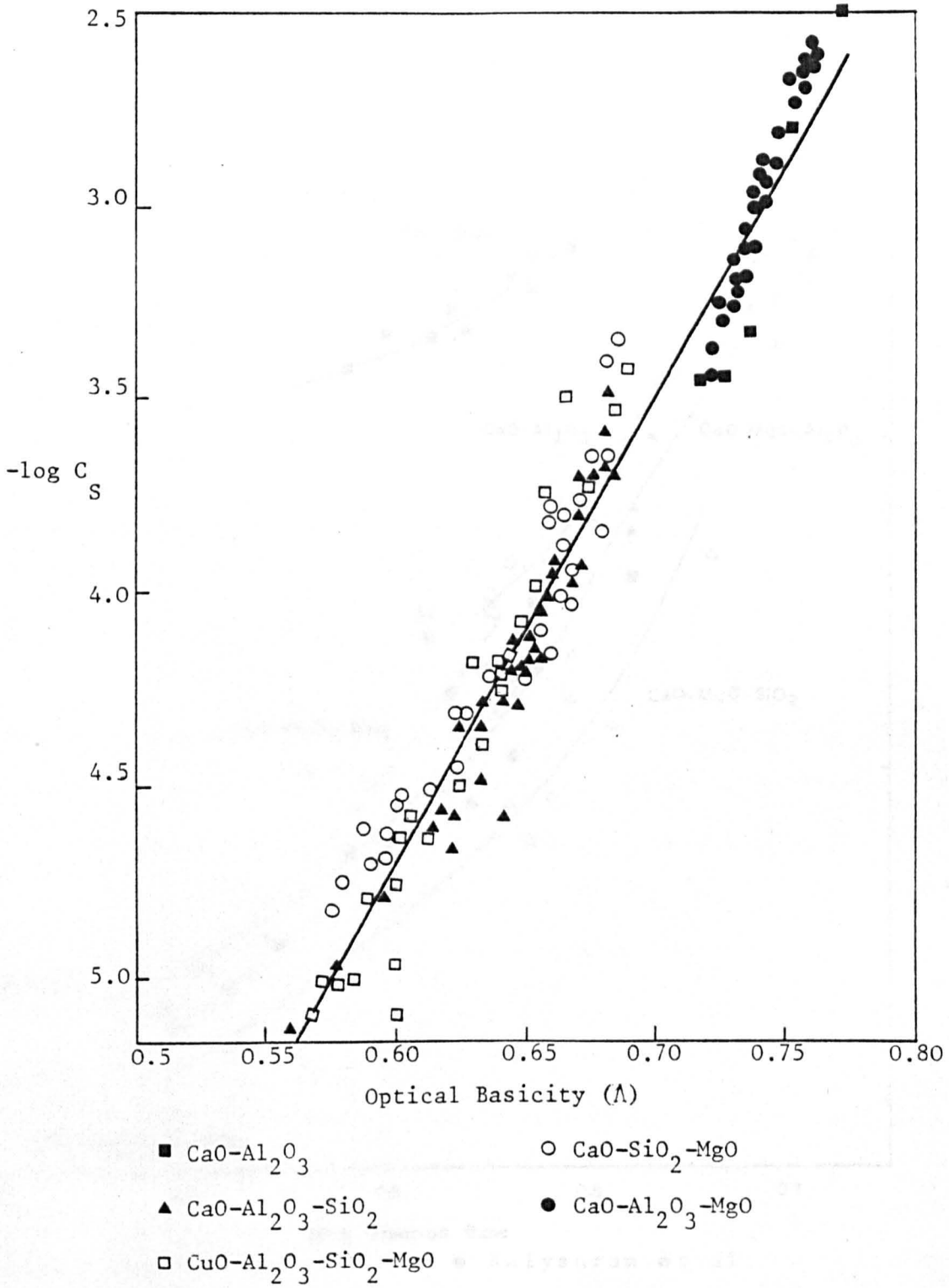

Fig. B.1.2 Variation of sulphide capacity with optical basicity at 1500°C.

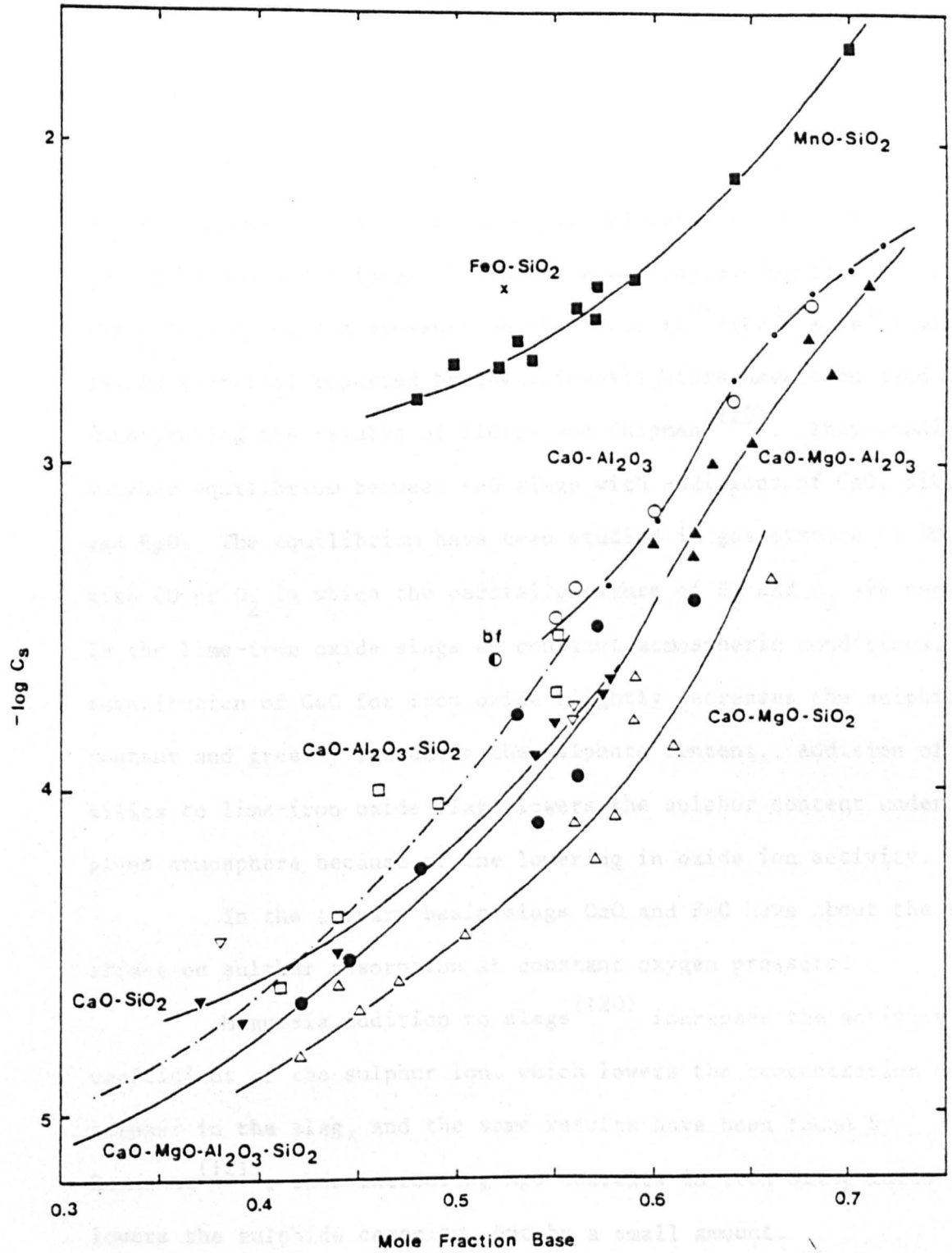

• Carter and Macfarlane
○ Kalyanram and Bell
▲ Kalyanram and Bell
△ Kalyanram et al
□ Kalyanram et al
● Kalyanram et al
■ Abraham et al
x Fincham and Richardson
▼ Carter and Macfarlane
▽ Fincham and Richardson

Fig. B.1.3 Sulphide capacities for slags free of titania at 1500°C

and gas depends upon the oxygen pressure of the gas. In the FeO slags, a change in oxygen pressure produces a change in ferric oxide content and a knowledge of the equilibrium is required for studies of sulphur distribution.

The data are found in the work of Darken and Gurry[25,26] on FeO systems and the more recent experiments of Gurry and Darken[90] and of Larson and Chipman[91] on FeO slags containing lime and silica. The effect of oxygen pressure on the ratio $Fe^{3+}/(Fe^{2+} + Fe^{3+})$ also called (j-ratio) reported by these investigators have been used in interpreting the results of Pierre and Chipman[120]. They studied sulphur equilibrium between FeO slags with additions of CaO, SiO_2 and MgO. The equilibrium have been studied in gas mixture of SO_2 with CO or O_2 in which the partial pressure of S_2 and O_2 are known. In the lime-iron oxide slags at constant atmospheric conditions, the substitution of CaO for iron oxide slightly decreases the sulphide content and greatly increases the sulphate content. Addition of silica to lime-iron oxide slags lowers the sulphur content under a given atmosphere because of the lowering in oxide ion activity.

In the ternary basic slags CaO and FeO have about the same effect on sulphur absorption at constant oxygen pressure.

Magnesia addition to slags[120] increases the activity coefficient of the sulphur ion, which lowers the concentration of sulphur in the slag, and the same results have been found by Earnshaw[121], that increasing MgO contents in iron oxide melts lowers the sulphide capacity, but by a small amount.

There is also an investigation of gas/slag equilibria by Lee and Bell[122]. Their studies have been made in the range of oxygen pressure 10^{-5} to 10^{-8} atmosphere, and about an oxygen pressure

10^{-5} the sulphate ion becomes predominate. The same effect of CaO additions to iron oxide slags have been found[122] by gas/slag equilibrium over a wide range of oxygen and sulphur potential, i.e. the amount of sulphur picked up by a slag is not changed by substituting CaO for FeO in the oxygen pressure range of 10^{-5} to 10^{-8} atmosphere. The sulphide capacity also remains constant in the same range of oxygen pressures.

The ratio FeO to Fe_2O_3 concentration at a given oxygen pressure increases with addition of CaO and it appears that the actual Fe_2O_3 concentration remains almost constant. The effect of adding silica to CaO-FeO-Fe_2O_3 melts is to reduce the sulphide capacity of the melt and this is the same effect reported by Pierre and Chipman[120]. This probably means that silica increases the activity coefficient of CaS, and may decrease the activity of lime or FeO in the slags and lowers the solubility of FeS and CaS in the melts.

Fincham and Richardson[81,98] also studied the addition of SiO_2 to FeO-FeS slags. The sulphide capacity decreases with silica additions to value 3×10^{-3} at mole fraction of silica of 0.50 at 1550°C. This effect is greater than the decrease in FeO activity and indicates a large increase in the activity coefficient of FeS with addition of silica (more than ten fold). Derici[123] studied the addition of FeO to Na_2O-SiO_2 slags up to 15 wt% FeO. High sulphur solubility in the melts was obtained due to increasing the iron oxide content in the melts. Sulphide capacities have been measured[123] at 1500°C on the silica saturation line of CaO-FeO-SiO_2 ternary. They were low mainly because of the higher polymerisation in the melts. On the silica saturation line sulphur solubilities have increased 4 to 5 times as the composition changes from the CaO-SiO_2

side to $FeO-SiO_2$ side of the ternary.

A study of steelmaking from pellets has been made by Cavaghan and Harris[124]. They found that the TiO_2 caused a marked reduction in the sulphur-holding capacity of the slags. With over 9% TiO_2 the desulphurising ability was very low and a modified basicity ratio had to be employed for control, i.e.

$$\text{Basicity} = \frac{CaO + MgO}{SiO_2 + Al_2O_3 + 2.2\ TiO_2}$$

A ratio well in excess of 1.5 is required. The reasons for this effect are not clear and insufficient data are available in the paper to analyse the effect, but it may be the presence of some iron oxide in the slag.

As shown by the data already given an increase in the iron oxide content increases the oxygen potential of the slag. It indicates that the slag/metal sulphur partition increases with increasing FeO content in the melts.

B.1. 3 SLAG-METAL SULPHUR PARTITION

A number of equations have in the past been suggested for evaluating the equilibrium sulphur distribution between slag and iron melts. It was shown by Schenck[125] that the sulphur partitions, i.e. $\frac{(\%S)}{[\%S]}$ could be related to the manganese content of the iron, and the ferrous oxide, calcium oxide and silica contents of the slag, and also the sulphur partition increased with temperature for given $\frac{\%CaO}{\%FeO}$ ratio.

Grant and Chipman[126] studied the sulphur distribution under simple $CaO-SiO_2-FeO$ slags and their results show that FeO (from

30% to 70%) has only a dilution effect on slag/metal sulphur distribution and when the FeO content in the slag was below 3% the sulphur partition improved. Temperature variations in the range 1540°C-1660°C showed no measureable effect on the sulphur ratio as confirmed by Earnshaw[121] and also by Trömel[127], shown in Figure (B.1.4). Temperatures greater than 1670°C or below 1540°C appear to have a small harmful effect.

There are also earlier investigations of slag/metal sulphur partition[94-98]. From the point of view of experimental simplicity, many of these have concerned carbon saturated iron and liquid slags using graphite crucibles. The use of graphite containers while limiting the range of variables which can be studied also leads to problems connected with silica reduction, which can slow down the rate of approach to equilibrium. Even so, the data are of interest in connection with ironmaking and as a link between the direct and indirect approaches to sulphur partition.

Turkdogan[128] also found that for ironmaking conditions the sulphur distribution can be related to the manganese distribution. When $\frac{[\%Mn]}{(\%Mn)}$ ratio is less than 5.0 and the temperature is within the 1400-1500°C range, the following equation applies:

$$(\%S)/[\%S] = 28[\%Mn]/(\%Mn)$$

Derge et al[129] studied the mechanism of sulphur transfer between slag and carbon-saturated iron. They found that sulphur crosses the interface in chemical combinations with iron which is later reduced to pellets accompanied by evolution of CO gas and formation of a stable calcium-sulphur compound in the slag. The mechanism for desulphurisation under reducing conditions is produced by the reaction

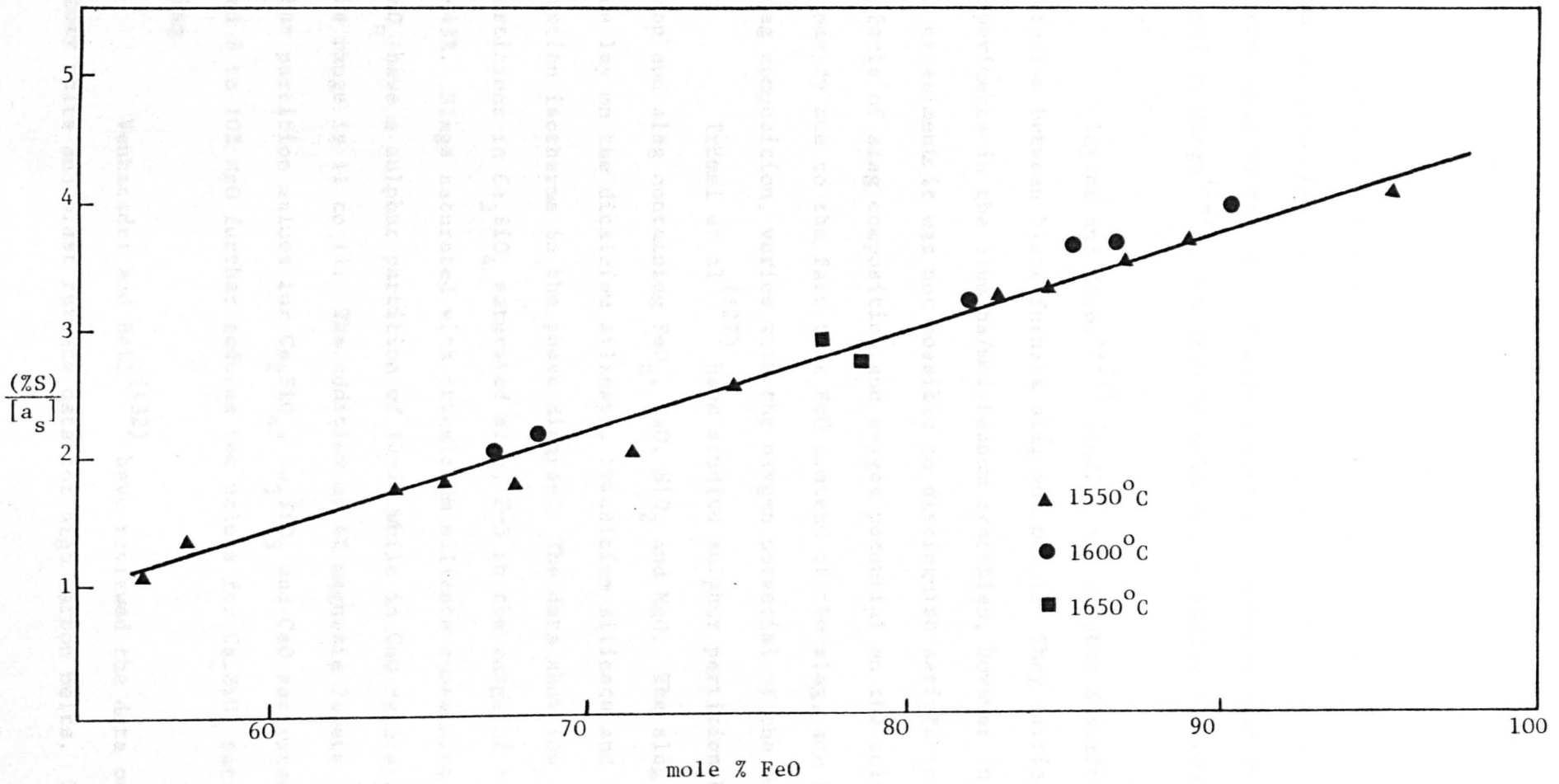

Fig. B.1.4 Variation of slag/metal sulphur partition with iron oxide[121].

$$FeS = (FeS)$$

$$(FeS) + (CaO) = (CaS) + (FeO)$$

$$(FeO) + [C] \rightarrow Fe + CO$$

The similar work was carried out by Ramachandran et al[130]. Their results show that the transfer of sulphur from metal to slag is accompanied by transfer of electropositive elements such as iron, as found by Derge[129], but also by silicon, aluminium and evaluation of CO.

Taylor and Stobo[131] studied the sulphur distribution reaction between blast furnace slag and metal. They carried out the experiments in the alumina/molybdenum crucibles, however in this type of experiments it was not possible to distinguish satisfactory the effects of slag composition and oxygen potential on the sulphide capacity due to the fact that FeO content of the slag, and hence the slag composition, varies with the oxygen potential of the metal.

Trömel et al[127] have studied sulphur partition between iron and slag containing FeO_n, CaO, SiO_2 and MgO. The slag composition lay on the dicalcium silicate, tricalcium silicate and lime saturation isotherms in the phase diagram. The data show low sulphur partitions in Ca_2SiO_4 saturated slag, 2-3 in the range of FeO_n or 8-43%. Slags saturated with tricalcium silicate containing 45% FeO_n have a sulphur partition of 10-11 while in CaO saturated slags the range is 11 to 14. The addition of 4% magnesia lowers the sulphur partition values for Ca_2SiO_4, Ca_3SiO_5 and CaO saturated slags and 8 to 10% MgO further reduces the values for Ca_2SiO_4 saturated slag.

Venkatadri and Bell[132] have reviewed the data on laboratory melts and blast furnace data for high carbon melts. Their work

showed that a_{FeO} was equal to the mole fraction of FeO in the slag, at low concentration of FeO, within the limits of accuracy. Several laboratory investigations have been made in graphite crucibles of the partition of sulphur between $CaO-Al_2O_3-MgO-SiO_2$ slags and liquid iron. They[132] have suggested that in the blast furnace, equilibrium between slag and metal is approached if the carbon monoxide pressure is taken as the total pressure in the system, i.e., the sulphur equilibrium between slag and metal in the blast furnace can be written as

$$CaO + S + C = CO + CaS$$

The major factor in systems of this type is the low oxygen pressure involved and the high activity coefficient of sulphur in the metal, i.e. high values of sulphur partition even though the sulphide capacities of the slagsare relatively low. The effect of varying oxygen potential on the slag/metal sulphur partition at 1500°C with $CaO-Al_2O_3-SiO_2$ slags containing small amounts of iron-oxide[115] is shown in Figure (B.1.5). Using the sulphide capacity data of Kalynaram and the various thermodynamic data, the relation between sulphide capacity and sulphur partition is

$$\log \frac{(\%S)}{[\%S]} = (5.55 - \frac{724}{T}) + \log C_S + \log \frac{a_C}{P_{CO}} \qquad (1.6)$$

The ferrous oxide content of the slag is often a better measurement of the oxygen potential than the carbon monoxide pressure, and equation (1.6) can be written as

$$\log \frac{(\%S)}{[\%S]} = [\frac{5543}{T} - 1.43] + \log C_S + \log \frac{a_{Fe}}{a_{FeO}}$$

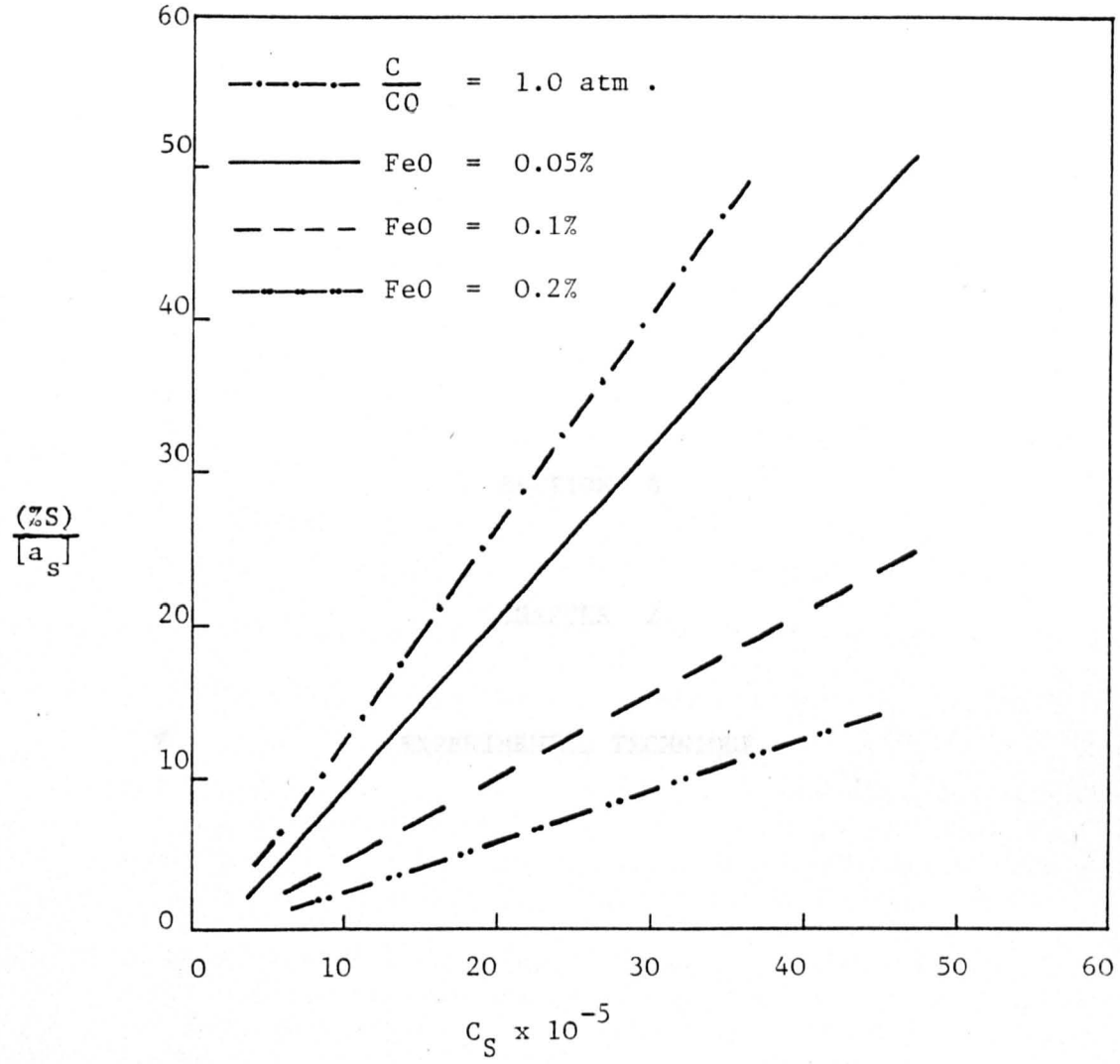

Fig. B.1.5 Effect of varying oxygen potential on the slag/metal sulphur partition of $CaO-Al_2O_3-SiO_2$ slags at 1500^oC [115].

SECTION B

CHAPTER 2

EXPERIMENTAL TECHNIQUE

B.2 EXPERIMENTAL TECHNIQUE

Two gas mixtures (techniques) were used in the present work. The first was a carbon dioxide, hydrogen, sulphur dioxide and nitrogen gas mixture, where all the gas flow rates were measured using separate gas flowmeters. This technique was used for most of the work i.e., for the $FeO-TiO_2-SiO_2$, $FeO-TiO_2-CaO$ and $FeO-TiO_2-SiO_2-CaO$ systems to give oxygen pressures around 10^{-8} atmosphere at $1500^{\circ}C$. A water vapour, hydrogen sulphide, hydrogen and argon gas mixture was also used to make measurements at a lower oxygen pressure.

The same method was used for gas flow measurement except that the water-vapour pressure was controlled by passing the hydrogen through an oxalic acid and anhydrous oxalic acid mixture. The oxygen pressure obtained by this technique was 10^{-14} atmosphere and sulphur pressure 10^{-6} atmosphere at the same temperature.

B.2.1 STARTING MATERIALS

a - Silica

b - Titania

C - Iron oxide

These were supplied and prepared as previously described in Section (A) Chapter (2).

B.2.1.1 Calcium Oxide

CaO was prepared from reagent grade calcium carbonate supplied by British Drug Houses laboratory. The carbonate was calcined in a muffle furnace at a temperature of $1000^{\circ}C$ for 12 hours according to the equation

$$CaCO_3 = CaO + CO_2$$

B.2.1.2 Alumina

Al_2O_3 was used as supplied by British Drug Houses of purity not less than 99%.

B.2.2 GAS-MIXTURE SYSTEM

The method used for controlling the oxygen and sulphur potential was simsilar to that used for controlling the oxygen pressure in Chapter A.2. To give an oxygen pressure of around 10^{-8} atmosphere and sulphur pressure of 10^{-4} atmosphere, a carbon dioxide, hydrogen, sulphur dioxide and nitrogen gas mixture was used. The flowmeters for N_2, CO_2 and H_2 were calibrated by using a soap-bubble meter as described previously, but SO_2 is soluble in water, and the flowmeter was calibrated by analysis, the technique used will be described later. A different gas mixture technique was used to give low oxygen pressure around 10^{-14} atmosphere. A hydrogen, water vapour, hydrogen sulphide and argon gas mixture was used. Nitrogen was not used in these experiments to prevent any possibility of the formation of TiN at low oxygen pressures. The argon flowmeter was calibrated using the same technique as for hydrogen.

As shown in Figure (B.2.1) high purity grade hydrogen was supplied to the system through magnesium perchlorate column(1) for drying and then through the flowmeter(3) which had been previously calibrated over a range of hydrogen flow rates. Any residual oxygen in the hydrogen was removed further by passing the hydrogen through platinised asbestos(2) which induced reaction at room temperature between the residual oxygen and the hydrogen to form water vapour. Then the hydrogen was passed through another anhydrous magnesium perchlorate granular column to ensure that all the water vapour was

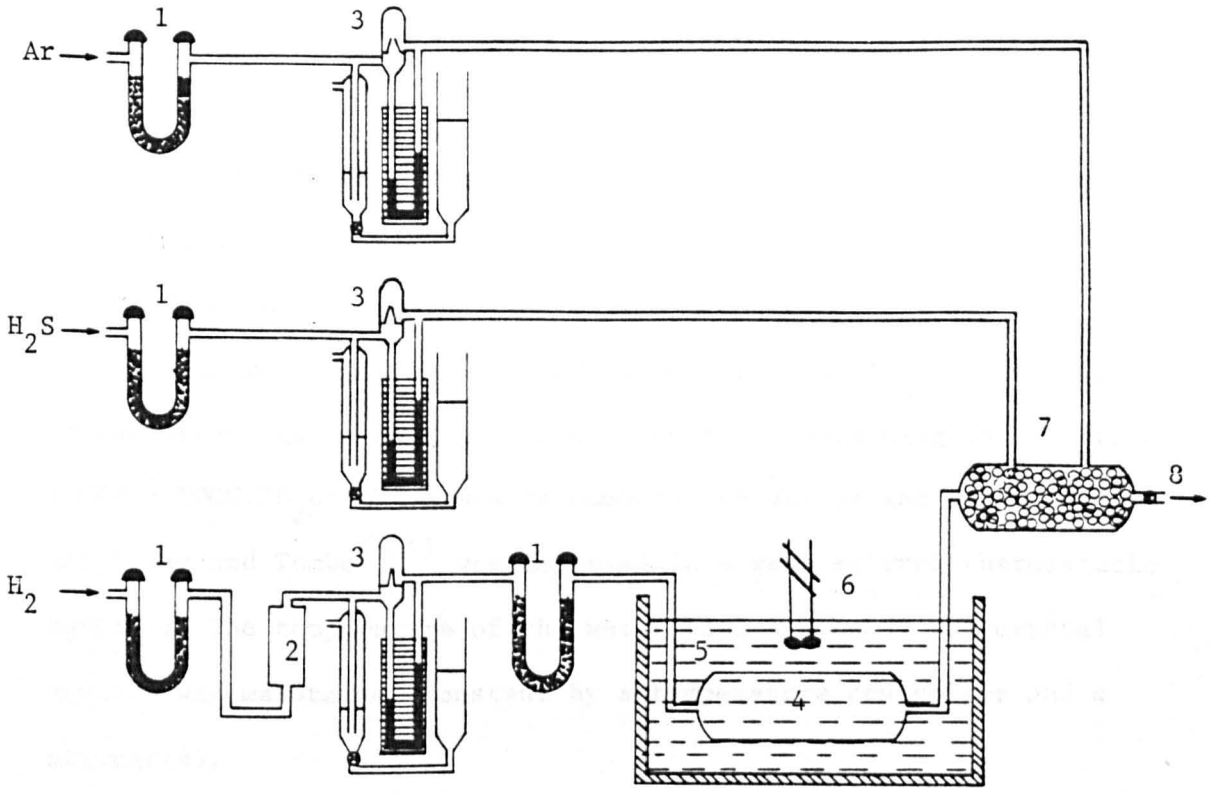

1 - Magnesium Perchlorate
2 - Platinised Asbestos
3 - Flowmeters
4 - Oxalic acid crystal mixture
5 - Water bath
6 - Stirrer
7 - Gas mixer
8 - To the furnace

Fig. B.2.1 Gas mixing apparatus for H_2O,H_2,H_2S and Ar mixture

removed. The flowmeter, catalytic purifier and drying columns were connected by thick walled polythene tubing. Thereafter all connections were made of copper tubing to minimise diffusion of moisture. The pure, dried hydrogen was diverted through the tube(4), (40cm long by 6cm diameter) which was filled with a two-component mixture consisting of 90% weight of oxalic acid dihydrate crystals and 10% weight of anhydrous oxalic acid crystals. The tube containing this mixture ($COOH + COOH.2H_2O$) which was recommended by Baxter and Lansing[133] and Booky and Tombs[134] was immersed in a well stirred thermostatic bath(5). The temperature of the water bath and hence the crystal mixture was maintained constant by a temperature controller and a stirrer(6).

Baxter and Lansing[133] derived an equation to determine the water vapour pressure, this was used during the present study

$$\log P = 18.053 - \frac{9661}{T + 250}$$

where P is the water vapour pressure in mmHg.

T is the temperature of oxalic acid mixture in ^{o}K

The controlled mixture of water vapour and hydrogen was mixed with the measured hydrogen sulphide and argon in a tall mixing cylinder packed with various sized glass beads.

In order to minimise errors due to thermal diffusion, an inert gas of high molecular weight was used to dilute the gas mixtures as described in Chapter A.2. Nitrogen and argon were used in this study as diluents.

B.2.2.1 The Calibration of the H_2S Flowmeter

Since hydrogen sulphide is soluble in water, its flowmeter was not calibrated by a bubble flowmeter. H_2S was bubbled for a

measured time-through an ammonical cadmium chloride solution (about 2% $CdCl_2$ in 10% NH_4OH)[135], where

$$CdCl_2 + H_2S = CdS + 2HCl \qquad (2.1)$$

The hydrochloric acid formed by this reaction is neutralised by the excess of ammonium hydroxide present, thus maintaining an alkaline absorbing solution. Two tubes each containing the excess chloride solution and the absorbent solution were used to ensure that all the hydrogen sulphide was removed from the gas phase. The contents of the two tubes were transferred to a conical flask containing a known volume of acidified iodine.

The following reactions occurred simultaneously:

i.e.
$$CdS + 2HCl = CdCl_2 + H_2S \qquad (2.2)$$
$$H_2S + I_2 = 2HI + S \qquad (2.3)$$

these reactions (2.2) and (2.3) can be combined to give the overall reaction

$$CdS + 2HCl + I_2 = CdCl_2 + 2HI + S \qquad (2.4)$$

The iodine left after all the cadmium sulphide has been converted was titrated against a standard sodium thiosulphate solution

i.e.
$$I_2 + 2Na_2S_2O_3 = 2NaI + Na_2S_2O_6 \qquad (2.5)$$

Hence knowing the amount of iodine present before and after reaction (2.4), it is possible to assess the amount of iodine equivalent to the hydrogen sulphide involved.

From equations (2.1) and (2.4) the net reaction is

$$H_2S + I_2 = 2HI + S \qquad (2.6)$$

It is possible to calculate from equation (2.6) that 1.0ml (0.1N iodine solution) is equivalent to 1.120ml hydrogen sulphide. Then the volume

of H_2S was corrected to the room temperature and atmospheric pressure at the time of calibration, according to the equation

$$V_a = V_{Sd} \cdot \frac{P_{Sd}}{Pa} \cdot \frac{Ta}{T_{Sd}} \qquad (2.7)$$

where V_a = volume of 1 mole of gas at the time of calibration

V_{Sd} = volume of 1 mole of gas in standard condition

Pa = atmospheric pressure at the time of calibration

P_{Sd} = atmospheric pressure in standard condition

Ta = temperature at the time of calibration (^oK)

T_{Sd} = temperature in standard condition (^oK)

$\therefore$ $Va = Vt \cdot e \cdot \frac{760}{Pa} \cdot \frac{Ta}{273.15}$

where Vt = volume of titrate

e = equivalence

B.2.2.2 The Calibration of SO_2 Flowmeter

At a certain flowmeter reading, the sulphur dioxide was passed through two tubes containing 100ml of acidulated water and 2ml of fresh starch solution, the second tube was used to ensure that all SO_2 was dissolved. The solution of sulphur dioxide in these tubes was continuously titrated with potassium iodate solution, according to the reaction:

$$KIO_3 + 5KI + 3SO_2 = 3I_2 + 3KSO_2 \qquad (2.9)$$

To stir the solution and to avoid "suck-backs" the titration was continued by bubbling argon through the titration tubes. The iodate solution contained 2.225gm KIO_3 per litre which gives an equivalence of 1.0ml $\equiv$ .001gm of sulphur where the amount of sulphur is Vt.e

$\therefore$ volume of $SO_2 = \frac{22.4}{32}$ Vt.e litre (2.10)

where (Vt) is the volume of titrate and (e) is the equivalence.

To correct the volume of SO_2 to the room temperature and atmospheric pressure at the time of calibration, equation(2.7) was used. From equation (2.7) and (2.10)

$$Va = 0.7\ V_t \cdot e.\frac{760}{Pa} \cdot \frac{T}{273.15}$$

$$= 1.948\ \frac{V_t \cdot e.\ Ta}{Pa}$$

B.2.3 SULPHIDE CAPACITY RUN TECHNIQUE

The furnace arrangement is shown in Figure (A.2.3), which has been described in Chapter A.2. The furnace was heated by six silicon carbide elements and the temperature was controlled by a Pt/Pt-13% Rh thermocouple with Eurotherm controller. For each run two 1.0g samples of slag were taken, they were placed in two platinum crucibles of 9.5mm diameter and 9.5-12.5mm high. The two crucibles were inserted slowly into the furnace heat zone which was approximately 50mm long ($\pm 3^{\circ}C$) at the centre of the furnace. A small flow of nitrogen or argon was started to flush out the furnace tube and the samples were kept for one hour, so that they would be completely molten. The inert gas was then switched off and the gas mixture turned on to give flow rate of 400ml/minute. The gas mixture was allowed to pass over the samples for four hours so that the gas and slag could reach equilibrium. After the samples reached equilibrium, the alumina tray was rapidly withdrawn from the furnace and the crucibles were immediately quenched to avoid oxidation of the sulphur in the slag. There was some trouble with slag creeping, but creeping phenomena was eliminated as described previously in Chapter (A.2). For lower oxygen pressure the hydrogen, water vapour, hydrogen sulphide and argon gas mixture was used. All these gases were calibrated

using separate gas flowmeters, as shown in Figure (B.2.1).

The heater-stirrer unit in the water bath was switched on and the thermostat adjusted to give the desired temperature of the oxalic acid crystal mixture which was allowed to stabilise overnight. The purified hydrogen was passed through the oxalic acid mixture in the water bath circuit. The same run technique was used as described previously. The exhaust gases from furnace were passed through a bubbler at the end of the furnace and into the atmosphere.

B.2.4 SLAG-SULPHUR ANALYSIS

Several methods of sulphur determination are available, the most convenient method being combustion by carbon dioxide. This method of analyis is based on the estimation of sulphur as sulphur dioxide. This technique of analysis for sulphur by combustion using CO_2 was developed as mentioned previously by Fincham and Richardson[113], as shown in Figure (B.2.2). Each slag to be analysed was crushed and a 0.05g sample accurately weighed out and placed in a pre-ignited fire-clay boat with approximately 0.05g "analar" sodium carbonate (maximum sulphur present as 0.02% sulphate), which acts as a fluxing agent. The combustion furnace, an electric carbolite furnace, is controlled at approximately 1400°C. The combustion boat is carefully introduced to the hot zone in the furnace. A stream of carbon dioxide was blown through the reaction tube at a flow rate of 250ml/minute, and the exhaust gases so evolved from the slag was absorbed into two flasks, each containing 100ml of a solution made up by mixing 5ml of 1:1 hydrochloric acid and 2ml of a starch solution. The evolution and absorption of sulphur dioxide is carried out by continuous titration against potassium iodide-potassium iodate solution, according to the

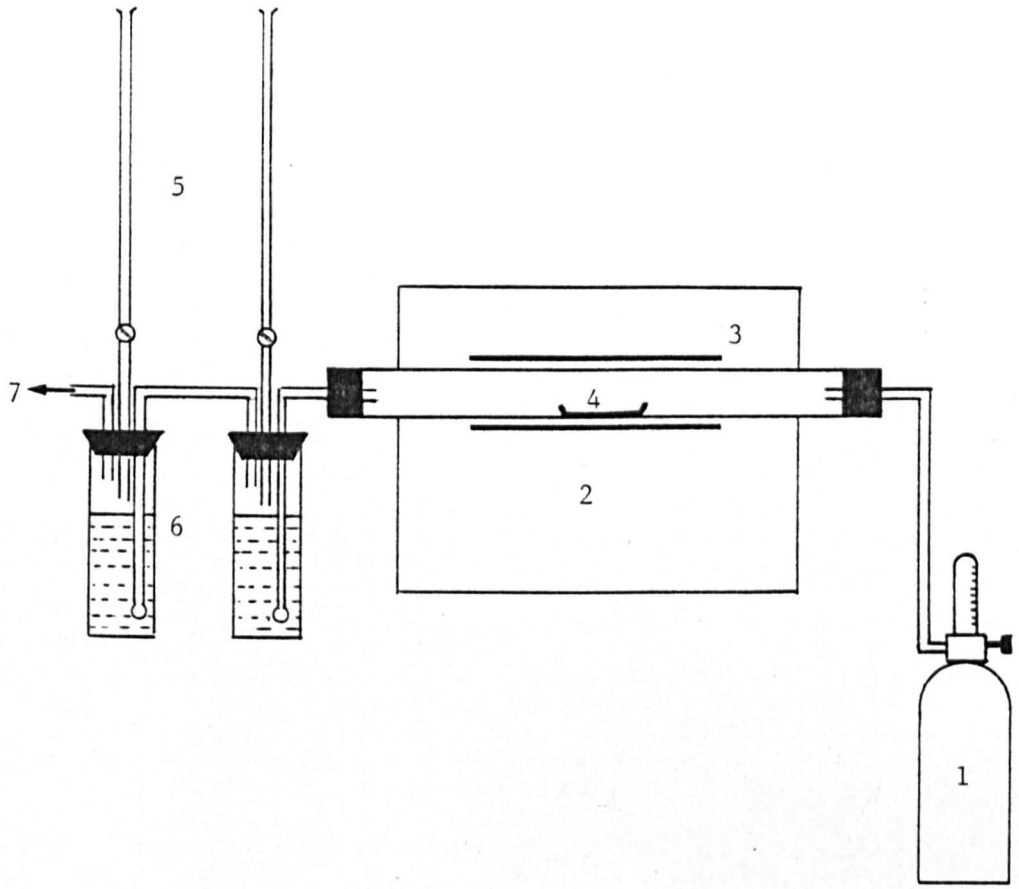

1 - Carbon dioxide supply
2 - Furnace
3 - Silicon-carbide heating elements
4 - Sample boat
5 - Titration bottles
6 - Microburettes
7 - Gas exit

Fig. B.2.2 Sulphur analysis apparatus.

reaction (2.9). Two flasks were used so that there was no chance of sulphur dioxide being swept away by the carbon dioxide. 40-60 minutes were allowed for the slag to be oxidised completely and then the boat was removed from the furnace. The starch solution was made up freshly each day the sulphur analysis was carried out. The iodate/iodide solution contained 0.2225g potassium iodate made up to one litre, which gives the equivalence of 1.0ml = 10^{-4}g sulphur[136].

To check the behaviour of the apparatus and the solution several runs were carried out using B.C.S. Basic slag No. 174/2 containing 0.11% sulphur. As a negligible amount of sulphur trioxide was formed when carbon dioxide was used, it was found that 97% of the sulphur from these slags was evolved. For smaller sulphur contents of the more acid slags the iodate/iodide solution was diluted to give a reasonable litre.

B.2.5 ANALYSIS OF SLAGS

B.2.5.1 a - Analysis of TiO_2

b - Analysis of SiO_2

c - Analysis of FeO

These components have previously been described in Section (A) Chapter (2).

B.2.5.2 Analysis of CaO

The method used for the analysis of calcium oxide was similar to that used for determination of silica and titania by using the atomic absorption spectrophotometry as described previously (A.2).

Lime stock standard solution was prepared by carefully heating 0.3g sodium tetraborate in a platinium crucible to remove the water of crystallisation and then melted. The sodium tetraborate was cooled and 1.78g of "analar" calcium carbonate was

added to it and then covered with 0.70g sodium carbonate and the mixture fused over a bunsen burner. After fusion the melt was cooled and taken up into solution by the addition of 20ml 1:1 hydrochloric acid. The solution was then transferred to a graduated flask and diluted to 100ml with deionized water. A 1000µg/ml lime stock standard solution was then obtained. Three standard solutions containing known concentration were within the range of calcium analysis, suitable dilutions were made and between 0.1-1.0% lanthanum oxide was added to each solution to remove the interference by silicon, aluminium, sulphate and titanium.

The matrix for each of the standard solutions was made the same as that of the slag by additions of titania, silica, alumina and iron oxide stock standard solutions. The stock standard solution prepared for silica and titania can be used for lime determination but with additions of lanthanum or strontium solution at concentration 0.1-1.0% (as the manual of the atomic absorption spectrophotometry recommends) to inhibit the interference by Si, Al, Ti and sulphate.

A.2.5.3 Analysis of Al_2O_3

Alumina sample solutions were prepared from the stock sample solution as for lime by diluting to bring them within the linear working range. Aluminium is partially ionized in the nitrous oxide-acetylene flame. This ionization must be controlled by the addition of alkali salt in the concentration (1000-2000µg/ml) to sample and standard solutions.

Alumina stock standard solution (1000µg/ml) was prepared from pure aluminium powder, dissolving 1.0g Al in (1:1)HCl, adding a small drop of mercury as a catalyst. The solution was diluted to

1.0 litre with 1% (v/v)HCl. To remove the mercury the solution was filtered. Three standard solutions containing known concentrations of alumina were prepared covering the whole range of Al_2O_3 compositions. The potassium solution (1000µg/ml) used to overcome the interference caused by ionization, was prepared by dissolving 19.04g KCl in dionized water and making it up to 1 litre. The matrices of the standard solutions were matched to that of the slag solution by making appropriate additions from the stock standard solution of the other elements.

SECTION B

CHAPTER 3

RESULTS AND DISCUSSION

B.3 RESULTS AND DISCUSSION

In this study the sulphide capacitiesof melts in the systems $FeO-SiO_2-TiO_2$, $FeO-TiO_2-CaO$ and $FeO-SiO_2-TiO_2-CaO$ were measured at an oxygen potential of 10^{-8} atmosphere, using an $H_2-SO_2-CO_2$ and N_2 gas mixture. The $CaO-SiO_2-TiO_2$ system study was made at an oxygen pressure of 10^{-14} atmosphere. by using a gas mixture consisting of $H_2O-H_2-H_2S$ and Ar at 1500°C.

The capacity of a melt to hold sulphur is defined as the sulphide capacity given by the relation:

$$C_S = (\text{wt\% S}) \cdot \frac{P_{O_2}^{\frac{1}{2}}}{P_{S_2}^{\frac{1}{2}}}$$

where P_{O_2} and P_{S_2} are the partial pressure of oxygen and sulphur in the gas atmosphere in equilibrium with the slag. By using ferrous oxide activity data and sulphide capacity values, slag/metal sulphur partition have been calculated for the same systems at the given temperature by using the expression:

$$\frac{(\%S)}{[\%S]} = \frac{C_S}{a_{FeO}} \cdot \frac{K_{FeO}}{K_{S_2}}$$

where

$$K_{FeO} = \frac{a_{FeO}}{P_{O_2}^{\frac{1}{2}}}$$

$$K_{S_2} = \frac{a_S}{P_{S_2}^{\frac{1}{2}}}$$

B.3.1 THE $FeO-SiO_2-TiO_2$ TERNARY SYSTEM

The results from the slags are shown in Table (B.1) and from an examination of Figure (B.3.1), it can be seen that the iso-sulphide capacity lines are parallel to lines of constant iron oxide content, and the sulphide capacity increases when the slag composition moves towards the FeO corner as shown in Figures (B.3.2) and (B.3.3). The activity of iron oxide in the $FeO-SiO_2-TiO_2$ system from the work reported by Abdelkarim[137] decreases when TiO_2 is added to $FeO-SiO_2$ melts and also when SiO_2 is added to $FeO-TiO_2$ melts as in Figures (B.3.4) and (B.3.5). Also evident is the fact that the activity of FeO in $FeO-SiO_2$ and $FeO-TiO_2$ melts shows almost exactly the same degree of negative deviation.

Examination of the equilibrium

$$FeO + \tfrac{1}{2} S_2 = FeS + \tfrac{1}{2} O_2 \qquad (3.1)$$

$$\Delta G^{\circ}_{1500^{\circ}C} = +20{,}330 \text{ cal.mole}^{-1}$$

The equilibrium constant expressed in terms of activities is then given by:

$$K_1 = \frac{a_{FeS}}{a_{FeO}} \cdot \frac{P_{O_2}^{\frac{1}{2}}}{P_{S_2}^{\frac{1}{2}}}$$

$$K_1 = \frac{\gamma_{FeS} \cdot N_{FeS}}{\gamma_{FeO} \cdot N_{FeO}} \cdot \frac{P_{O_2}^{\frac{1}{2}}}{P_{S_2}^{\frac{1}{2}}}$$

As can be seen from equation (3.1) the sulphide capacity is proportional to the term $N_{FeS} \cdot \frac{P_{O_2}^{\frac{1}{2}}}{P_{S_2}^{\frac{1}{2}}}$ and this has been shown in Figure (B.3.1) to be almost constant when TiO_2 replaces SiO_2 in $FeO-SiO_2-TiO_2$ slags.

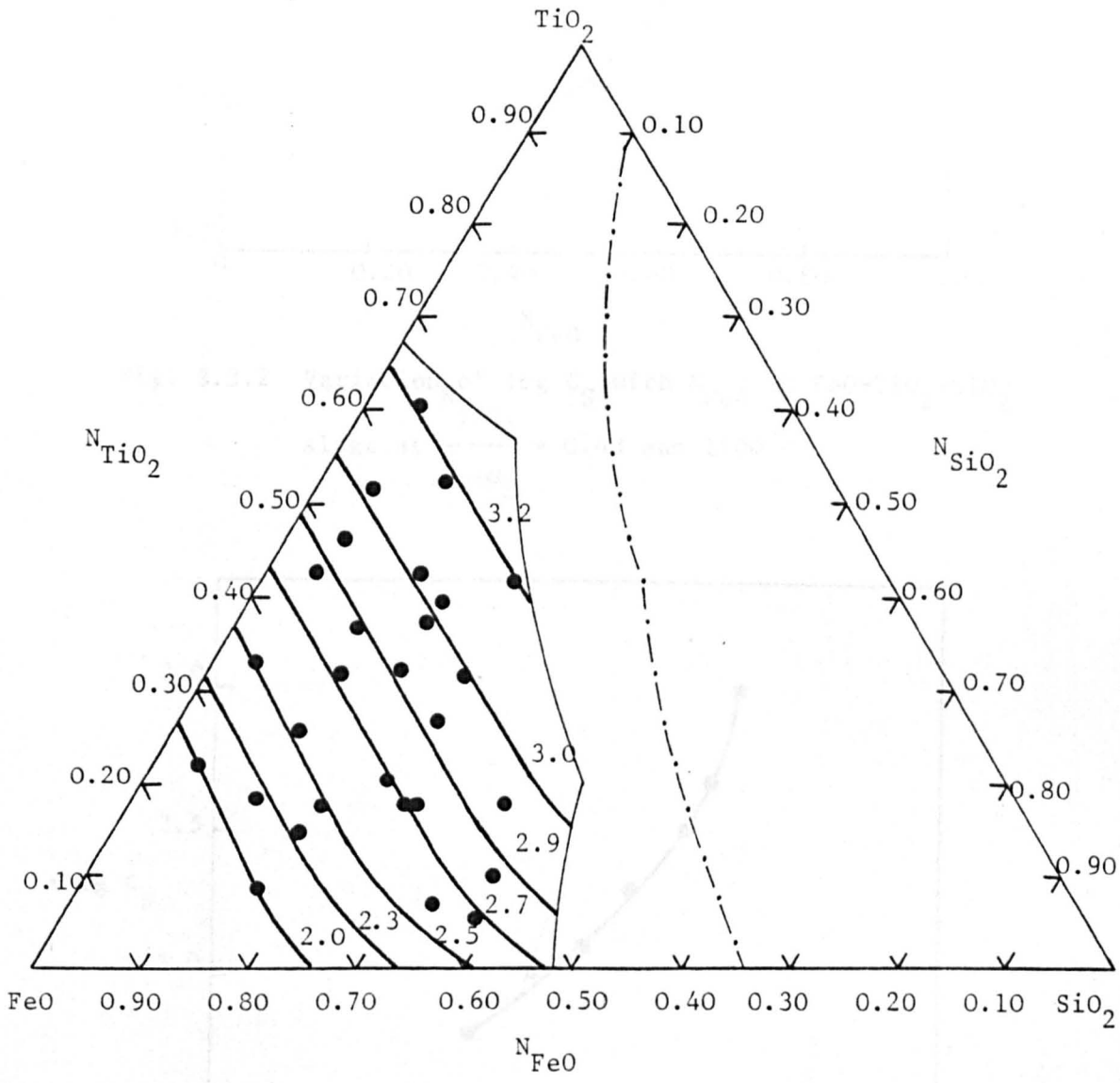

Fig. B.3.1 Sulphide capacities (-log C_S) of the FeO-SiO_2-TiO_2 slags at 1500°C.

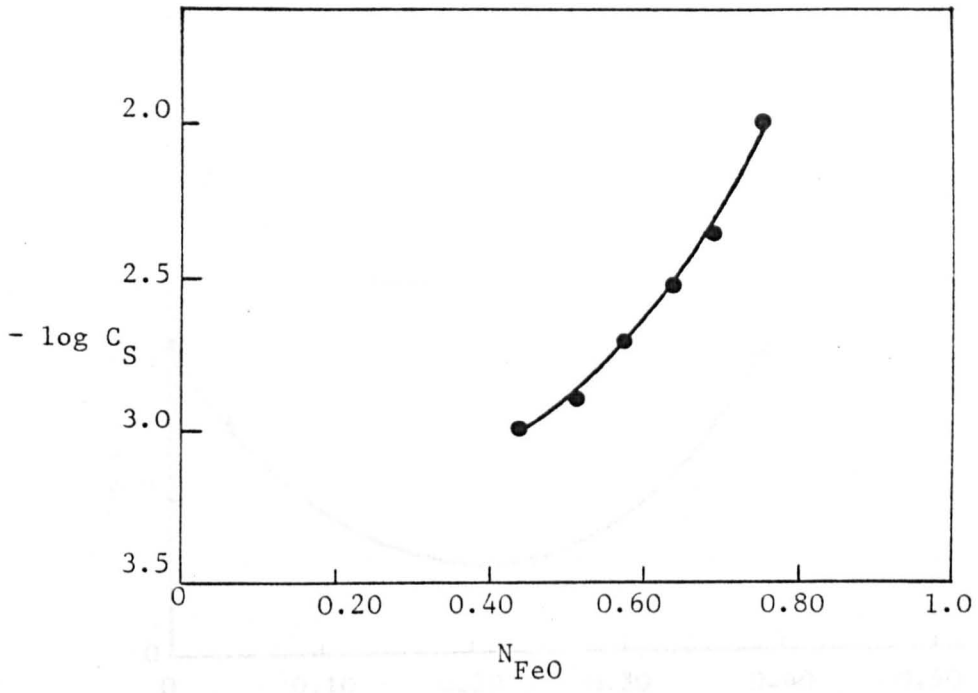

Fig. B.3.2 Variation of log C_S with N_{FeO} in $FeO-TiO_2-SiO_2$ slags at $\frac{N_{TiO_2}}{N_{SiO_2}} = 0.43$ and 1500°C.

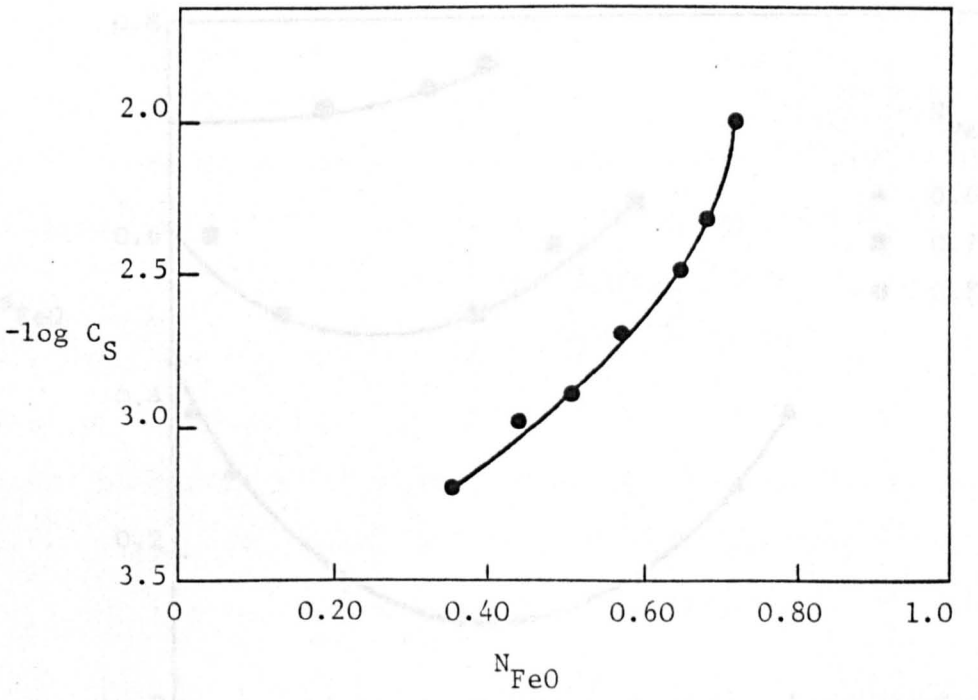

Fig. B.3.3 Variation of log C_S with N_{FeO} in $FeO-TiO_2-SiO_2$ slags at $\frac{N_{TiO_2}}{N_{SiO_2}} = 2.33$ and 1500°C.

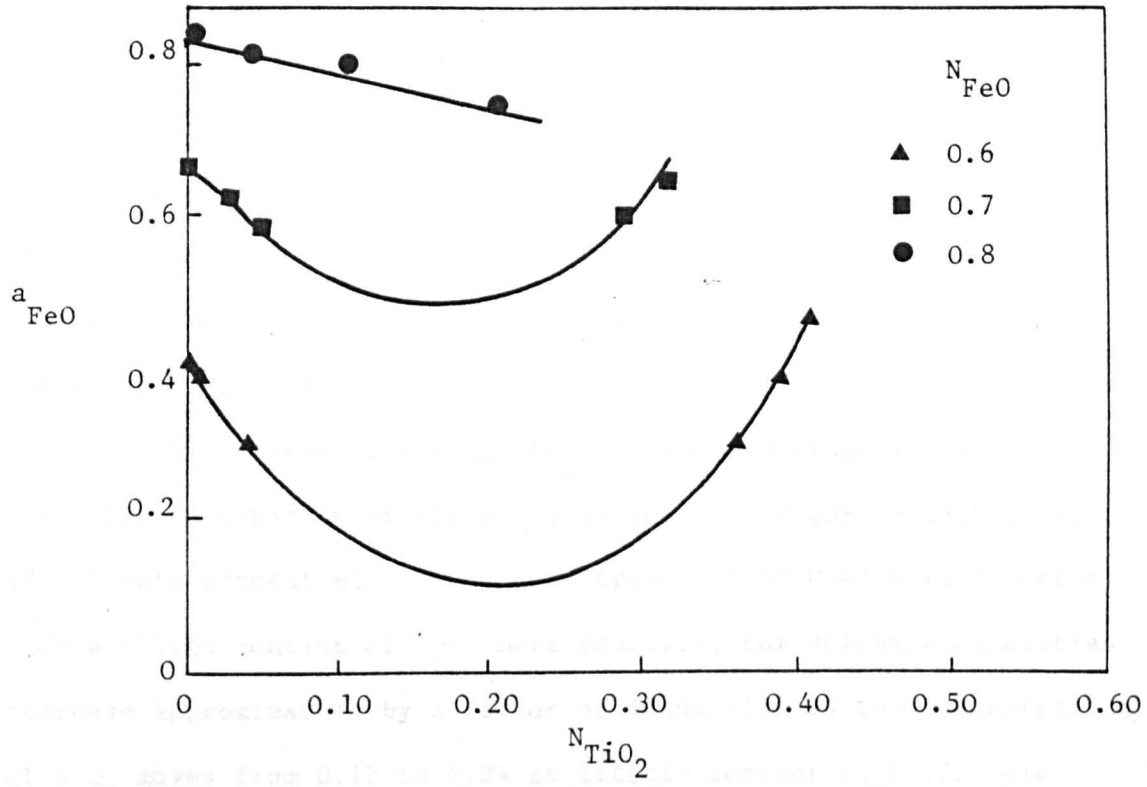

Fig. B.3.4 The effect of replacement of SiO_2 by TiO_2 on FeO activity in FeO-SiO_2-TiO_2 slags at 1475°C(137).

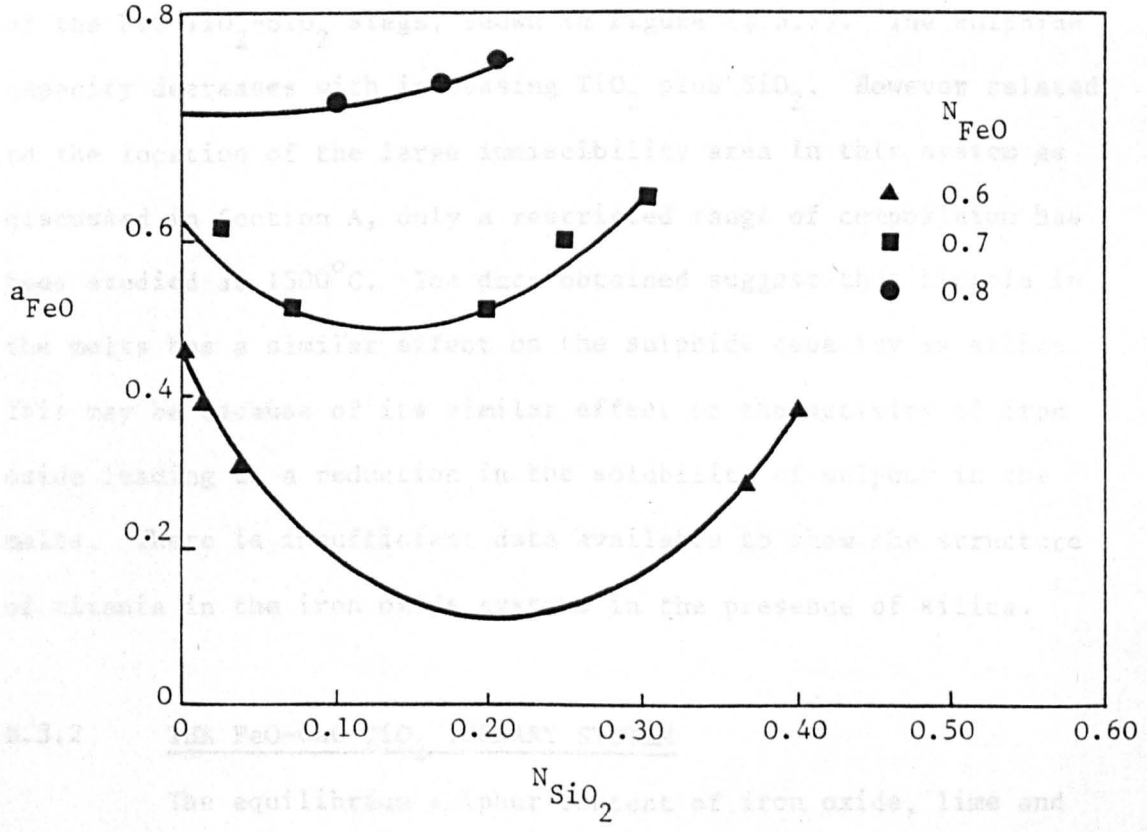

Fig. B.3.5 The effect of replacement of TiO_2 by SiO_2 on FeO activity in FeO-SiO_2-TiO_2 slags at 1475°C (137).

In the melts held under an oxygen pressure of about 10^{-8} atmosphere at 1500°C the sulphide capacities increased with increase in FeO content in the slag. This behaviour was similar to that reported by Derici[123] for CaO-FeO-SiO_2 slags. It is a known fact that the increase in silica in slag would result in a decrease in the sulphide capacities of these melts.

The effect of adding TiO_2 to SiO_2-FeO slags is to reduce the sulphide capacity of the melt, as shown in Figure (B.3.6). As the titania concentration increases from 0.17 to 0.41 mole fraction with a silica content of 0.24 mole fraction, the sulphide capacities decrease approximately by a factor of 4 and also as the concentration of SiO_2 moves from 0.12 to 0.34 at titania content of 0.175 mole fraction.

The effect of titania plus silica on the sulphide capacity of the FeO-TiO_2-SiO_2 slags, shown in Figure (B.3.7). The sulphide capacity decreases with increasing TiO_2 plus SiO_2. However related to the location of the large immiscibility area in this system as discussed in Section A, only a restricted range of composition has been studied at 1500°C. The data obtained suggest that titania in the melts has a similar effect on the sulphide capacity as silica. This may be because of its similar effect on the activity of iron oxide leading to a reduction in the solubility of sulphur in the melts. There is insufficient data available to show the structure of titania in the iron oxide systems in the presence of silica.

B.3.2 THE FeO-CaO-TiO_2 TERNARY SYSTEM

The equilibrium sulphur content of iron oxide, lime and titania melts was investigated at an oxygen pressure of approximately 10^{-8} atmosphere, and sulphur pressure of approximately

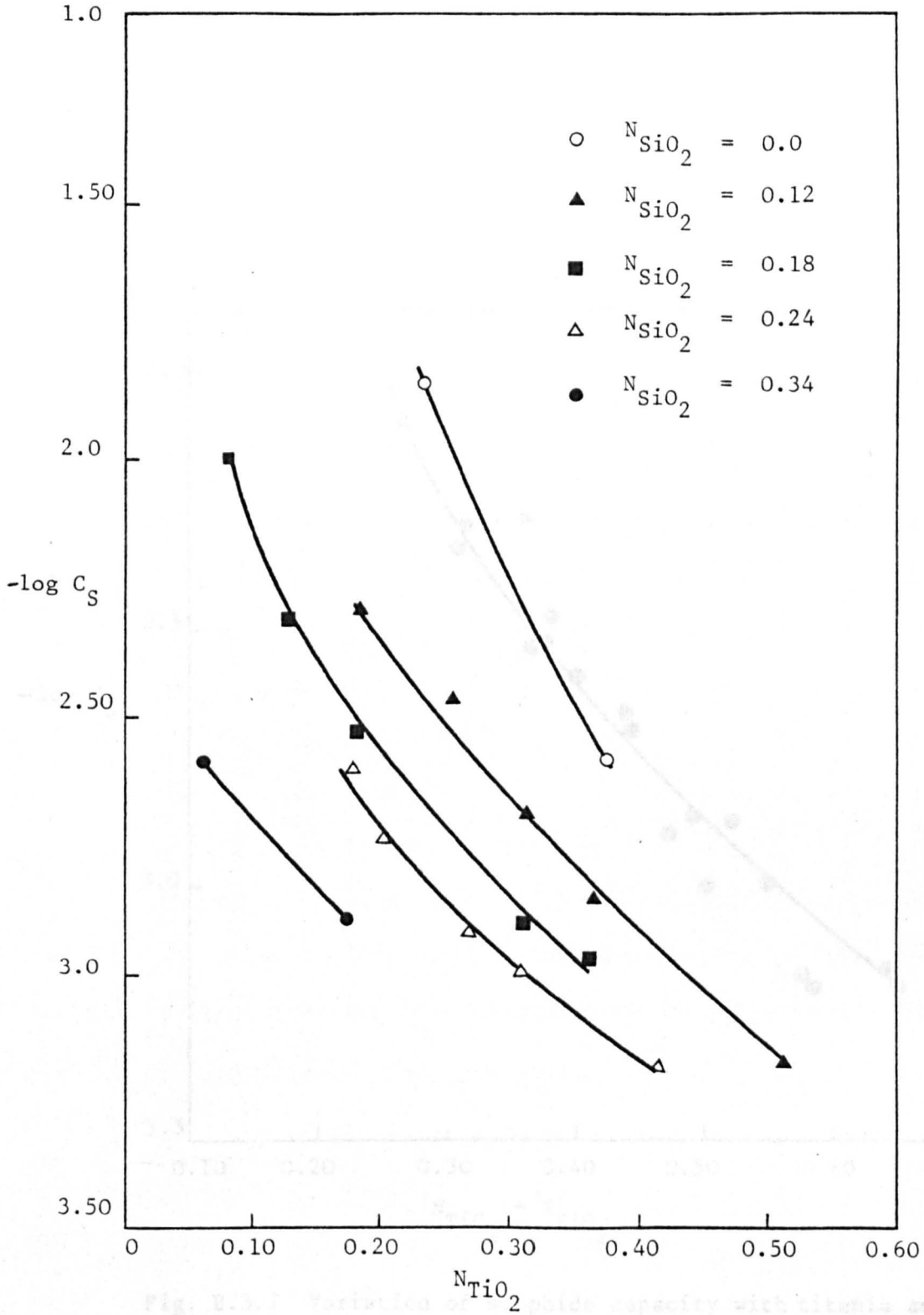

Fig. B.3.6 Variation of sulphide capacity with titania at constant silica of $FeO-TiO_2-SiO_2$ slags at 1500°C.

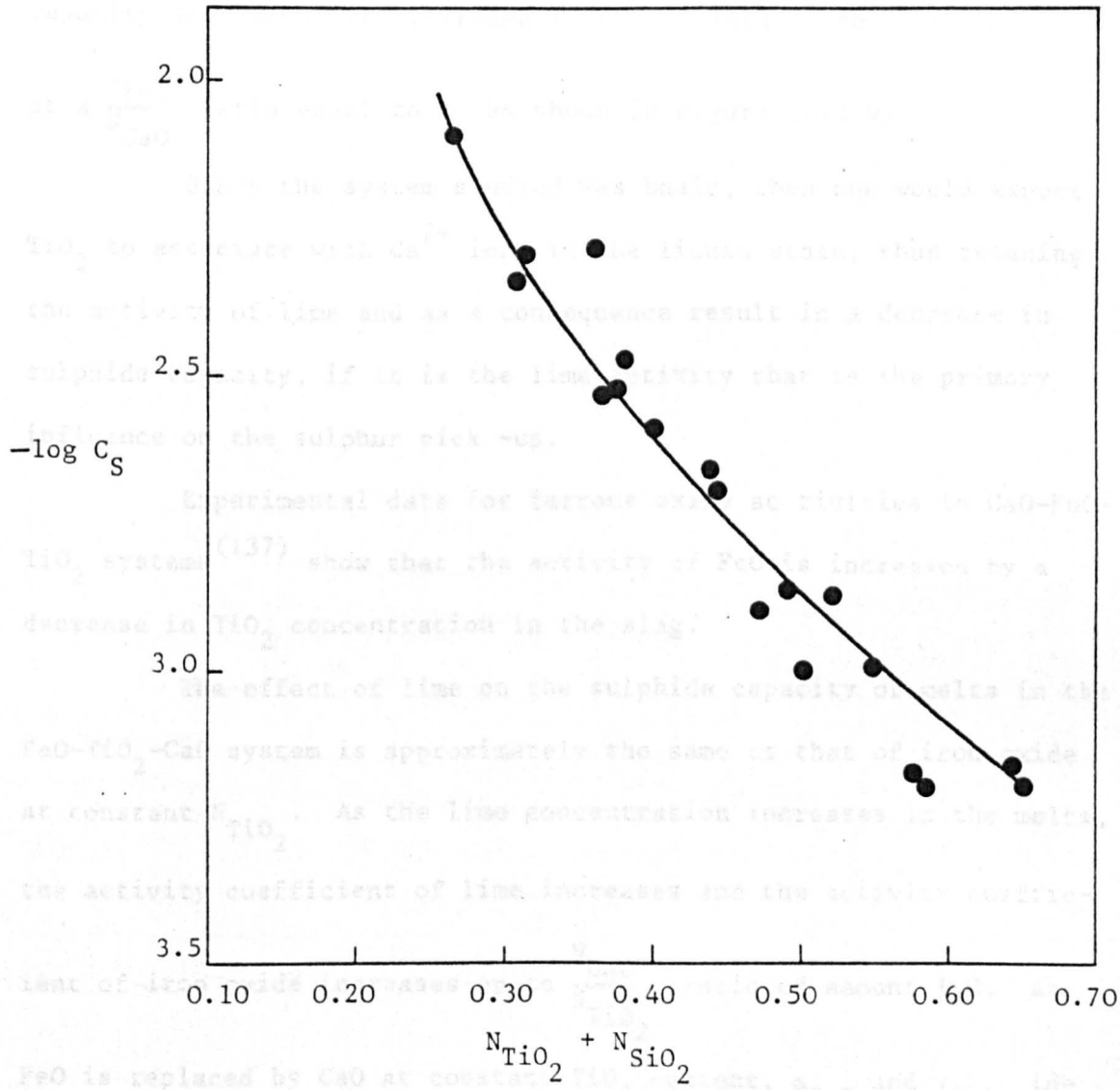

Fig. B.3.7 Variation of sulphide capacity with titania and silica of $FeO-TiO_2-SiO_2$ slags at 1500°C.

10^{-4} atmosphere at 1500°C. The results obtained are shown in Table (B.2). The compositions of the melts examined are shown in Figure (B.3.8). The data show that the sulphide capacity values do not change much by replacement of iron oxide by calcium oxide at a given oxygen pressure and constant mole fraction of titania. The sulphide capacity decreases with increase in the titania content of the melts at a $\frac{N_{FeO}}{N_{CaO}}$ ratio equal to $\frac{3}{2}$ as shown in Figure (B.3.9).

Since the system studied was basic, then one would expect TiO_2 to associate with Ca^{2+} ions in the liquid state, thus reducing the activity of lime and as a consequence result in a decrease in sulphide capacity, if it is the lime activity that is the primary influence on the sulphur pick -up.

Experimental data for ferrous oxide ac tivities in CaO-FeO-TiO_2 systems[137] show that the activity of FeO is increased by a decrease in TiO_2 concentration in the slag.

The effect of lime on the sulphide capacity of melts in the FeO-TiO_2-CaO system is approximately the same as that of iron oxide at constant N_{TiO_2}. As the lime concentration increases in the melts, the activity coefficient of lime increases and the activity coefficient of iron oxide increases up to $\frac{N_{CaO}}{N_{TiO_2}}$ ratio of amount 1.0. As FeO is replaced by CaO at constant TiO_2 content, a_{CaO} and γ_{CaO} increase, i.e. the number of free O^{2-} ions is increasing, but a_{FeO} and γ_{FeO} are decreasing, so reducing the number of free O^{2-} ions. Also, as CaO increases, Fe^{3+} is stabilised relative to Fe^{2+} and this tends to form ferrite ions which decreases the number of free O^{2-} ions in the melt.

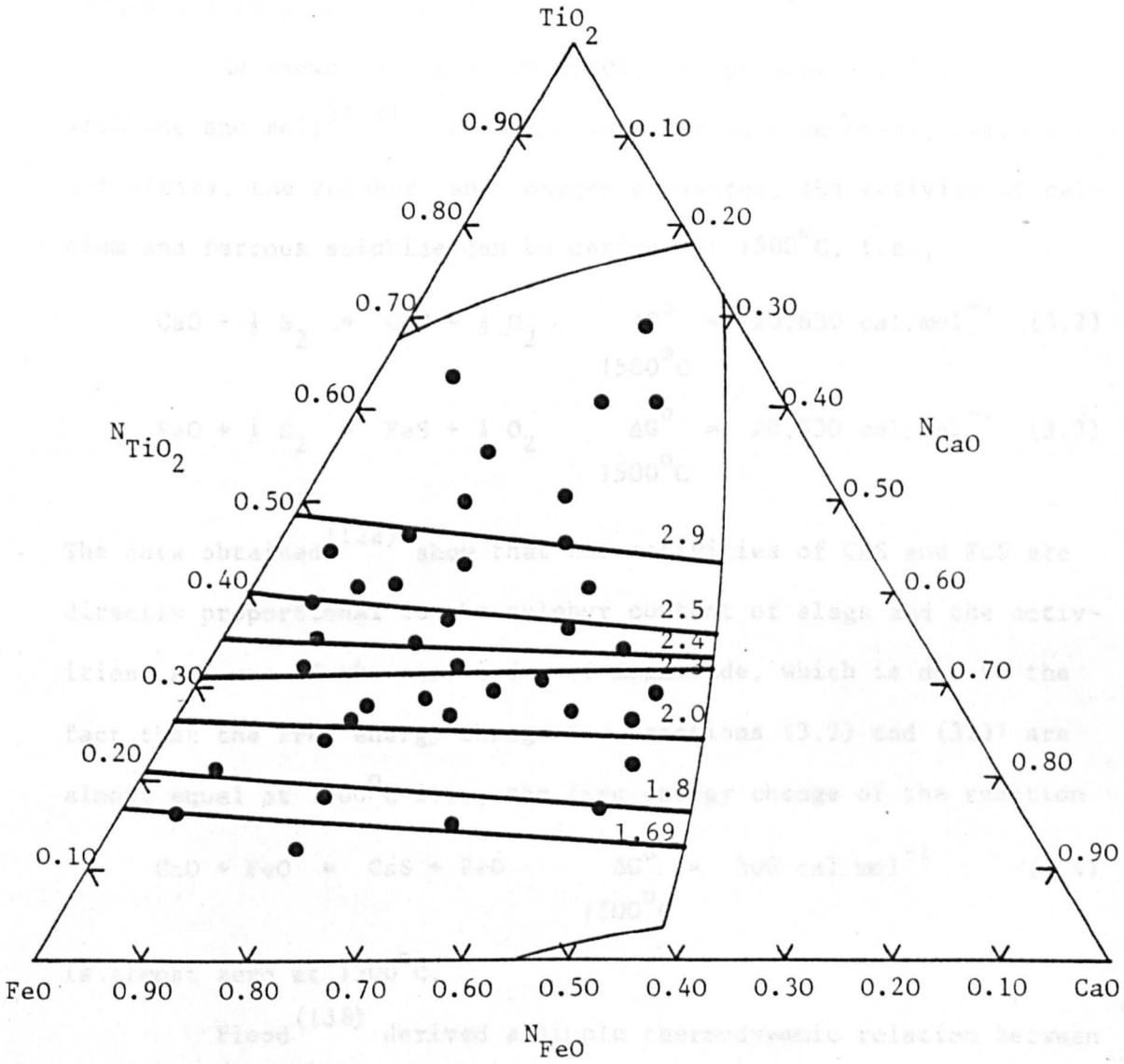

Fig. B.3.8 Sulphide capacities (-log C_S) of the FeO-CaO-TiO_2 slags at 1500°C.

From the sulphide capacities it would seem as though the factor causing an increase in the number of O^{2-} ions is almost exactly counter balanced by the two factors causing a decrease, so that the number of O^{2-} ions replaceable by sulphur ions is constant at a given oxygen and sulphur potential.

As shown in Figure (B.3.10), the present results agree well with Lee and Bell[122]. From the data for calcium oxide, ferrous oxide activities, the sulphur and oxygen pressures, the activity of calcium and ferrous sulphide can be derived at 1500°C, i.e.,

$$CaO + \tfrac{1}{2} S_2 = CaS + \tfrac{1}{2} O_2 \qquad \Delta G^{\circ}_{1500^{\circ}C} = 20{,}630 \text{ cal.mol}^{-1} \qquad (3.2)$$

$$FeO + \tfrac{1}{2} S_2 = FeS + \tfrac{1}{2} O_2 \qquad \Delta G^{\circ}_{1500^{\circ}C} = 20{,}330 \text{ cal.mol}^{-1} \qquad (3.3)$$

The data obtained[122] show that the activities of CaS and FeS are directly proportional to the sulphur content of slags and the activities, and are of the same order of magnitude, which is due to the fact that the free energy change for reactions (3.2) and (3.3) are almost equal at 1500°C i.e., the free energy change of the reaction

$$CaO + FeO = CaS + FeO \qquad \Delta G^{\circ}_{1500^{\circ}C} = 300 \text{ cal.mol}^{-1} \qquad (3.4)$$

is almost zero at 1500°C.

Flood[138] derived a simple thermodynamic relation between the equilibrium constant and the concentrations of ions not entering into the equilibrium equation. The equilibrium constant of the sulphur equilibrium of the equation

$$O'' + \tfrac{1}{2} S_2 = S'' + \tfrac{1}{2} O_2$$

can be in the present case expressed as

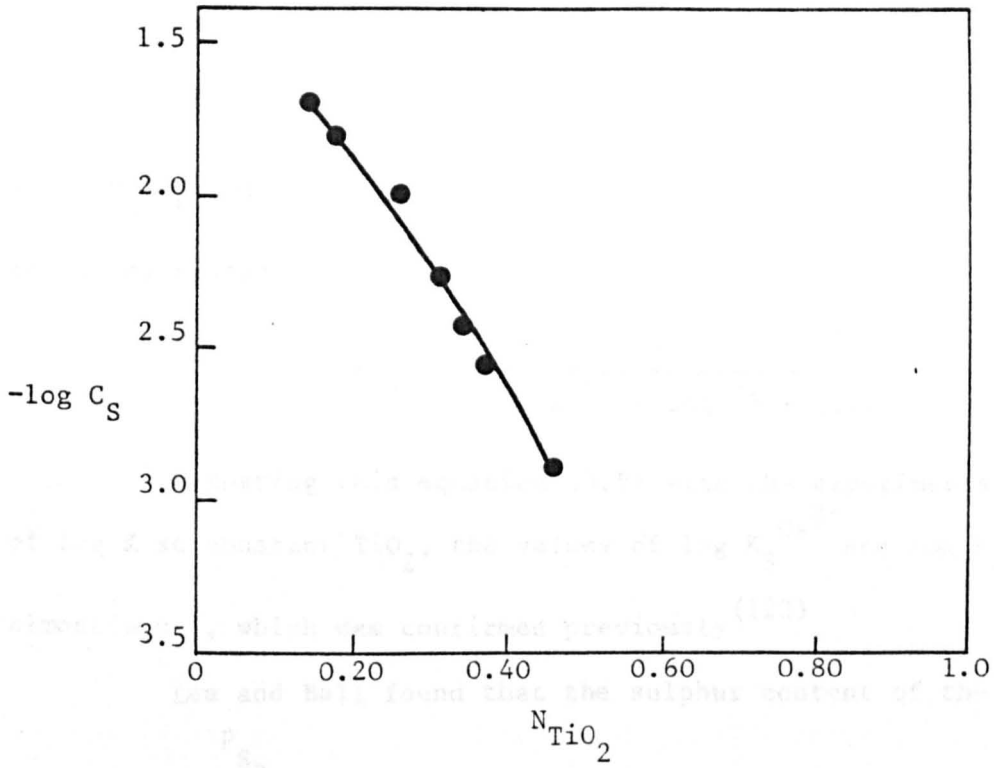

Fig. B.3.9 Variation of sulphide capacity with titania at $\frac{N_{FeO}}{N_{CaO}} = 1.5$ in FeO-CaO-TiO_2 slags at 1500°C.

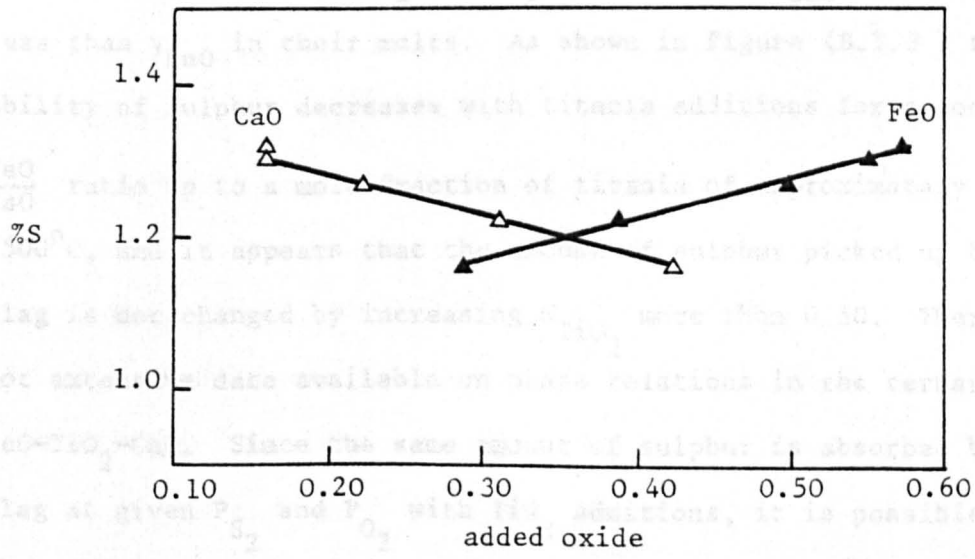

Fig. B.3.10 Sulphur solubility in the FeO-CaO-TiO_2 slags at $N_{TiO_2} = 0.28$ and 1500°C.

$$\log K = N_{Ca^{2+}} \log K_S^{Ca^{2+}} + N_{Fe^{2+}} \log K_S^{Fe2+} \qquad (3.5)$$

where $N_{Ca^{2+}}$ and $N_{Fe^{2+}}$ are the equivalent cation fractions in the melts, expressed at

$$N_{cation} = \frac{n^{(+)}}{n^{(+)} + 2n(^{++}) + \ldots.}$$

Comparing this equation (3.5) with the experimental value of log K at constant TiO_2, the values of log $K_S^{Ca^{2+}}$ and log $K_S^{Fe^{2+}}$ almost equal, which was confirmed previously[122].

Lee and Bell found that the sulphur content of the slags for a given $\frac{P_{S_2}}{P_{O_2}}$ ratio does not vary with the calcium oxide concentration for $CaO-FeO-Fe_2O_3$ melts over a range of oxygen pressures up to 10^{-5} atmosphereand also the activity coefficients of FeS and CaS in the slags were similar. They[122] studied iron oxide melts free of titania or silica, TiO_2 or SiO_2 might reduce γ_{CaO}, which would be less than γ_{FeO} in their melts. As shown in Figure (B.3.8) the solubility of sulphur decreases with titania additions for a constant $\frac{FeO}{CaO}$ ratio up to a mole fraction of titania of approximately 0.50 at 1500°C, and it appears that the amount of sulphur picked up by a slag is not changed by increasing N_{TiO_2} more than 0.50. There are not extensive data available on phase relations in the ternary system $FeO-TiO_2-CaO$. Since the same amount of sulphur is absorbed by the slag at given P_{S_2} and P_{O_2} with TiO_2 additions, it is possible that a a new phase is formed in this region. It is suggested from data for $FeO-TiO_2-SiO_2$ system which has been studied in this work that sulphide capacities decrease with increase in the concentration of titania up

to N_{TiO_2} equal to 0.67 in melts in the binary system TiO_2-FeO. There are insufficient data available to show the effect of varying the titania to lime ratio in melts in the TiO_2-CaO binary system, due to a very limited range of composition which can be studied at 1500°C. At mole ratios $\frac{CaO}{TiO_2}$ between 1.0 to 1.5, TiO_2 and CaO form a series of compounds of formula 3 CaO.2 TiO_2 melting at 1740°C, 4 CaO.3 TiO_2 melting at 1755°C and CaO.TiO_2 melting at 1970°C in the CaO-TiO_2 binary system as shown in Figure (B.3.11)[139]. In the FeO-TiO_2 binary system[2] a series of compounds of the formula 2 FeO.TiO_2 melting at 1395°C, FeO.TiO_2 melting at 1400°C and FeO.2 TiO_2 melting at 1494°C are formed at $\frac{N_{FeO}}{N_{TiO_2}}$ ratio between 1.0 and 1.5, as shown in Figure (A.1.1).

Sulphide capacities of melts in the system FeO-CaO-SiO_2 have been studied at 1500°C by Derici[123] on the silica saturation line sulphide capacities increased 4 to 5 times as the composition changes from CaO-SiO_2 to FeO-SiO_2 side of the ternary. Melts which are not saturated with silica and lie between the Rankinite and Wallastonite phase fields showed high ferric oxide concentration at a given oxygen pressure due to the increase in the activity coefficient of ferrous oxide and decrease in coefficient of ferric oxide in these compositions. Derici[123] showed the effect on the sulphide capacity of melts at constant silica concentrations. The C_S values increase with increase in the $\frac{FeO}{CaO}$ ratio the effect was relatively very small and decreased with increase in silica concentration as in Figures (B.3.12 and (B.3.13), which has been confirmed by this study for FeO-TiO_2-CaO system.

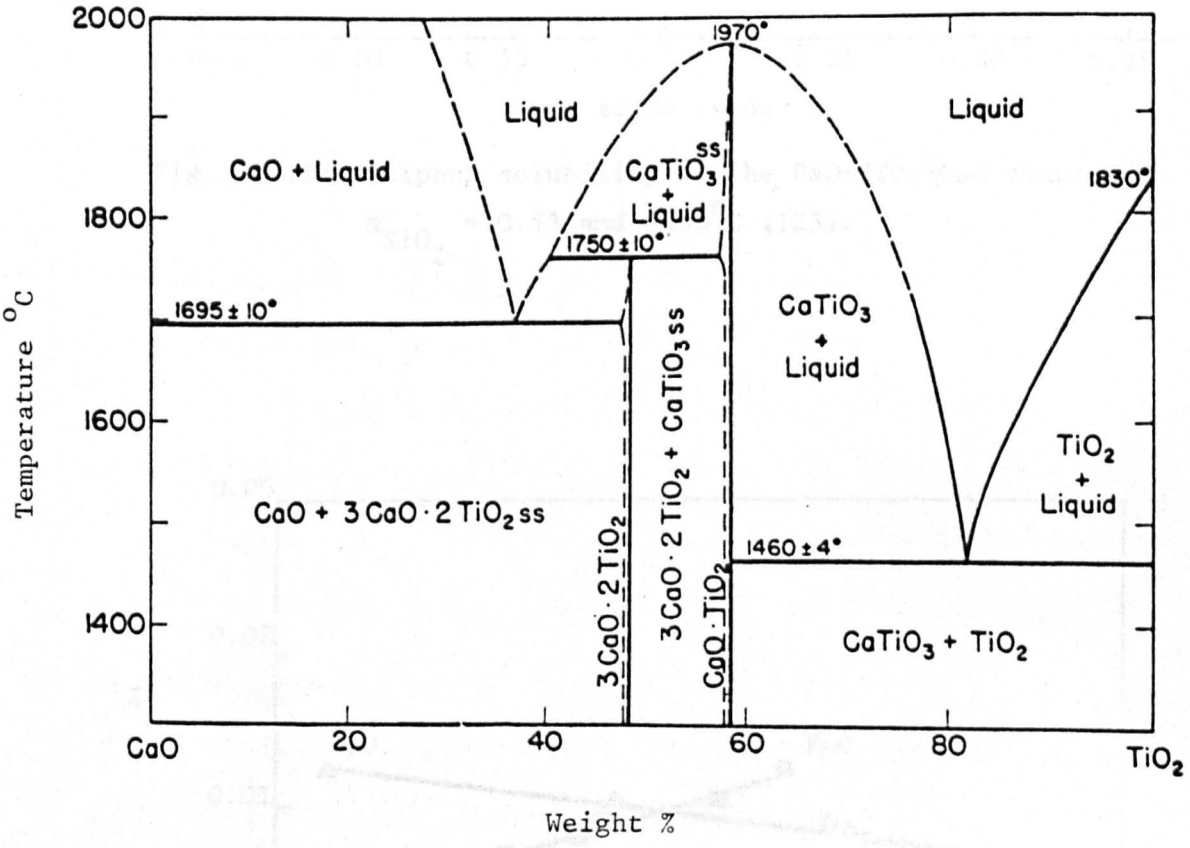

Fig. B.3.11 Phase diagram for the system $CaO-TiO_2$ (139)

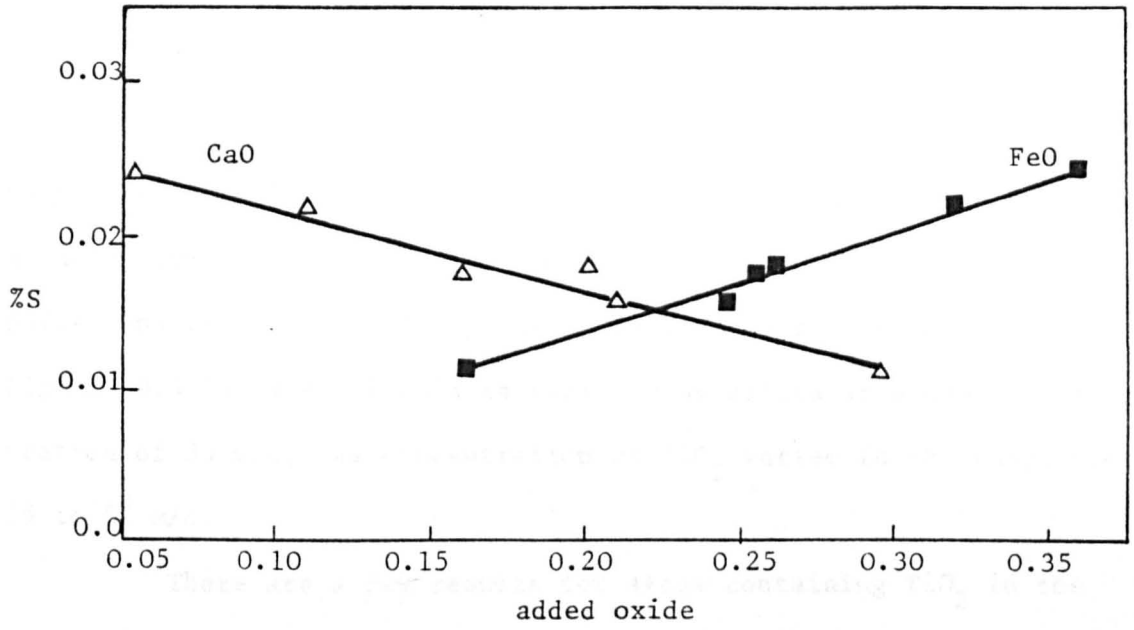

Fig. B.3.12 Sulphur solubility of the FeO-SiO_2-CaO slags at N_{SiO_2} = 0.53 and 1500°C (123).

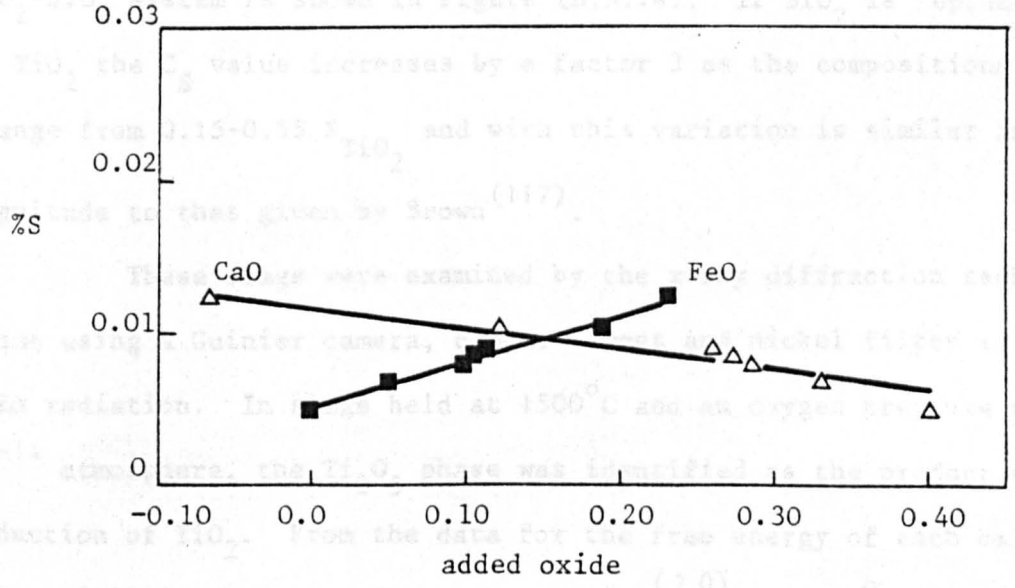

Fig. B.3.13 Sulphur solubility of the FeO-SiO_2-CaO slags at N_{SiO_2} = 0.65 and 1500°C (123).

B.3.3 THE $CaO-TiO_2-SiO_2$ TERNARY SYSTEM

Brown[117] has studied the sulphide capacities for the ternary system $CaO-TiO_2-SiO_2$ at oxygen pressure 10^{-8} atmosphere using a gas mixture consisting of $H_2-CO_2-SO_2$ and Ar at 1500°C. The sulphide capacity is reduced approximately by a factor of two, as in Figure (B.3.14) when titania is replaced by silica at a CaO concentration of 33 m/o, the concentration of TiO_2 varied in the range from 15 to 57 m/o.

There are a few results for slags containing TiO_2 in the $SiO_2-CaO-TiO_2$ system which have been made at an oxygen pressure of 10^{-14} atmosphere, as given in Table (B.3). A water vapour, hydrogen, hydrogen sulphide and argon, gas mixture was used to control the oxygen and sulphur potential of the melt. The graph of the logarithm of the sulphide capacity versus the mole fraction titania of the $CaO-TiO_2-SiO_2$ system is shown in Figure (B.3.14). If SiO_2 is replaced by TiO_2 the C_S value increases by a factor 3 as the compositions change from 0.15-0.55 N_{TiO_2} and with this variation is similar in magnitude to that given by Brown[117].

These slags were examined by the x-ray diffraction technique using a Guinier camera, copper target and nickel filter to give CuKα radiation. In slags held at 1500°C and an oxygen pressure of 10^{-14} atmosphere, the Ti_2O_3 phase was identified as the product of reduction of TiO_2. From the data for the free energy of each oxide, and equilibrium constant for each reaction[70] at 1500°C, i.e.

$$\Delta G = -RT \ln K_p$$

the range of stability of some oxides of titanium, can be calculated at 1500°C as shown in Table (B.4).

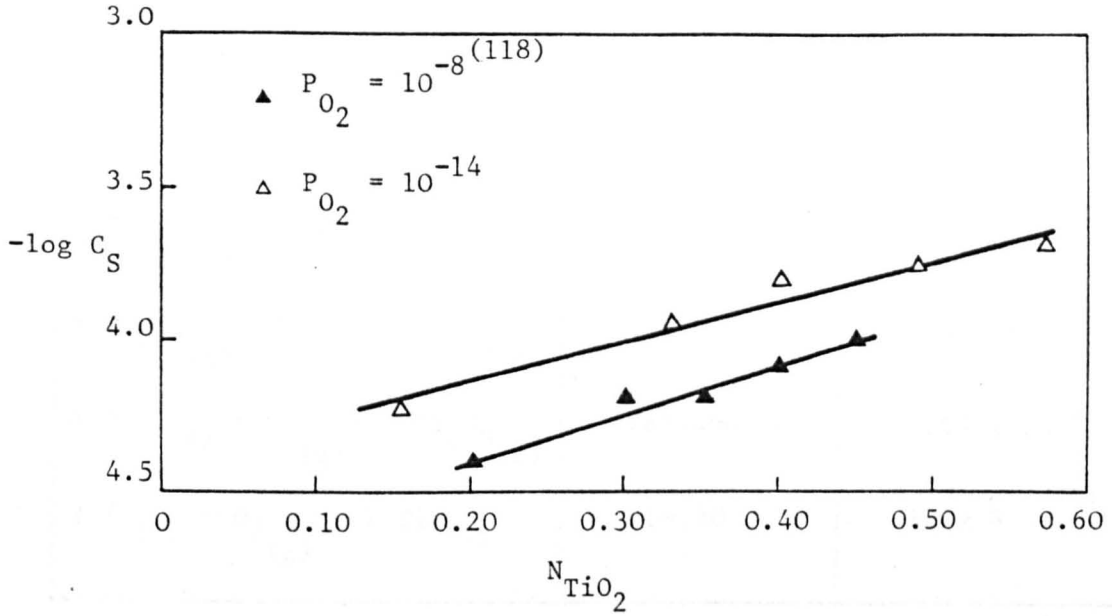

Fig. B.3.14 Variation of sulphide capacity with titania in the TiO_2-CaO-SiO_2 slags at N_{CaO} = 0.30 and 1500°C.

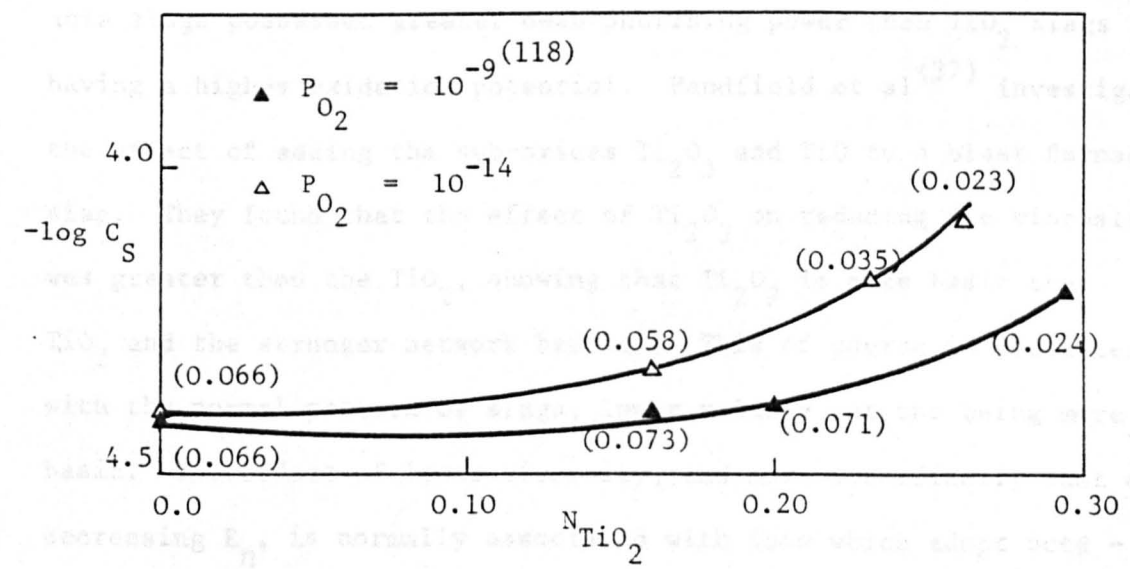

Fig. B.3.15 Variation of sulphide capacity with titania in the TiO_2-CaO-SiO_2-Al_2O_3 slags at N_{CaO} = 0.34 and 1500°C, figures in brackets give the $N_{Al_2O_3}$ content of the melt.

TABLE 8.4

Equilibrium Reaction	ΔG^{o} cal.mol^{-1}	Partial pressure of oxygen (atm)
$2\ Ti_3O_{5(s)} + O_{2(g)} = 6\ TiO_{2(s)}$	- 92,800	3.62×10^{-12}
$6\ Ti_2O_{3(s)} + O_{2(g)} = 4\ Ti_3O_{5(s)}$	-106,000	8.5×10^{-14}
$4\ Ti\ O_{(s)} + O_{2(g)} = 2\ Ti_2O_{3(s)}$	-162,400	9.53×10^{-21}
$2\ Ti_{(s)} + O_{2(g)} = 2\ TiO_{(s)}$	-169,80	1.16×10^{-21}

This table shows that around an oxygen pressure of 10^{-14} atmosphere, TiO_2 can be reduced to Ti_2O_3, this fits with the observation made in the present study. An increase of C_S values with increased Ti_2O_3 content comes from the fact that highly reduced titania slags possessed greater desulphurising power than TiO_2 slags having a higher oxidation potential. Handfield et al[37] investigated the effect of adding the sub-oxides Ti_2O_3 and TiO to a blast furnace slag. They found that the effect of Ti_2O_3 on reducing the viscosity was greater than the TiO_2, showing that Ti_2O_3 is more basic than TiO_2 and the stronger network breaker. This of course is consistent with the normal pattern of slags, lower valency cations being more basic. The effect of lower viscosity, and more specifically that of decreasing E_η, is normally associated with ions which adopt octahedral co-ordination, so that the Ti^{3+} ion is seen to have an even stronger preference for six-fold co-ordination than Ti^{4+}, which again is consistent with its large size. In fact, Handfield and Charette[18] found that by studying viscosities on Sorelslags similar values were

obtained for both low and high FeO contents. The effect of FeO reduction is counterbalanced by the effect of increasing the Ti_2O_3 content, which in turn implies that Ti_2O_3 has much the same effect on slag structure as FeO, in agreement with Handfield et al[37].

The effect of titania on the sulphide capacity of some melts in $CaO-TiO_2-TiO_2-Al_2O_3$ system at an oxygen pressure of 10^{-14} atmosphere, and 1500°C is given in Table (B.3A) and Figure (B.3.15).

B.3.4 THE $FeO-SiO_2-CaO-TiO_2$ QUATERNARY SYSTEM

Sulphide capacities have been measured for melts in the $FeO-TiO_2-SiO_2-CaO$ system at an oxygen pressure of 10^{-8} atmosphere and 1500°C, and data is given in Table (B.5). As shown in Figure (B.3.16) the iso-sulphide capacity lines are parallel to lines of constant iron oxide content, and that C_S increases when the slag compositions move towards the iron oxide corner in pseudo ternary system $FeO-TiO_2-SiO_2$ with 12 m/o CaO added at given P_{O_2} and temperature. The Figure (B.3.17) shows the pick-up of sulphur decreases with increase in titania content in the slag at constant lime. From a comparison of Figures (B.3.7) and (B.3.18) it can be seen that by adding TiO_2 plus silica in $FeO-TiO_2-SiO_2$ ternary system and in $FeO-SiO_2-TiO_2-CaO$ quaternary system, the sulphide capacities are reduced, the effect being slightly greater in the quaternary system. Abdelkarim[137] found that the bowing of the FeO iso-activity towards the FeO corner was maintained with CaO contents of 6 m/o in the quaternary system $FeO-TiO_2-SiO_2-CaO$, as shown in Figure (B.3.19). With further additions of lime to the basic ternary, the direction of bowing of the ferrous oxide, iso-activity curves was reversed. This indicates that an increase of CaO in the melts increased the FeO

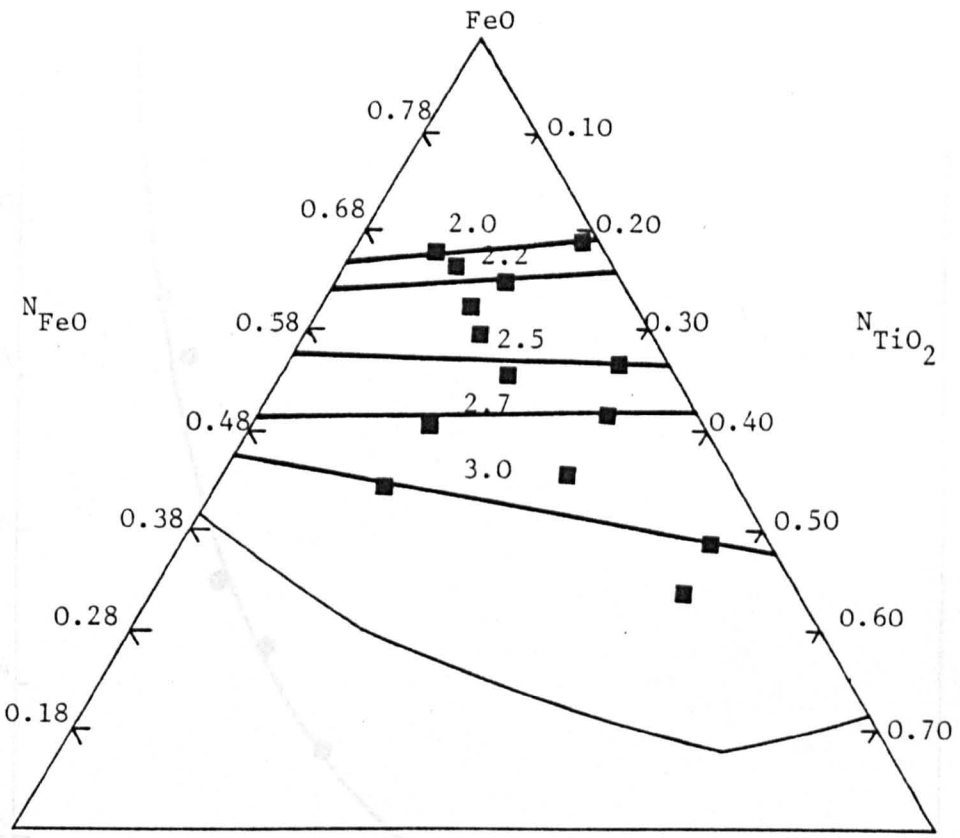

Fig. B.3.16 Sulphide capacities (-log C_S) of FeO-TiO_2-SiO_2-CaO slags at constant N_{CaO} = 0.12 and 1500°C.

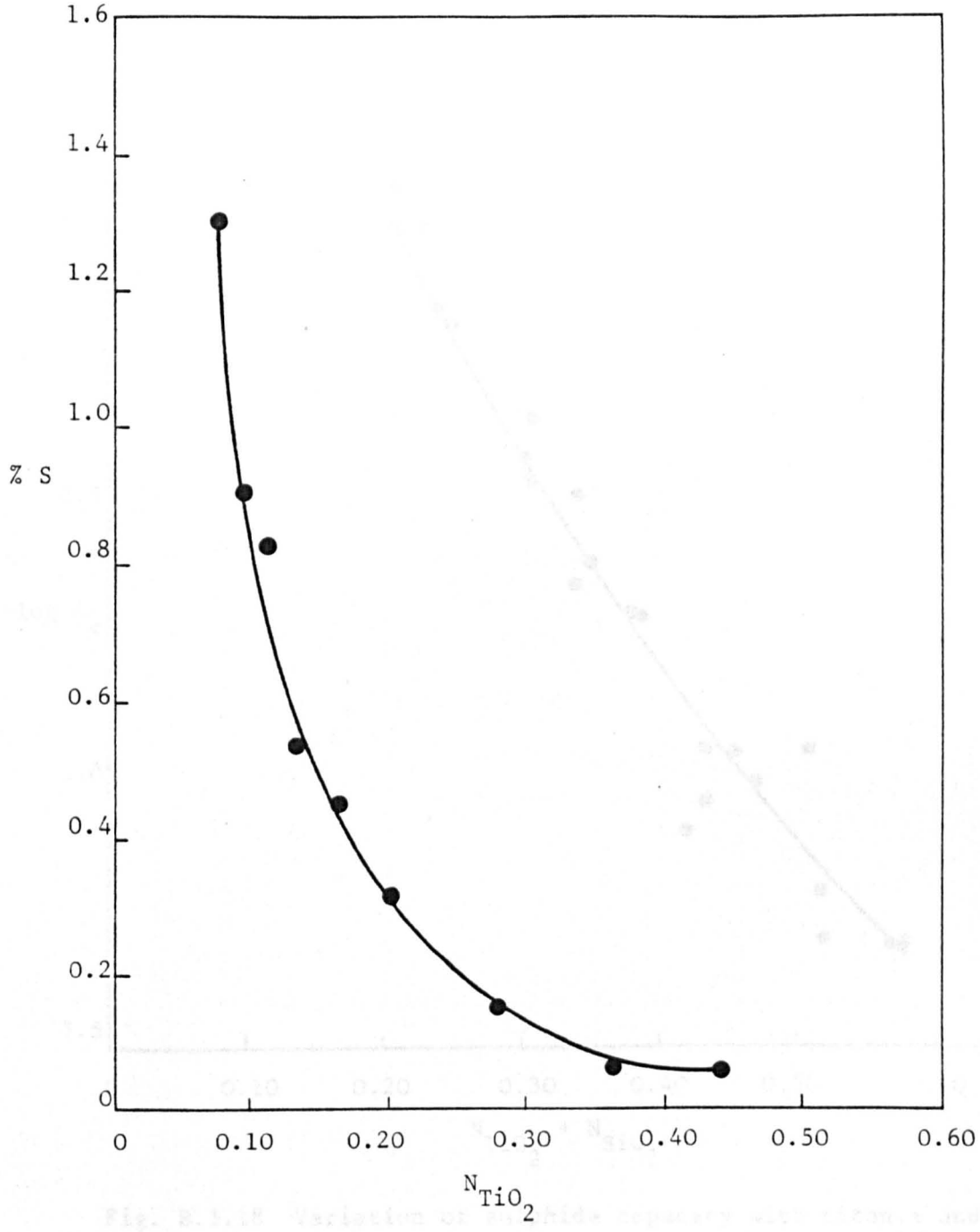

Fig. B.3.17 Sulphur solubility of the $FeO-TiO_2-SiO_2-CaO$ slags at $N_{SiO_2} = 0.15$, $N_{CaO} = 0.12$ and $1500^{o}C$.

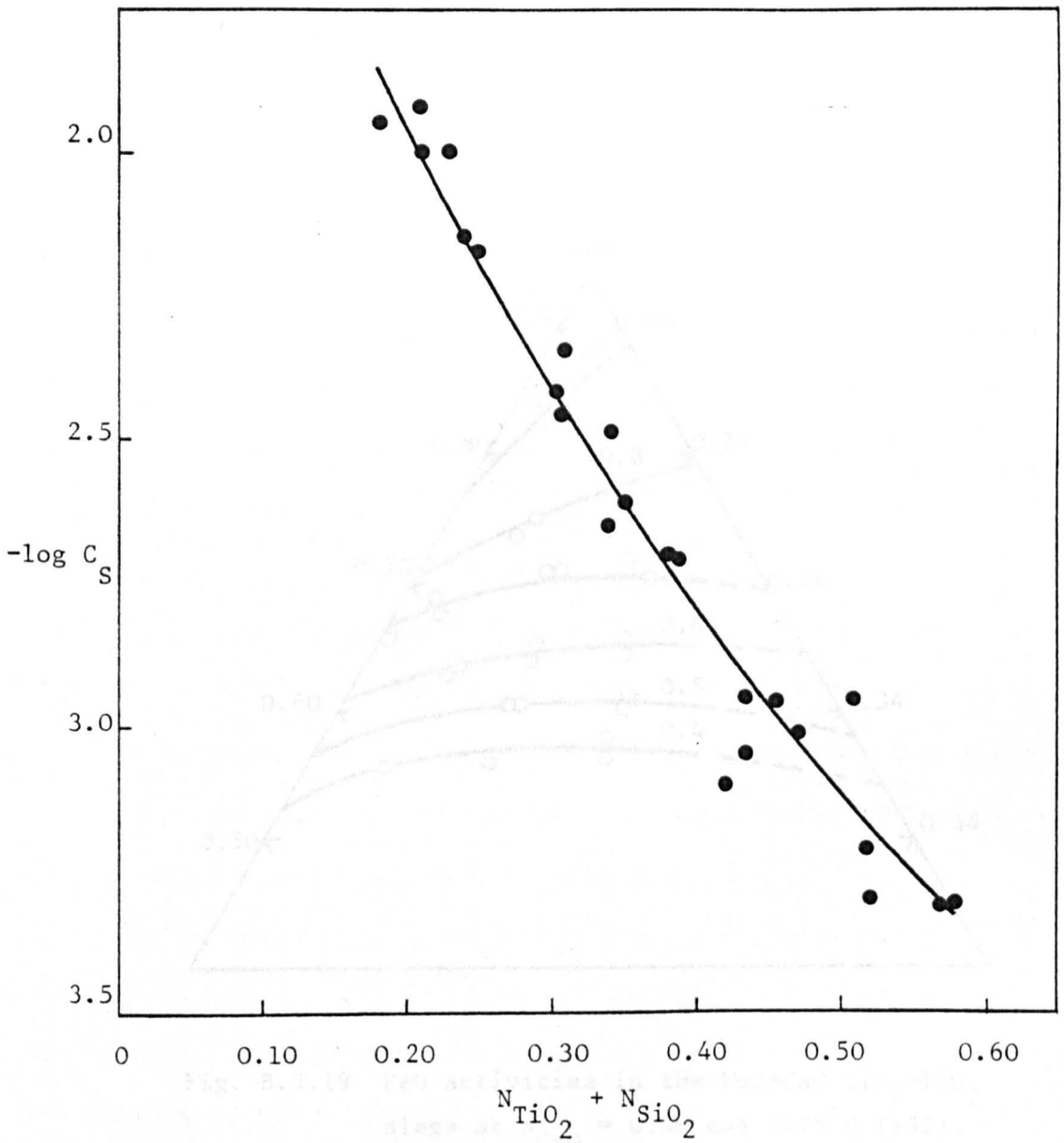

Fig. B.3.18 Variation of sulphide capacity with titania and silica of $FeO-TiO_2-SiO_2-CaO$ slags at 1500^oC.

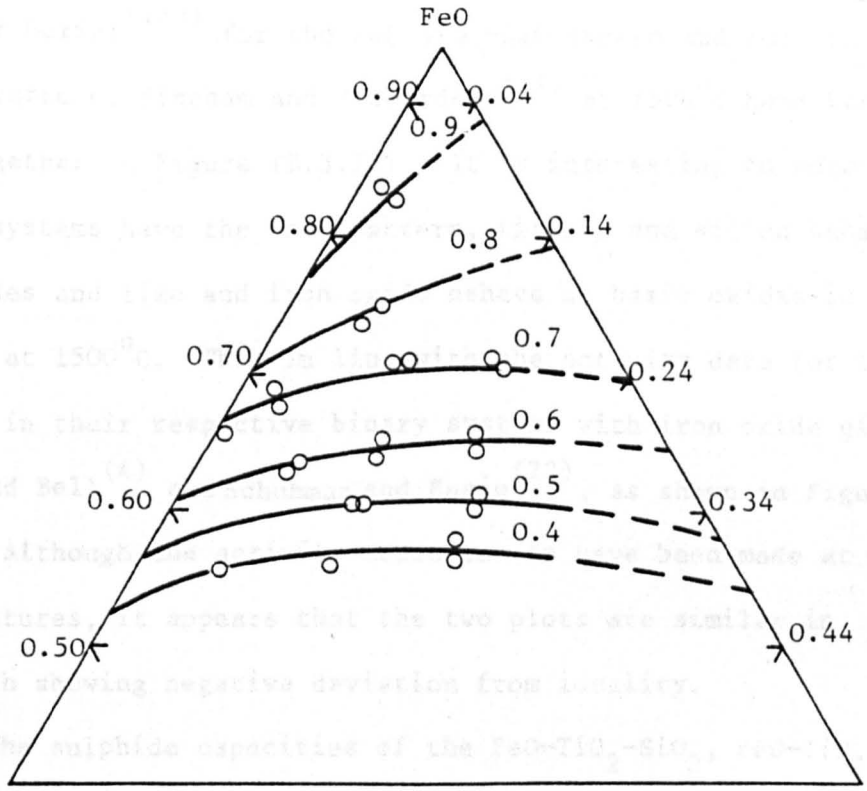

Fig. B.3.19 FeO activities in the FeO-CaO-SiO_2-TiO_2 slags at N_{CaO} = 0.06 and 1475°C (137).

activity coefficients. The variation of C_S with FeO content at a mole percentage of lime of 0.125 is shown in Figure (B.3.20). It can be seen that as mentioned previously replacement of CaO by FeO has only a very small effect on the sulphide capacity values as in Figure (B.3.21).

To compare the behaviour of the sulphide capacities of the systems, $FeO-TiO_2$, $FeO-TiO_2-SiO_2$, $FeO-TiO_2-CaO$, $FeO-TiO_2-SiO_2-CaO$, the data of Derici[123] for the $FeO-SiO_2-CaO$ system and for the $FeO-SiO_2$ system of Fincham and Richardson[81] at 1500°C have been plotted together on Figure (B.3.22). It is interesting to note that all these systems have the same pattern, titania and silica behave as acidic oxides and lime and iron oxide behave as basic oxides in the iron slags at 1500°C. This in line with the activity data for titania and silica in their respective binary systems with iron oxide given by Smith and Bell[4] and Schuhman and Ensio[22], as shown in Figure (B.3.23). Although the activity measurements have been made at different temperatures, it appears that the two plots are similar in nature, both showing negative deviation from ideality.

The sulphide capacities of the $FeO-TiO_2-SiO_2$, $FeO-TiO_2-CaO$, $FeO-SiO_2-CaO$ and TiO_2-SiO_2-CaO ternary systems have been measured, and they form the boundaries of the quaternary system $FeO-TiO_2-SiO_2-CaO$, this diagram is given in Figure (B.3.24).

The results for the system $CaO-TiO_2-SiO_2$[117] show that the sulphide capacity does not show a large change with increasing titania content in the melt, but when silica is replaced by titania on a molar or weight percent, there is a slight increase in the sulphide capacity. It is interesting to note that sulphide capacities for all systems are consistent with one another. The data from Carter and

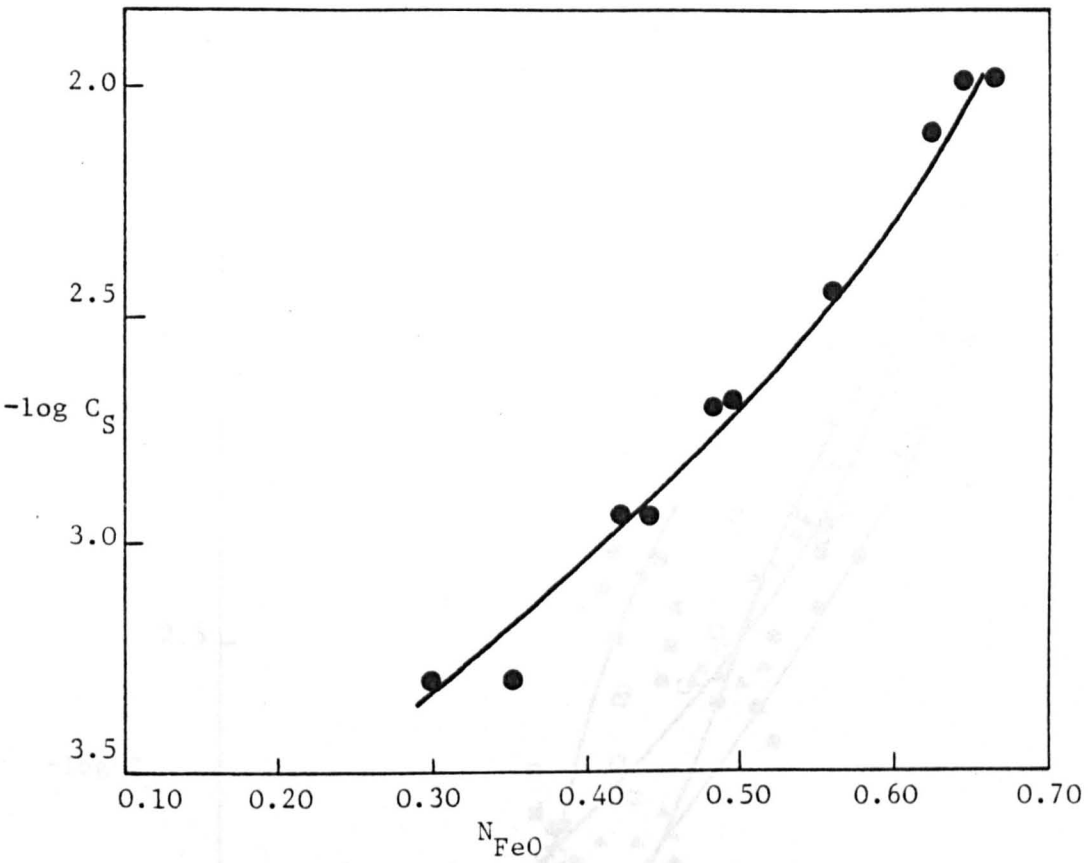

Fig. B.3.20 Variation of sulphide capacity with iron oxide at N_{CaO} = 0.125 in FeO-TiO_2-SiO_2-CaO slags and 1500°C.

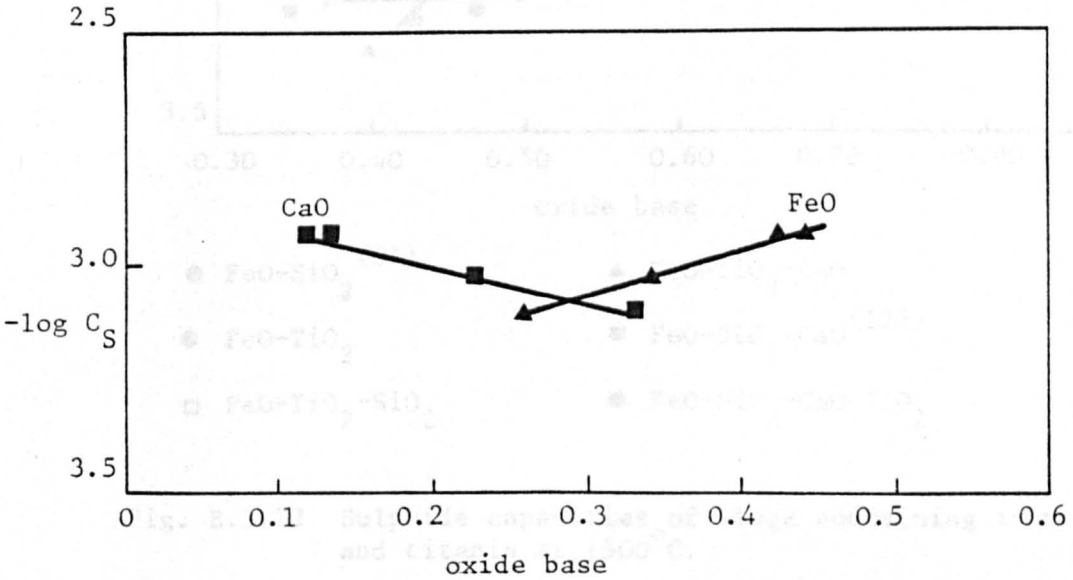

Fig. B.3.21 Variation of sulphide capacity with oxide base in the FeO-CaO-TiO_2-SiO_2 slags at 1500°C.

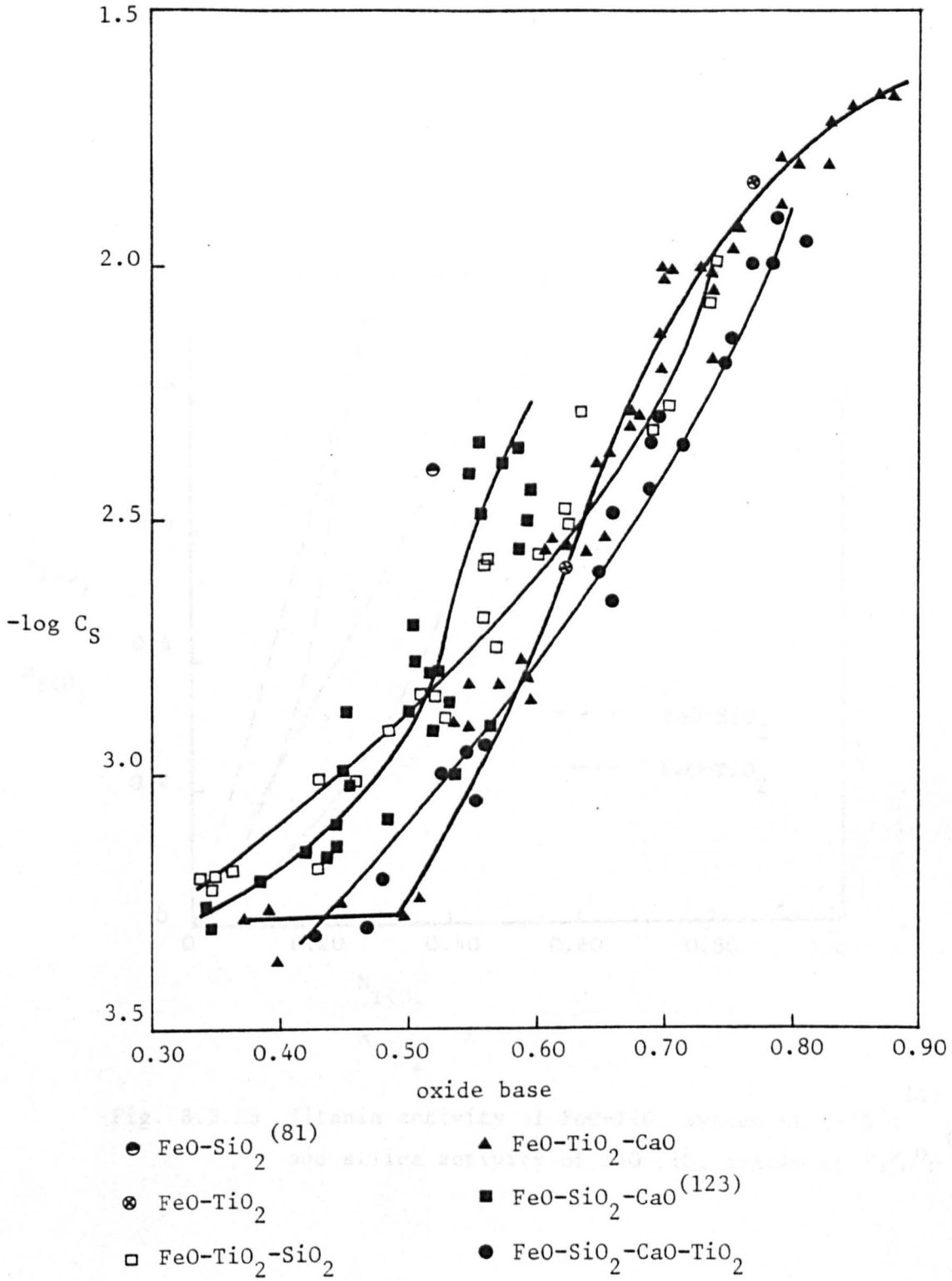

Fig. B.3.22 Sulphide capacities of slags containing iron oxide and titania at 1500°C.

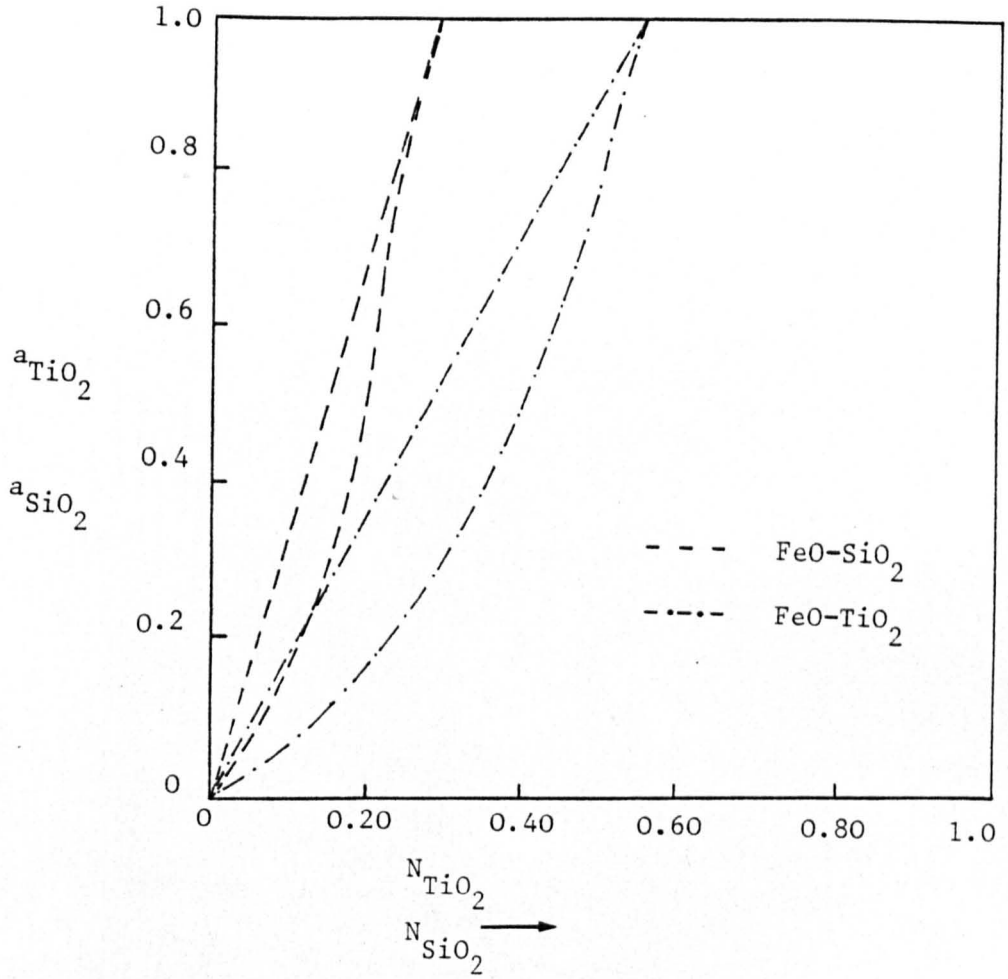

Fig. B.3.23 Titania activity of FeO-TiO_2 system at 1475°C [4] and silica activity of FeO-SiO_2 system at 1350°C [22]

■ The SiO_2-CaO system of Carter and MacFarlane[99]

● The SiO_2-CaO-TiO_2 system of Brown[117]

The FeO-CaO-SiO_2 system of Derici[123]

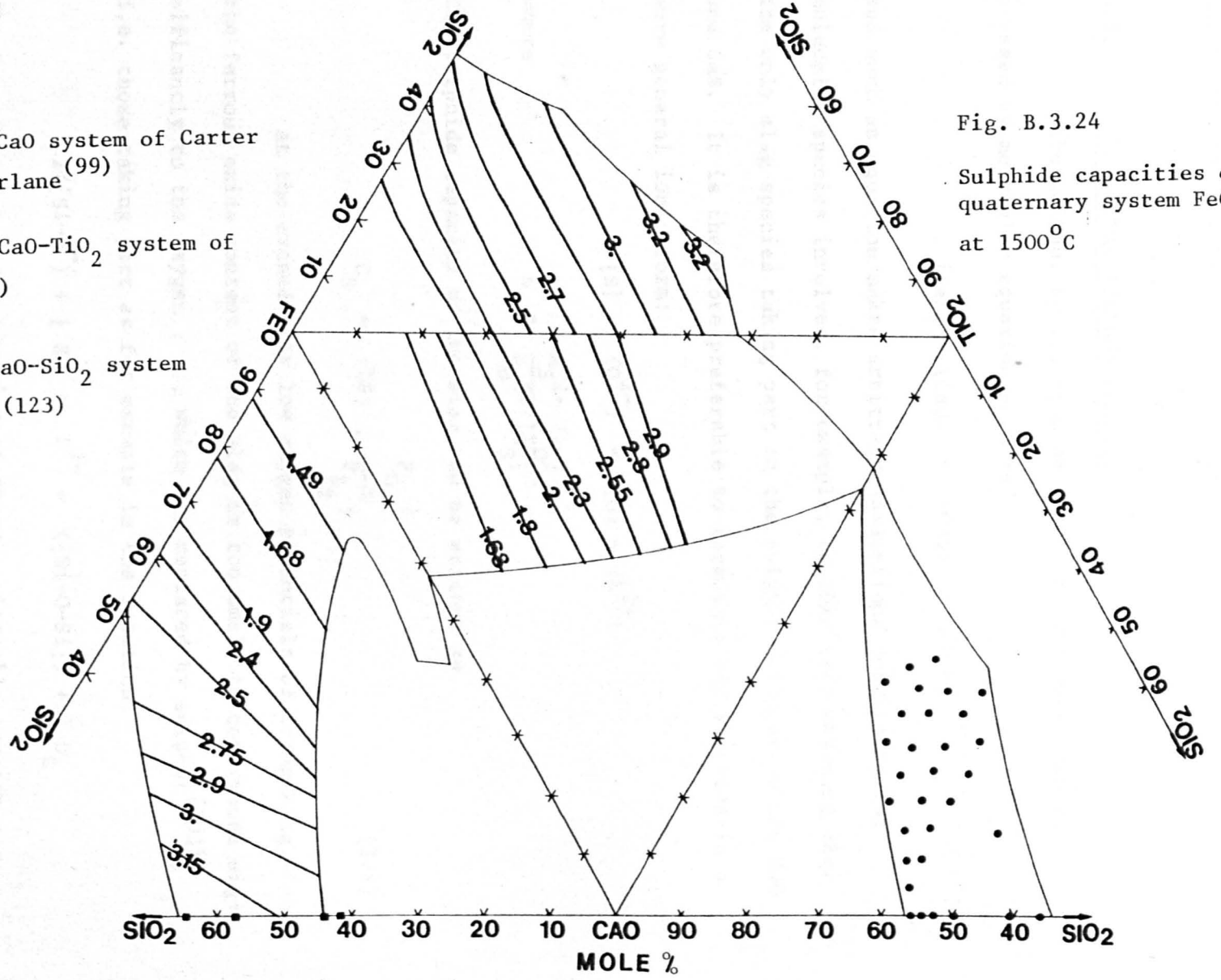

Fig. B.3.24

Sulphide capacities of the quaternary system FeO-CaO-TiO_2-SiO_2 at 1500°C

MacFarlane[99] on the $CaO-SiO_2$ binary system are consistent with these of Brown [118] where they overlap on the binary diagram. The sulphide capacity values of the $FeO-SiO_2$ binary diagram found by Derici[123] agree with those obtained in the present work on the same system.

B.3.5 SLAG-METAL SULPHUR PARTITION

The sulphur equilibrium between slag and metal can be expressed by molecular equation such as

$$[FeS] + (CaO) = (CaS) + [FeO]$$

but such an equation makes arbitrary assumptions concerning the molecular species involved, for example, in this case assuming that the only slag species taking part in the sulphur equilibrium are CaO and CaS. It is therefore preferable to formulate the reaction in a more general ionic form:

$$[S] + (O^{2-}) = [O] + (S^{2-})$$

where $$K = \frac{a_{S^{2-}} [a_O]}{a_{O^{2-}} [a_S]}$$

The sulphide capacity of the slag can be written as

$$C_S = (\%S) \cdot \frac{P_{O_2}^{\frac{1}{2}}}{P_{S_2}^{\frac{1}{2}}} \qquad (3.6)$$

At the exceedingly low oxygen potentials of ironmaking, the ferrous oxide content of the slag is too small to contribute significantly to the oxygen , which are replaced by sulphur[103], i.e. those taking part as for example in the reaction:

$$2(\vdots Si\text{-}O^{-}) + \tfrac{1}{2} S_2 = S^{2-} + (\vdots Si\text{-}O\text{-}Si \vdots) + \tfrac{1}{2} O_2$$

The concentration and activities of these replaceable oxygens are determined primarily by the ratio of metal oxides to silica.

Nevertheless in the presence of iron, the ferrous oxide content of the slag must be proportional to $[a_O]$ or $P_{O_2}^{\frac{1}{2}}$ by virtue of the equilibrium,

$$Fe_{(l)} + [\tfrac{1}{2}\, O_2] = (FeO)_{(l)} \qquad \Delta G = 56{,}900 + 11.82T \text{ cal.mol}^{-1} \tag{3.7}$$

where $K_7 = \dfrac{a_{FeO}}{P_{O_2}^{\frac{1}{2}}}$ in contact with iron

The free energy of solution of sulphur in iron can be written as

$$\tfrac{1}{2}\, S_2 = \underline{S\%} \qquad \Delta G = -31{,}520 + 5.27T \text{cal.atom}^{-1} \tag{3.8}$$

where $K_8 = \dfrac{a_S}{P_{S_2}^{\frac{1}{2}}}$

From equation (3.6)

$$C_S = \frac{(\%S)}{[\%S]} \cdot \frac{a_{FeO} \cdot K_8}{K_7} \qquad \text{where } [\%S] = [a_S]$$

i.e.
$$\frac{(\%S)}{[\%S]} = \frac{C_S}{a_{FeO}} \cdot \frac{K_7}{K_8} \tag{3.9}$$

where $\log K_7 = 4.431$ and $\log K_8 = 2.734$ at 1500^oC, can be derived from the equation (3.7) and (3.8) respectively

hence
$$\frac{(\%S)}{[\%S]} = 50 \times \frac{C_S}{a_{FeO}} \tag{3.10}$$

Also, it can be noted from equation (3.10) that the FeO concentration in the slag reflects the prevailing oxygen potential. As the FeO concentration increases or sulphide capacity decreases, the $\frac{(\%S)}{[\%S]}$ ratio must decrease proportionately. Measurements have been made of iron oxide activities in $FeO\text{-}TiO_2\text{-}SiO_2$ and $FeO\text{-}TiO_2\text{-}CaO$ systems at 1475^oC using a gas/slag equilibrium technique[137], as shown in Figure (B.3.25) and (B.3.26). This holds in the range investigated of

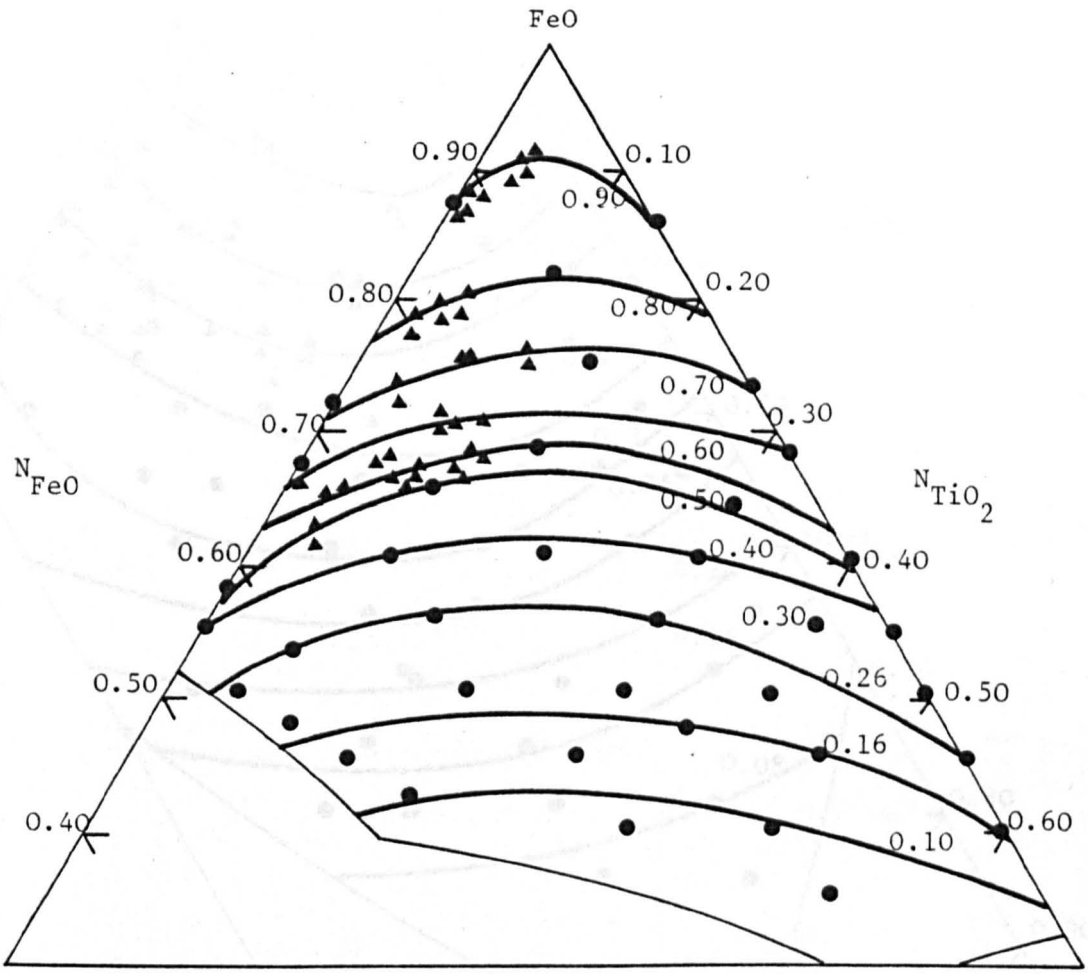

Fig. B.3.25 FeO activities of the $FeO-SiO_2-TiO_2$ slags at 1475^oC.

▲ Experimental points (137)

● Calculated points.

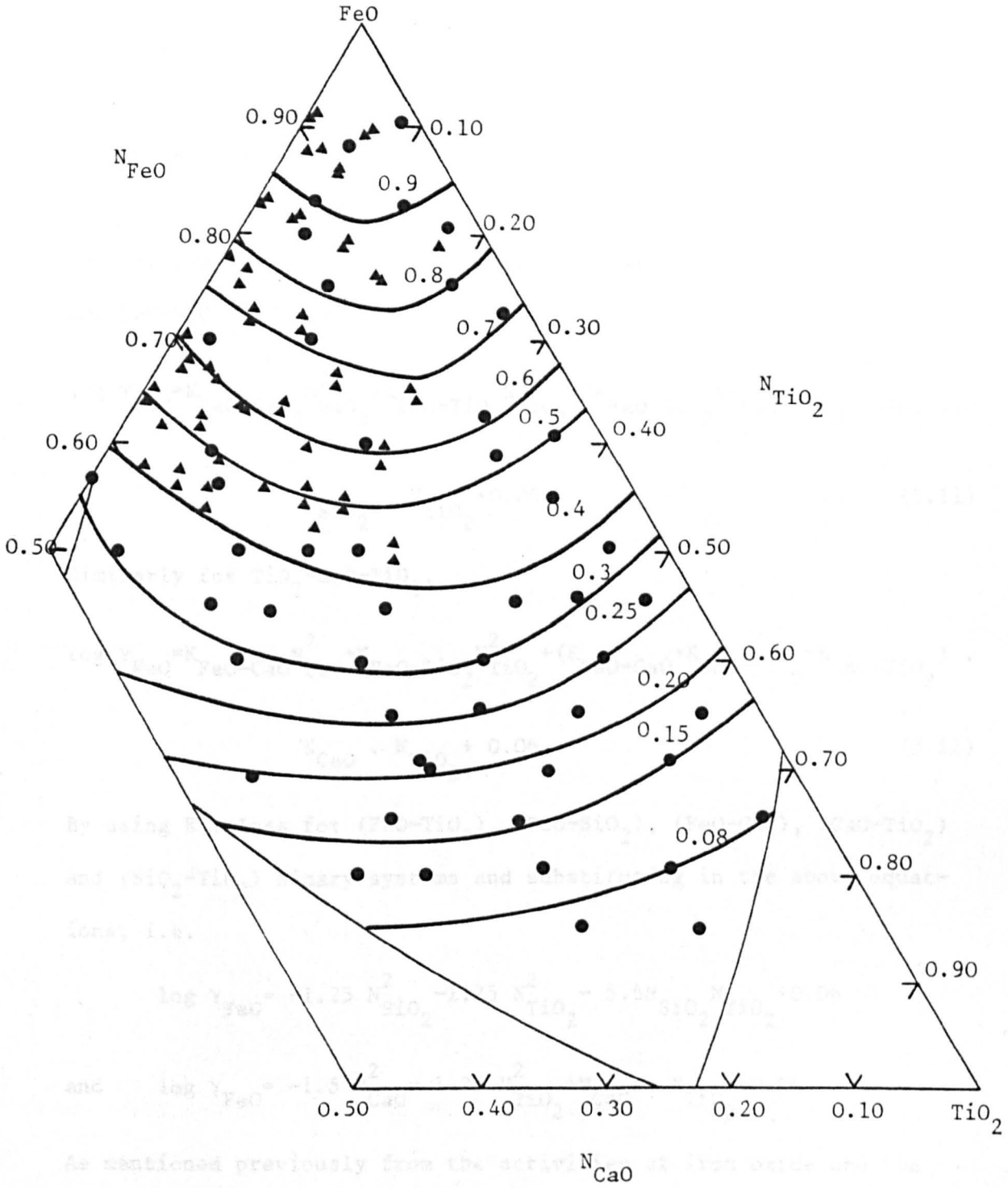

Fig. B.3.26 FeO activities of the FeO-CaO-TiO_2 slags at 1475°C.

▲ Experimental points (137)

● Calculated points.

N_{FeO} from 0.55 to 0.93, i.e., activity of iron oxide 0.40 to 0.90. Sommerville and Bell[141] have used a model based on random mixing of cations for these systems to represent the a_{FeO} in the range of N_{FeO} up to 0.55 at 1745°K. Taking both binary and ternary data together, it was found that they could be represented by the expressions:

For $FeO-SiO_2-TiO_2$ system,

$$\log \gamma_{FeO} = K_{FeO-SiO_2} N^2_{SiO_2} + K_{FeO-TiO_2} N^2_{TiO_2} + (K_{FeO-SiO_2} + K_{FeO-TiO_2} - K_{SiO_2-TiO_2}) \cdot N_{SiO_2} \cdot N_{TiO_2} + 0.06 \quad (3.11)$$

Similarly for $TiO_2-CaO-TiO_2$,

$$\log \gamma_{FeO} = K_{FeO-CaO} N^2_{CaO} + K_{FeO-TiO_2} N^2_{TiO_2} + (K_{FeO-CaO} + K_{FeO-TiO_2} - K_{CaO-TiO_2}) \cdot N_{CaO} \cdot N_{TiO_2} + 0.06 \quad (3.12)$$

By using K values for $(FeO-TiO_2)$, $(FeO-SiO_2)$, $(FeO-CaO)$, $(CaO-TiO_2)$ and (SiO_2-TiO_2) binary systems and substituting in the above equations, i.e.

$$\log \gamma_{FeO} = -1.25\, N^2_{SiO_2} - 1.25\, N^2_{TiO_2} - 5.6 N_{SiO_2} N_{TiO_2} + 0.06$$

and $$\log \gamma_{FeO} = -1.5\, N^2_{CaO} - 1.25\, N^2_{TiO_2} + N_{CaO} \cdot N_{TiO_2} + 0.06$$

As mentioned previously from the activities of iron oxide and the sulphide capacity data, it is possible to determine the slag/metal sulphur distribution for the systems $FeO-SiO_2-TiO_2$ and $FeO-CaO-TiO_2$. These are shown in Tables (B.6), (B.7) and Figures (B.3.27) and (B.3.28) respectively. By increasing the titania content in the melts, the sulphur partition decreases and similarly with the addition of silica to the slag. The iso-sulphur partition lines are

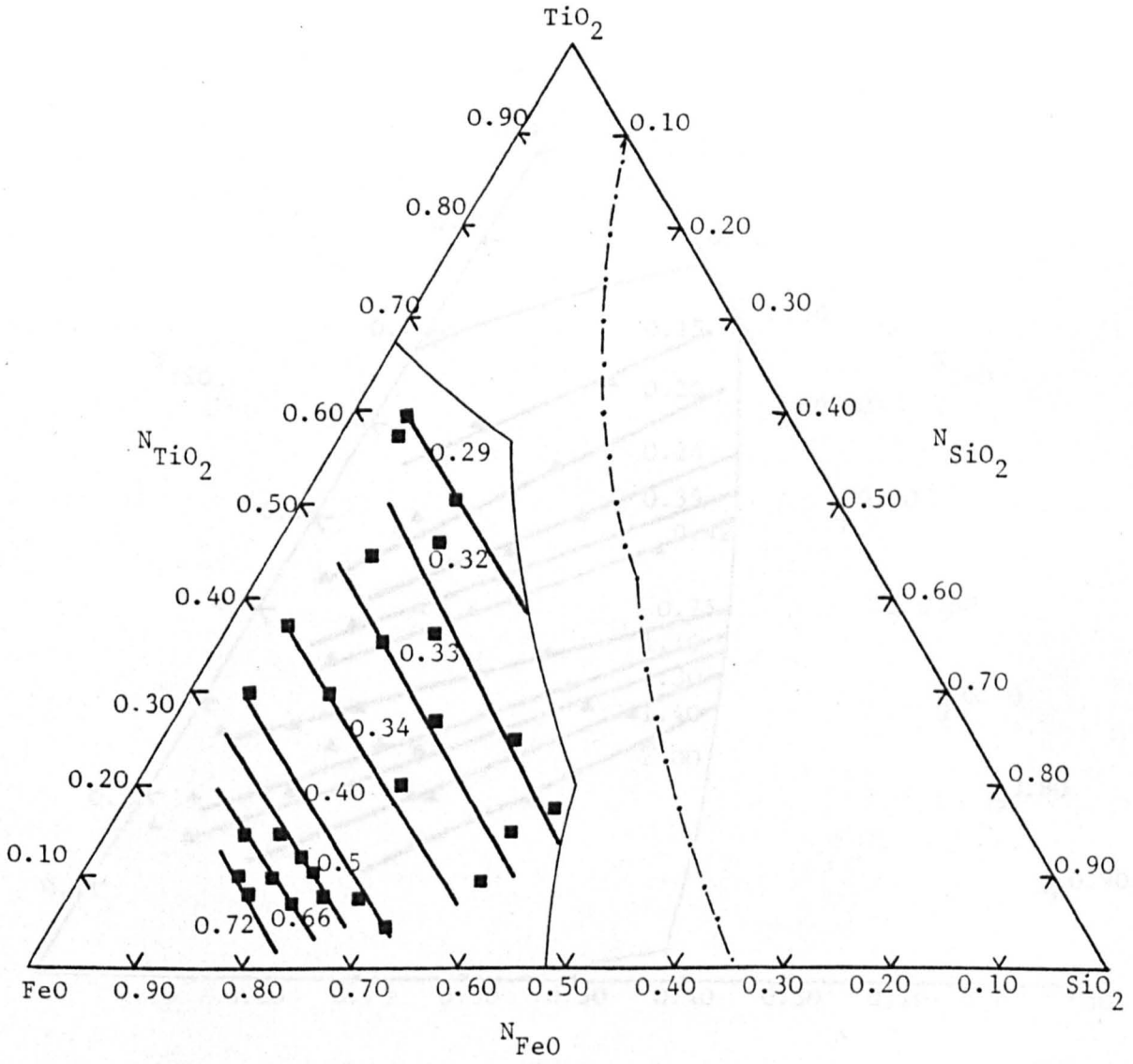

Fig. B.3.27 Slag-metal sulphur partition of the $FeO-TiO_2-SiO_2$ slags at 1500°C

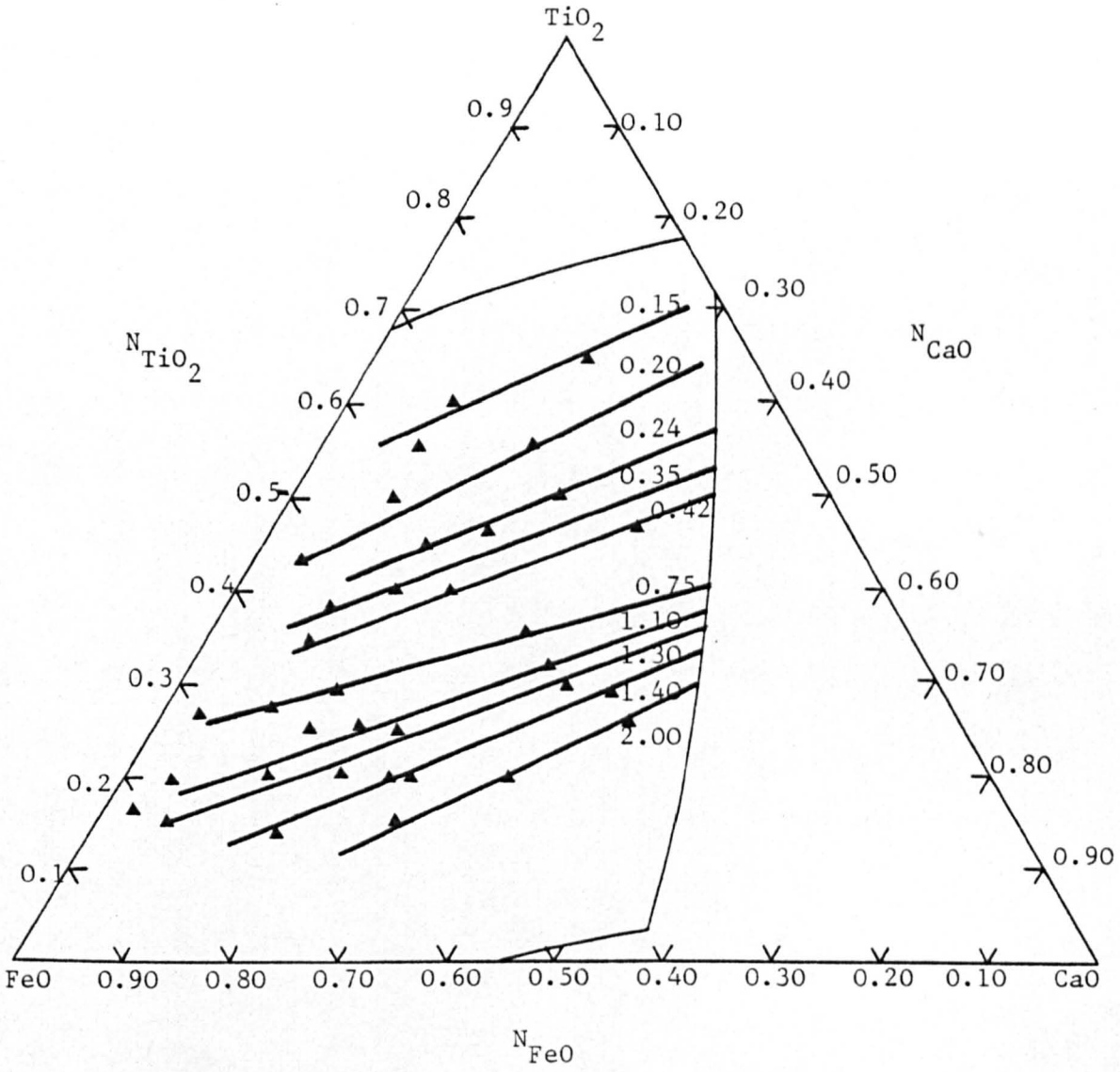

Fig. B.3.28 Slag-metal sulphur partition of the FeO-TiO_2-CaO slags at 1500°C.

slightly different from the constant iron oxide lines in the melts and there is not a great variation between these lines and iso-sulphide capacity lines in $FeO-SiO_2-TiO_2$ system. This is not surprising because if the TiO_2 and SiO_2 concentration increases in the melts, the sulphide capacities decrease and the iron oxide activities also decrease.

In the $FeO-CaO-TiO_2$ system the iso-sulphide partition lines are different from the sulphide capacity lines, as shown in Figure (B.3.28). As dicsussed before lime behaves as iron oxide in its influence on C_S, thus the sulphide capacity increases with the addition of lime to the slag and from equation (3.10), it is found that lime increases the slag/metal sulphur partition with the melts. It is interesting to note that increasing titania content in the slag decreases $\frac{(\%S)}{[\%S]}$ up to N_{TiO_2} of 0.50, above this concentration the effect is less. This is because the sulphide capacity in this area is almost constant, i.e. a factor affecting the sulphur partition is removed.

Trömel et al[127] have measured the slag/metal sulphur distribution for slag compositions on the dicalcium silicate, tricalcium silicate and lime saturation isotherms in the system $CaO-FeO_n-SiO_2-MgO$. The data show that the slag/metal sulphur partition increases with addition of FeO in the melt and decreases with increase of SiO_2 in the slag. The effect of silica on the sulphur partition between silica saturated in $FeO-CaO-SiO_2$ slags and metal has also been studied[123] by gas/slag equilibria at 1500°C over the range of oxygen and sulphur potentials. The $\frac{(\%S)}{[\%S]}$ ratio decreases with increase in both oxygen potential and mole fraction of silica. A similar effect of silica on the slag/metal sulphur distribution in

systems examined in the present study has been found.

By using the iron oxide activity data of Elliot[142] and Lee and Bell[122], and the sulphide capacity data of Derici[123] the slag/metal sulphur partition can be evaluated at 1500°C for $FeO-SiO_2-CaO$ system, as shown in Figure (B.3.29). It is noted that the data obtained by Lee give high $\frac{(\%S)}{[\%S]}$ ratio, this might be due to the presence of some ferric oxides in the melts. The slag/metal sulphur partition by Trömel agree with the values calculated. The effect of oxygen pressure on slag/metal sulphur partition is also illustrated in steelmaking processes. In the BOS process where the oxygen potential in the slag emulsion has been quoted as high as 10^{-6}, sulphur has been found to revert from slag to metal, whereas in the reducing period in the electric arc furnace sulphur partition improves. The quantitive effects can be shown by considering a slag containing titania and silica.

If a_{FeO} in slags is 0.4, $P_{O_2} = 3.38 \times 10^{-8}$ atmosphere and the sulphide capacity 3.30×10^{-3}, then at 1500°C

$$\frac{(\%S)}{[\%S]} = 4.13 \times 10^{-1}$$

A slag containing titania and lime with sulphide capacity of 1.04×10^{-2}, $a_{FeO} = 0.4$ and $P_{O_2} = 3.38 \times 10^{-8}$, then at 1500°C

$$\frac{(\%S)}{[\%S]} = 13 \times 10^{-1}$$

A slag[115] with a C_S value of 4×10^{-2}, $P_{O_2} = 10^{-6}$ atmosphere and temperature is 1600°C

$$\tfrac{1}{2} S_2 = \underline{S} \qquad \Delta G = -31{,}520 + 5.27T \text{ cal.mole}^{-1}$$

Then $\frac{(\%S)}{[\%S]} = \frac{1.17 \times 10^{-4}}{P_{O_2}^{\frac{1}{2}}} = 1.17 \times 10^{-1}$

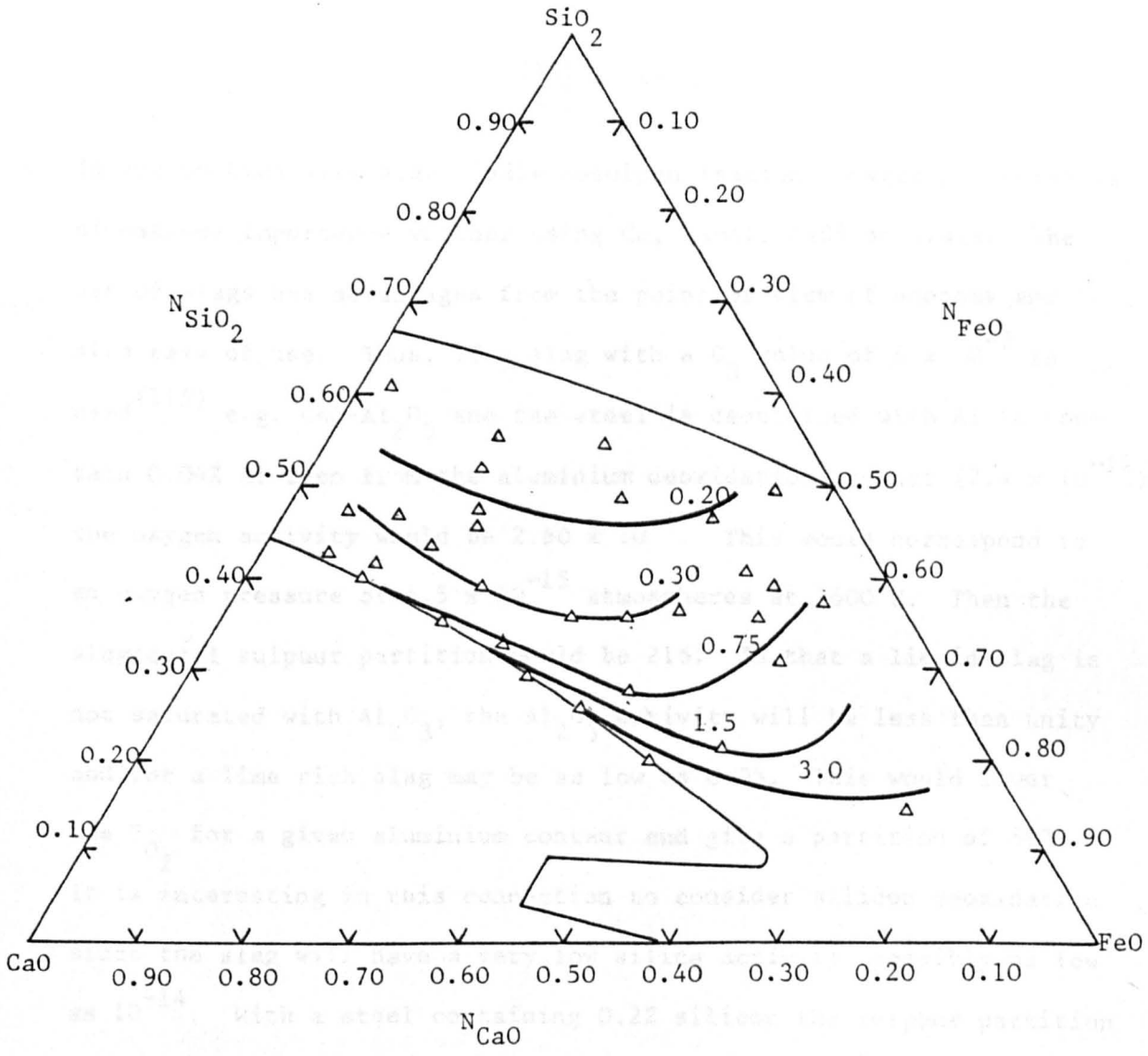

Fig. B.3.29 Slag-metal sulphur partition of the FeO-CaO-SiO_2 slags at 1500°C.

If P_{O_2} is for 0.21 carbon steel in equilibrium with P_{CO} of two atmospheres, then $P_{O_2} = 5.52 \times 10^{-11}$ atmosphere and

$$\frac{(\%S)}{[\%S]} = 15.7$$

if a_{FeO} in slag is 0.05, then $P_{O_2} = 1.8 \times 10^{-11}$ atmosphere and

$$\frac{(\%S)}{[\%S]} = 27.6$$

In conjunction with steel ladle desulphurisation oxygen potential is of extreme importance whether using Ca, Ca-Al, CaSi or slags. The use of slags has advantages from the point of view of economy and also ease of use. Thus, if a slag with a C_S value of 6×10^{-3} is used[115] e.g. $CaO-Al_2O_3$ and the steel is deoxidised with Al to contain 0.04% Al then from the aluminium deoxidation product (2.4×10^{-14}) the oxygen activity would be 2.50×10^{-4}. This would correspond to an oxygen pressure of 4.5×10^{-15} atmospheres at 1600°C. Then the slag/metal sulphur partition would be 216. In that a liquid slag is not saturated with Al_2O_3, the Al_2O_3 activity will be less than unity and for a lime rich slag may be as low as 0.05. This would lower the P_{O_2} for a given aluminium content and give a partition of 593. It is interesting in this connection to consider silicon deoxidation since the slag will have a very low silica activity, possibly as low as 10^{-14}. With a steel containing 0.2% silicon the sulphur partition ratio could be about 460 with a slag of $C_S = 6 \times 10^{-3}$, as reported by Bell[115].

From these data given above, it is interesting to note that slag/metal sulphur partition in steelmaking is lower than in ironmaking and that is not surprising since FeO does not play a significant part in the desulphurisation process in ironmaking.

With iron-oxide present in the slag, titania behaves as silica and decreases the slag/metal sulphur distribution. Cavaghan and Harris[124] in a study of steelmaking from pellets also found that TiO_2 had a large effect in reducing the ability of the slag to desulphurise and lowering the sulphur partition between slag and metal. On the other hand, and as mentioned previously, titania is considered as basic oxide and increases the sulphide capacity in iron-making as found by Brown[117] and Roxburgh[65], as shown in Figure (B.3.30).

B.3.6 THE BASICITY OF SLAGS

Probably the most useful outcome of the molecular theory of slags has been the concept of a numerical basicity index which summarises the composition of slag, and serves as a single parameter with which the chemical behaviour of the slag can be correlated. The dominating influence of lime and silica was early realised and data relating to desulphurisation and dephosphorisation were correlated with the simple "vee ratio"

$$V = \text{wt\% } CaO/\text{wt\% } SiO_2$$

which is still used as a measure of slag basicity in works practiced today. The ratio devised by the following authors is based on this ratio, Roxburgh[65] for $CaO-MgO-TiO_2$ system, Kalyanram et al[106] for $CaO-MgO-SiO_2-Al_2O_3$ system and McRae et al[42] for $CaO-MgO-SiO_2-Al_2O_3-TiO_2$. Comparison of these data[42,65,106] suggest that titania would be considered as an acidic oxide. Cavaghan and Harris[124] also found that TiO_2 caused a marked reduction in the sulphur holding capacity of the slag in a study of steelmaking from pellets. The

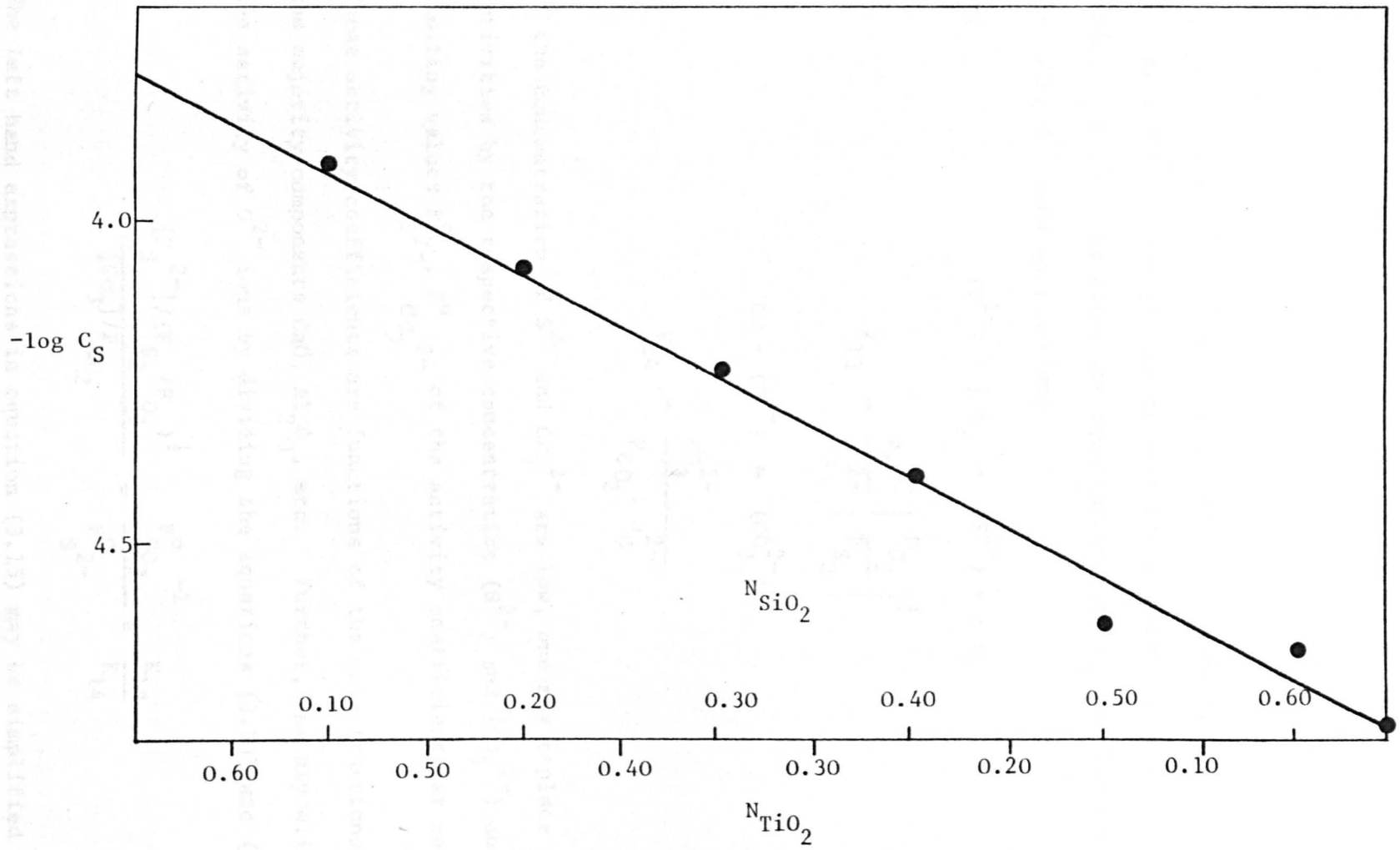

Fig. B.3.30 Variation of sulphide capacity with titania and silica in slags containing 0.20 N_{CaO} and 0.15 N_{MgO} (65).

desulphurising ability was very low, almost independent of the slag basicity with over 9% TiO_2. A modified basicity ratio had to be employed for sulphur control expressed as $\frac{MgO + CaO}{SiO_2 + Al_2O_3 + 2.2\ TiO_2}$ where the concentrations are in weight percent. The reasons for this are not clear, as mentioned previously.

Wagner[143] recently examined the concept of the basicity of a slag and the possibility of defining a quantitative measure of basicity in order to correlate equilibrium data for various reactions involving O^{2-} ions as reactions

e.g. $$(O^{2-}) + \tfrac{1}{2} S_2 = (S^{2-}) + \tfrac{1}{2} O_2 \qquad (3.13)$$

$$K_{13} = \frac{a_S^{2-}}{a_O^{2-}} \left[\frac{P_{O_2}}{P_{S_2}} \right]^{\frac{1}{2}}$$

$$CO + (O^{2-}) = (CO_3^{2-}) \qquad (3.14)$$

$$K_{14} = \frac{CO_3^{2-}}{P_{CO_2} \cdot a_O^{2-}}$$

If the concentration of S^{2-} and CO_3^{2-} are low, one may replace the activities by the respective concentration (S^{2-}) and (CO_3^{2-}) and the limiting values $F^{o}_{S^{2-}}$, $F^{o}_{CO_3^{2-}}$ of the activity coefficients at zero. These activity coefficients are functions of the mole fractions of the majority components CaO, Al_2O_3, etc. Further, one may eliminate the activity of O^{2-} ions by dividing the equations (3.13) and (3.14)

$$\frac{[P_S{}^{2-}]/(P_{S_2}/P_{O_2})^{\frac{1}{2}}}{[CO_3]/P_{CO_2}} = \frac{F^{o}_{CO_3}{}^{-2}}{F^{o}_{S^{2-}}} = \frac{K_{13}}{K_{14}} \qquad (3.15)$$

The left hand expressions in equation (3.15) may be simplified by

introducing "capacities" C_i of species i which are defined semi-largely to the sulphide capacity of a slag according to Richardson et al[81,144] with concentrations in weight percent and partial pressures in the gas phase atmosphere

$$C_{S^{2-}} = (\text{weight \% } S^{2-}) \cdot (P_{O_2}/P_{S_2})^{\frac{1}{2}} \qquad (3.16)$$

$$C_{CO_3^{2-}} = (\text{weight \% } CO_3^{2-})/ P_{O_2} \qquad (3.17)$$

Furthermore, one may define the basicity of a slag of arbitrary composition with the carbonate capacity $C_{CO_3^{2-}}$ by

$$B = \frac{C_{CO_3^{2-}}}{C^*_{CO_3^{2-}}}$$

where CO_3^{*2-} is the carbonate capacity in a reference slag, e.g. 0.4 CaO + 0.4 SiO_2 + 0.2 Al_2O_3 which is liquid above about 1300°C.

From equation $\left[\frac{C''_j}{C'_j}\right]^{1/V_j} \simeq \left[\frac{C''_i}{C'_J}\right]^{1/V_i}$ (3.18)

where I and j are capacities of species in different slags denoted by prime and double prime superscripts, V_i and V_j are the number of O^{2-} ions involved in reactions (3.13) and (3.14).

In view of equation (3.18) one may also use the capacity of a species other than CO_3^{2-} for the definition of basicity, e.g.

$$B_{sulf.} = \frac{C_{S^{2-}}}{C^*_{S^{2-}}}$$

So far, the difficulty in this approach is that the solubility of CO_2 in steelmaking slags has not been determined.

Kalyanram et al[106] studied the activity of lime in the systems CaO-MgO-SiO_2, CaO-Al_2O_3-SiO_2 and CaO-MgO-Al_2O_3-SiO_3 at 1500°C

and found the following relationship

$$R = \frac{N_{CaO} + \frac{1}{2} N_{MgO}}{N_{SiO_2} + \frac{1}{3} N_{Al_2O_3}}$$

The basicity ratio of Kalyanram et al[106] and its relationship with sulphide capacity is found by Shuja[145] as

$$\log C_S = -5.57 + 1.39 \left| \frac{N_{CaO} + \frac{N}{2} MgO}{N_{SiO_2} + \frac{N}{3} Al_2O_3} \right|$$

Duffy, Ingram and sommerville[119] used an optical basicity scale in which it is not necessary to separate the slag components into acidic and basic oxides. The theory of optical basicity assumed all oxides (acidic and basic) contain O^{2-} ions, the basicity of these O^{2-} ions being reduced to a greater or lesser extent through interaction with acidic cations (Si^{4+}, Al^{3+}, ...). The technique involves the determination of the $S_0^1 \rightarrow P_1^3$ frequency shift for Pb^{2+} probe ion. From these measurements basicity moderating parameter (γ) are assigned to different cations and the optical basicity calculated as

$$\Lambda = \frac{X_A}{\gamma_A} + \frac{X_B}{\gamma_B} + ... \qquad (3.19)$$

γ_A, γ_B are basicity moderating parameters for the constituent cations and X_A, X_B are the corresponding equivalent cation fractions of A and B, based on the fraction of negative charge "neutralised" by the charge (oxidation number) of each cation. The γ-parameter is calculated from the Pauling electronegativity (x) by

$$\gamma = 1.36(x - 0.26)$$

hence

$$\Lambda = \frac{1}{\gamma}$$

Equation (3.19) can be rewritten in the form

$$\Lambda = X_A\Lambda_A + X_B\Lambda_B + \ldots$$

where Λ_A, Λ_B are the basicity values of the component oxides. Duffy et al give a correlation between C_S value at 1500°C and optical basicity (Λ) as

$$\log C_S = -11.9 + 12.0\ \Lambda$$

for slags without titania, as listed in Tables (B.8-B.11) and (B.15). As shown in Tables (B.8-B.16) and Figure (B.3.31), the slags replotted with slags containing titania[65,117,118], and the equation of the best straight line is given by

$$\log C_S = -11.07 + 10.86\ \Lambda$$

Steelmaking slags are always formed under considerably more oxidising conditions than those which prevail in the blast furnace. For this reason these slags contain an appreciable amount of FeO, MnO and other transition metal oxides. This difference complicates the quantitive treatments of basicity, and also makes it highly unlikely that for steelmaking slags, there will be a simple correlation between $\log C_S$ and Λ.

Due to the reasons mentioned above, the measurements of sulphide capacities in the present study for the $FeO-SiO_2-TiO_2$, $FeO-CaO-TiO_2$ and $FeO-SiO_2-CaO-TiO_2$ systems do not correlate to this type of basicity. A major difficulty also is that the basicity moderating parameters (γ) are known for main group elements only, and therefore at present there is no reliable way of calculating a basicity value for multi-component systems containing certain transition metal oxides.

Although the oxides can be labelled as either acid or basic,

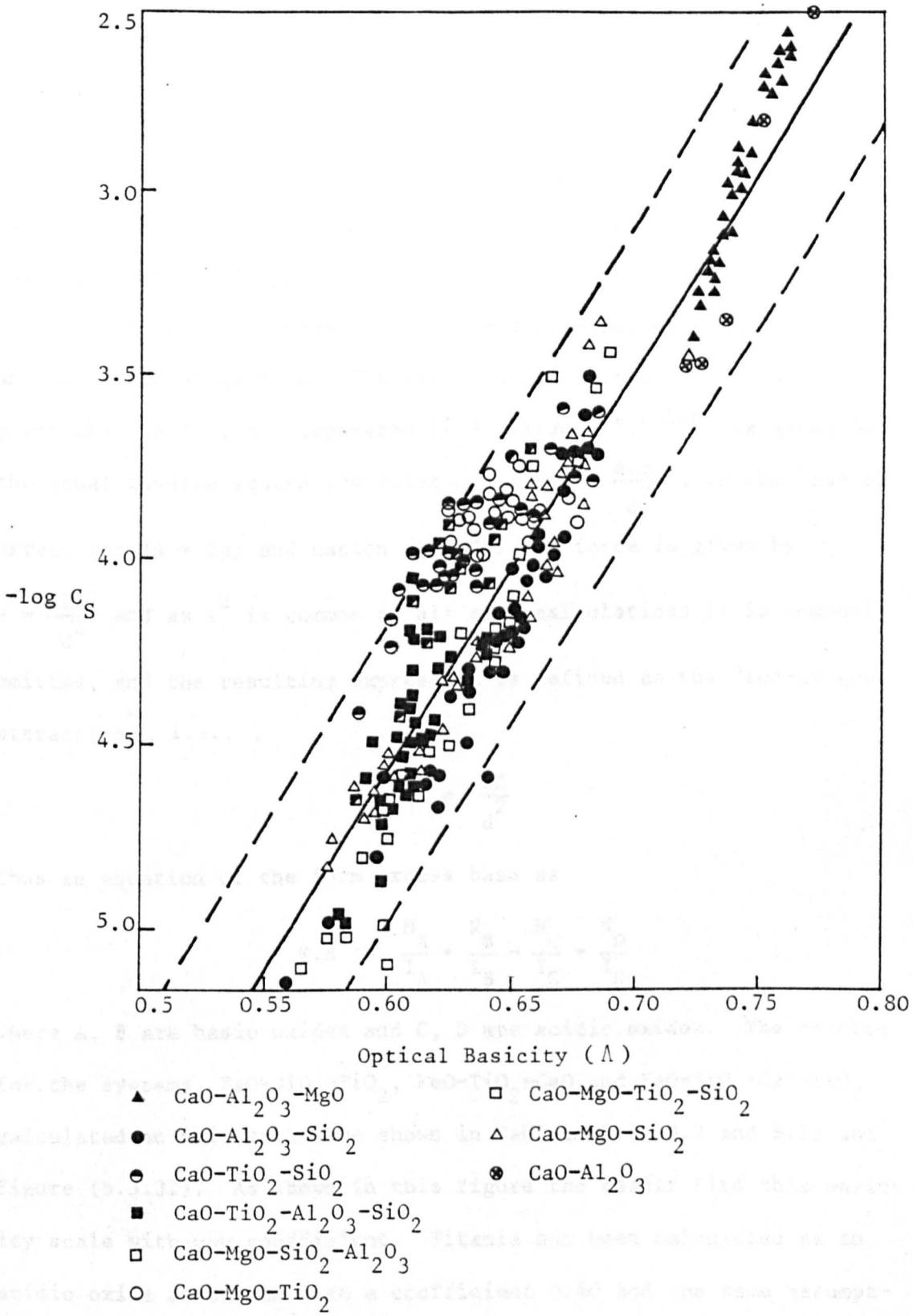

Fig. B.3.31 Variation of sulphide capacities with optical basicity for slags containing titania at 1500°C.

an examination of the properties of oxides shows that they form a continuous series from those strongly basic to those with strongly acidic behaviour. It is necessary to have a parameter by which to describe the degree of basicity of an oxide, and the attractive force between a metal ion and an O^{2-} ion has often been used.

Brown[118] suggested an excess base parameter based on such an ion-oxygen attraction. The electrostatic attraction between two point charges (a^-, b^+) separated by a distance "d"[146] is given by the usual inverse square low relation as $F = \frac{a.b}{d^2}$, in the case of oxygen ion (a = 2e) and cation (b = Ze) the force is given by $F = \frac{2Ze^2}{d^2}$ and as e^2 is common to all such calculations it is commonly omitted, and the resulting expression is defined as the "ion-oxygen attraction", i.e.,

$$I = \frac{2Z}{d^2}$$

Thus an equation of the form excess base as

$$E.B = \frac{N_A}{I_A} + \frac{N_B}{I_B} - \frac{N_C}{I_C} - \frac{N_D}{I_D}$$

where A, B are basic oxides and C, D are acidic oxides. The results for the systems, $FeO-SiO_2-TiO_2$, $FeO-TiO_2-CaO$ and $FeO-SiO_2-CaO-TiO_2$ calculated on this scale are shown in Tables (B.1, B.2 and B.5) and Figure (B.3.32). As shown in this figure the result fits this basicity scale with new coefficient. Titania has been calculated as an acidic oxide as silica with a coefficient 0.40 and the same assumption has been made for iron oxide which is considered a basic oxide as lime with a coefficient 1.45.

i.e.
$$E.B = \frac{N_{FeO} + N_{CaO}}{I_{CaO}} - \frac{N_{SiO_2} + N_{TiO_2}}{I_{SiO_2}}$$

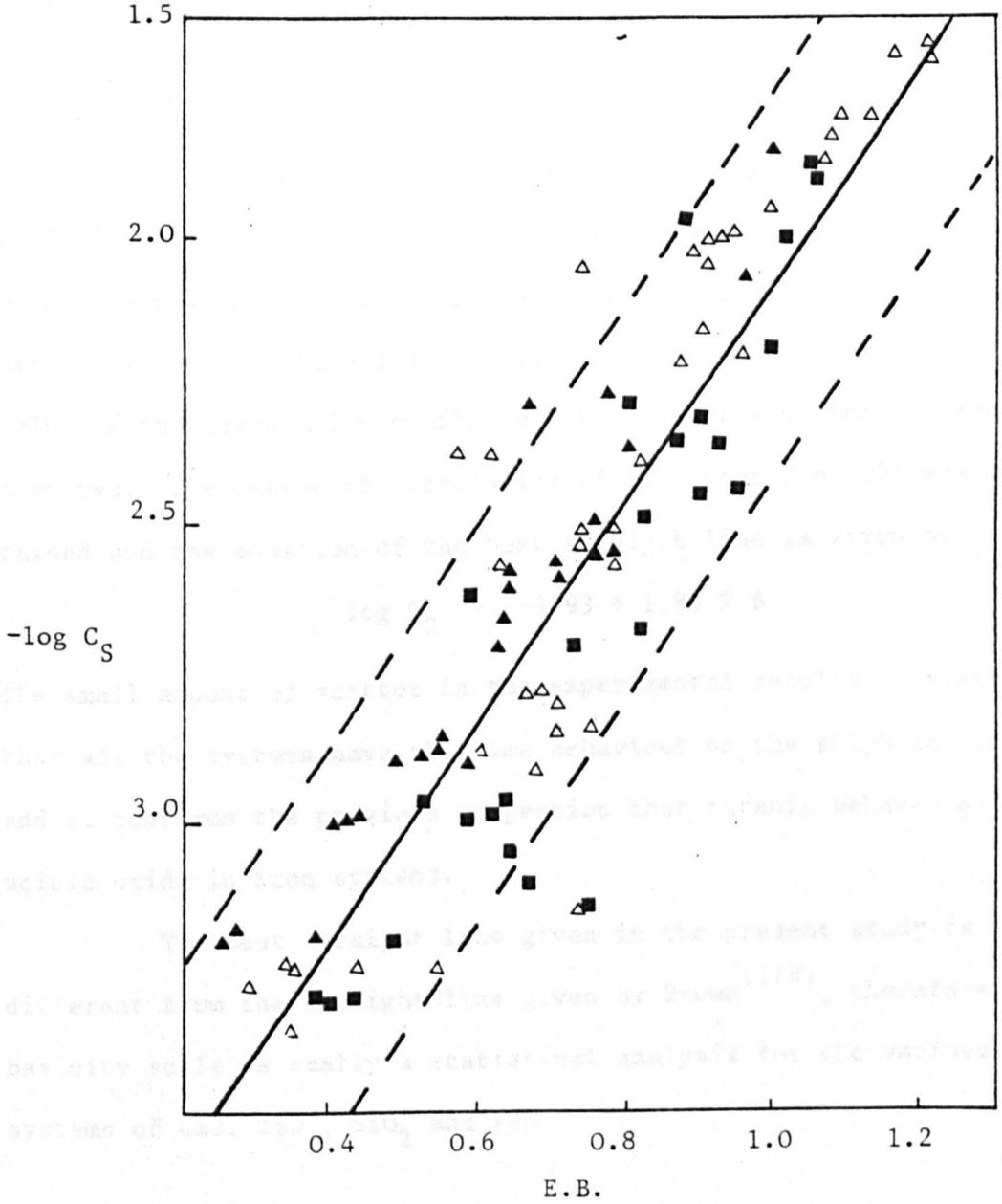

Fig. B.3.32 Variation of sulphide capacities with excess base at 1500°C.

$$\therefore \quad E.B = 1.45(N_{FeO} + N_{CaO}) - 0.40(N_{SiO_2} + N_{TiO_2})$$

The close approach of the numerical value of the correlation coefficient to unity indicates that the representation of the experimental data by the best straight line shown is very reli able. The good reliability of the best straight line representation is substantiated by the narrow band widths of the 95% confidence limits drawn on either side of the line since these take into account not only the value of the correlation coefficient but also the number of results involved. The degree of correlation of the order r = 0.91 was obtained and the equation of the best straight line is given by

$$\log C_S = -3.93 + 1.85 \text{ E.B.}$$

The small amount of scatter in the experimental results indicates that all the systems have the same behaviour on the sulphide capacity and it confirms the previous suggestion that titania behaves as acidic oxide in iron systems.

The best straight line given in the present study is different from the straight line given by Brown[118], therefore this basicity scale is really a statistical analysis for the various systems of CaO, TiO_2, SiO_2 and FeO.

CONCLUSIONS

The system $FeO-TiO_2-SiO_2$ is noteworthy because of the immiscibility among both liquid and crystalline structures. A two-liquid region characterizes much of the liquidus surface, extending completely across the diagram from the SiO_2-TiO_2 side line to the SiO_2-FeO side line. The liquidus surface in the region of liquid immiscibility slopes from these two side lines to the boundary curve separating the fields in which cristobalite is in equilibrium with two liquids from that in which rutile is in equilibrium with two liquids. This boundary curve is at the invariant temperature of $1540 \pm 10^{\circ}C$ while crossing the two-liquid region.

The large compositional range and high liquidus temperatures characterizing the two-liquid region can be very significant in explaining or predicting phenomena in titania-bearing slags and refractories.

Extrapolating from data on the system $FeO-TiO_2-SiO_2$ under inert gas, it was noted that TiO_2 will serve in general to increase liquidus temperatures, but will also contribute significantly to the extension of the two-liquid region.

The system $FeO-TiO_2-SiO_2$ can be divided into five composition triangles, each corresponding to a simple eutectic point at which three different crystalline compounds at liquid are in equilibrium, within the composition range studied.

The crystalline phases which were found to be in equilibrium with melts containing FeO, TiO_2 and SiO_2 were fayalite-$2FeO.SiO_2$, uvöspinel-$2FeO.TiO_2$, ilmenite-$FeO.TiO_2$, pseudobrookite-$FeO.2TiO_2$,

rutile-TiO_2, silica-SiO_2 and wüstite-FeO. Interesting cases exist where, for instance, during cooling under equilibrium conditions certain mixtures have two separate temperature intervals during which two liquids appear in equilibrium with crystals.

The use of liquidus measurements to assist in the selection of slag composition for maximum removal of sulphur is an accepted principle. The results obtained in the present study of the liquidus show how it can be of assistance in the study of the high temperature properties of steelmaking slags.

The important fact which has been established in this work is that the liquidus temperature is not affected by the titania content in the slag from $\frac{N_{SiO_2}}{\Sigma N_{Fe}} = 0.67$ to the two-liquid region, at constant $\frac{N_{SiO_2}}{\Sigma N_{Fe}}$ of the $FeO-Fe_2O_3-SiO_2-TiO_2$ slags at given oxygen pressures.

The lowest liquidus temperature at which liquid can exist under equilibrium conditions in the FeO, SiO_2 and TiO_2 mixture was approximately 1300 ± 10°C at an oxygen pressure of about 10^{-6} atmosphere. With further increase of the oxygen pressure to approximately 10^{-2} atmosphere the lowest liquidus temperature was 1450 ± 10°C, i.e. liquidus temperatures in general decrease as the oxygen pressure is lowered.

There is a large liquid immiscibility in the molten Fe-Ti-Si-O system, with increasing the oxygen potential the composition range of the two-liquid region increases.

Titania and silica have the same effect on the $\frac{Fe^{3+}}{Fe^{2+}}$ ratio in $FeO-TiO_2-SiO_2$ melts and decrease it, but silica decreases the

$\frac{Fe^{3+}}{Fe^{2+}}$ ratio more than does titania.

From the work on the measurements of the sulphide capacity in the $FeO-TiO_2-SiO_2$, $FeO-TiO_2-CaO$ and $FeO-TiO_2-SiO_2-CaO$ systems, the main conclusion that titania content in the melts decreases the sulphide capacity at oxygen pressure of 10^{-8} atmosphere at temperature of $1500^{o}C$, according to the reaction

$$\tfrac{1}{2} S_2 + O^{2-} = S^{2-} + \tfrac{1}{2} O_2$$

$$K = \frac{a_s^{2-} \cdot P_{O_2}^{\frac{1}{2}}}{a_O^{2-} \cdot P_{S_2}^{\frac{1}{2}}}$$

It was suggested that there is a decrease in the number of oxygen ions which can be replaced by sulphur ions in the presence of titania. The results obtained from the present work show that titania behaves as silica, i.e. acidic oxide in the presence of iron oxide in the melts.

On the other hand titania increases the sulphide capacity for the blast furnace slags at oxygen pressure of 10^{-14} atmosphere and $1500^{o}C$. The expected sulphur pick-up of a slag can be determined by calculating the oxygen pressure, according to the reaction

$$C + \tfrac{1}{2} O_2 = CO$$

$$P_{O_2}^{\frac{1}{2}} = \frac{P_{CO}}{a_C \cdot K_C}$$

Similarly an equilibrium will be set up for the sulphur introduced to the furnace

$$\underline{S} = \tfrac{1}{2} S_2$$

$$P_{S_2}^{\frac{1}{2}} = K_S \cdot a_S$$

By definition of sulphide capacity of slag

$$C_S = \%S \cdot \frac{P_{O_2}^{\frac{1}{2}}}{P_{S_2}^{\frac{1}{2}}}$$

$$= \%S \cdot \frac{P_{CO}}{K_C \cdot a_C} \cdot \frac{1}{K_S \cdot a_S}$$

$$\therefore \quad \%S = a_{\underline{S}} \cdot C_S \cdot \frac{K_C \cdot K_S \cdot a_C}{P_{CO}}$$

where $a_{\underline{S}}$ is a function of the total sulphur introduced to the furnace. C_S, K_C and K_S are all constant for a given slag temperature and composition. P_{CO} is a function of the furnace conditions, while a_C depends on the metal composition.

This equilibrium calculation indicates a maximum figure for the expected sulphur removal which can be obtained.

Duffy et al[119] using an optical basicity scale have shown a correlation with sulphide capacity of slags. The results of the previous work on slags containing titania (iron oxide free) have been plotted against this basicity and a similar relationship was found to that on the slags without titania and iron oxide.

The results obtained in the present work on the slag/metal sulphur partition show that the system $FeO-TiO_2-CaO$ has a higher slag/metal sulphur distribution than for $FeO-TiO_2-SiO_2$ system.

APPENDICES

APPENDIX 1

The calculation of oxygen pressure of the Gas Mixture CO, CO_2 and N_2

The value of partial pressure of oxygen in the system can be calculated from the equilibrium constant for the reaction

$$CO_2 = CO + \tfrac{1}{2} O_2 \qquad \Delta G = 31{,}000 \text{ cal mole}^{-1} \qquad (1)$$

$$1500^{\circ}C$$

Hence

$$\Delta G = -RT \ln K$$

$$\log K = \frac{-\Delta G}{RT} = \frac{(-31010)}{4.575 \times (1773)}$$

$$K = 1.50 \times 10^{-4}$$

From equation (1)

$$P_{O_2}^{\frac{1}{2}} = K \cdot \frac{P_{CO_2}}{P_{CO}}$$

$$= 1.50 \times 10^{-4} \cdot \frac{P_{CO_2}}{P_{CO}}$$

APPENDIX 2

The calculation of oxygen and sulphur potential of Gas Mixture CO_2, H_2, SO_2 and N_2

As mentioned previously the gas mixtures which have been used contain CO_2, H_2, SO_2 and N_2. The latter does not take part in any chemical reaction. Once the initial gas mixture composition has been fixed, it is necessary to evaluate the equilibrium sulphur and oxygen potentials at the required temperature (1500°C).

When gas mixtures such as these reach equilibrium at 1500°C a number of chemical species are formed. The species which are expected to appear in significant amounts are CO_2, CO, SO_2, H_2, H_2O, H_2S, S_2, S, SO, HS, COS and O_2. It can be shown that other chemical species such as SO_3 and CS_2 will be present but not in sufficient quantity as to affect the equilibrium sulphur and oxygen pressures under the conditions of these experiments.

By considering the reaction

$$SO_2 + \tfrac{1}{2} O_2 = SO_3$$

$$K = \frac{P_{SO_3}}{P_{SO_2} \cdot P_{O_2}^{\frac{1}{2}}}$$

$$= 3.24 \times 10^{-5} \text{ at } 1500^{\circ}C$$

Hence the experiments are carried out under oxygen pressure approximately of 10^{-9} atmosphere.

Thus $$P_{SO_3} = 3.24 \times 10^{-5} \times P_{SO_2} \times P_{O_2}^{\frac{1}{2}}$$

$$= 3.24 \times 10^{-5} \times 0.01 \times 3.16 \times 10^{-5}$$

$$\simeq 10^{-11} \text{ atmosphere}$$

This is too small a value to have a significant effect on the sulphur potential of the gas mixture.

Also, for carbon disulphide, and from the reaction

$$CO_2 + 2\ SO_2 = CS_2 + 3\ O_2$$

$$K_{1500^oC} = \frac{P_{CS_2} \times P_{O_2}^3}{P_{CO_2} \times P_{SO_2}}$$

$$= 6.9 \times 10^{-58}$$

Thus

$$P_{CS_2} = \frac{6.9 \times 10^{-58} \times 0.25 \times (0.01)^2}{10^{-27}}$$

$$\simeq 10^{-35} \text{ atmosphere}$$

Therefore carbon disulphide need not be considered to have an effect on the sulphur pressure.

There is some doubt concerning sulphur monoxide. Meschi and Myers[140] quoted that sulphur monoxide has the chemical composition S_2O and not SO. The JANAF tables[111] quote values for its free energy of formation but it is pointed out that there has been no direct measurement of sulphur monoxide free energy of formation. In the present study S_2O has been ignored since the expected sulphur monoxide pressures were very low and the free energy of formation of S_2O and SO at 1500°C are similar and therefore only SO will be considered.

To calculate the sulphurising potential of a gas mixture of initial composition P_{CO_2}, P_{H_2} and P_{SO_2}, it is first necessary to calculate an approximate oxygen pressure from the H_2/CO_2 equilibrium:

$$H_2 + CO_2 = CO + H_2O$$

At equilibrium of 1500°C

$$\frac{pCO \cdot pH_2O}{pCO_2 \cdot pH_2} = \frac{2.09 \times 10^{-12} \times 2.41 \times 10^{-4}}{1.36 \times 10^{-8}}$$

$$= 3.71$$

If $pCO = X$, $pH_2O = X$

$$pCO_2 = P_{CO_2} - X \text{ , } pH_2 = P_{H_2} - X$$

$$\therefore \quad \frac{X^2}{(P_{CO_2} - X)(P_{H_2} - X)} = 3.71$$

Now knowing P_{CO_2} and P_{H_2} from the initial gas mixture, they can be used in the standard quadratic in X, in the form $aX^2 - bX + C = 0$, thus enabling a satisfactory solution of X to be determined by the equation

$$X = \frac{-b \pm \sqrt{b^2 - 4aC}}{2a}$$

Hence values of pH_2, pCO, pCO_2 and pH_2O can be determined.

An oxygen pressure can be calculated by using the CO/CO_2 equilibrium,

$$CO_2 = CO + \tfrac{1}{2} O_2$$

$$\therefore \quad pO_2 = \frac{2.09 \times 10^{-12}}{1.36 \times 10^{-8}} \times \frac{pCO_2}{pCO}$$

It is possible to calculate all the sulphur containing species in terms of sulphur partial pressure, by using the above information which is readily obtained.

$$SO_2 = \tfrac{1}{2} S_2 + O_2 \qquad K_1 = \frac{pS_2 \times pO_2}{pSO_2} \qquad (1)$$

$$pSO_2 = \frac{pS_2^{\frac{1}{2}} \times pO_2}{1.38 \times 10^{-7}}$$

$$SO = \tfrac{1}{2} S_2 + \tfrac{1}{2} O_2 \qquad K_2 = \frac{pS_2^{\frac{1}{2}} \times pO_2^{\frac{1}{2}}}{pSO} \qquad (2)$$

$$pSO = \frac{pS_2^{\frac{1}{2}} \times pO_2^{\frac{1}{2}}}{7.92 \times 10^{-3}}$$

$$\tfrac{1}{2} S_2 = S \qquad K_3 = \frac{pS}{pS_2^{\frac{1}{2}}} \qquad (3)$$

$$pS = 5.74 \times 10^{-4} \times pS_2^{\frac{1}{2}}$$

$$\tfrac{1}{2} S_2 + H_2 = H_2S \qquad K_4 = \frac{pH_2S}{pS_2^{\frac{1}{2}} \times pH_2} \qquad (4)$$

$$pH_2S = 1.10 \times pS_2^{\frac{1}{2}} \times pH_2$$

$$\tfrac{1}{2} S_2 + \tfrac{1}{2} H_2 = HS \qquad K_5 = \frac{pHS}{pS_2^{\frac{1}{2}} \times pH_2^{\frac{1}{2}}} \qquad (5)$$

$$pHS = 1.21 \times pS_2^{\frac{1}{2}} \times pH_2^{\frac{1}{2}}$$

$$\tfrac{1}{2} S_2 + CO = COS \qquad K_6 = \frac{pCOS}{pS_2^{\frac{1}{2}} \times pCO} \qquad (6)$$

$$pCOS = 5.38 \times 10^{-2} \times pS_2^{\frac{1}{2}} \times pCO$$

The sulphur potential of the system can also be found, i.e.

$$P_{SO_2} = 2\,pS_2 + pSO_2 + pSO + pS + pH_2S + pHS + pCOS$$

Once pS_2 has been evaluated a partial pressure for all sulphur containing species can be calculated. However, it will be found that a mass balance for all the above reactions will not be satisfied. It is necessary to make a correction to the starting gas pressures of H_2 and CO_2 allow for the formation of H_2S, HS and COS. Thus

$$P'_{CO_2} = P_{CO_2} - pCOS$$

$$P'_{H_2} = P_{H_2} - (pH_2S + pHS)$$

There will also be some reduction of sulphur dioxide for which some oxygen will not be accounted for in the reactions above. This excess oxygen is given by

$$XO = 2\,P_{SO_2} - (2pSO_2 + pSO + pCOS)$$

To apply these conditions it is necessary to return to the H_2/CO_2 equilibrium. If it is assumed that the excess oxygen is associated with the water, the equilibrium becomes,

$$\frac{pCO \times pH_2O}{pCO_2 \times pH_2} = \frac{X(X + XO)}{(P'_{CO_2} - X)(p'_{H_2} - X - XO)}$$

From these partial pressures a new oxygen pressure can be recalculated and the process repeated until the mass balance of input and output partial pressures is correct.

From previous discussions it can be seen that there exists a variety of gas species present at 1500°C and as a consequence a computer must be employed to solve the equations by successive approximation to evaluate the equilibrium sulphur and oxygen pressures. The limitation of the repetitive process was set by:

$$\left| \frac{P_S^{(1)} - P_{(S)}^{(2)}}{P_{S_2}^{(2)}} \right| < 10^{-8}$$

and

$$\left| \frac{P_{O_2}^{(1)} - P_{O_2}^{(2)}}{P_{O_2}^{(2)}} \right| < 10^{-8}$$

Therefore the sulphurising power of a gas mixture $A = \frac{P_{S_2}^{\frac{1}{2}}}{P_{O_2}^{\frac{1}{2}}}$, can be calculated from the values of P_{S_2} and P_{O_2}.

APPENDIX 3

The calculations of oxygen and sulphur potentials of Gas Mixtures H_2, H_2O, H_2S and Ar.

Consider an initial gas mixture consisting of :

$$P_{H_2} = 0.496 \text{ atmosphere}$$
$$P_{H_2S} = 2.00 \times 10^{-3} \text{ "}$$
$$P_{H_2O} = 2.00 \times 10^{-3} \text{ "}$$
$$P_{N_2} = 0.500 \text{ "}$$

Using these values of P_{H_2} and P_{H_2O} as an approximation of the equilibrium values, P_{O_2} can be calculated from

$$H_2O = H_2 + \tfrac{1}{2} O_2 \qquad K_6 = \frac{P_{H_2} \times P_{O_2}^{\frac{1}{2}}}{P_{H_2O}} \qquad (6)$$

$$P_{O_2}^{\frac{1}{2}} = \frac{K_6 \times P_{H_2O}}{P_{H_2}} \qquad P_{O_2} = 3.89 \times 10^{-14} \text{ atm.}$$

Simultaneous solution of five equations (1-5) representing the formation of SO_2, SO, S, H_2S and HS can now be carried out.

There are two unknowns in each equation, the value for $P_{S_2}^{\frac{1}{2}}$ and the partial pressure of one of the species. By applying a sulphur balance to the reaction gas, solution of $P_{S_2}^{\frac{1}{2}}$ reduces to:

Initial partial pressure of H_2S = partial pressure of all sulphur containing gases at 1500°C.

i.e. $$P_{H_2S} = 2 P_{S_2} + PSO_2 + pSO + pS + pH_2S + pH_S$$

$$0.002 = 2 P_{S_2} + 0.6384 P_{S_2}^{\frac{1}{2}}$$

By solving the positive root of the quadratic equation it was found that

$$P_{S_2}^{\frac{1}{2}} = 3.102 \times 10^{-3} \text{ atmosphere}$$

$$\therefore \quad P_{S_2} = 9.622 \times 10^{-6} \text{ atmosphere}$$

Substitution of this value for $P_{S_2}^{\frac{1}{2}}$ in the preceding five equations (1-5), yield values of

$$pSO_2 = 9.08 \times 10^{-10}$$

$$pSO = 7.86 \times 10^{-8}$$

$$pS = 1.77 \times 10^{-6}$$

$$pH_2S = 1.85 \times 10^{-3}$$

$$pHS = 1.33 \times 10^{-4}$$

and ends the first approximation. The first estimation of A value $\frac{P_{S_2}^{\frac{1}{2}}}{P_{O_2}^{\frac{1}{2}}}$ was 15,727.

The total pressure of such a gas equilibrium, however, greater than 0.50 atmosphere and, as the six new species must have been formed from the three initial gases, it is necessary to correct the starting values of P_{H_2} and P_{H_2O} to maintain

$$P_{H_2} + P_{H_2S} + P_{H_2O} = 0.50 \text{ atmosphere}$$

This correction can be seen from the following gas reaction:

$$H_2S = H_2 + \tfrac{1}{2} S_2$$

$$2H_2O + H_2S = 3H_2 + SO_2$$

$$H_2O + H_2S = 2H_2 + SO$$

$$H_2S = H_2 + S$$

$$H_2S = \tfrac{1}{2}H_2 + H_S$$

$$H_2O = H_2 + \tfrac{1}{2}O_2$$

From a consideration of the volume changes in each of these reactions, it was observed that the hydrogen content is increased at

the expense of hydrogen sulphide and water vapour.

Where

$$P_{H_2} = \text{initial } P_{H_2} + 2pS_2 + 3pSO_2 + 2pSO + PS + \tfrac{1}{2}pHS + 2PO_2$$

$$P_{H_2O} = \text{initial } P_{H_2O} - pSO_2 - pSO - 2pO_2$$

Therefore from the second estimation of P_{S_2} and P_{O_2} can be calculated the sulphurising power of a gas mixture

$$\text{i.e. } A = \frac{P_{S_2}^{\frac{1}{2}}}{P_{O_2}^{\frac{1}{2}}} = 12{,}634$$

APPENDIX 4

Linear Correlation of the Experimental Results

The experimental results have been illustrated graphically and, in some cases it was assumed that the best form of representation of the relationship between the two variables involved was the single straight line. The statistical significance of this assumption is investigated and discussed. This straight line may be expressed in more mathematical terms, represented by the equation $y = a + bX$, in which X and y are independent and dependent variables respectively, by the Formula[147]

$$b = \frac{N\Sigma XY - (\Sigma X) \cdot (\Sigma Y)}{N\Sigma X^2 - (\Sigma X)^2}$$

and

$$a = \frac{\Sigma Y - b\Sigma X}{N}$$

where N is the number of individual results.

The computation of the equation of the best straight line was carried out on a computer. To test for the significance of an apparently linear relation, the correlation coefficient (r) was defined[147] by

$$r = \frac{N\Sigma XY - (\Sigma X)(\Sigma Y)}{\sqrt{[N\Sigma X^2 - (\Sigma X)^2][N\Sigma Y^2 - (\Sigma Y)^2]}}$$

This correlation coefficient gives a measure of the significance of the assumption that a linear relationship exists between the two variables, X and Y. It has the characteristics such that if the relationship between the data can be represented exactly by a straight line then $r \pm 1$, positive if the straight line has a positive

slope and negative if the line has a negative slope, if on the other hand there is no relation at all between the variables then r = 0.

The residual variance about the regression line of Y upon X was also taken into account. This was done by calculating the standard deviation (δ_r) of the scatter of the points about the regression line, measured in units of Y parallel to the Y-axis, using the formula[148]

$$\delta_r = \sqrt{1 - r^2} \sqrt{\frac{\Sigma Y^2 - (\Sigma Y)^2/N}{N - 2}}$$

The value of the standard deviation provides a good measure of the usefulness and reliability of the equation of regression line for predicting values of Y for given values of X. In particular, it allows confidence limits to be drawn on either side of the regression line at a Y axis distance equal $t_x \delta_r$ units[149] on the two lines drawn parallel to the regression line on the downwards and upwards. The student's "t" value is obtained from statistical table for N-2 degrees of freedom.

In the present study, the value of "τ" from statistical tables was taken at the 5% level of significance and this allowed 95% confidence limits to be drawn on either side of the regression line.

APPENDIX 5

TABLES

Table A.1

Liquidus Temperatures and Phase Identifications for Fe_2TiO_2-Fe_2SiO_4-FeO System

No.	TiO_2 %	SiO_2 %	FeO %	Liquidus Temp. ± 10°C	Phase identified
A 1	5.09	7.71	87.20	1285	FeO
2	4.96	22.91	74.13	1155	FeO-F_2S
3	7.45	18.56	73.99	1180	F_2T-FeO
4	9.58	20.14	70.28	1185	F_2T-F_2S
5	7.75	24.69	67.56	1160	F_2S
6	6.10	23.20	70.70	1135	F_2S-F_2T-FeO
7	19.19	7.58	72.43	1370	F_2T
8	22.84	5.96	71.20	1380	F_2T
9	6.54	23.21	70.26	1170	F_2S
10	6.77	25.44	67.79	1175	-
11	6.51	25.65	67.84	1180	F_2S
12	5.22	11.25	83.53	1255	FeO
13	6.54	17.57	75.89	1220	FeO
14	5.01	16.64	78.35	1225	FeO
15	2.19	15.28	82.53	1245	-
16	13.52	5.91	80.57	1325	F_2T
17	17.17	3.88	78.35	1355	F_2T
18	13.65	14.25	72.10	1335	F_2T
19	30.00	1.20	68.80	1390	-
20	15.00	9.70	75.30	1350	-
21	8.50	13.00	78.50	1260	F_2T-FeO
22	2.50	9.00	88.50	1320	FeO
23	10.88	10.46	78.66	1315	F_2T
24	10.89	11.97	77.14	1325	F_2T
25	10.25	12.11	77.64	1290	F_2T-FeO
26	20.00	4.00	76.00	1370	F_2T
27	8.00	7.50	84.00	1210	FeO-F_2T
28	10.50	8.50	81.00	1305	F_2T
29	7.90	14.08	78.02	1200	F_2T-FeO
30	22.20	2.80	75.00	1375	F_2T

Table A.1 contd/

No.	TiO_2 %	SiO_2 %	FeO %	Liquidus Temp. ± 10°C	Phase identified
A31	28.00	1.00	71.00	1390	F_2T
32	25.20	3.50	71.30	1385	F_2T
33	25.00	2.00	73.00	1385	-
34	17.52	8.30	74.18	1365	F_2T
35	3.20	5.10	91.70	1350	-
36	8.00	1.00	91.00	1320	FeO
37	20.24	12.24	67.52	1365	F_2T
38	13.24	20.00	66.76	1185	F_2T-F_2S
39	3.25	30.74	66.01	1205	F_2S
40	15.05	17.93	67.02	1310	F_2T
41	26.58	5.88	67.54	1385	-
42	27.57	3.50	68.93	1390	F_2T
43	3.50	28.50	68.00	1190	-
44	3.00	21.50	75.50	1200	F_2T
45	17.50	12.00	70.50	1255	F_2T
46	6.10	23.20	70.70	1145	F_2T-F_2S-FeO
47	9.10	13.50	87.40	1280	F_2T-FeO
48	9.00	7.00	84.00	1215	FeO-F_2T
49	7.00	14.50	78.50	1200	FeO-F_2T

Compositions are in mole percentage.

Table A.2

Liquidus Temperatures and Phase Identification for Fe_2TiO_4-Fe_2SiO_4-SiO_2 System.

No.	TiO_2 %	SiO_2 %	FeO %	Liquidus Temp. ± 10°C	Phase identified
A19	30.00	1.20	68.80	1390	-
A37	20.24	12.24	67.52	1365	F_2T
A38	13.24	20.00	66.76	1185	F_2T-F_2S
A39	3.25	30.74	66.01	1205	F_2S
A40	15.05	17.93	67.02	1310	F_2T-F_2S
A41	26.58	5.88	67.54	1385	F_2T
A42	27.57	3.50	68.93	1390	F_2T
B 1	7.34	27.60	65.66	1200	F_2S
2	8.13	28.90	62.97	1175	-
3	10.94	28.44	60.62	1170	F_2S
4	24.00	13.50	62.50	1370	F_2T
5	15.79	20.73	63.53	1310	F_2T
6	20.00	20.00	60.00	1335	-
7	20.00	14.20	66.80	1365	F_2T-F_2S
8	13.35	23.16	63.49	1180	F_2T-F_2S
9	19.19	23.44	56.66	1305	F_2T
10	19.80	24.50	55.70	1330	SiO_2-F_2T
11	20.99	25.96	53.05	1360	SiO_2
12	16.85	35.10	48.05	1385	SiO_2
13	12.90	34.95	52.15	1380	-
14	10.40	38.30	51.30	1420	SiO_2
15	8.17	44.18	47.65	1490	SiO_2
16	11.24	31.08	57.68	1145	F_2S-SiO_2
17	13.04	28.95	58.01	1140	F_2S-F_2T-SiO_2
18	29.50	3.25	67.25	1390	F_2T
19	27.00	12.50	60.50	1350	F_2T
20	20.40	28.90	50.70	1370	SiO_2
21	23.98	23.80	52.22	1365	SiO_2
22	25.20	19.30	55.50	1330	SiO_2-F_2T

Table A.2 contd/

No.	TiO_2 %	SiO_2 %	FeO %	Liquidus Temp. ± 10°C	Phase identified
B23	20.00	35.00	45.00	1480	SiO_2
24	17.91	40.34	41.75	1525	SiO_2
25	12.40	30.00	57.60	1145	F_2S-SiO_2
26	7.05	35.25	57.25	1150	F_2S
27	4.30	40.20	55.50	1170	F_2S-SiO_2
28	13.20	25.00	61.80	1170	F_2S
29	1150	28.00	60.50	1170	F_2S
30	30.00	1.20	68.00	1390	F_2T
31	18.00	25.00	57.00	1335	SiO_2-F_2T
32	15.00	37.50	47.50	1380	SiO_2
33	15.00	45.00	40.00	1620	-
34	10.20	49.91	39.89	1645	-
35	3.51	50.20	46.29	1552	SiO_2
36	13.04	28.95	58.01	1185	F_2S
37	20.24	12.24	67.52	1365	F_2T
38	14.20	22.30	63.50	1165	F_2T-F_2S
39	18.00	43.50	38.50	1605	-
40	4.50	48.00	47.50	1585	-
41	5.50	46.50	48.00	1555	-
42	6.00	45.00	49.00	1505	-
43	9.00	40.00	51.00	1445	-
44	14.00	30.50	55.50	1340	-

Compositions are in mole percentage

Table A.3

Liquidus Temperatures and Phase Identification for Fe_2TiO_4-$FeTiO_3$-SiO_2 System

No.	TiO_2 %	SiO_2 %	FeO %	Liquidus Temp. ± 10°C	Phase identified
B18	29.50	3.25	67.25	1390	F_2T
19	27.00	12.50	60.50	1350	F_2T
21	23.98	23.80	52.22	1365	SiO_2
22	25.20	19.30	55.50	1330	SiO_2-F_2T
23	20.00	35.00	45.00	1480	SiO_2
24	17.91	40.34	41.75	1525	SiO_2
33	15.00	45.00	40.00	1620	-
39	18.00	43.50	38.50	1605	-
C 1	26.22	34.91	38.87	1525	-
2	26.47	24.38	44.15	1420	SiO_2
3	31.04	29.52	39.44	1490	-
4	32.33	22.72	44.95	1430	SiO_2
5	37.37	17.23	45.50	1380	SiO_2
6	32.65	16.92	50.43	1360	SiO_2-FT
7	41.53	5.22	53.25	1360	FT_2
8	37.09	6.18	56.73	1380	FT
9	32.50	15.00	52.50	1360	SiO_2
10	31.50	12.20	56.30	1355	F_2T
11	35.00	10.00	55.00	1365	F_2T
12	37.50	10.00	52.50	1320	F_2T-FT-SiO_2
13	42.55	12.00	45.45	1350	FT-SiO_2
14	38.00	12.00	50.00	1340	FT-SiO_2
15	36.20	12.94	50.86	1350	SiO_2
16	43.05	12.58	44.37	1365	FT-SiO_2
17	39.91	18.28	41.81	1415	SiO_2
18	37.35	24.02	38.63	1460	SiO_2
19	35.03	29.09	35.88	1520	-
20	26.47	29.50	44.03	1480	-
21	27.50	20.00	52.50	1345	SiO_2
22	16.00	45.00	39.00	1620	-

Compositions are in mole percentage

Table A.3 Contd/

No.	TiO_2 %	SiO_2 %	FeO %	Liquidus Temp. ± 10°C	Phase identified
C23	26.10	40.05	33.85	1635	-
24	21.50	41.50	37.00	1625	-
25	45.50	6.50	48.00	1385	-
26	29.00	34.50	36.50	1555	-
27	25.50	34.00	40.50	1525	-
28	24.00	37.50	38.50	1560	-
29	34.00	24.00	42.00	1445	-
30	33.00	32.50	34.50	1550	-
31	28.50	26.00	45.50	1460	-
32	36.00	26.50	37.50	1490	-

Table A.4

Liquidus Temperatures and Phase Identifications for $FeTiO_3$-$FeTi_2O_5$-SiO_2 System

No.	TiO_2 %	SiO_2 %	FeO %	Liquidus Temp. ± 10°C	Phase identified
C16	43.05	12.58	44.37	1365	FT-SiO_2
17	39.91	18.28	41.81	1415	SiO_2
18	37.35	24.02	38.63	1460	SiO_2
19	35.02	29.09	35.88	1520	-
D 1	63.80	5.00	32.20	1480	FT_2
2	60.02	10.07	29.91	1450	FT_2-SiO_2
3	56.50	15.00	28.50	1495	SiO_2
4	53.10	20.00	26.90	1530	SiO_2
5	49.80	24.90	25.30	1570	SiO_2
6	60.00	5.00	35.00	1455	FT_2
7	54.75	5.00	40.25	1425	FT-FT_2

Table A.4 Contd/

No.	TiO_2 %	SiO_2 %	FeO %	Liquidus Temp. ± 10°C	Phase identified
D 8	55.00	9.85	35.15	1440	FT_2-SiO_2
9	50.10	4.80	45.10	1380	FT
10	50.20	10.10	39.70	1370	SiO_2
11	50.00	15.10	34.90	1460	SiO_2
12	50.02	20.18	29.80	1570	-
13	45.00	14.92	40.08	1420	SiO_2
14	44.78	20.00	35.22	1450	SiO_2
15	45.00	24.83	30.17	1575	-
16	40.10	25.30	34.60	1520	SiO_2
17	35.50	35.00	31.50	1590	-
18	52.50	7.50	40.00	1330	FT-FT_2-SiO_2
19	50.00	9.23	40.77	1360	FT
20	55.01	15.10	29.89	1489	SiO_2
21	41.50	20.00	38.50	1480	SiO_2
22	36.50	30.00	31.50	1554	SiO_2
23	39.92	30.10	29.98	1540	-
24	43.11	31.21	25.68	1543	SiO_2
25	53.50	9.00	37.50	1435	FT_2-SiO_2
26	55.00	12.00	33.00	1510	-
27	52.50	17.50	30.00	1450	-

Compositions are in mole percentage

Table A.5

Experimental Results on Fe-Ti-Si-O System at P_{O_2} = 0.021 atm. at 1500°C

No.	Weight Percent				Mole Fraction				'Atom Fraction'					$\frac{Fe^{3+}}{Fe^{2+}}$	Liquidus Temp. ±10°C
	TiO_2	SiO_2	FeO	Fe_2O_3	TiO_2	SiO_2	FeO	Fe_2O_3	Ti^{4+}	Si^{4+}	Fe^{2+}	Fe^{3+}	O^{2-}		
1	4.43	22.62	28.68	44.27	0.050	0.340	0.360	0.250	0.016	0.108	0.115	0.159	0.602	1.38	1490
2	9.15	23.35	28.55	38.95	0.100	0.340	0.347	0.213	0.033	0.110	0.113	0.138	0.606	1.22	1535
3	25.15	5.88	24.47	44.50	0.305	0.095	0.330	0.270	0.095	0.030	0.103	0.168	0.604	1.63	1535
4	21.08	9.50	25.93	43.49	0.250	0.150	0.342	0.258	0.074	0.045	0.101	0.154	0.626	1.52	1470
5	16.32	13.54	26.88	43.26	0.190	0.210	0.348	0.252	0.060	0.067	0.110	0.160	0.603	1.45	1420
6	4.98	23.46	30.29	41.27	0.055	0.345	0.372	0.228	0.018	0.112	0.120	0.148	0.602	1.23	1488
7	24.60	4.97	25.00	45.43	0.301	0.081	0.340	0.278	0.093	0.025	0.106	0.173	0.173	1.63	1550
8	14.57	4.95	24.97	55.50	0.190	0.086	0.362	0.362	0.054	0.026	0.107	0.215	0.598	2.01	1535
9	9.68	4.47	25.90	59.95	0.130	0.080	0.387	0.403	0.038	0.023	0.113	0.236	0.590	2.09	1530
10	5.42	4.64	26.28	63.66	0.070	0.080	0.378	0.412	0.022	0.024	0.116	0.252	0.586	2.17	1520
11	35.88	5.19	23.16	35.77	0.415	0.080	0.298	0.207	0.132	0.026	0.096	0.133	0.613	1.38	1560
12	25.67	15.40	25.82	33.71	0.275	0.225	0.315	0.185	0.090	0.074	0.103	0.121	0.612	1.17	1455
13	20.79	19.08	26.34	33.79	0.225	0.275	0.317	0.183	0.074	0.090	0.104	0.120	0.612	1.15	1500
14	15.13	24.15	27.64	33.08	0.160	0.340	0.325	0.175	0.053	0.112	0.107	0.116	0.612	1.08	1554
15	12.66	26.23	27.82	33.29	0.133	0.367	0.325	0.175	0.044	0.121	0.107	0.116	0.612	1.08	1570
16	33.17	8.30	24.41	34.12	0.375	0.125	0.307	0.193	0.122	0.041	0.100	0.125	0.612	1.25	1475
17	26.35	14.33	25.73	33.59	0.290	0.210	0.315	0.185	0.095	0.069	0.103	0.121	0.612	1.74	1450

Table A.5 Contd/

No.	Weight Percent				Mole Fraction				'Atom Fraction'					$\frac{Fe^{3+}}{Fe^{2+}}$	Liquidus Temp. ±10°C
	TiO_2	SiO_2	FeO	Fe_2O_3	TiO_2	SiO_2	FeO	Fe_2O_3	Ti^{4+}	Si^{4+}	Fe^{2+}	Fe^{3+}	O^{2-}		
18	14.29	25.05	28.28	32.38	0.150	0.350	0.330	0.170	0.050	0.115	0.111	0.116	0.608	1.05	1565
19	5.01	5.00	24.33	65.66	0.07	0.093	0.378	0.459	0.020	0.025	0.107	0.260	0.588	2.43	1525
20	9.95	5.00	25.55	59.50	0.133	0.089	0.380	0.398	0.039	0.026	0.111	0.233	0.591	2.10	1540
21	14.99	5.02	24.82	55.17	0.195	0.087	0.359	0.359	0.058	0.026	0.107	0.214	0.595	2.00	1530
22	25.04	4.99	25.17	44.80	0.305	0.081	0.341	0.273	0.095	0.025	0.106	0.170	0.604	1.60	1555
23	5.03	14.98	26.33	53.66	0.062	0.246	0.361	0.331	0.019	0.075	0.109	0.200	0.597	1.83	1453
24	10.03	15.01	26.32	48.64	0.120	0.239	0.350	0.291	0.037	0.074	0.108	0.180	0.601	1.67	1442
25	15.06	15.03	26.53	43.44	0.174	0.232	0.342	0.252	0.055	0.073	0.108	0.159	0.604	1.47	1430
26	25.03	14.96	26.18	33.83	0.275	0.219	0.320	0.186	0.090	0.072	0.105	0.122	0.611	1.16	1455
27	5.03	24.99	29.60	40.38	0.055	0.364	0.360	0.221	0.018	0.118	0.117	0.143	0.604	1.22	1530
28	10.40	21.88	29.63	38.09	0.125	0.350	0.396	0.229	0.037	0.104	0.118	0.136	0.605	1.15	1523
29	14.52	24.30	29.02	32.16	0.158	0.352	0.315	0.175	0.053	0.117	0.133	0.117	0.580	0.880	1584
30	25.01	25.00	24.80	25.19	0.254	0.338	0.280	0.128	0.086	0.114	0.094	0.084	0.622	0.894	1605
31	3.22	9.70	34.33	52.75	0.040	0.160	0.473	0.327	0.013	0.050	0.149	0.206	0.582	1.38	1491
32	11.62	9.98	30.92	47.48	0.140	0.160	0.414	0.286	0.044	0.051	0.131	0.181	0.593	1.38	1487
33	17.63	8.83	29.07	44.47	0.210	0.140	0.385	0.265	0.069	0.046	0.145	0.176	0.564	1.21	1520
34	21.94	9.93	35.17	32.96	0.290	0.175	0.517	0.218	0.082	0.050	0.147	0.124	0.597	0.84	1463
35	28.02	15.28	22.36	34.34	0.310	0.225	0.275	0.190	0.100	0.072	0.089	0.122	0.617	1.37	1470
36	35.53	6.92	23.19	34.36	0.405	0.105	0.294	0.196	0.131	0.034	0.095	0.127	0.613	1.34	1548
37	34.50	10.09	22.81	32.60	0.385	0.150	0.283	0.182	0.125	0.050	0.092	0.118	0.615	1.28	1475

Table A.6

Experimental Results on Fe-Ti-Si-O System at $\frac{P_{CO_2}}{P_{CO}} = 249$ at 1500°C

No.	Weight Percent				Mole Fraction				'Atom Fraction'					$\frac{Fe^{3+}}{Fe^{2+}}$	Liquidus Temp. ±10°C
	TiO_2	SiO_2	FeO	Fe_2O_3	TiO_2	SiO_2	FeO	Fe_2O_3	Ti^{4+}	Si^{4+}	Fe^{2+}	Fe^{3+}	O^{2-}		
1	4.67	23.83	34.57	36.93	0.050	0.340	0.412	0.198	0.017	0.114	0.138	0.132	0.599	0.956	1450
2	9.64	24.62	34.51	31.23	0.100	0.340	0.398	0.162	0.034	0.116	0.136	0.111	0.603	0.816	1485
3	20.20	25.79	31.79	22.22	0.200	0.340	0.350	0.110	0.070	0.118	0.122	0.077	0.614	0.631	1573
4	3.63	24.56	30.40	41.41	0.040	0.360	0.372	0.228	0.013	0.117	0.120	0.148	0.602	1.233	1425
5	14.75	14.98	27.62	42.65	0.170	0.230	0.354	0.246	0.054	0.073	0.113	0.157	0.603	1.390	1360
6	26.31	4.94	24.39	44.36	0.320	0.080	0.330	0.270	0.100	0.025	0.103	0.168	0.604	1.630	1490
7	37.06	5.57	31.82	25.55	0.400	0.080	0.382	0.138	0.138	0.028	0.132	0.095	0.607	0.72	1490
8	21.81	5.44	35.61	37.14	0.250	0.083	0.454	0.213	0.084	0.028	0.153	0.143	0.592	0.940	1477
9	12.40	5.09	36.26	46.25	0.150	0.082	0.488	0.280	0.049	0.027	0.159	0.182	0.583	1.140	1475
10	8.08	4.85	37.04	50.04	0.100	0.080	0.510	0.310	0.032	0.026	0.164	0.199	0.579	1.210	1476
11	3.50	4.67	36.06	55.77	0.045	0.080	0.516	0.359	0.014	0.014	0.163	0.227	0.582	1.390	1463
12	25.04	17.36	31.61	25.99	0.260	0.240	0.365	0.135	0.090	0.082	0.126	0.093	0.609	0.738	1430
13	15.00	26.29	33.73	24.98	0.150	0.350	0.375	0.125	0.053	0.122	0.130	0.087	0.608	0.669	1571
14	11.11	29.58	34.07	25.24	0.110	0.390	0.375	0.125	0.038	0.136	0.131	0.087	0.608	0.664	1600
15	10.21	30.66	35.06	24.07	0.100	0.400	0.382	0.118	0.035	0.140	0.134	0.083	0.608	0.619	1605
16	14.46	22.05	19.70	43.79	0.165	0.335	0.250	0.250	0.050	0.103	0.077	0.154	0.616	2.000	1510
17	27.73	25.08	31.39	25.80	0.290	0.210	0.365	0.135	0.100	0.072	0.126	0.093	0.609	0.738	1420
18	37.00	6.95	29.79	26.26	0.400	0.100	0.358	0.142	0.135	0.034	0.122	0.097	0.612	0.795	1492

Table A.6. Contd./

No.	Weight Percent				Mole Fraction				'Atom Fraction'					$\frac{Fe^{3+}}{Fe^{2+}}$	Liquidus Temp. $\pm 10^{0}C$
	TiO_2	SiO_2	FeO	Fe_2O_3	TiO_2	SiO_2	FeO	Fe_2O_3	Ti^{4+}	Si^{4+}	Fe^{2+}	Fe^{3+}	O^{2-}		
19	5.01	4.99	35.15	54.85	0.064	0.085	0.500	0.351	0.020	0.027	0.156	0.219	0.578	1.400	1458
20	10.04	4.99	35.61	49.36	0.124	0.082	0.489	0.305	0.040	0.026	0.157	0.195	0.582	1.240	1469
21	15.02	4.98	34.75	45.25	0.181	0.080	0.466	0.273	0.059	0.026	0.151	0.177	0.587	1.170	1471
22	25.04	5.00	34.09	35.87	0.286	0.076	0.433	0.205	0.095	0.026	0.146	0.138	0.595	0.945	1488
23	5.01	15.02	37.71	42.26	0.057	0.227	0.476	0.240	0.019	0.076	0.158	0.160	0.587	1.010	1362
24	4.96	24.91	36.60	33.53	0.052	0.347	0.426	0.175	0.017	0.118	0.145	0.120	0.600	0.828	1473
25	15.05	15.00	37.44	35.51	0.162	0.215	0.448	0.175	0.056	0.074	0.154	0.121	0.595	0.786	1345
26	14.95	24.99	33.93	26.13	0.151	0.336	0.381	0.132	0.051	0.112	0.127	0.168	0.542	1.322	1533
27	25.17	15.05	32.45	27.33	0.265	0.211	0.380	0.144	0.084	0.067	0.091	0.166	0.592	1.820	1394
28	10.00	24.95	34.95	30.10	0.103	0.342	0.400	0.155	0.032	0.107	0.089	0.127	0.645	1.430	1485
29	11.09	16.66	35.17	37.08	0.122	0.244	0.430	0.204	0.042	0.084	0.148	0.114	0.612	0.770	1380
30	24.97	25.04	30.43	19.56	0.245	0.327	0.332	0.096	0.086	0.114	0.116	0.067	0.617	0.577	1597
31	40.66	9.71	22.85	26.78	0.440	0.140	0.275	0.145	0.146	0.046	0.091	0.096	0.621	1.055	1457
32	37.68	14.15	22.19	25.98	0.400	0.200	0.262	0.138	0.133	0.066	0.087	0.092	0.622	1.057	1442
33	35.79	17.20	21.64	25.37	0.375	0.240	0.252	0.133	0.124	0.080	0.084	0.088	0.624	1.048	1487
34	20.93	8.52	32.55	38.00	0.240	0.130	0.412	0.218	0.079	0.043	0.137	0.144	0.597	1.050	1453
35	18.91	14.20	30.70	36.19	0.210	0.210	0.379	0.201	0.142	0.064	0.116	0.122	1.556	1.052	1365
36	17.62	15.27	30.80	36.31	0.195	0.225	0.379	0.201	0.064	0.074	0.125	0.125	0.612	1.00	1351

Table A.7.

Experimental Results on Fe-Ti-Si-O System at $\frac{CO_2}{CO}$ = 135.36 at 1500°C

No.	Weight Percent				Mole Fraction				"Atom Fraction"					$\frac{Fe^{3+}}{Fe^{2+}}$	Liquidus Temp. ±10°C
	TiO_2	SiO_2	FeO	Fe_2O_3	TiO_2	SiO_2	FeO	Fe_2O_3	Ti^{4+}	Si^{4+}	Fe^{2+}	Fe^{3+}	O^{2-}		
1	4.86	24.82	39.43	30.89	0.050	0.340	0.451	0.159	0.021	0.119	0.158	0.112	0.590	0.70	1380
2	10.03	25.60	39.12	25.25	0.100	0.340	0.434	0.126	0.043	0.122	0.156	0.091	0.588	0.58	1410
3	20.73	26.47	34.77	18.03	0.200	0.340	0.373	0.087	0.087	0.125	0.137	0.064	0.587	0.467	1500
4	31.78	27.05	28.68	12.49	0.300	0.340	0.301	0.059	0.132	0.126	0.111	0.044	0.587	0.396	1598
5	10.66	10.83	24.36	54.15	0.170	0.230	0.432	0.168	0.049	0.055	0.104	0.208	0.584	2.00	1380
6	9.59	21.60	37.77	31.05	0.100	0.300	0.438	0.162	0.042	0.105	0.154	0.114	0.585	0.740	1327
7	4.88	25.67	38.99	30.46	0.050	0.350	0.444	0.156	0.021	0.123	0.156	0.110	0.590	0.705	1409
8	5.85	24.88	38.90	30.38	0.060	0.340	0.444	0.156	0.025	0.119	0.156	0.110	0.590	0.705	1407
9	11.91	19.68	37.54	30.87	0.125	0.275	0.438	0.162	0.053	0.097	0.154	0.114	0.582	0.740	1325
10	14.94	16.83	35.77	32.42	0.160	0.240	0.426	0.174	0.067	0.084	0.149	0.120	0.580	0.805	1374
11	32.41	5.56	35.56	26.47	0.350	0.080	0.427	0.143	0.151	0.029	0.159	0.105	0.556	0.660	1476
12	24.86	5.43	38.28	31.43	0.275	0.080	0.471	0.174	0.118	0.029	0.170	0.126	0.557	0.741	1470
13	14.77	5.01	46.63	34.39	0.175	0.079	0.601	0.205	0.071	0.027	0.206	0.139	0.557	0.675	1468
14	9.51	4.91	38.97	46.61	0.115	0.079	0.524	0.282	0.046	0.026	0.175	0.188	0.565	1.074	1455
15	4.83	4.83	39.21	51.13	0.060	0.080	0.542	0.318	0.024	0.026	0.176	0.207	0.567	1.176	1452
16	24.19	14.13	37.41	24.27	0.225	0.275	0.387	0.113	0.109	0.071	0.158	0.092	0.570	0.582	1408

Table A.7 Contd/

No.	Weight Percent				Mole Fraction				'Atom Fraction'					$\frac{Fe^{3+}}{Fe^{2+}}$	Liquidus ±10°C
	TiO_2	SiO_2	FeO	Fe_2O_3	TiO_2	SiO_2	FeO	Fe_2O_3	Ti^{4+}	Si^{4+}	Fe^{2+}	Fe^{3+}	O^{2-}		
17	14.62	27.40	36.12	21.86	0.143	0.357	0.393	0.107	0.052	0.110	0.121	0.066	0.651	0.545	1469
18	10.42	31.29	37.47	20.82	0.100	0.400	0.400	0.100	0.047	0.156	0.078	0.078	0.641	1.00	1547
19	24.97	25.03	32.47	17.53	0.242	0.323	0.350	0.085	0.106	0.118	0.128	0.062	0.586	0.484	1507
20	11.43	30.43	37.37	20.77	0.110	0.390	0.400	0.100	0.052	0.152	0.078	0.078	0.640	1.00	1510
21	17.20	25.07	35.49	22.24	0.170	0.330	0.390	0.110	0.076	0.124	0.163	0.083	0.553	0.509	1466
22	31.28	7.83	18.38	42.51	0.375	0.125	0.245	0.255	0.144	0.040	0.078	0.163	0.575	2.090	1455
23	14.98	15.02	37.65	32.35	0.161	0.215	0.450	0.174	0.420	0.047	0.099	0.076	0.358	0.768	1380
24	46.45	7.12	25.58	20.85	0.490	0.100	0.300	0.110	0.213	0.037	0.110	0.080	0.560	0.727	1501
25	10.07	12.37	42.80	34.76	0.110	0.180	0.520	0.190	0.046	0.064	0.185	0.135	0.570	0.730	1400
26	18.37	10.35	39.33	31.95	0.200	0.150	0.476	0.174	0.085	0.054	0.170	0.124	0.566	0.729	1420

Table A.8

Experimental Results on Fe-Ti-S-O System at $\frac{P_{CO_2}}{P_{CO}} = 20.99$ at $1500^{o}C$

No.	Weight Percent				Mole Fraction				'Atom Fraction'					$\frac{Fe^{3+}}{Fe^{2+}}$	Liquidus Temp. $\pm 10^{o}C$
	TiO_2	SiO_2	FeO	Fe_2O_3	TiO_2	SiO_2	FeO	Fe_2O_3	Ti^{4+}	Si^{4+}	Fe^{2+}	Fe^{3+}	O^{2-}		
1	5.00	26.00	44.00	25.00	0.050	0.340	0.488	0.122	0.018	0.124	0.175	0.090	0.593	0.514	1365
2	10.00	27.00	44.00	19.00	0.100	0.340	0.470	0.090	0.035	0.127	0.173	0.067	0.598	0.387	1402
3	19.00	24.00	40.00	17.00	0.200	0.340	0.400	0.060	0.067	0.112	0.156	0.060	0.605	0.385	1505
4	28.99	24.66	37.46	11.59	0.300	0.340	0.320	0.040	0.099	0.112	0.133	0.040	0.616	0.301	1597
5	26.49	8.03	37.61	27.87	0.285	0.115	0.450	0.150	0.100	0.040	0.158	0.105	0.597	0.665	1400
6	19.14	14.38	39.51	26.97	0.200	0.200	0.459	0.141	0.072	0.094	0.165	0.101	0.568	0.612	1305
7	10.00	22.53	42.89	24.58	0.100	0.300	0.477	0.123	0.036	0.108	0.172	0.089	0.595	0.517	1350
8	4.08	27.53	43.96	24.43	0.040	0.360	0.480	0.120	0.014	0.131	0.174	0.087	0.594	0.500	1370
9	2.05	29.31	44.61	24.02	0.020	0.380	0.483	0.117	0.007	0.138	0.176	0.085	0.594	0.483	1399
10	33.73	12.33	34.68	19.26	0.343	0.167	0.392	0.098	0.122	0.060	0.140	0.070	0.608	0.500	1355
11	27.46	16.87	36.11	19.56	0.275	0.225	0.402	0.098	0.098	0.081	0.144	0.070	0.607	0.486	1345
12	18.13	25.28	38.38	18.21	0.175	0.325	0.412	0.088	0.121	0.130	0.164	0.070	0.515	0.427	1453
13	8.59	33.88	40.77	16.76	0.080	0.420	0.422	0.078	0.022	0.160	0.153	0.058	0.606	0.379	1515
14	6.47	35.60	40.70	17.23	0.060	0.440	0.420	0.080	0.023	0.160	0.153	0.058	0.606	0.379	1620
15	18.62	24.86	38.32	18.20	0.180	0.320	0.412	0.088	0.065	0.116	0.149	0.064	0.606	0.430	1470
16	37.78	8.01	34.85	19.36	0.390	0.110	0.400	0.100	0.139	0.039	0.143	0.072	0.607	0.497	1424
17	2.05	30.03	43.33	24.59	0.020	0.390	0.470	0.120	0.007	0.141	0.169	0.087	0.596	0.515	1424
18	24.99	24.97	34.79	15.25	0.239	0.318	0.370	0.073	0.083	0.111	0.114	0.051	0.641	0.447	1553

Table A.8 Contd/

No.	Weight Percent				Mole Fraction				'Atom Fraction'					$\frac{Fe^{3+}}{Fe^{2+}}$	Liquidus Temp. $\pm 10^{0}C$
	TiO_2	SiO_2	FeO	Fe_2O_3	TiO_2	SiO_2	FeO	Fe_2O_3	Ti^{4+}	Si^{4+}	Fe^{2+}	Fe^{3+}	O^{2-}		
19	12.32	30.03	38.03	19.62	0.118	0.383	0.405	0.094	0.042	0.138	0.145	0.068	0.607	0.469	1530
20	17.06	25.00	39.33	18.61	0.165	0.322	0.423	0.090	0.060	0.117	0.153	0.065	0.605	0.425	1440
21	39.10	10.83	32.50	17.57	0.397	0.147	0.367	0.089	0.141	0.052	0.130	0.064	0.613	0.492	1342
22	32.02	5.01	38.76	24.21	0.341	0.071	0.459	0.129	0.122	0.025	0.163	0.092	0.598	0.564	1433
23	9.62	4.99	45.87	39.52	0.115	0.076	0.583	0.226	0.039	0.027	0.204	0.158	0.572	0.774	1441
24	9.72	12.43	50.72	27.13	0.101	0.172	0.586	0.141	0.037	0.064	0.217	0.105	0.577	0.484	1368
25	8.74	14.59	50.07	26.60	0.090	0.200	0.573	0.137	0.033	0.074	0.212	0.102	0.579	0.481	1345
26	26.08	5.34	44.69	23.89	0.275	0.075	0.525	0.126	0.100	0.027	0.192	0.092	0.589	0.479	1445
27	20.65	4.23	49.04	26.08	0.220	0.060	0.581	0.139	0.081	0.022	0.215	0.103	0.578	0.479	1447
28	19.24	10.12	46.03	24.61	0.200	0.140	0.532	0.128	0.073	0.052	0.195	0.094	0.586	0.482	1385
29	5.82	28.05	45.70	20.43	0.061	0.391	0.441	0.107	0.021	0.132	0.180	0.072	0.595	0.400	1477
30	35.52	12.59	33.36	18.53	0.360	0.170	0.376	0.094	0.128	0.061	0.134	0.067	0.610	0.500	1350
31	34.02	16.15	32.03	17.80	0.340	0.215	0.356	0.089	0.121	0.076	0.126	0.063	0.613	0.500	1394
32	32.89	18.99	30.93	17.19	0.325	0.250	0.340	0.085	0.115	0.088	0.120	0.061	0.616	0.508	1500
33	31.61	21.05	30.43	16.91	0.310	0.275	0.332	0.083	0.111	0.098	0.122	0.059	0.610	0.484	1547

Table A.9

Experimental Results on Fe-Ti-Si-O System at $\frac{P_{CO_2}}{P_{CO}} = 6.71$ at 1500°C

No.	Weight Percent				Mole Fraction				'Atom Fraction'					$\frac{Fe^{3+}}{Fe^{2+}}$	Liquidus Temp. ±10°C
	TiO_2	SiO_2	FeO	Fe_2O_3	TiO_2	SiO_2	FeO	Fe_2O_3	Ti^{4+}	Si^{4+}	Fe^{2+}	Fe^{3+}	O^{2-}		
1	5.12	26.25	46.09	22.54	0.050	0.340	0.500	0.110	0.d8	0.125	0.184	0.081	0.592	0.44	1290
2	10.83	27.25	48.50	13.42	0.100	0.335	0.498	0.062	0.038	0.128	0.191	0.048	0.595	0.251	1330
3	21.99	28.31	42.01	7.69	0.202	0.343	0.425	0.035	0.076	0.129	0.160	0.026	0.609	0.163	1467
4	33.36	28.56	34.30	3.78	0.300	0.342	0.343	0.017	0.106	0.126	0.126	0.012	0.630	0.095	1554
5	20.23	15.19	46.19	18.19	0.200	0.200	0.510	0,090	0.075	0.075	0.191	0.067	0.592	0.351	1330
6	8.95	22.40	53.55	15.10	0.090	0.300	0.599	0.076	0.033	0.109	0.218	0,055	0.585	0,252	1220
7	4.37	29.52	53.02	13.09	0.040	0.360	0.540	0.060	0.015	0.140	0.209	0.047	0.589	0,225	1304
8	2.74	30.87	53.24	13.15	0.025	0.375	0.540	0.060	0.008	0.284	0.176	0.039	0.493	0.222	1300
9	8.73	19.66	55.56	16.05	0.075	0.325	0.531	0.069	0.033	0.097	0.230	0.060	0.580	0.260	1241
10	33.34	14.08	42.16	10.42	0.320	0.180	0.450	0.050	0.120	0.068	0.170	0.038	0.604	0.224	1325
11	25.75	20.95	44.08	9.22	0.240	0.260	0.457	0.043	0.091	0.099	0.174	0.033	0.603	0.190	1353
12	13.80	31.09	45.18	9.93	0.125	0.375	0.455	0.045	0.045	0.142	0.172	0.034	0.607	0.198	1440
13	6.22	38.21	46.98	8.59	0.055	0.450	0.462	0.038	0,021	0.171	0.176	0.030	0.603	0.170	1498
14	4.58	39.57	47.38	8.47	0.040	0.460	0.463	0.037	0.015	0.177	0.177	0.028	0.603	0.158	1505
15	38.83	9.72	42.55	8.90	0.375	0.125	0.457	0.043	0.142	0.048	0.174	0.033	0.603	0.190	1370
16	16.91	28.27	44.35	10.47	0.155	0.345	0.452	0.048	0.059	0.130	0.171	0.036	0.604	0.211	1409
17	26.19	20.47	43.73	9.61	0.245	0.255	0.455	0.045	0.092	0.096	0.171	0.034	0.607	0.199	1350
18	36.17	13.38	47.00	3.45	0.335	0.165	0.484	0.016	0.131	0.065	0.191	0.013	0.600	0.068	1344

Table A.9 Contd/

No.	Weight Percent				Mole Fraction				'Atomic Fraction'					$\frac{Fe^{3+}}{Fe^{2+}}$	Liquidus Temp. ±10°C
	TiO_2	SiO_2	FeO	Fe_2O_3	TiO_2	SiO_2	FeO	Fe_2O_3	Ti^{4+}	Si^{4+}	Fe^{2+}	Fe^{3+}	O^{2-}		
19	38.27	26.28	29.99	5.46	0.350	0.320	0.305	0.025	0.127	0.117	0.111	0.018	0.627	0.162	1552
20	24.81	25.11	40.16	9.92	0.230	0.310	0.414	0.046	0.086	0.116	0.155	0.034	0.609	0.219	1433
21	10.04	24.21	49.90	15.85	0.095	0.305	0.525	0.075	0.036	0.116	0.200	0.057	0.591	0.285	1229
22	14.94	24.04	47.79	13.23	0.140	0.300	0.498	0.062	0.053	0.114	0.190	0.047	0.596	0.247	1301
23	40.80	13.74	37.96	7.50	0.435	0.195	0.450	0.040	0.145	0.065	0.151	0.027	0.612	0.179	1360
24	33.32	14.94	40.92	10.82	0.320	0.191	0.437	0.052	0.135	0.080	0.184	0.043	0.558	0.234	1330
25	25.43	14.96	46.75	12.86	0.245	0.192	0.501	0.062	0.093	0.073	0.190	0.470	0.595	0.245	1290
26	17.37	14.88	50.80	16.95	0.170	0.194	0.553	0.083	0.065	0.074	0.212	0.063	0.586	0.297	1299
27	49.91	4.54	36.08	9.47	0.495	0.060	0.398	0.047	0.183	0.022	0.148	0.035	0.512	0.236	1395
28	39.92	4.65	42.46	12.97	0.400	0.062	0.473	0.065	0.151	0.023	0.178	0.049	0.599	0.275	1400
29	25.48	4.78	51.13	18.61	0.260	0.065	0.580	0.095	0.100	0.025	0.222	0.073	0.580	0.329	1397
30	21.33	4.44	53.29	20.94	0.220	0.061	0.611	0.108	0.084	0.023	0.235	0.083	0.575	0.353	1402
31	-	10.05	61.87	28.08	-	0.139	0.715	0.146	-	0.055	0.277	0.133	0.555	0.408	1304
32	-	17.32	60.07	21.91	-	0.227	0.665	0.108	-	0.091	0.268	0.087	0.594	0.327	1375
33	-	32.09	53.27	14.64	-	0.391	0.542	0.067	-	0.151	0.209	0.052	0.588	0.249	1298
34	11.34	17.11	54.24	17.31	0.110	0.221	0.585	0.084	0.043	0.085	0.227	0.065	0.580	0.286	1284
35	7.53	9.96	60.35	22.16	0.076	0.134	0.678	0.112	0.030	0.053	0.266	0.088	0.563	0.331	1340
36	5.00	17.48	57.30	20.22	0.049	0.228	0.624	0.099	0.019	0.087	0.252	0.076	0.566	0.302	1270
37	5.74	17.15	57.66	19.45	0.056	0.223	0.626	0.095	0.022	0.087	0.244	0.074	0.573	0.303	1276
38	15.44	21.98	49.39	13.19	0.145	0.275	0.517	0.063	0.056	0.106	0.198	0.048	0.592	0.242	1254
39	29.34	16.53	42.40	11.73	0.280	0.210	0.454	0.056	0.106	0.079	0.170	0.042	0.603	0.247	1300
40	24.23	33.07	33.46	9.24	0.220	0.400	0.338	0.042	0.080	0.146	0.123	0.031	0.620	0.252	1565

Table A.9 Contd /

No	Weight Percent				Mole Fraction				'Atomic Fraction					$\frac{Fe^{3+}}{Fe^{2+}}$	Liquidus Temp. $\pm 10^{o}C.$
	TiO_2	SiO_2	FeO	Fe_2O_3	TiO_2	SiO_2	FeO	Fe_2O_3	Ti^{4+}	Si^{4+}	Fe^{2+}	Fe^{3+}	O^{2-}		
41	28.31	22.52	39.34	9.83	0.265	0.280	0.409	0.046	0.099	0.104	0.152	0.035	0.610	0.230	1400
42	25.43	29.05	38.67	6.85	0.230	0.350	0.389	0.031	0.086	0.131	0.145	0.021	0.617	0.145	1500

TABLE B.1

Sulphide Capacity of $FeO-SiO_2-TiO_2$ slags at 1500°C

No.	N_{FeO}	N_{SiO_2}	N_{TiO_2}	A	%S	$C_S \times 10^3$	$-\log C_S$	E.B.*
M1	0.502	0.181	0.317	131.56	0.158	1.20	2.92	0.529
M2	0.634	0.178	0.178	131.56	0.392	2.98	2.53	0.777
M3	0.690	0.177	0.133	131.56	0.584	4.44	2.35	0.877
M4	0.455	0.182	0.363	131.56	0.140	1.06	2.97	0.442
M5	0.700	0.120	0.180	131.56	0.642	4.88	2.31	0.895
M6	0.561	0.263	0.176	131.56	0.318	2.42	2.60	0.639
M7	0.635	0.204	0.161	131.56	0.690	5.24	2.28	0.775
M8	0.481	0.346	0.173	131.56	0.169	1.29	2.89	0.488
M9	0.511	0.122	0.367	131.56	0.182	1.38	2.86	0.544
10	0.625	-	0.375	131.56	0.354	2.69	2.57	0.756
11	0.352	0.241	0.407	131.56	0.084	0.64	3.19	0.251
12	0.448	0.239	0.313	131.56	0.139	1.05	2.98	0.430
13	0.496	0.237	0.267	131.56	0.158	1.20	2.92	0.516
14	0.518	0.062	0.420	131.56	0.182	1.38	2.86	0.558
15	0.736	0.176	0.088	131.56	1.210	9.20	2.00	0.961
16	0.419	0.063	0.518	131.56	0.082	0.62	3.20	0.376
17	0.363	0.124	0.513	131.56	0.087	0.66	3.18	0.271
18	0.769	-	0.231	131.56	1.840	1.40	1.85	1.022
19	0.350	0.050	0.600	131.56	0.083	0.63	3.20	0.247
20	0.735	0.045	0.220	131.56	1.124	8.54	2.07	0.960
21	0.620	0.125	0.255	131.56	0.436	3.31	2.48	0.747
22	0.530	0.370	0.100	131.56	0.138	1.20	2.92	0.581
23	0.430	0.150	0.420	131.56	0.132	1.00	3.00	0.396
24	0.560	0.125	0.315	131.56	0.257	1.95	2.71	0.636
25	0.560	0.390	0.050	131.56	1.010	7.68	2.11	0.636
26	0.598	0.340	0.062	131.56	0.379	2.88	2.54	0.706
27	0.430	0.060	0.510	131.56	0.085	0.65	3.19	0.396
28	0.575	0.225	0.200	131.56	0.225	1.71	2.77	0.664
29	0.625	0.050	0.325	131.56	0.39)	2.96	2.53	0.756

* E.B. $= 1.45\ (N_{FeO}+N_{CaO})-0.40(N_{TiO_2}+N_{SiO_2})$

TABLE B.2

Sulphide Capacity of $FeO-CaO-TiO_2$ slags at $1500^{o}C$

No.	N_{FeO}	N_{CaO}	N_{TiO_2}	A	%S	$C_S \times 10^3$	$-\log C_S$	E.B.
Z1	0.549	0.160	0.291	131.56	1.300	9.88	2.01	0.912
Z2	0.373	0.359	0.268	131.56	1.250	9.50	2.02	0.954
Z3	0.282	0.422	0.296	131.56	1.160	8.81	2.05	0.902
Z4	0.387	0.309	0.304	131.56	1.220	9.27	2.03	0.888
Z5	0.423	0.280	0.297	131.56	0.950	7.22	2.14	0.901
Z6	0.492	0.221	0.287	131.56	1.270	9.65	2.02	0.926
Z7	0.328	0.312	0.360	131.56	0.364	2.77	2.56	0.783
Z8	0.546	0.305	0.149	131.56	2.700	20.50	1.69	1.170
Z9	0.223	0.286	0.491	131.56	0.076	0.57	3.24	0.543
10	0.288	0.368	0.344	131.56	0.501	3.80	2.42	0.813
11	0.385	0.493	0.122	131.56	2.720	20.70	1.68	1.220
12	0.617	0.189	0.194	131.56	2.080	15.80	1.80	1.091
13	0.382	0.193	0.425	131.56	0.198	0.20	2.82	0.664
14	0.295	0.081	0.624	131.56	0.069	0.53	3.28	0.295
15	0.421	0.118	0.461	131.56	0.172	1.31	2.88	0.600
16	0.693	0.175	0.132	131.56	2.697	20.50	1.69	1.206
17	0.173	0.222	0.605	131.56	0.071	0.54	3.27	0.331
18	0.283	0.313	0.414	131.56	0.186	1.41	2.85	0.703
19	0.347	0.445	0.208	131.56	1.776	1.35	1.87	1.061
20	0.572	0.160	0.268	131.56	1.320	10.00	2.00	0.953
21	0.190	0.426	0.384	131.56	0.378	2.87	2.54	0.739
22	0.487	0.250	0.263	131.56	0.838	6.37	2.19	0.969
23	0.545	0.066	0.389	131.56	0.378	2.87	2.54	0.732
24	0.458	0.130	0.412	131.56	0.218	1.65	2.78	0.688
25	0.300	0.150	0.550	131.56	0.073	0.55	3.26	0.433
26	0.110	0.290	0.600	131.56	0.064	0.45	3.35	0.340
27	0.400	0.430	0.170	131.56	2.190	16.70	1.78	1.132
28	0.605	0.150	0.245	131.56	2.480	11.00	1.94	0.982
29	0.495	0.100	0.405	131.56	0.207	1.57	2.80	0.701
30	0.350	0.150	0.500	131.56	0.074	0.56	3.25	0.525

TABLE B.2(Contd.)

No.	N_{FeO}	N_{CaO}	N_{TiO_2}	A	%S	$C_S \times 10^3$	$-\log C_S$	E.B.
31	0.250	0.250	0.500	131.56	0.073	0.55	3.25	0.652
32	0.500	0.250	0.450	131.56	0.195	1.48	2.83	0.752
33	0.280	0.270	0.450	131.56	0.158	1.20	2.92	0.660
34	0.425	0.200	0.375	131.56	0.370	2.81	2.55	0.623
35	0.559	0.090	0.351	131.56	0.533	4.05	2.39	0.568
36	0.475	0.185	0.340	131.56	0.547	4.15	2.38	0.614
37	0.317	0.420	0.263	131.56	1.160	8.81	2.05	0.726
38	0.615	0.145	0.240	131.56	2.480	11.00	1.94	0.591
39.	0.728	0.060	0.212	131.56	2.080	15.80	1.80	0.548
40	0.780	0.051	0.169	131.56	2.697	20.50	1.69	0.541

TABLE B.3

Sulphide Capacity of the SiO_2-CaO-TiO_2 slags at 1500°C

No.	N_{SiO_2}	N_{CaO}	N_{TiO_2}	P_{O_2} atm.	P_{S_2} atm.	A	%S	$C_S \times 10^4$	-log C_S	
R1	0.410	0.400	0.190	3.89×10^{-14}	6.21×10^{-6}	12634.9	1.050	0.83	4.08	
R2	0.206	0.306	0.489	3.89×10^{-14}	6.21×10^{-6}		2.246	1.78	3.75	
R3	0.333	0.334	0.333	3.89×10^{-14}	6.21×10^{-6}		1.462	1.16	3.94	
R4	0.117	0.313	0.570	3.89×10^{-14}	6.21×10^{-6}		3.782	3.00	3.52	
R5	0.267	0.333	0.400	3.89×10^{-14}	6.21×10^{-6}		1.864	1.48	3.83	
R6	0.515	0.330	0.155	3.89×10^{-14}	6.21×10^{-6}		0.797	0.63	4.20	
23	0.500	0.300	0.200	1.06×10^{-8}	4.67×10^{-3}	664	0.026	0.39	4.41	*
24	0.400	0.300	0.300	1.06×10^{-8}	4.67×10^{-3}		0.037	0.67	4.17	*
25	0.350	0.300	0.350	1.06×10^{-8}	4.67×10^{-3}		0.045	0.68	4.17	*
26	0.300	0.300	0.400	1.06×10^{-8}	4.67×10^{-3}		0.055	0.83	4.08	*
27	0.250	0.300	0.450	1.06×10^{-8}	4.67×10^{-3}		0.067	1.02	3.99	*

* Reference (118)

TABLE B.3A

Sulphide Capacity of SiO_2-CaO-TiO_2-Al_2O_3 slags at 1500°C.

No.	N_{SiO_2}	N_{CaO}	N_{TiO_2}	$N_{Al_2O_3}$	P_{O_2} atm.	P_{S_2} atm.	A	%S	$C_S \times 10^4$	-log C_S
R7	0.500	0.434	-	0.066	3.89×10^{-14}	6.21×10^{-6}	12634.9	0.846	0.67	4.17
R8	0.384	0.351	0.230	0.035	3.89×10^{-14}	6.21×10^{-6}		0.570	0.45	4.35
R9	0.418	0.36o	0.164	0.058	3.89×10^{-14}	6.21×10^{-6}		0.506	0.40	4.40
R10	0.373	0.344	0.260	0.023	3.89×10^{-14}	6.21×10^{-6}		1.04	0.82	4.08
2	0.356	0.325	0.295	0.024	7.28×10^{-10}	2.29×10^{-3}	1774	0.108	0.61	4.21 *
12	0.500	0.434	-	0.066	1.38×10^{-9}	8.93×10^{-4}	804	0.030	0.37	4.43 *
28	0.404	0.328	0.197	0.071	1.38×10^{-9}	8.93×10^{-4}		0.035	0.43	4.36 *
35	0.421	0.347	0.162	0.070	1.38×10^{-9}	8.93×10^{-4}		0.032	0.40	4.40 *

* Reference (118)

TABLE B.5

Sulphide Capacity of $FeO-SiO_2-TiO_2-CaO$ slags at 1500^oC

No.	N_{FeO}	N_{SiO_2}	N_{TiO_2}	N_{CaO}	A	%S	$C_S \times 10^3$	$-\log C_S$	E.B.
ZM 1	0.364	0.055	0.451	0.130	131.56	0.144	1.09	2.96	0.516
ZM 2	0.440	0.158	0.277	0.125	131.56	0.152	1.16	2.94	0.646
ZM 3	0.493	0.231	0.154	0.122	131.56	0.260	1.98	2.70	0.736
ZM 4	0.645	0.155	0.077	0.123	131.56	1.310	9.96	2.00	1.017
ZM 5	0.563	0.155	0.157	0.125	131.56	0.450	3.56	2.45	0.947
ZM 6	0.423	0.304	0.152	0.121	131.56	0.142	1.08	2.97	0.607
ZM 7	0.627	0.145	0.107	0.121	131.56	0.830	6.40	2.19	0.979
ZM 8	0.253	0.082	0.341	0.324	131.56	0.100	0.70	3.12	0.665
ZM 9	0.188	0.042	0.348	0.422	131.56	0.088	0.67	3.17	0.727
ZM10	0.348	0.171	0.356	0.125	131.56	0.064	0.48	3.31	0.402
ZM11	0.352	0.126	0.221	0.301	131.56	0.066	5.01	2.29	0.807
ZM12	0.396	0.186	0.124	0.294	131.56	0.57	4.32	2.36	0.876
ZM13	0.518	0.124	0.062	0.296	131.56	1.46	11.10	1.96	0.882
ZM14	0.355	0.085	0.256	0.304	131.56	0.28	2.10	2.67	0.820
ZM15	0.490	0.084	0.126	0.300	131.56	1.59	12.00	1.92	1.062
ZM16	0.305	0.184	0.121	0.391	131.56	0.490	3.72	2.43	0.899
ZM17	0.211	0.224	0.295	0.270	131.56	0.080	0.61	3.22	0.492
ZM18	0.192	0.173	0.389	0.246	131.56	0.066	0.50	3.30	0.412
ZM19	0.357	0.441	0.030	0.172	131.56	0.128	0.97	3.01	0.579
ZM20	0.485	0.090	0.300	0.125	131.56	0.146	1.98	2.70	0.728
ZM21	0.665	0.014	0.200	0.121	131.56	1.310	9.96	2.00	1.054
ZM22	0.298	0.140	0.440	0.122	131.56	0.066	0.50	3.30	0.377
ZM23	0.340	0.085	0.350	0.225	131.56	0.118	0.90	3.05	0.645
ZM24	0.631	0.149	0.095	0.125	131.56	0.920	6.99	2.16	0.999
ZM25	0.587	0.151	0.135	0.127	131.56	0.540	4.10	2.39	0.921
ZM26	0.526	0.151	0.200	0.123	131.56	0.310	2.36	2.63	0.590
ZM27	0.536	0.050	0.290	0.124	131.56	0.426	3.24	2.49	0.821

TABLE B.6

Slag/metal sulphur partition of $FeO-SiO_2-TiO_2$ slags at 1500°C

No.	N_{FeO}	N_{SiO_2}	N_{TiO_2}	a_{FeO}	A	$C_S \times 10^3$	$\frac{(\%S)}{[\%S]}$
1	0.640	0.310	0.050	0.40	131.56	3.24	0.40
2	0.640	0.060	0.300	0.40	131.56	3.16	0.39
3	0.680	0.180	0.200	0.40	131.56	3.98	0.50
4	0.680	0.195	0.125	0.40	131.56	3.30	0.41
5	0.650	0.280	0.070	0.40	131.56	3.31	0.41
6	0.660	0.340	-	0.40	131.56	2.18	0.27
7	0.665	0.285	0.050	0.50	131.56	4.46	0.45
8	0.680	0.070	0.250	0.50	131.56	5.01	0.50
9	0.680	0.245	0.075	0.50	131.56	5.01	0.50
10	0.690	0.160	0.150	0.50	131.56	5.01	0.50
11	0.690	0.210	0.100	0.50	131.56	5.01	0.50
12	0.620	-	0.380	0.50	131.56	2.69	0.27
13	0.700	0.250	0.050	0.60	131.56	7.94	0.66
14	0.720	0.130	0.150	0.60	131.56	7.94	0.66
15	0.720	0.180	0.100	0.60	131.56	7.94	0.66
16	0.710	0.215	0.075	0.60	131.56	7.94	0.66
17	0.750	0.175	0.075	0.70	131.56	10.10	0.72
18	0.750	0.150	0.100	0.70	131.56	10.10	0.72
19	0.750	0.100	0.150	0.70	131.56	12.50	0.89
20	0.570	0.050	0.380	0.31	131.56	2.09	0.34
21	0.560	0.140	0.300	0.26	131.56	1.78	0.34
22	0.550	0.250	0.200	0.25	131.56	1.78	0.36
23	0.530	0.370	0.100	0.25	131.56	1.70	0.34
24	0.500	0.150	0.350	0.18	131.56	1.20	0.33
25	0.490	0.250	0.260	0.18	131.56	1.20	0.33
26	0.480	0.370	0.150	0.16	131.56	1.05	0.33
27	0.450	0.100	0.450	0.16	131.56	1.02	0.32
28	0.440	0.200	0.360	0.12	131.56	0.79	0.33
29	0.425	0.325	0.250	0.10	131.56	0.63	0.31
30	0.425	0.400	0.175	0.11	131.56	0.71	0.32
31	0.350	0.050	0.600	0.10	131.56	0.50	0.25
32	0.350	0.140	0.510	0.08	131.56	0.50	0.31
33	0.380	0.150	0.470	0.08	131.56	0.52	0.32
34	0.360	0.050	0.390	0.10	131.56	0.56	0.28

TABLE B.7

Slag/metal sulphur partition of $FeO-CaO-TiO_2$ slags at 1500°C

No.	N_{FeO}	N_{CaO}	N_{TiO_2}	a_{FeO}	A	$C_S \times 10^3$	$\frac{(\%S)}{[\%S]}$
1	0.51	0.165	0.325	0.40	131.56	6.30	0.79
2	0.525	0.055	0.420	0.40	131.56	1.78	0.22
3	0.515	0.105	0.380	0.40	131.56	2.75	0.34
4	0.515	0.235	0.250	0.40	131.56	10.40	1.30
5	0.525	0.275	0.200	0.40	131.56	10.40	1.30
6	0.560	0.100	0.340	0.50	131.56	3.98	0.40
7	0.550	0.150	0.300	0.50	131.56	7.90	0.79
8	0.550	0.200	0.250	0.50	131.56	11.20	1.12
9	0.550	0.250	0.200	0.50	131.56	14.10	1.41
10	0.570	0.280	0.150	0.50	131.56	20.00	2.00
11	0.650	0.040	0.310	0.60	131.56	5.01	0.42
12	0.620	0.100	0.280	0.60	131.56	8.90	0.74
13	0.600	0.150	0.250	0.60	131.56	12.60	1.05
14	0.600	0.200	0.200	0.60	131.56	15.80	1.32
15	0.700	0.040	0.260	0.70	131.56	11.00	0.79
16	0.675	0.075	0.250	0.70	131.56	7.90	0.56
17	0.660	0.140	0.200	0.70	131.56	15.80	1.13
18	0.675	0.175	0.150	0.70	131.56	20.00	1.43
19	0.800	0.040	0.160	0.80	131.56	20.00	1.25
20	0.775	0.075	0.150	0.80	131.56	20.00	1.25
21	0.775	-	0.225	0.75	131.56	14.00	0.93
22	0.620	-	0.380	0.52	131.56	2.69	0.26
23	0.350	0.100	0.550	0.20	131.56	0.56	0.14
24	0.750	0.050	0.200	0.75	131.56	16.60	1.11
25	0.400	0.150	0.450	0.29	131.56	1.45	0.25
26	0.450	0.150	0.400	0.35	131.56	2.50	0.35
27	0.450	0.350	0.200	0.35	131.56	14.00	2.00
28	0.400	0.100	0.500	0.24	131.56	1.00	0.21
29	0.400	0.200	0.400	0.30	131.56	2.50	0.42
30	0.300	0.100	0.600	0.15	131.56	5.49	0.18

TABLE B.7 (Contd.)

No.	N_{FeO}	N_{CaO}	N_{TiO_2}	a_{FeO}	A	$C_S \times 10^3$	$\frac{(\%S)}{[\%S]}$
31	0.250	0.250	0.500	0.15	131.56	0.72	0.24
32	0.240	0.210	0.550	0.14	131.56	0.56	0.20
33	0.150	0.20	0.650	0.07	131.56	0.28	0.20
34	0.351	0.199	0.450	0.25	131.56	1.29	0.26
35	0.212	0.318	0.470	0.12	131.56	1.00	0.42
36	0.221	0.379	0.400	0.12	131.56	1.62	0.68
37	0.352	0.288	0.360	0.25	131.56	3.71	0.74
38	0.449	0.231	0.320	0.25	131.56	5.60	1.12
39	0.351	0.349	0.300	0.26	131.56	6.92	1.33
40	0.298	0.392	0.310	0.20	131.56	5.60	1.40
41	0.301	0.437	0.262	0.20	131.56	7.90	1.98

TABLE B.8

Optical basicity of $CaO-Al_2O_3$ slags at 1500°C *

No.	N_{CaO}	$N_{Al_2O_3}$	$C_S \times 10^4$	$-\log C_S$	Λ
CA1	0.551	0.449	3.30	3.48	0.720
CA2	0.564	0.436	4.16	3.38	0.725
CA3	0.598	0.402	7.16	3.14	0.737
CA4	0.642	0.358	15.50	2.80	0.753
CA5	0.679	0.321	31.82	2.50	0.769

* Reference (107)

TABLE B.9

Optical basicity of $CaO-MgO-SiO_2$ slags at $1500^{o}C$ *

No.	N_{CaO}	N_{MgO}	N_{SiO_2}	$C_S \times 10^5$	$-\log C_S$	Λ
1	0.345	0.057	0.598	2.82	4.55	0.601
2	0.326	0.112	0.562	2.51	4.60	0.609
3	0.307	0.165	0.527	2.63	4.58	0.616
4	0.287	0.217	0.496	3.54	4.45	0.622
5	0.268	0.267	0.465	4.47	4.35	0.629
6	0.252	0.315	0.434	6.02	4.22	0.636
7	0.395	0.057	0.548	4.57	4.34	0.623
8	0.372	0.112	0.516	5.13	4.29	0.629
9	0.351	0.165	0.484	5.37	4.27	0.636
10	0.330	0.216	0.453	6.61	4.18	0.642
11	0.311	0.266	0.424	8.13	4.09	0.649
12	0.289	0.314	0.397	11.20	3.95	0.654
13	0.449	0.057	0.495	5.49	4.26	0.647
14	0.427	0.111	0.462	6.61	4.18	0.654
15	0.397	0.164	0.439	7.94	4.10	0.657
16	0.373	0.216	0.411	9.55	4.02	0.663
17	0.349	0.265	0.386	13.50	3.87	0.668
18	0.328	0.313	0.359	20.40	3.69	0.674
19	0.481	0.057	0.462	9.12	4.04	0.662
20	0.455	0.111	0.434	11.00	3.96	0.667
21	0.421	0.166	0.413	16.20	3.79	0.669
22	0.401	0.215	0.384	22.40	3.65	0.677
23	0.376	0.265	0.360	38.00	3.42	0.681
24	0.349	0.313	0.338	44.70	3.35	0.685
25	0.321	0.057	0.622	1.41	4.58	0.592
26	0.275	0.113	0.613	2.57	4.59	0.589
27	0.231	0.166	0.603	1.95	4.71	0.585
28	0.146	0.269	0.585	1.74	4.76	0.578
29	0.106	0.318	0.576	1.48	4.83	0.575
30	0.371	0.057	0.572	3.09	4.51	0.613

* Reference (106)

TABLE B.9(Contd.)

No.	N_{CaO}	N_{MgO}	N_{SiO_2}	$C_S \times 10^5$	$-\log C_S$	Λ
31	0.325	0.112	0.562	2.95	4.53	0.609
32	0.281	0.166	0.554	2.82	4.55	0.605
33	0.237	0.218	0.545	2.09	4.68	0.601
34	0.195	0.268	0.537	2.04	4.69	0.597
35	0.154	0.317	0.529	2.04	4.69	0.594
36	0.523	0.070	0.407	22.40	3.65	0.687
37	0.475	0.124	0.401	13.50	3.87	0.682
38	0.429	0.177	0.395	19.10	3.72	0.677
39	0.384	0.228	0.389	19.10	3.72	0.672
40	0.351	0.265	0.384	14.20	3.84	0.667

* Reference (106)

TABLE B.10

Optical basicity of $CaO-Al_2O_3-MgO$ slags at 1500^oC*

No.	N_{CaO}	$N_{Al_2O_3}$	N_{MgO}	$C_S \times 10^4$	$-\log C_S$	Λ
1	0.501	0.400	0.091	3.56	3.45	0.724
2	0.492	0.400	0.108	4.28	3.37	0.724
3	0.482	0.393	0.125	4.94	3.31	0.725
4	0.473	0.385	0.142	5.47	3.26	0.725
5	0.464	0.378	0.158	5.19	3.28	0.726
6	0.453	0.372	0.175	5.89	3.23	0.726
7	0.513	0.397	0.090	5.18	3.29	0.728
8	0.503	0.390	0.107	5.21	3.28	0.728
9	0.494	0.382	0.124	6.13	3.21	0.729
10	0.475	0.368	0.157	6.61	3.18	0.730
11	0.580	0.393	0.027	8.80	3.06	0.737
12	0.566	0.380	0.054	9.61	3.01	0.738
13	0.555	0.373	0.072	10.03	3.00	0.736

* Reference (106)

TABLE B.10(Contd.)

No.	N_{CaO}	$N_{Al_2O_3}$	N_{MgO}	$C_S \times 10^4$	$-\log C_S$	Λ
14	0.546	0.366	0.088	10.84	2.96	0.739
15	0.536	0.359	0.105	11.60	2.94	0.740
16	0.525	0.353	0.122	10.84	2.96	0.740
17	0.516	0.346	0.138	12.61	2.90	0.741
18	0.506	0.340	0.154	13.27	2.88	0.741
19	0.586	0.328	0.086	18.75	2.73	0.755
20	0.575	0.322	0.103	19.19	2.72	0.755
21	0.565	0.316	0.119	20.49	2.69	0.755
22	0.555	0.310	0.135	19.51	2.71	0.756
23	0.545	0.304	0.151	21.05	2.68	0.756
24	0.534	0.300	0.166	21.46	2.67	0.756
25	0.621	0.295	0.084	36.63	2.44	0.769
26	0.610	0.289	0.101	37.09	2.43	0.770
27	0.599	0.284	0.117	37.93	2.43	2.70
28	0.550	0.396	0.054	6.20	3.21	0.732
29	0.534	0.394	0.072	5.68	3.25	0.731
30	0.518	0.392	0.090	5.54	3.26	0.729
31	0.578	0.352	0.070	14.80	2.83	0.747
32	0.563	0.349	0.088	12.90	2.89	0.746
33	0.547	0.348	0.105	11.79	2.93	0.744
34	0.532	0.346	0.122	11.51	2.94	0.743
35	0.517	0.345	0.138	10.55	2.98	0.741
36	0.502	0.343	0.155	7.76	3.11	0.739
37	0.488	0.341	0.171	7.76	3.11	0.738
38	0.656	0.318	0.026	26.90	2.57	0.767
39	0.632	0.316	0.052	26.28	2.58	0.764
40	0.617	0.314	0.069	24.17	2.62	0.763
41	0.601	0.313	0.086	24.35	2.61	0.761

* Reference (106)

TABLE B.11

Optical basicity of $CaO-SiO_2-Al_2O_3$ slags at 1500°C +

No.	N_{CaO}	N_{SiO_2}	$N_{Al_2O_3}$	$C_S \times 10^5$	$-\log C_S$	Λ
1	0.546	0.425	0.029	19.90	3.70	0.678
2	0.546	0.395	0.059	24.00	3.62	0.682
3	0.546	0.364	0.091	30.50	3.52	0.685
4	0.403	0.574	0.023	2.27	4.64	0.164
5	0.410	0.543	0.047	2.15	4.67	0.620
6	0.416	0.511	0.072	4.10	4.39	0.626
7	0.424	0.478	0.098	4.29	4.37	0.633
8	0.431	0.444	0.125	5.03	4.30	0.639
9	0.437	0.418	0.145	6.84	4.17	0.644
10	0.442	0.391	0.166	6.09	4.22	0.649
11	0.450	0.354	0.196	7.63	4.12	0.656
12	0.434	0.506	0.060	3.17	4.50	0.632
13	0.441	0.474	0.085	3.10	4.51	0.638
14	0.449	0.440	0.111	4.71	4.33	0.645
15	0.457	0.405	0.138	6.20	4.21	0.652
16	0.459	0.396	0.145	6.31	4.20	0.653
17	0.465	0.369	0.166	10.40	3.98	0.658
18	0.479	0.499	0.022	5.82	4.23	0.646
19	0.483	0.473	0.044	6.72	4.17	0.651
20	0.487	0.445	0.068	8.61	4.06	0.656
21	0.490	0.419	0.092	11.20	3.95	0.660
22	0.494	0.378	0.128	10.40	3.98	0.666
23	0.487	0.484	0.029	6.77	4.17	0.650
24	0.494	0.454	0.051	9.07	4.04	0.657
25	0.502	0.424	0.074	11.00	3.95	0.663
26	0.512	0.387	0.101	14.60	3.84	0.671
27	0.544	0.437	0.019	14.80	3.84	0.676
28	0.552	0.410	0.038	19.30	3.71	0.682
29	0.539	0.402	0.059	20.00	3.70	0.680
30	0.405	0.274	0.321	6.11	4.21	0.653
31	0.227	0.702	0.072	0.70	5.16	0.558

+ Reference (106)

TABLE B.11(Contd.)

No.	N_{CaO}	N_{SiO_2}	$N_{Al_2O_3}$	$C_S \times 10^5$	$-\log C_S$	Λ	
32	0.326	0.607	0.067	1.56	4.81	0.591	
33	0.442	0.501	0.057	4.63	4.33	0.635	
34	0.268	0.641	0.092	1.04	4.98	0.574	
35	0.395	0.518	0.087	2.54	4.60	0.620	
36	0.457	0.456	0.037	8.73	4.06	0.650	
37	0.280	0.600	0.123	0.65	5.19	0.583	
38	0.405	0.495	0.100	2.63	4.58	0.626	
39	0.514	0.373	0.113	1.46	3.84	0.673	
10	0.478	0.501	0.021	5.80	4.24	0.647	*
11	0.456	0.501	0.043	4.65	4.33	0.641	*
12	0.434	0.500	0.066	3.70	4.43	0.632	*
13	0.410	0.500	0.090	3.00	4.52	0.627	*
14	0.387	0.500	0.113	2.20	4.66	0.617	*
16	0.333	0.502	0.165	1.14	4.94	0.610	*
17	0.306	0.501	0.193	0.90	5.05	0.604	*

* Reference (118)

TABLE B.12

Optical basicity of $CaO-SiO_2-TiO_2$ slags at 1500°C +

No.	N_{CaO}	N_{SiO_2}	N_{TiO_2}	$C_S \times 10^4$	$-\log C_S$	Λ	
1	0.543	0.395	0.062	1.68	3.77	0.683	
2	0.546	0.102	0.352	2.53	3.60	0.683	
3	0.500	0.100	0.400	1.86	3.73	0.643	
4	0.500	0.151	0.349	1.97	3.71	0.667	
5	0.501	0.202	0.297	1.72	3.59	0.672	
6	0.498	0.252	0.250	1.69	3.77	0.677	
7	0.450	0.150	0.400	1.54	3.81	0.645	
8	0.401	0.250	0.349	1.45	3.84	0.649	
9	0.450	0.250	0.300	1.34	3.87	0.654	
10	0.450	0.300	0.250	1.32	3.88	0.658	
11	0.449	0.350	0.201	0.89	4.05	0.663	
12	0.400	0.200	0.400	1.41	3.85	0.628	
13	0.400	0.250	0.350	1.48	3.83	0.632	
14	0.400	0.300	0.300	1.43	3.84	0.636	
15	0.400	0.350	0.250	1.27	3.90	0.641	
16	0.300	0.400	0.300	0.83	4.08	0.605	
17	0.350	0.150	0.500	0.58	4.24	0.603	
18	0.350	0.250	0.400	0.87	4.06	0.620	
19	0.350	0.300	0.350	1.08	3.96	0.615	
20	0.350	0.350	0.300	0.95	4.02	0.620	
21	0.350	0.400	0.250	1.05	3.98	0.624	
22	0.360	0.441	0.199	1.62	3.79	0.627	
23	0.300	0.200	0.500	0.39	4.41	0.588	
24	0.300	0.450	0.250	1.02	3.99	0.609	
25	0.300	0.350	0.350	0.67	4.17	0.601	
18	0.469	0.471	0.060	0.90	4.05	0.652	*
19	0.454	0.456	0.090	0.90	4.05	0.639	*
20	0.438	0.440	0.122	0.88	4.06	0.637	*
21	0.422	0.429	0.154	0.92	4.04	0.633	*
22	0.405	0.408	0.187	0.90	4.05	0.627	*
23	0.387	0.392	0.221	0.91	4.04	0.625	*
24	0.369	0.375	0.256	0.90	4.05	0.619	*
25	0.351	0.358	0.291	0.88	4.06	0.615	*

* Reference (118)

\+ Reference (117)

TABLE B.13

Optical basicity of $CaO-MgO-TiO_2$ slags at 1500°C*

No.	N_{CaO}	N_{MgO}	N_{TiO_2}	$C_S \times 10^4$	$-\log C_S$	Λ
1	0.240	0.169	0.591	1.51	3.82	0.643
2	0.160	0.230	0.610	1.20	3.92	0.628
3	0.280	0.130	0.590	1.45	3.84	0.648
4	0.230	0.280	0.490	1.07	3.97	0.663
5	0.280	0.090	0.630	1.29	3.89	0.640
6	0.310	0.090	0.610	1.41	3.85	0.649
7	0.180	0.180	0.640	1.12	3.95	0.625
8	0.200	0.280	0.520	1.23	3.91	0.651
9	0.250	0.120	0.630	1.20	3.92	0.635
10	0.200	0.330	0.470	1.35	3.87	0.663
11	0.220	0.310	0.470	1.20	3.92	0.666
12	0.250	0.090	0.660	1.07	3.97	0.630
13	0.210	0.370	0.420	1.23	3.91	0.676
14	0.180	0.240	0.580	1.12	3.95	0.636
15	0.240	0.200	0.560	1.38	3.86	0.649
16	0.270	0.170	0.560	1.41	3.85	0.653
17	0.180	0.200	0.620	2.09	3.86	0.628
18	0.220	0.340	0.440	1.48	3.83	0.673
19	0.230	0.240	0.530	1.70	3.77	0.653
20	0.280	0.040	0.680	1.35	3.87	0.630
21	0.320	-	0.680	1.12	3.95	0.636

* Reference (65)

TABLE B.14

Optical basicity of $CaO-TiO_2-Al_2O_3-SiO_2$ slags at 1500°C *

No.	N_{CaO}	N_{TiO_2}	$N_{Al_2O_3}$	N_{SiO_2}	$C_S \times 10^4$	$-\log C_S$	Λ
2	0.325	0.296	0.023	0.355	0.61	4.21	0.609
3	0.320	0.267	0.048	0.365	0.50	4.30	0.608
4	0.310	0.233	0.072	0.387	0.40	4.40	0.605
5	0.300	0.201	0.096	0.403	0.32	4.49	0.603
6	0.292	0.169	0.121	0.419	0.25	4.60	0.601
7	0.283	0.136	0.146	0.435	0.21	4.68	0.597
8	0.278	0.103	0.171	0.448	0.19	4.72	0.598
9	0.266	0.069	0.197	0.468	0.13	4.89	0.595
29	0.320	0.166	0.095	0.419	0.33	4.48	0.608
30	0.312	0.133	0.119	0.426	0.31	4.51	0.604
31	0.305	0.101	0.145	0.449	0.22	4.66	0.604
32	0.292	0.068	0.169	0.468	0.21	4.68	0.601
33	0.362	0.225	0.023	0.390	0.63	4.20	0.617
35	0.346	0.162	0.070	0.421	0.40	4.40	0.609
36	0.339	0.131	0.094	0.437	0.30	4.52	0.611
37	0.331	0.099	0.118	0.453	0.26	4.59	0.609
38	0.323	0.066	0.142	0.469	0.24	4.62	0.606
39	0.38	0.190	0.023	0.407	0.61	4.21	0.621
40	0.372	0.160	0.046	0.422	0.50	4.30	0.619
41	0.365	0.129	0.069	0.438	0.37	4.43	0.618
42	0.357	0.097	0.093	0.453	0.31	4.51	0.616
43	0.349	0.065	0.116	0.469	0.24	4.62	0.612
44	0.397	0.157	0.022	0.432	0.63	4.20	0.639
45	0.39	0.126	0.045	0.439	0.50	4.30	0.625
46	0.38	0.094	0.068	0.459	0.42	4.38	0.625
47	0.375	0.064	0.091	0.469	0.35	4.46	0.618
48	0.415	0.124	0.022	0.439	0.63	4.20	0.620
51	0.394	0.032	0.09	0.485	0.40	4.40	0.621
52	0.431	0.092	0.022	0.455	0.62	4.21	0.633
53	0.424	0.062	0.044	0.470	0.51	4.29	0.626

* Reference (118)

TABLE B.14(Contd.)

No.	N_{CaO}	N_{TiO_2}	$N_{Al_2O_3}$	N_{SiO_2}	$C_S \times 10^4$	$-\log C_S$	Λ
54	0.417	0.031	0.067	0.485	0.50	4.30	0.630
55	0.447	0.061	0.022	0.471	0.62	4.21	0.639
60	0.255	0.134	0.12	0.491	0.11	4.96	0.586
61	0.264	0.166	0.095	0.474	0.16	4.98	0.587
62	0.273	0.198	0.071	0.458	0.19	4.72	0.588
63	0.280	0.230	0.047	0.443	0.27	4.57	0.591
64	0.289	0.261	0.023	0.426	0.32	4.49	0.492
65	0.228	0.132	0.094	0.546	0.08	5.10	0.570

* Reference (118)

TABLE B.15

Optical basicity of $CaO-MgO-SiO_2-Al_2O_3$ slags at 1500°C *

No.	N_{CaO}	N_{MgO}	N_{SiO_2}	$N_{Al_2O_3}$	$C_S \times 10^5$	$-\log C_S$	Λ
1	0.210	0.015	0.649	0.066	0.79	5.10	0.567
2	0.194	0.146	0.599	0.061	0.97	5.01	0.577
3	0.178	0.214	0.551	0.056	0.91	5.04	0.586
4	0.302	0.074	0.562	0.062	1.70	4.77	0.599
5	0.274	0.146	0.522	0.058	2.20	4.66	0.606
6	0.257	0.212	0.478	0.053	3.01	4.52	0.616
7	0.409	0.073	0.464	0.053	5.76	4.24	0.641
8	0.379	0.143	0.429	0.049	7.73	4.11	0.649
9	0.349	0.210	0.396	0.045	10.80	3.97	0.655
10	0.247	0.076	0.592	0.085	1.03	4.99	0.583
11	0.228	0.148	0.546	0.078	1.57	4.80	0.592
12	0.210	0.216	0.502	0.072	2.20	4.66	0.602
13	0.364	0.075	0.477	0.084	3.14	4.50	0.627
14	0.334	0.147	0.442	0.078	3.86	4.41	0.634
15	0.309	0.214	0.405	0.071	5.86	4.23	0.642
16	0.423	0.075	0.422	0.080	13.7	3.85	0.652
17	0.390	0.146	0.390	0.074	16.90	3.77	0.658
18	0.359	0.213	0.359	0.068	30.40	3.52	0.664
19	0.259	0.077	0.551	0.113	0.74	5.13	0.592

* Reference (106)

TABLE B.15(Contd.)

No.	N_{CaO}	N_{MgO}	N_{SiO_2}	$N_{Al_2O_3}$	$C_S \times 10^5$	$-\log C_S$	Λ
20	0.238	0.150	0.507	0.105	1.07	4.97	0.601
21	0.219	0.219	0.466	0.096	2.41	4.62	0.610
22	0.374	0.076	0.458	0.093	4.37	4.36	0.633
23	0.345	0.147	0.422	0.036	5.38	4.27	0.640
24	0.317	0.215	0.388	0.078	7.29	4.14	0.647
25	0.475	0.076	0.344	0.105	19.60	3.71	0.678
26	0.438	0.147	0.318	0.097	27.00	3.57	0.684
27	0.403	0.216	0.293	0.089	37.70	3.42	0.689

* Reference (106)

TABLE B.16

Optical basicity of $CaO-MgO-TiO_2-SiO_2$ slags at 1500^oC*

Run	N_{CaO}	N_{MgO}	N_{TiO_2}	N_{SiO_2}	$C_S \times 10^5$	$-\log C_S$	Λ
1	0.220	0.290	0.440	0.050	12.90	3.89	0.657
2	0.230	0.160	0.560	0.060	11.10	3.95	0.643
3	0.240	0.080	0.620	0.060	11.20	3.95	0.620
4	0.220	0.080	0.580	0.120	7.59	4.12	0.610
5	0.160	0.220	0.510	0.110	8.71	4.06	0.616
6	0.200	0.280	0.420	0.100	8.32	4.08	0.642
7	0.270	0.080	0.540	0.110	12.00	3.92	0.625
8	0.210	0.150	0.530	0.110	9.77	4.01	0.619
9	0.200	0.220	0.470	0.110	10.70	3.97	0.629
10	0.200	0.210	0.030	0.560	2.19	4.66	0.588
11	0.200	0.210	0.110	0.480	2.40	4.62	0.595
12	0.210	0.220	0.180	0.390	3.98	4.40	0.608
13	0.210	0.220	0.260	0.310	5.89	4.23	0.615
14	0.220	0.230	0.350	0.200	9.77	4.01	0.630
15	0.230	0.240	0.430	0.100	12.30	3.91	0.645

* Reference (65)

ACKNOWLEDGEMENTS

The author wishes to express his sincere thanks to Professor H.B. Bell for his constructive supervision, enthusiastic guidance and infinite patience, throughout the course of this work.

The author also wishes to thank Dr. I.D. Sommerville for many useful discussions.

Thanks are also due to other members of the academic staff and to the technical staff for their assistance.

Finally, a special acknowledgement and appreciation is extended to my wife, Violet Rose, for her patience and understanding during this research.

REFERENCES

1. Grieve, J.
White J.
J. Roy. Tech. Coll.(Glasgow) (1939), Vol. 4, p.444.

2. MacChesney, J.B.
Muan, A.
Am. Mineral, (1961), Vol. 46, p.572.

3. Grau, A.E.
Can. Met. Quart, (1979), Vol. 18, p. 313.

4. Smith, I.C.
Bell, H.B.
Trans. Inst. Min. Metall., (1970) Vol. C79, p.C253.

5. Bigger, G.M.
J. Am. Cerm. Soc.,(1970), Vol. 47 No. 3, p.286.

6. Rase, D.E.
Roy, R.
J. Am. Cerm. Soc.,(1955), Vol. 38 p.102.

7. Bunting, E.N.
Bureau Standards Journal of Research (1933), Vol.11, No. 5, p.719.

8. DeVries, R.C.
Roy, R.
Osborn, E.F.
Trans. of Brit. Ceram. Soc. (1954), Vol. 53, p.525.

9. Coughanour, L.
Pross, V.A.
J. of Research, National Bureau of Standards,(1953), Vol. 51, p.85.

10. Tuset, J.K.
Norwegian Journal of Chem.,Min. and Met., Metallurgy, (1968), Vol. 28,(11), p.232.

11. Bowen, N.L.
Schairer, J.F.
Am. J. Sci., (1932), Vol. 24, p.177.

12. Greig, J.W.
Am. J. Sci., (1927), Vol. 14, p.473.

13. Darken, L.S.
J. Am. Chem. Soc., (1948), Vol. 70, p.2046.

14. Muan, A.
Trans. A.I.M.E.,(1955), Vol. 203, p.965.

15. Muan, A.
Am. J. Sci., (1958), Vol. 25,p.171.

16. Waseda, Y.
Toguri, J.M.
Met. Trans. (1978), Vol. 9B, p.595.

17. Waseda, Y.
Shiarishi, Y.
Trans. I.S.I.J. (1978), Vol. 18, p.783.

18.	Handfield, G. Charette, G.G.	Can. Met. Quart. (1971), Vol. 10, No. 3, p.235
19.	Mori, K.	Tetsu to Hagane, (1956), Vol. 42, p.1024.
20.	Reznichenko, V.A.	Izv. Akad, Nauk, SSSR Metal (1967) Vol. 5, p.43.
21.	Denisov, S.I. Degtyarev, V.S. Reznichenko, V.A.	Izv. Akad, Nauk, SSSR Metal, (1970) Vol. 6, p.80
22.	Schuhmann, R. Ensio, J.P.	Trans. A.I.M.E. (1951), Vol.191, p.401.
23.	Smith, I.C.	Ph.D. Thesis (1969), University of Strathclyde.
24.	White, J.	I.S.I. Carnegie School. Mem., (1938) Vol. 27, p.175.
25.	Darken, L.S. Gurry, R.W.	J. Am. Chem., Soc.,(1945), Vol. 67, p.1398
26.	Darken, L.S. Gurry, R.W.	J. Am. Chem. Soc., (1946), Vol. 68, p.798.
27.	Michal, E.J. Schuhmann, R.	Trans. A.I.M.E., (1952), Vol. 194, p.723.
28.	Schuhmann, R. Powell, G.G. Michal, E.J.	Trans. A.I.M.E. (1953), Vol. 197, p.1097.
29.	Turkdogan, E.T. Bills, P.M.	J.I.S.I. (1957) Vol, 186, p.329.
30.	Markhanavala, M.D. Momina, A.C.	J. Am. Ceram. Soc., (1959), Vol. 42, p.399.
31.	Vicent, E.A. Wright, J.B. Chevallier, R. Mathie, S.	Mineralog, Mag., (1957), Vol. 31 p.624.
32.	Webster, A.H. Bright, F.H.	J. Am. Ceram. Soc., (1961), Vol. 44, p.110.
33.	Akimoto, S. Katsura, T.	Nature, (1957), Vol. 179, p.37.
34.	MacChesney, J.B. Muan, A.	Am. Mineral., (1959), Vol. 44, p.938.

35. Schmahl, N.G.
Frisch, B.
Hargarter, E.
Z.anorg. allgen.chem., (1960) Vol. 305, p.40

36. Muan, A.
Osborn, E.F.
"Phase Equilibrium Among Oxides in Steelmaking", Addison Wesby, (1965).

37. Handfield, G.
Charette, G.G.
Lee, H.Y.
J. Metals, (1972), Vol. 24, p.37

38. Frohberg, M.G.
Weber, R.
Arch. Eisenhüttenw, (1965), Vol. 36, p.447.

39. Schenck, H.
Frohberg, M.G.
Arch. Eisenhüttenw, (1962), Vol. 33, p.421

40. Ohno, A.
Ross, H.N.
Can. Met. Quart., (1963), Vol. 2, p.259.

41. Pliner, Ya. L.
Shtengelmeier, S.V.
Ignatenko, G.F.
Rubinshtein, E.A.
Stal in English, (1966), Vol. 4, p.284.

42. McRae, L.B.
Pothas, E.
Jochens, P.R.
Howat, D.D.
J.S.A. Ins. of Min. and Metal., (1969), Vol. 69, p.577.

43. Gruzdev, Yu. A.
Zhilo, N.L.
Pershina, R.F.
Steel in USSR, (1974), Vol. 4. p. 105.

44. Mikhailov, V.
Belyakova, E.
Ural. Metal., (1939), Vol. 6, p.7.

45. Van der Colf, J.C.G.
Ph.D. Thesis, (1974), University of the Witwatersrand, Johannesburg, South Africa.

46. Reznichenko, V.A.
Izv., Akad. Nauk. SSSR Metal, (1967), Vol. 5, p.43.

47. Inouye, H.
Tomlinson, J.W.
Chipman, J.
Trans. Faraday Soc., (1953), Vol. 49, p.796.

48. Nikitin, Yu.P.
Lopatin, V.M.
Barmin, L.N.
Steel in the USSR, (1973), Vol. 3, p.121.

49. Mori, K.
Tetsu to Hagane, (1960) Vol. 46, p.548.

50.	Kato, M. Minowa	Trans. Iron Steel Inst., Japan, (1969), Vol. 9, p.39
51.	Degtyarev, V.S. Denisov, S.I. Denisov, N.V. Gobov, A.P.	Izv. Akad. Nauk, SSSR Metal, (1970) Vol. 6, p.27.
52.	Musithin, V.I. Lepinshikh, V.M. Formichev, Yu A.	Trans. Inst. Met. Sverdlovsk, (1969), Vol. 18, p.293
53.	Wyatt, J.L.	Trans. A.I.M.E. (1950) Vol. 188, p. 989.
54.	Marboe, E.C. Meyl, W.A.	J. Soc. Glass Tech., (1955), Vol. 37, p.16
55.	Asbrink, S. Magnali, A.	Acta Cryst. (1959), Vol. 12, p.575.
56.	Esin, O.A. Lepinskikh, B.M.	Doklad. Akad. Nauk. SSSR (1954), Vol. 95, p.135.
57.	Sommerville, I.D. Bell, H.B.	"International Symposium on Metallurgical Slags", Halifax, Nova Scotia (1980)
58.	Rao, Bh. V.J.	Phys. Chem. Glasses, (1963), Vol. 4.
59.	Iwamoto, N. Fuji, M. Tsunawaki, Y.	Trans. Japan Welding Research Inst. (1974), Vol. 3, p.53.
60.	Ohno, A. Ross, H.V.	Can. Met. Quart. (1964), Vol. 3, p.257.
61.	Chukukere, E.U. Ross, H. V.	Can. Met. Quart. (1967), Vol. 6, p.137.
62.	Sommerville, I.D. Grieveson, P. Taylor, T.	Ironmaking and Steelmaking (1980) Vol. 7, p.25.
63.	De Vries, R C. Roy, R. Osborn, E.F.	J. Am. Ceram. Soc. (1955), Vol. 38, p.161.
64.	Abdur Rouf, Md.	Ph.D. Thesis, (1968), University of Strathclyde.
65.	Roxburgh, R.J.	Ph.D. Thesis, (1971), University of Strathclyde.
66.	Mansor, Y.B.	Ph.D. Thesis, (1976), University of Strathclyde.

67. Johnston, J. Walker, A.C. — J. Am. Chem. Soc., (1925), Vol. 47, p.1807.

68. Young, R.S. — "Chemical Analysis in Extractive Metallurgy", Griffin & Co. Ltd. London, 1971, p.73.

69. Burgess, G.K. — "The Measurement of High Temperatures" Pub. John Wiley and Sons (1912)

70. Elliot, J.F. Gleiser, M. Ramakrishma, V. — "Thermochemistry for Steelmaking" Vol. 2, Addison-Wesbey Co. (1963).

71. Gillespie, L.T. — J. Chem. Physics, (1939), Vol. 7, p.530.

72. Emmet, P.H. Schultz, J.F. — J. Am. Chem., Soc.,(1933), Vol. 55, p.1376.

73. Fontana, M.G. Chipman, J. — Trans. Am. Soc. Metals, (1936), Vol. 24, p.313.

74. Dastur, M.N. Chipman, J. — Trans. A.I.M.E.,(1949), Vol. 185, p.441

75. Floridis. T.P. Chipman, J. — Trans. Met. Soc. A.I.M.E.,(1958), Vol. 212, p.549.

76. MacLean, A. Bell, H.B. — J.I.S.I. (1965), Vol. 203, p.123.

77. Charlton, K. — Ph.D. Thesis, (1963), University of Glasgow.

78. Aziz, A. — Ph.D. Thesis, (1965), University of Glasgow.

79. Smellie, A.M. — Ph.D. Thesis, (1969) University of Strathclyde.

80. Tankims, E.S. Grokcen, N.A. Belton, G.R. — Trans. Met. Soc., A.I.M.E., (1964), Vol. 230, p.820

81. Fincham, C.J. Richardson, F.D. — Proc. Roy. Soc., (1954), Vol. 223, Series A, p.40.

82. Levin, E.M. Robbins, C.R. MacMurdie, H.F. — "Phase Diagrams for Ceramists" (1964), p.17, The Am. Ceram.Soc.

83. MacChesney, J.B. Muan, A. — J. Am. Ceram. Soc.,(1960), Vol.43, No. 11, p.586.

84.	Holmes, W.T. Banning, L.H Brown, L.L.	U.S. Bureau of Mines Report of Investigation 7801, (1967).
85.	Fine, H.A. Arac, S.	Ironmaking and Steelmaking (1980), No. 4, p.160.
86.	Baldwin, B.G.	J.I.S.I. (1957), Aug. p.388.
87.	Herty, C.H. Gaines, J.M. Larsey, B.M. Simkins, W.A.	Mining and Metallurgical Investigation Bulletin (1927), Vol. 34.
88.	Fetters, K.L. Chipman, J.	Trans. A.I.M.E., (1941), Vol. 145, p.45.
89.	Taylor, C.R. Chipman, J.	Trans. A.I.M.E. (1943), Vol. 154, p.228.
90.	Gurry, R.W. Darken, L.S.	J. Am. Chem. Soc., (1950), Vol. 72, p.3906.
91.	Larson, H. Chipman, J.	Trans. A.I.M.E. (1953), Vol. 197, p.1089.
92.	Turkdogan, E.T. Bills, P.M.	J.I.S.I. (1958), February, p.143.
93.	Timucin, M. Morris, A.E.	Metal. Trans., (1970), Vol. 1, p.3193.
94.	Holbrook, W.F. Joseph, T.L.	Trans. A.I.M.E. (1936), Vol. 120, p.99.
95.	Holbrook, W.F.	Trans. A.I.M.E. (1938), Vol. 131, p.127.
96.	Hatch, G. Chipman, J.	Trans. A.I.M.E., (1949), Vol. 185, p.274.
97.	Grant, N.J. Kalling, V. Chipman, J.	Trans. A.I.M.E., (1951), Vol. 191, p.666.
98.	Fincham, C.J. Richardson, F.D.	J.I.S.I. (1954), Vol. 178, p.4.
99.	Carter, P.T. Macfarlane, T.G.	J.I.S.I. (1957), Vol. 185, p.54.
100.	Rosenquist, T.	Trans. A.I.M.E. (1959), Vol. 215, p.529.
101.	Filipovska, N.J. Bell, H.B.	Documenta Chemico Yugoslavia, (1975), Vol. 40, p.499.

102.	Kor, G.T.W. Richardson, F.D.	J.I.S.I. (1968), Vol. 206, p.700.
103.	Sharma, R.A. Richardson, F.D.	Trans. A.I.M.E. (1965), Vol. 233, p.1586.
104.	Sharma, R.A Richardson, F.D.	J.I.S.I. (1961), Vol. 198, p.386.
105.	Cameron, J. Gibbons, T.B. Taylor, J.	J.I.S.I. (1966), Vol. 204, p.1223.
106.	Kalyanram, M.R. Macfarlane, T.G. Bell, H.B.	J.I.S.I. (1960), Vol. 195, p.58.
107.	Kalyanram, M.R. Bell, H.B.	Trans. Brit. Ceram. Soc., (1961), Vol. 60, p.135.
108.	Sharma, R.A. Richardson, F.D.	J.I.S.I. (1962), Vol. 200, p.373.
109.	Abraham, K.P. Davies, M.W. Richardson, F.D.	J.I.S.I. (1960), Vol. 195, p.309.
110.	Wagner, C.	Met. Trans. (1975), Vol. 6B, p.398.
111.	JANAF	"Thermochemical tables", Dow Chemical Co., Midland, Michigan (1965),(1966).
112.	Piere, G. St. Chipman, J.	J. Am. Chem. Soc., (1954), Vol. 76, p.4787.
113.	Fincham, C.J. Richardson, F.D.	J.I.S.I. (1952), Vol. 172, p.53.
114.	Schürmann, E. Bruderm, R. Richter, H.	Arch. Eisenhut., (1979), Vol. 50, p.139.
115.	Bell, H.B.	"International Symposium on Metallurgical Slags", Halifax, Nova Scotia, (1980).
116.	Abraham, K.P. Richardson, F.D.	J.I.S.I. (1958), Vol. 188, p.360.
117.	Brown, S.D.	M.Sc. Thesis, (1975), University of Strathclyde.
118.	Brown S.D.	Ph.D. Thesis,(1977), University of Strathclyde.

119. Duffy, J.A.
Ingram, M.D.
Sommerville, I.D.
J. Chem. Soc., Faraday Trans. (1978) Vol. 74, p.1410.

120. Pierre, St. G.
Chipman, J.
Trans. A.I.M.E. (1956), Vol. 206, p.1474.

121. Earnshaw, I.
Ph.D. Thesis, (1959), University of Glasgow.

122. Lee, B.E.
Bell, H.B.
Unpublished work.

123. Derici, R.H.
Ph.D. Thesis, (1980) University of Strathclyde.

124. Cavaghan, N.J.
Harris, T.H.
J.I.S.I. (1970), Vol. 208, p.528.

125. Schenck, H.
"Physical Chemistry of Steelmaking" (1945), p.472, London, B.I.S.R.A.

126. Grant, N.J.
Chipman, J.
Trans. A.I.M.E., (1946), Vol. 167, p.134.

127. Trömel, G.
Knoch, K.
Wolfdietrich, F.
Arch. Esin., (1969), Vol. 40, p.969.

128. Turkdogan, E.T.
J.I.S.I. (1955), Feb. p.147.

129. Derge, G.
Philbrook, W.O.
Goldman, K.M.
Trans. A.I.M.E., (1950), Vol. 188, p.1111.

130. Ramachandran, S.
King, T.B.
Grant, N.J.
Trans. A.I.M.E. (1956), Vol. 206, p.1549.

131. Taylor, J.
Stobo, J.J.
J.I.S.I. (1954), Vol. 178 , p.360.

132. Venkatadri, A.S.
Bell, H.B.
J.I.S.I. (1969), Vol, 207, p.1110.

133. Baxter, G.P.
Lansing, J.E.
J. Am. Chem. Soc., (1920), Vol. 42, p.419.

134. Booky, J.B.
Tombs, N.C.
J.I.S.I. (1952), Vol. 172, p.86.

135. Naish, W.R.
Clennell, J.E.
"Select Methods of Metallurigcal Analysis", (1953), Chapman & Hall Ltd., London.

136.	A.S.T.M.	"Chemical Analysis of Metal Sampling and analysis of Metal Bearing Ore" (1969)
137.	Abdelkarim, O.I.	Ph.D. Thesis, (1977), University of Strathclyde.
138.	Flood, H. Grjothein, K.	J.I.S.I. (1952), Vol. 171, p.64.
139.	De Vries, R.C. Roy, R. Osborn, E.F.	J. Phy. Chem., (1954), Vol. 58, p.1069.
140.	Meshi, D. Myers, R.	J. Mol. Spectro, (1959), Vol. 3, p.405.
141.	Sommerville, I.D. Bell, H.B.	Unpublished work.
142.	Elliot, J.F.	J.I.S.I. (1952), Vol. 171, p.64.
143.	Wagner, C.	Met. Trans., (1975), Vol. 6B, p.405.
144.	Richardson, F.D.	"Physical Chemistry of Metals in Steelmaking", (1974), Vol. 2,p.29.
145.	Shuja, M.S	Ph.D. Thesis, (1970), University of Strathclyde.
146.	Ward, R.G.	"The Physical Chemistry of Iron and Steelmaking", (1962), Pub. Arnold, London.
147.	British Olivetti Ltd. Glasgow.	Programmes Library - programma 101, Model Computer, programme No.132.
148.	H.M.S.O., London	"Industrial Experimentation", (1949), 4th Edition, p.65.
149.	Ibid	p.32.